PB86-112299

REPORT NO.
UCB/EERC-85/01
FEBRUARY 1985

EARTHQUAKE ENGINEERING RESEARCH CENTER

SIMPLIFIED METHODS OF ANALYSIS FOR EARTHQUAKE RESISTANT DESIGN OF BUILDINGS

by

ERNESTO F. CRUZ
ANIL K. CHOPRA

A Report on Research Conducted Under
Grants CEE-8105790 and CEE-8402271
from the National Science Foundation

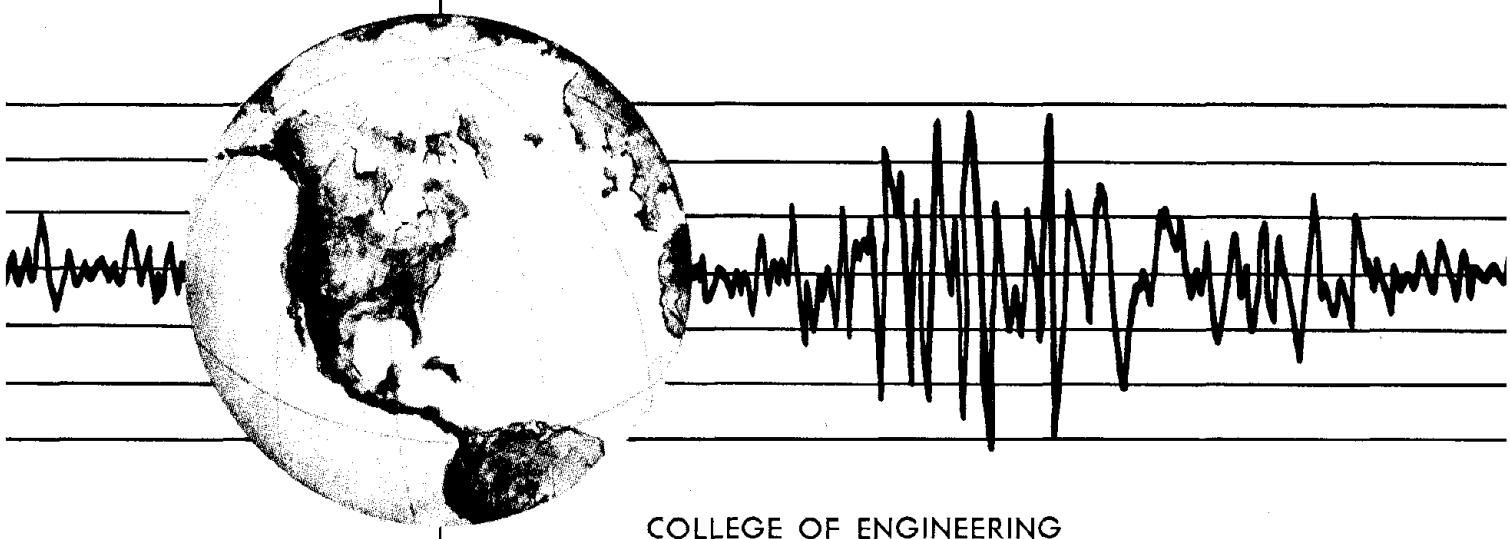

COLLEGE OF ENGINEERING

UNIVERSITY OF CALIFORNIA · Berkeley, California

For sale by the National Technical Information Service, U.S. Department of Commerce, Springfield, Virginia 22161.

See back of report for up to date listing of EERC reports.

50272-101

REPORT DOCUMENTATION PAGE	1. REPORT NO. NSF/ENG-85020	2.	3. Recipient's Accession No. PB86 112299/AS

4. Title and Subtitle
Simplified Methods of Analysis for Earthquake Resistant Design of Buildings

5. Report Date
February 1985

6.

7. Author(s)
Ernesto F. Cruz and Anil K. Chopra

8. Performing Organization Rept. No.
UCB/EERC-85/01

9. Performing Organization Name and Address
Earthquake Engineering Research Center
University of California, Berkeley
1301 So. 46th Street
Richmond, Calif. 94804

10. Project/Task/Work Unit No.

11. Contract(C) or Grant(G) No.
(C)
(G) CEE-8105790
CEE-8402271

12. Sponsoring Organization Name and Address
National Science Foundation
1800 G Street, N.W.
Washington, D.C. 20550

13. Type of Report & Period Covered

14.

15. Supplementary Notes

16. Abstract (Limit: 200 words)

In Part I, the accuracy of the response spectrum analysis (RSA) for estimating the maximum response of a building directly from the earthquake design spectrum is evaluated with the objective of developing better simplified analysis procedures suitable for preliminary design of buildings and for inclusion in building codes.

In Part II, recognizing that the earthquake response of many buildings can be estimated by considering only the first two vibration modes in the response spectrum analysis (RSA) procedure, a simplified response spectrum analysis (SRSA) procedure is presented. The SRSA method should be very useful in practical application because, although much simpler than the RSA method, it provides very similar estimates of design forces for many buildings.

In Part III, formulas for base shear, height-wise distribution of lateral forces, and computation of overturning moments specified in three design documents -- Uniform Building Code, Mexico's Federal District Building Code, and ATC-3 design provisions -- are evaluated in light of the results of dynamic analysis of buildings. It is demonstrated that these formulas do not properly recognize the effects of important building parameters which control the significance of higher mode contributions in the building response; an improved procedure, which does recognize them is presented. The procedure represents a major conceptual improvement over present building codes with very little increase in computational effort.

17. Document Analysis a. Descriptors

b. Identifiers/Open-Ended Terms

c. COSATI Field/Group

18. Availability Statement: Release Unlimited	19. Security Class (This Report)	21. No. of Pages 260
	20. Security Class (This Page)	22. Price A12

SIMPLIFIED METHODS OF ANALYSIS FOR EARTHQUAKE RESISTANT DESIGN OF BUILDINGS

by

Ernesto F. Cruz

and

Anil K. Chopra

A Report on Research Conducted Under
Grants CEE-8105790 and CEE-8402271
from the National Science Foundation

Report No. UCB/EERC-85/01
Earthquake Engineering Research Center
University of California
Berkeley, California

February, 1985

ia

ABSTRACT

This work on the development of simplified methods of analysis which are suitable for application to earthquake resistant design of buildings is organized in three parts.

In Part I, the accuracy of the response spectrum analysis (RSA) for estimating the maximum response of a building directly from the earthquake design spectrum is evaluated with the objective of developing better simplified analysis procedures suitable for preliminary design of buildings and for inclusion in building codes. It is demonstrated that: (1) For a fixed fundamental period T_1 of the building, the response contributions of the higher vibration modes increase, and consequently the errors in the RSA results increase, with decreasing beam-to-column stiffness ratio ρ. (2) For a fixed ρ, the response contributions of the higher vibration modes increase, and consequently the errors in the RSA results increase, with increasing T_1 in the medium- and long-period regions of the design spectrum. (3) The RSA results are accurate enough for design applications.

In Part II, recognizing that the earthquake response of many buildings can be estimated by considering only the first two vibration modes in the response spectrum analysis (RSA) procedure, a simplified response spectrum analysis (SRSA) procedure is presented. The SRSA method should be very useful in practical application because, although much simpler than the RSA method, it provides very similar estimates of design forces for many buildings. With the development of the SRSA, a hierarchy of four analysis procedures to determine the earthquake forces are available to the building designer: code-type procedure, SRSA, RSA, and RHA -- response history analysis. The criteria presented to evaluate the results from each of procedure, and to decide whether it is necessary to improve results by proceeding to the next procedure in the hierarchy, utilize all the preceding computations and are therefore convenient.

In Part III, formulas for base shear, height-wise distribution of lateral forces, and computation of overturning moments specified in three design documents --Uniform Building Code, Mexico's Federal District Building Code, and ATC-3 design provisions-- are evaluated in light

of the results of dynamic analysis of buildings. It is demonstrated that these formulas do not properly recognize the effects of important building parameters which control the significance of higher mode contributions in the building response. An improved procedure, which recognizes the influence of these parameters, to compute the earthquake forces for the initial, preliminary design of buildings is presented. Starting with the earthquake design spectrum for elastic or inelastic design and the overall, general description of the proposed building, this procedure provides an indirect approach to estimate the response in the first two vibrations modes of the building. The procedure recognizes the important influence of those building properties and parameters that significantly influence its earthquake response without requiring the computations inherent in standard dynamic analysis by the response spectrum method. The procedure represents a major conceptual improvement over present building codes with very little increase in computational effort.

ACKNOWLEDGEMENTS

This research investigation was supported by the National Science Foundation under Grants CEE81-05790 and CEE84-02271. The authors are grateful for this support.

The report is the same, except for some editorial changes, as Ernesto F. Cruz's doctoral dissertation which has been submitted to the University of California, Berkeley. The dissertation committee consisted of Professors A.K. Chopra (Chairman), S.A. Mahin, and B.A. Bolt. The authors are grateful to Professors Mahin and Bolt for reviewing the manuscript and suggesting improvements.

PREFACE

This work on the development of simplified methods of analysis which are suitable for application to earthquake resistant design of buildings is organized in three parts:

- Part I: Elastic Earthquake Response of Building Frames
- Part II: Simplified Procedures for Elastic Analysis of Buildings
- Part III: An Improved Code-type Analysis Procedure for Preliminary Design

TABLE OF CONTENTS

PART I

ELASTIC EARTHQUAKE RESPONSE OF BUILDING FRAMES

1. INTRODUCTION

The response spectrum method plays an important role in practical analysis of multistory buildings for earthquake motions. The maximum response of the building is estimated directly from the elastic or inelastic design spectrum characterizing the design earthquake for the site and considering the performance criteria for the building. The resulting estimates of maximum forces and deformations provide a basis for preliminary design for buildings. These estimates may be accurate for the final design of many buildings but could be refined for the unusual or important buildings by response history analysis. Furthermore, most building codes specifications for earthquake forces are based on simplifications of the response spectrum method of analysis.

In order to develop better simplified analysis procedures suitable for preliminary design of buildings and for inclusion in building codes, it is therefore necessary to evaluate the accuracy of the response spectrum estimates of maximum building response. Because the errors in these estimates are related to the significance of the contributions of the vibration modes higher than the fundamental mode, it should be useful to investigate the contributions of the various vibration modes to the response of buildings.

These issues are, of course, not new. They have been the subject of many investigations, most of them restricted to idealized shear buildings. For example, the response of idealized 4-story shear buildings with three different values of the fundamental vibration period due to recorded and simulated ground motions was determined by response history analysis, response spectrum analysis, and random vibration analysis and the results were compared [11]. Modal contributions in the response of 10-story shear buildings to simple ground motions, described by a half-cycle displacement pulse, and to El Centro 1940 ground motion were investigated for a wide range of fundamental vibration periods of the building [13]. One of the most comprehensive investigations was due to Roehl [9], wherein the response of five-story moment-resisting plane frames to a half-cycle displacement pulse was determined for a wide range of

parameters. The beam-to-column stiffness ratio was varied to cover the complete range of frame behavior, from the vertical flexural beam at one extreme to the vertical shear beam at the other end. The fundamental vibration period was also varied over a wide range. Among other issues, the significance of the higher mode contributions in building response was investigated and its dependence on the beam-to-column stiffness ratio and fundamental vibration period was identified.

The work of Roehl is extended to study the response of the same class of moment-resisting plane frames to an ensemble of earthquake ground motions. The ensemble average of the maximum response is determined by response history analysis and response spectrum analysis for a wide range of values of the beam-to-column stiffness ratio and fundamental vibration period. Based on these results, the response contributions of the various vibration modes are studied and the accuracy of the response spectrum estimates of maximum response is investigated. The results of this investigation provide a basis for developing improved simplified analysis procedures for preliminary design of buildings in Part II of this report.

2. SYSTEMS AND GROUND MOTIONS

2.1 Systems analyzed

The systems analyzed are idealized as single-bay, five story moment resisting plane frames with constant story height $= h$, and bay width $= 2h$ (Figure 1). All members are prismatic with constant cross-section. Only flexural deformations are considered in the analysis of these frames. All the beams have the same flexural stiffness (EI_b) and the column stiffness (EI_c) does not vary with height. The structure is idealized as a lumped mass system with the same mass m at all the floor levels. The rotational inertia of the sections is neglected in all members. The damping ratio for all the natural modes of vibration is assumed to be 5 percent.

As shown by Roehl [9], only two additional parameters are needed to completely define the system: the fundamental mode period T_1 and the stiffness ratio ρ. This ratio was originally defined by Blume [1], as a joint rotation index, based on the properties of beams and columns in the story closest to the mid-height of the frame:

$$\rho = \frac{\sum_{beams} EI_b \ / \ L_b}{\sum_{columns} EI_c \ / \ L_c} \tag{1}$$

where I_b is the moment of inertia of a beam, L_b is the beam length, I_c is the moment of inertia of a column, and L_c is the column length; and the summations include all the beams and columns in the mid-height story. For the selected class of building frames defined in the preceding paragraph, equation (1) reduces to

$$\rho = I_b \ / \ 4 \ I_c \tag{2}$$

For this selected class of building frames with a particular ρ value, as noted by Roehl [9], the natural vibration mode shapes ϕ_n and the ratios between the natural vibration frequencies ω_n / ω_1 are independent of the fundamental vibration period T_1 (Appendix B). By varying the stiffness ratio ρ, the complete range of behavior of the frame can be covered, from the flexural

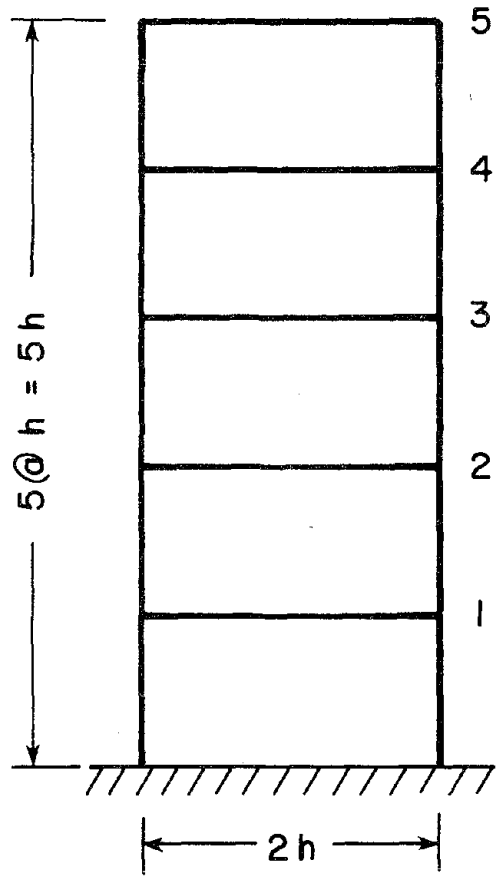

UNIFORM FRAME

$m_j = m$

$I_b = 4\rho I$

$I_c = I$

FIGURE 1 Idealized building frame.

beam with the beams imposing no restraint to joint rotation ($\rho = 0$) to the shear beam ($\rho = \infty$) in which the joint rotations are completely restrained and deformations occur only through double-curvature bending of the columns. Intermediate values of ρ represent frames with both beams and columns undergoing bending deformations with joint rotations.

The ratios of the natural frequencies for a wide range of ρ values are presented in Table 1 and plotted in Figure 2. The natural vibration mode shapes for six differents values of ρ are presented in Table 2 and three of these cases are plotted in Figure 3. It is readily apparent from this data that the stiffness ratio ρ must have great importance in determining the dynamic (and static) behavior of the frame. The mode shapes for the two extreme cases $\rho = 0$ and $\rho = \infty$ are quite different, and the values of the frequency ratios show important changes with ρ especially for the higher modes. The effects of these differences in the mode shapes and frequency ratios on earthquake response of frames will be discussed later.

2.2 Ground Motions

Eight simulated motions were generated to model the properties of ground motions recorded on firm ground in the region of strong shaking during magnitude 6.5 to 7.5 earthquakes in the Western United States [5]. The random process model, its parameter values, and the simulation procedure used is identical to earlier studies [4,6,10]. The simulation procedure consisted of generating samples of stationary Gaussian white noise, multiplying the white noise by an intensity function of time (Figure 4) to represent a segment of strong shaking at constant intensity preceded by a quadratic build-up of intensity and followed by an exponential decay in intensity; passing the resulting function through a second order linear filter with frequency = 2.5 cps and damping ratio = 60 percent to impart the desired frequency content, as indicated by the spectral density (Figure 4), and finally performing a base line correction on the filtered function [3]. The resulting motions are shown in Figure 5 and the maximum values of acceleration, integrated velocity, and displacement are listed in Table 3. They differ from the values presented in reference [5] by an intensity-scaling factor. As will

Table 1: Ratios of natural vibration frequencies of idealized frames.

Adapted from Roehl (1971).

ρ	$\frac{\omega_1}{\left(\frac{EI}{mh^3}\right)^{1/2}}$	$\frac{\omega_2}{\omega_1}$	$\frac{\omega_3}{\omega_1}$	$\frac{\omega_4}{\omega_1}$	$\frac{\omega_5}{\omega_1}$
0	0.16563	6.3853	18.0923	34.9637	52.0702
0.00001	0.16574	6.3817	18.0806	34.9404	52.0349
0.0001	0.16679	6.3500	17.9768	34.7330	51.7215
0.001	0.17638	6.0659	17.0435	32.8660	48.8987
0.0125	0.26284	4.5691	11.8654	22.3609	32.9174
0.05	0.40661	3.7267	8.4281	14.9965	21.4433
0.1	0.51813	3.4755	7.2294	12.2209	16.9698
0.125	0.56051	3.4119	6.9167	11.4699	15.7401
0.5	0.88165	3.1343	5.5716	8.1628	10.2844
1	1.05563	3.0507	5.1829	7.2279	8.7764
2	1.18110	2.9947	4.9299	6.6406	7.8534
5	1.29510	2.9526	4.7451	6.2254	7.2155
10	1.34184	2.9364	4.6757	6.0727	6.9844
50	1.38336	2.9226	4.6168	5.9443	6.7915
500	1.39328	2.9193	4.6030	5.9145	6.7470
∞	1.39439	2.9190	4.6015	5.9112	6.7421

Table 2: Natural vibration mode shapes of idealized frame.

Adapted from Roehl (1971).

ρ	Story	Mode Number				
		1	2	3	4	5
0	1	0.0611	-0.4403	1.4150	-3.2749	6.4358
	2	0.2221	-1.0746	1.5795	0.6731	-7.0564
	3	0.4508	-1.1156	-0.7390	2.3497	6.2089
	4	0.7178	-0.3224	-1.5389	-2.7989	-3.6567
	5	1.0000	1.0000	1.0000	1.0000	1.0000
0.05	1	0.1115	-0.4579	1.2817	-2.8617	5.3933
	2	0.3439	-1.0078	1.2578	0.7755	-6.1182
	3	0.5997	-0.8996	-0.8400	1.9148	5.5105
	4	0.8250	-0.0762	-1.2992	-2.5404	-3.3954
	5	1.0000	1.0000	1.0000	1.0000	1.0000
0.125	1	0.1419	-0.5101	1.2314	-2.5538	4.5184
	2	0.4023	-1.0339	1.0544	0.8755	-5.3428
	3	0.6608	-0.8281	-0.9240	1.5715	4.9384
	4	0.8658	0.0410	-1.1414	-2.3426	-3.1829
	5	1.0000	1.0000	1.0000	1.0000	1.0000
0.5	1	0.1953	-0.6351	1.2434	-2.1092	3.0955
	2	0.4738	-1.0897	0.7575	1.0995	-4.1252
	3	0.7201	-0.7349	-1.0726	1.0276	4.0680
	4	0.9002	0.1881	-0.9210	-2.0539	-2.8654
	5	1.0000	1.0000	1.0000	1.0000	1.0000
2	1	0.2448	-0.7499	1.2903	-1.8411	2.2930
	2	0.5176	-1.1010	0.5316	1.2873	-3.4903
	3	0.7476	-0.6557	-1.1643	0.6949	3.6537
	4	0.9129	0.2670	-0.7896	-1.9006	-2.7232
	5	1.0000	1.0000	1.0000	1.0000	1.0000
∞	1	0.2846	-0.8308	1.3099	-1.6825	1.9188
	2	0.5462	-1.0882	0.3728	1.3979	-3.2284
	3	0.7634	-0.5943	-1.2036	0.5212	3.5132
	4	0.9189	0.3098	-0.7154	-1.8310	-2.6822
	5	1.0000	1.0000	1.0000	1.0000	1.0000

Table 3: Properties of simulated ground motions.

Simulation No.	Ground Motion Maxima		
	Acceleration (g' s)	Velocity (in/sec)	Displacement (in)
1	0.3145	23.199	10.006
2	0.2375	24.278	23.070
3	0.2795	20.536	11.866
4	0.3512	16.363	16.856
5	0.2807	17.526	12.381
6	0.3024	13.872	8.790
7	0.3152	22.001	21.930
8	0.3325	22.227	13.870
Average Values	0.3017	20.000	14.772

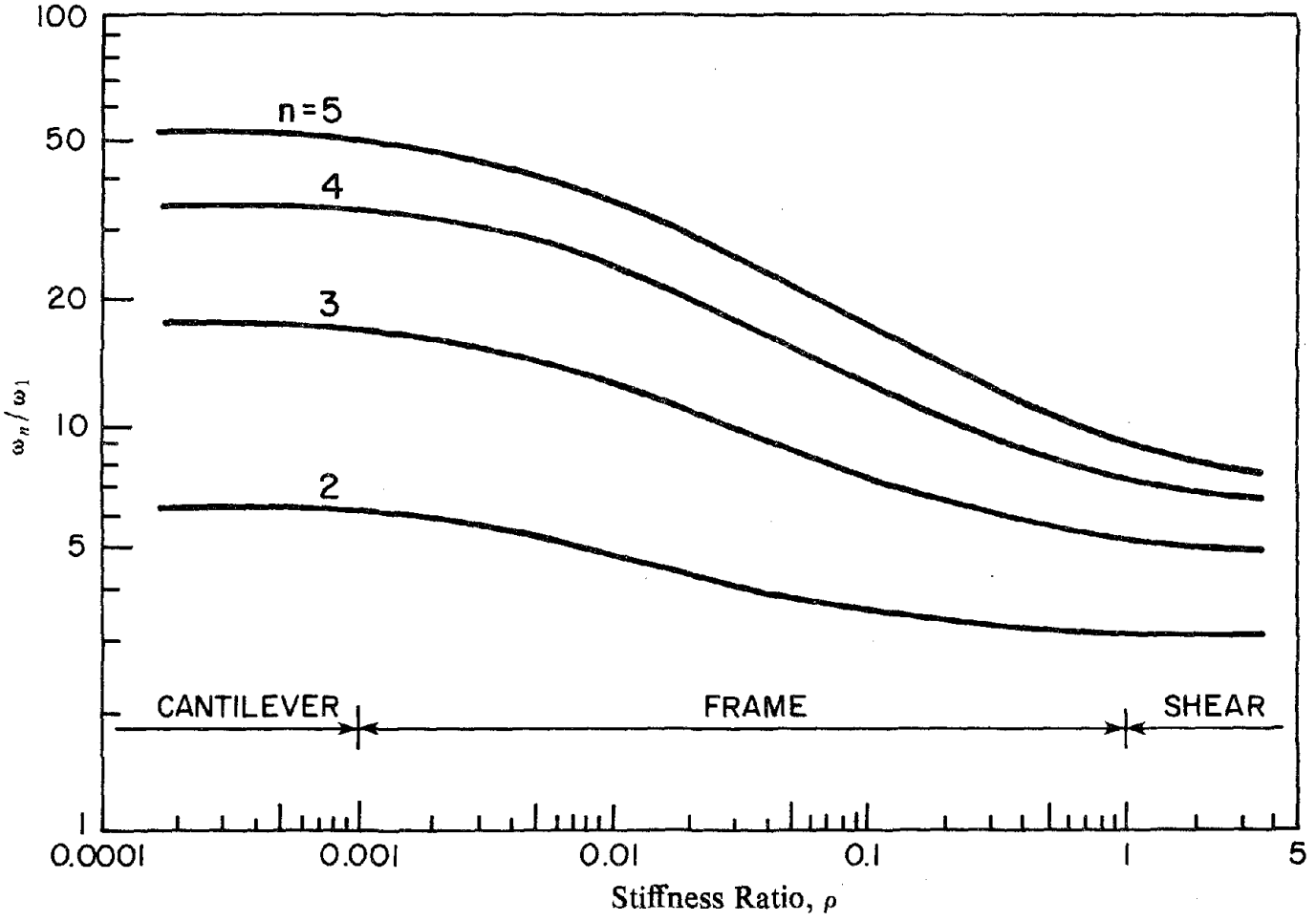

FIGURE 2 Natural frequency ratios for single-bay frame. Adapted from Roehl (1971).

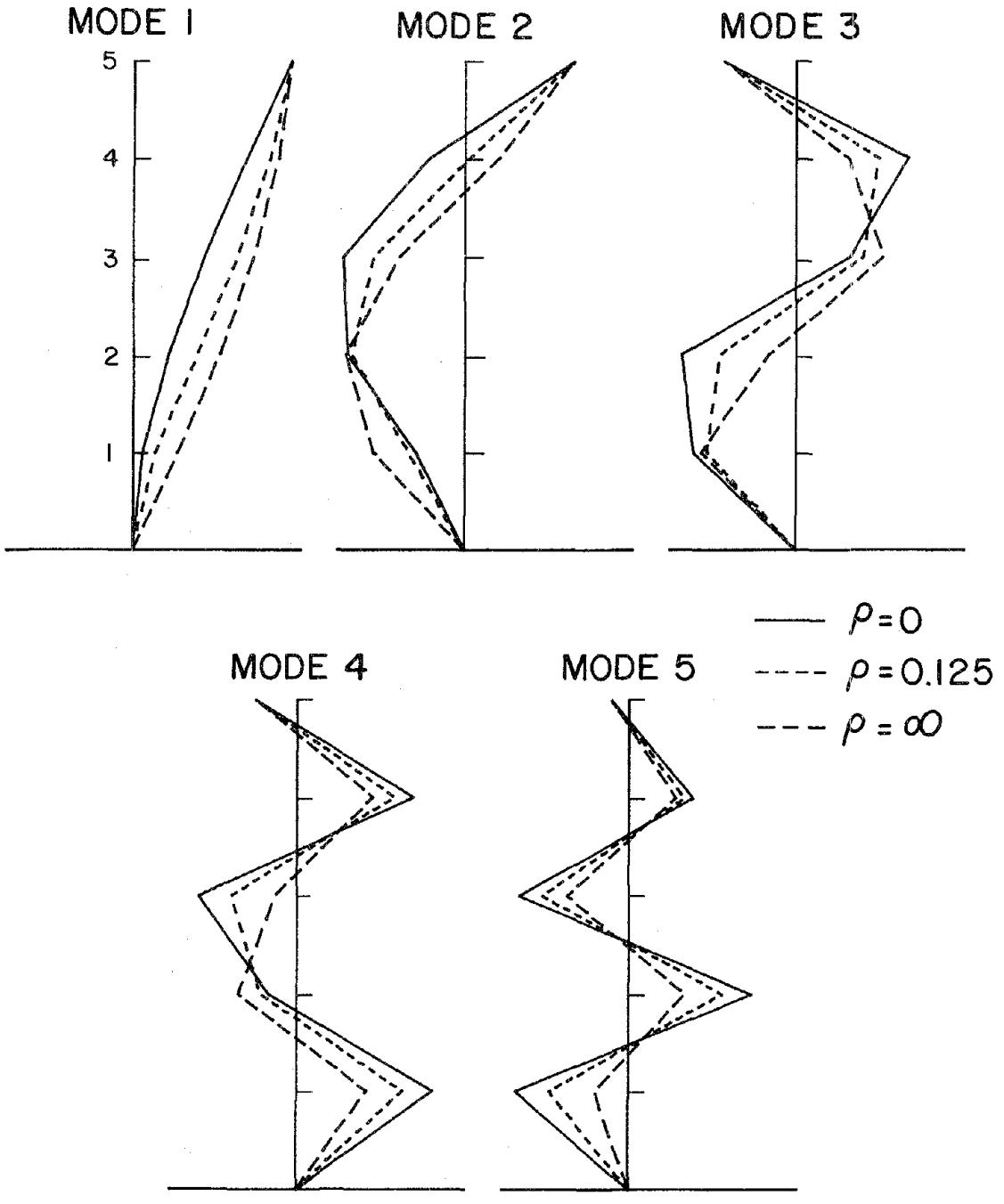

FIGURE 3 Natural vibration mode shapes.

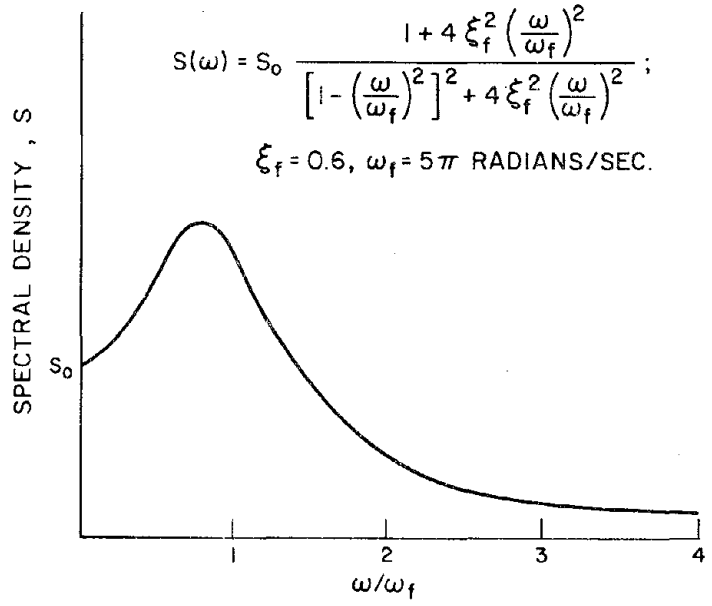

(a) SPECTRAL DENSITY OF FILTERED WHITE NOISE ACCELERATION

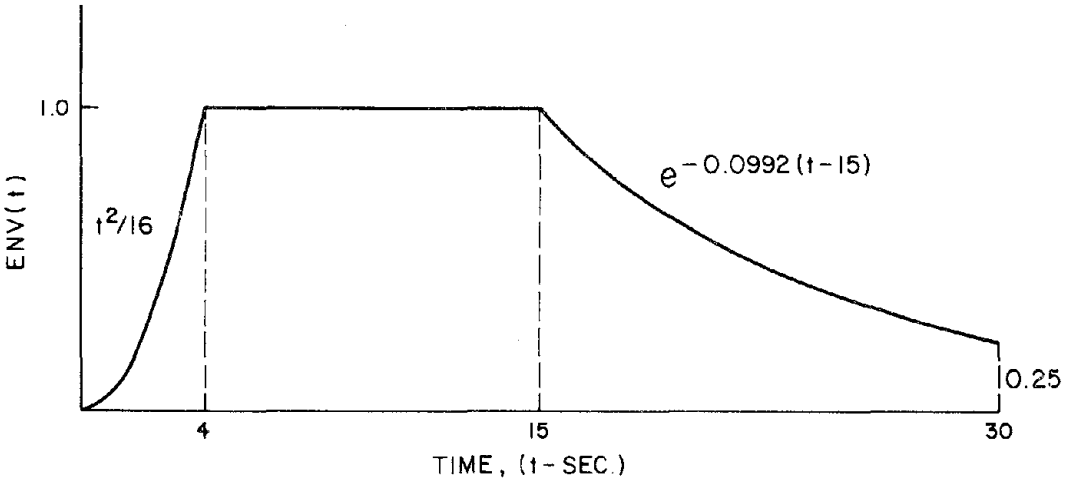

(b) INTENSITY - TIME FUNCTION

FIGURE 4 Simulated ground motion spectral density and intensity time-function. Adapted from Lopez (1978).

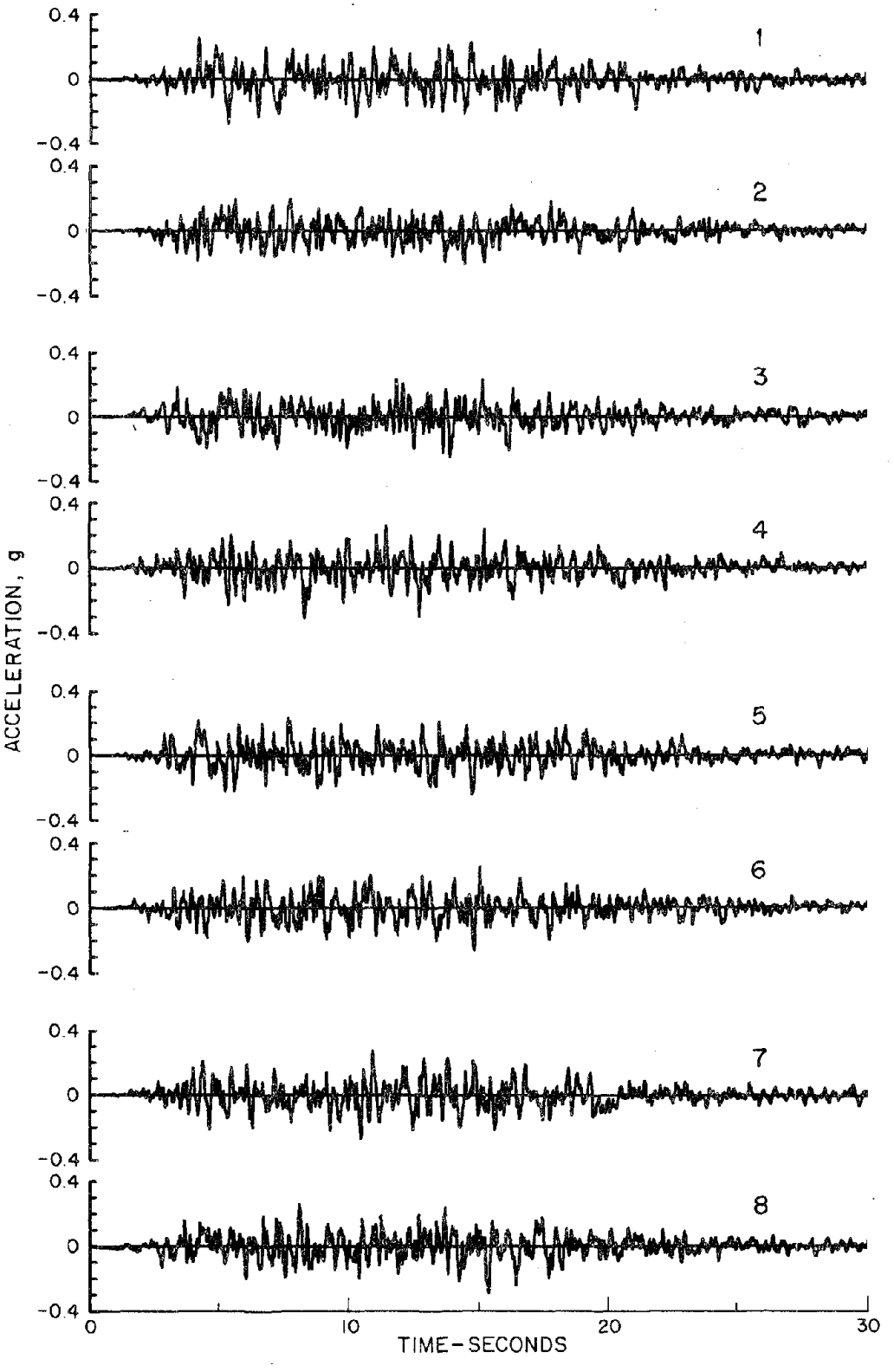

FIGURE 5 Simulated ground motions accelerograms. Adapted from Lopez (1978).

be seen later, the response of the building frames will be normalized so that they will be independent of the ground motion intensity.

The elastic response spectrum for 5 percent damping for each of the eight ground motions was computed using a modified version of the computer program SPECEQ [8]. The average of the eight response spectra is presented in Figure 6 together with the ensemble averages of the maximum ground acceleration, velocity, and displacement.

The concept of frequency (or period) regions based on the shape of the pseudo-velocity response spectrum plotted on log-log paper, which is useful in interpreting earthquake response spectra and structural response, is taken from [7]: When plotted in this form, the central portion of the spectrum can be approximated by a horizontal line and two 45° diagonal lines as shown by the dashed lines in Figure 7. The region to the left of the intersection point b is defined as the "low-frequency" region of the spectrum, the region between points b and c is defined as the "medium-frequency" region, and the portion to the right of point c is defined as the "high-frequency" region. It is sometimes desirable to subdivide the low-frequency region into an "extremely low-frequency" sub-region for which the displacement response spectrum S_d is equal to or less than the maximum ground displacement $\bar{u}_g$ and a "moderately low-frequency" sub-region where S_d is greater than $\bar{u}_g$. The high-frequency region is similarly subdivided into a "moderately high-frequency" sub-region for which the pseudo-acceleration response spectrum S_a is greater than the maximum ground acceleration $\bar{a}_g$, and an "extremely high-frequency" sub-region for which S_a is for all practical purposes equal to $\bar{a}_g$. The boundaries of these sub-regions are identified in Figure 7 by the points a and d.

For the average response spectrum of Figure 6 the trapezoidal approximation to the spectrum and the boundaries of the frequency regions are as shown. The relative positions of points b, c, and d are reversed because the spectrum is plotted against period rather than frequency. In the rest of this study the equivalent terms long-period region, medium-period region, and short-period region will be used to refer to the different regions of the spectrum because the response results are presented in terms of period rather than frequency.

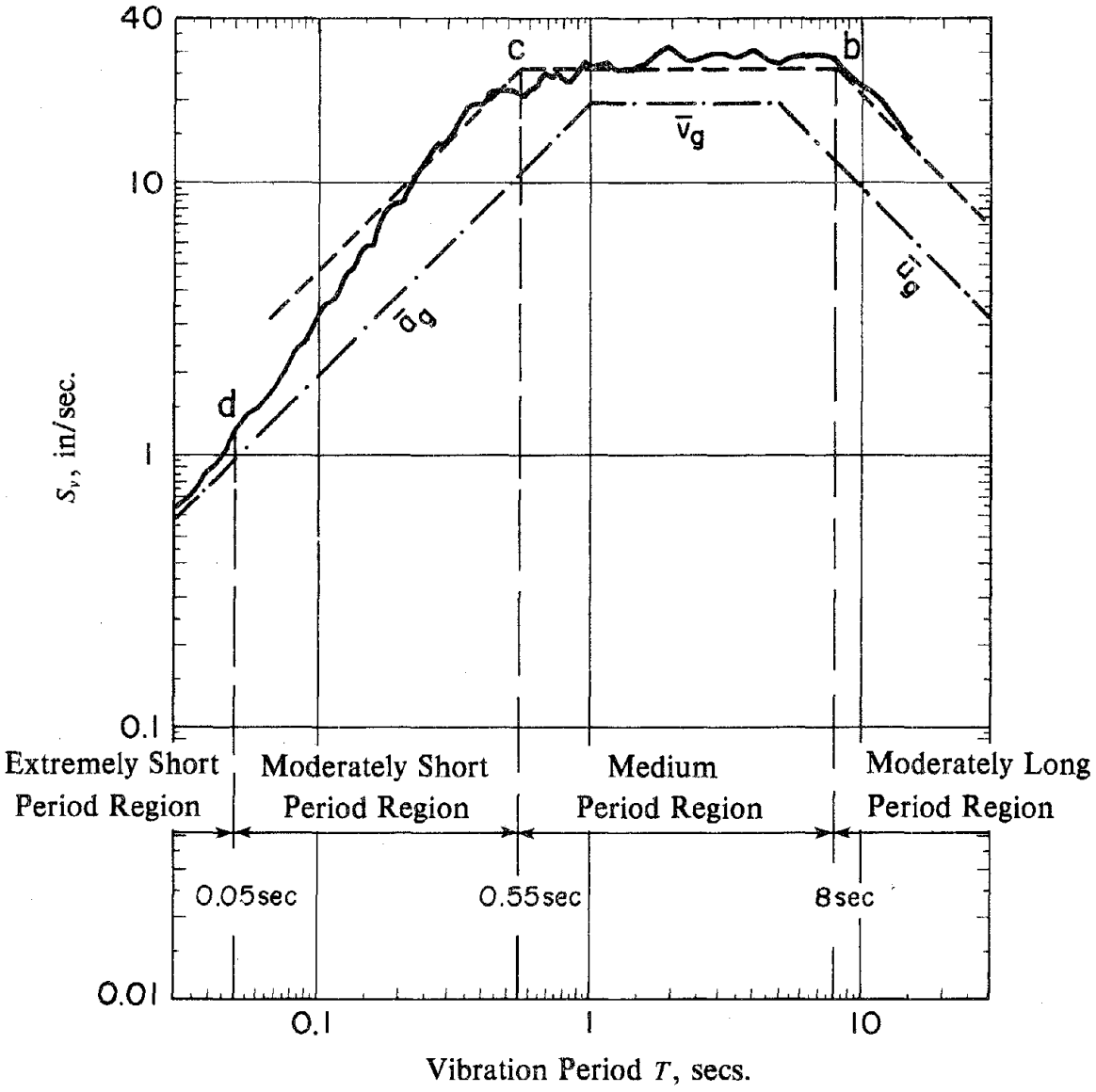

FIGURE 6 Average response spectrum (5 % damping) and definition of spectral period regions for simulated ground motions.

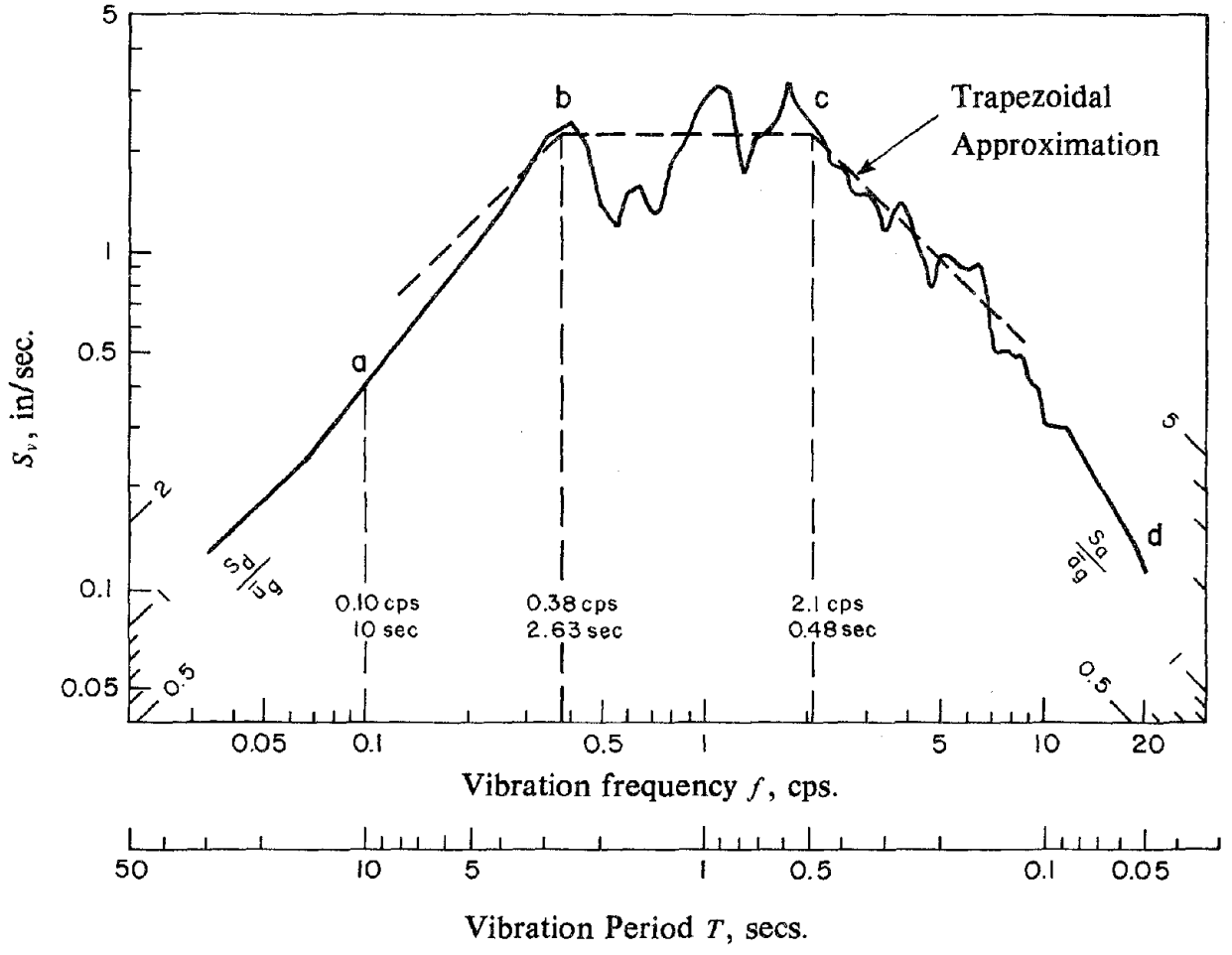

FIGURE 7 Definition of spectral frequency regions. El Centro ground motion; damping = 2 percent. Adapted from Veletsos (1969).

The shapes of the spectra in Figures 6 and 7 have the same general characteristics but the boundaries between the different regions occur at rather different values of period (or frequency). In particular, the period values at points b and a for the average spectrum of the simulated earthquake motions (Figure 6) are much longer than for the El Centro spectrum (Figure 7). This is due to the different values of the spectrum amplification factors [7] for the average and El Centro response spectra. The amplification factor is the ratio of an ordinate of the trapezoidal approximation to the response spectrum to a ground motion parameter. In the moderately short period region it is the ratio between the constant spectral pseudo-acceleration and the maximum ground acceleration. In the medium period region, it is the ratio between the constant spectral pseudo-velocity and the maximum ground velocity. In the moderately long period region, it is the ratio between the constant spectral displacement and the maximum ground displacement. For the average spectrum of Figure 6 these ratios are approximately: 2.5, 1.4, and 2.5 respectively which are much different than the values of: 3.1, 2.1, and 1.5, respectively, for the El Centro spectrum of Figure 7. Furthermore, the maximum ground acceleration, velocity, and displacement are not in the same proportions for both spectra, which is yet another reason for the observed differences in the period values for the two spectra at the boundaries of the various period regions.

3. ANALYSIS PROCEDURES

The idealized building frame described in Section 2.1 is analyzed using standard methods of dynamic structural analysis: response history analysis and response spectrum analysis. Only a summary of these procedures is presented here but more details including their implementation are available in Appendices A and B.

3.1 Response History Analysis

The time-variation of response of the idealized building frame to earthquake ground motion can be computed by the following procedure [2]:

1. Define the ground acceleration $a_g(t)$ by the numerical ordinates of the accelerogram.
2. Define structural properties
   (a) Compute the mass matrix **m** as a diagonal matrix of masses lumped at the floor levels
   (b) Compute the lateral stiffness matrix **k** of the building frame having one degree-of-freedom, the lateral displacement, per floor. This matrix is computed by static condensation of the vertical and rotational degrees of freedom from the complete stiffness matrix determined from the stiffness matrices of structural elements.
   (c) Estimate modal damping ratios ξ_n.
3. Solve the eigen-problem

$$\mathbf{k}\,\boldsymbol{\phi} = \omega^2\,\mathbf{m}\,\boldsymbol{\phi} \tag{3}$$

   to determine the natural frequencies ω_n (natural periods $T_n = 2\pi/\omega_n$) and modes $\boldsymbol{\phi}_n$ of vibration.
4. Compute the response in individual modes of vibration by repeating the following steps for each mode:

(a) Compute the modal response $Y_n(t)$ by solving

$$\ddot{Y}_n(t) + 2\xi_n \omega_n \dot{Y}_n(t) + \omega_n^2 Y_n(t) = -\frac{L_n}{M_n} a_g(t) \tag{4}$$

where $L_n = \boldsymbol{\phi}_n^T \mathbf{m}\, \mathbf{1}$, $M_n = \boldsymbol{\phi}_n^T \mathbf{m}\, \boldsymbol{\phi}_n$, and $\mathbf{1}$ is a vector of as many elements as the number of stories, all equal to unity.

(b) Compute the lateral floor displacements from

$$\mathbf{u}_n(t) = Y_n(t)\, \boldsymbol{\phi}_n \tag{5}$$

(c) Compute equivalent lateral forces from

$$\mathbf{f}_n(t) = \omega_n^2\, Y_n(t)\, \mathbf{m}\, \boldsymbol{\phi}_n \tag{6}$$

(d) Compute the forces in structural elements --beams and columns-- story shears and story overturning moments by static analysis of the structure subjected to the equivalent lateral forces. In particular the base shear and the base moment are calculated from

$$V_{on}(t) = \sum_{j=1}^{N} f_{jn}(t) \tag{7a}$$

$$M_{on}(t) = \sum_{j=1}^{N} f_{jn}(t)\, h_j \tag{7b}$$

where f_{jn} is the equivalent lateral force at the jth floor and h_j is the height of this floor above the base.

5. Determine the total value of the response quantity $r(t)$ from

$$r(t) = \sum_{n=1}^{N} r_n(t) \tag{8}$$

by combining the modal contributions $r_n(t)$ to the response quantity.

Such response history analyses were carried out for each of the eight simulated ground motions described in the preceding section. The maximum of each of the response quantities of interest during each simulated motion was determined. The ensemble average of the

maximum response was obtained by averaging the maximum value corresponding to each of the eight simulated ground motions.

3.2 Response Spectrum Analysis

The maximum response of the idealized buildings frame during a specified earthquake ground motion can be estimated by the following procedure [2]:

1. Determine the average of the response spectra for the eight simulated ground motions.
2. Define structural properties as outlined in computational step 2 of Section 3.1.
3. Solve the eigen-problem of equation (3) as mentioned in computational step 3 of Section 3.1.
4. Compute the maximum response in individual modes of vibration by repeating the following steps for each mode:
   (a) Corresponding to period T_n and damping ratio ξ_n, read the ordinate S_{an} of the pseudo-acceleration response spectrum of the earthquake ground motion.
   (b) Compute maximum values of the lateral floor displacements from

$$\bar{\mathbf{u}}_n = \frac{L_n}{M_n} \frac{S_{an}}{\omega_n^2} \boldsymbol{\phi}_n \tag{9}$$

   (c) Compute the maximum values of the equivalent lateral forces from

$$\bar{\mathbf{f}}_n = \frac{L_n}{M_n} S_{an} \mathbf{m} \boldsymbol{\phi}_n \tag{10}$$

   (d) Compute the maximum values of forces in structural elements, story shears and overturning moments by static analysis of the structure subjected to the equivalent lateral forces of equation (10). In particular the base shear and base overturning moment are calculated from

$$\bar{V}_{0n} = \frac{L_n^2}{M_n} S_{an} = W_n^* \frac{S_{an}}{g} \tag{11a}$$

$$\overline{M}_{on} = \frac{L_n}{M_n} S_{an} \sum_{j=1}^{N} h_j \, m_j \, \phi_{jn} = h_n^* \, \overline{V}_{on} \tag{11b}$$

where W_n^* and h_n^* are known as the effective weight and effective height for the nth mode.

5. Determine an estimate of the maximum $\overline{r}$ of any response by combining the modal maxima $\overline{r}_n$ for the response quantity in accordance with

$$\overline{r} = \left[\sum_{n=1}^{N} \overline{r}_n^2 \right]^{1/2} \tag{12}$$

The square-root-of-the-sum-of-the squares (SRSS) combination of the individual modal maxima is adequate because the idealized frame analyzed here has well separated vibration frequencies.

3.3 Computer Program Implementation

A special purpose computer program was developed to implement the analysis procedures outlined on the preceding section. It takes advantage of some special features of the problem to improve computational efficiency. The details of the implementation of the analysis procedure, a flow chart of the program, and the necessary input data are presented in Appendix B. Although the program can only analyze the idealized frame described in Section 2.1, it allows the choice of performing only response-history analysis (RHA), only response spectrum analysis (RSA), or both analyses for any number of earthquake ground motions and pseudo-acceleration response spectra. The input to the program is the fundamental period, the value of the stiffness ratio ρ, the modal damping ratio (assumed to be the same in all modes) for the frame to be analyzed; and the time variations of the ground accelerations for RHA and the pseudo-acceleration response spectrum for RSA.

4. EFFECT OF FRAME ACTION

The ensemble average of the maximum response computed by response history analysis (RHA) is plotted against the fundamental vibration period T_1 of the building in the form of response spectra. Such plots are presented in Figures 8 and 9 for the values of $\rho = 0$, 0.125, and ∞ and six response quantities: top floor displacement $\overline{u}_5$ relative to the base, base shear $\overline{V}_0$, base overturning moment $\overline{M}_0$, the largest moment $\overline{M}_b$ among all the beams, the largest moment $\overline{M}_c$ among all the columns, and the largest axial force $\overline{P}_c$ among all the columns. The response quantities $\overline{u}_5$, $\overline{V}_0$, and $\overline{M}_0$ are selected as representative of the overall behavior of the system, and $\overline{M}_b$, $\overline{M}_c$, and $\overline{P}_c$ as indicative of its local behavior.

The response quantities are presented in dimensionless form as defined in the figures, where $\overline{u}_g$ and $\overline{\ddot{u}}_g$ are the ensemble averages of the maximum ground displacement and ground acceleration, respectively; W_1^* and h_1^* are the effective weight and effective height for the first vibration mode of the building. The normalization factors for $\overline{V}_0$ and $\overline{M}_0$ are the base shear and moment for a rigid (i.e. zero vibration period) single-degree-of-freedom system with lumped weight W_1^* and height h_1^*. They depend on the geometry of the frame and stiffness ratio ρ, but not separately on m, I_c or I_b. Similarly the normalized responses depend on the time variation of the ground motions but not on their intensity.

Over a wide range of fundamental periods T_1, the top floor displacement does not vary appreciably with ρ, i.e. it is not sensitive to variations in the ratio of stiffness between beams and columns (Figure 8). The base shear $\overline{V}_0$ and base overturning moment $\overline{M}_0$ vary significantly with ρ for T_1 in the medium- and long-period regions of the earthquake response spectrum (Figure 8), with the variation in $\overline{M}_0$ not as great as in $\overline{V}_0$. In the short period region, they do not vary appreciably with ρ (Figure 8) and a significant part of the variation is because the normalizing factors, W_1^* and h_1^*, depend on ρ (Table 4). The variation of responses with ρ is closely related to the significance of the higher mode contributions in response, which as will be shown in Section 5, generally increase with decreasing ρ and also

Table 4: Effective weight and height for fundamental vibration mode.

ρ	$\frac{W_1^*}{\text{Total Weight}}$	$\frac{h_1^*}{\text{Total Height}}$
0	0.6787	0.7936
0.05	0.7642	0.7568
0.125	0.7963	0.7420
0.5	0.8350	0.7238
2	0.8615	0.7113
∞	0.8795	0.7027

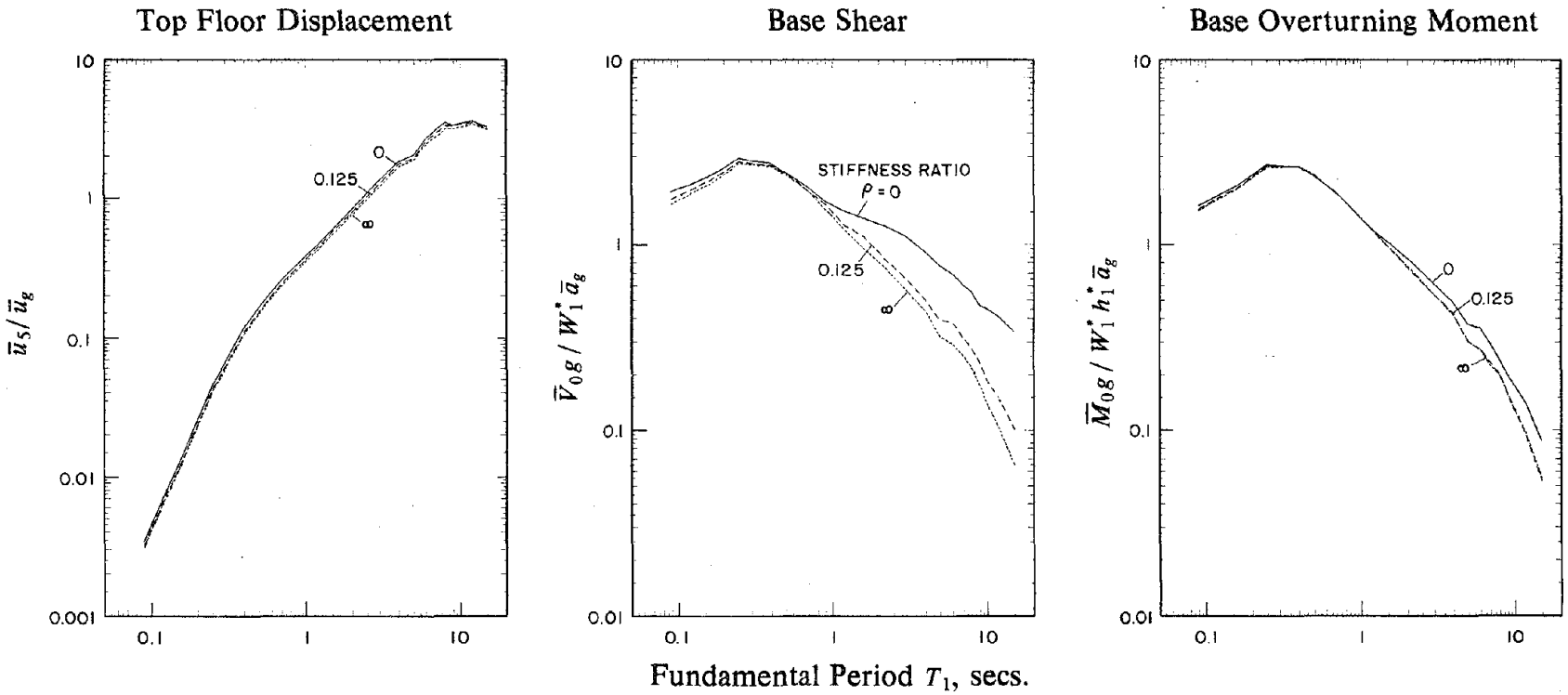

FIGURE 8 Effect of ρ on top floor displacement, base shear, and base overturning moment.

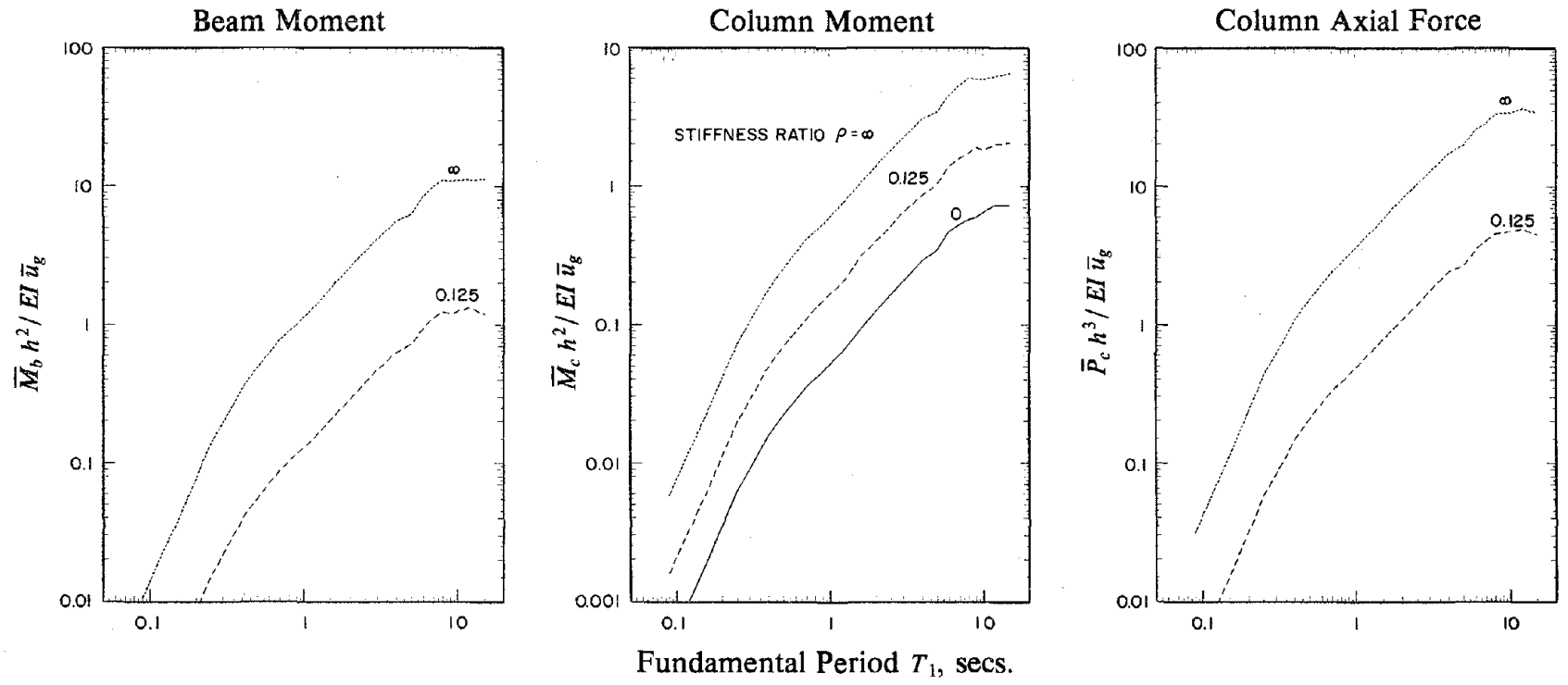

FIGURE 9 Effect of ρ on maximum beam moment, maximum column moment, and maximum column axial force.

depend on T_1 and the response quantity considered.

The general trends in the variation of the three local response quantities --beam moment, column moment, and column axial force-- with ρ are the same (Figure 9). As ρ decreases, $\overline{M}_b$ and $\overline{P}_c$ tend to zero and $\overline{M}_c$ decreases to the values for a cantilever bending beam. Actually what decreases is the normalized value of $\overline{M}_c$, expressed in terms of the flexural stiffness of the column which increases when ρ decreases. For a fixed value of T_1, the column stiffness increases as ρ decreases, and therefore the actual $\overline{M}_c$ may increase even though its normalized value decreases.

In Figure 9, $\overline{M}_b$ is the largest moment over all beams, and $\overline{M}_c$ and $\overline{P}_c$ are the largest moment and axial force over all columns of the building frame. In order to examine the locations of the largest member forces, response spectra for the forces in the beams and columns of each story are presented in Figures 10-12. These results demonstrate that, over a wide range of T_1 values, the maximum forces occur in the first or second story of the frame. The magnitudes of these forces decrease at higher stories with the rate of reduction tending to be greater for the larger values of ρ.

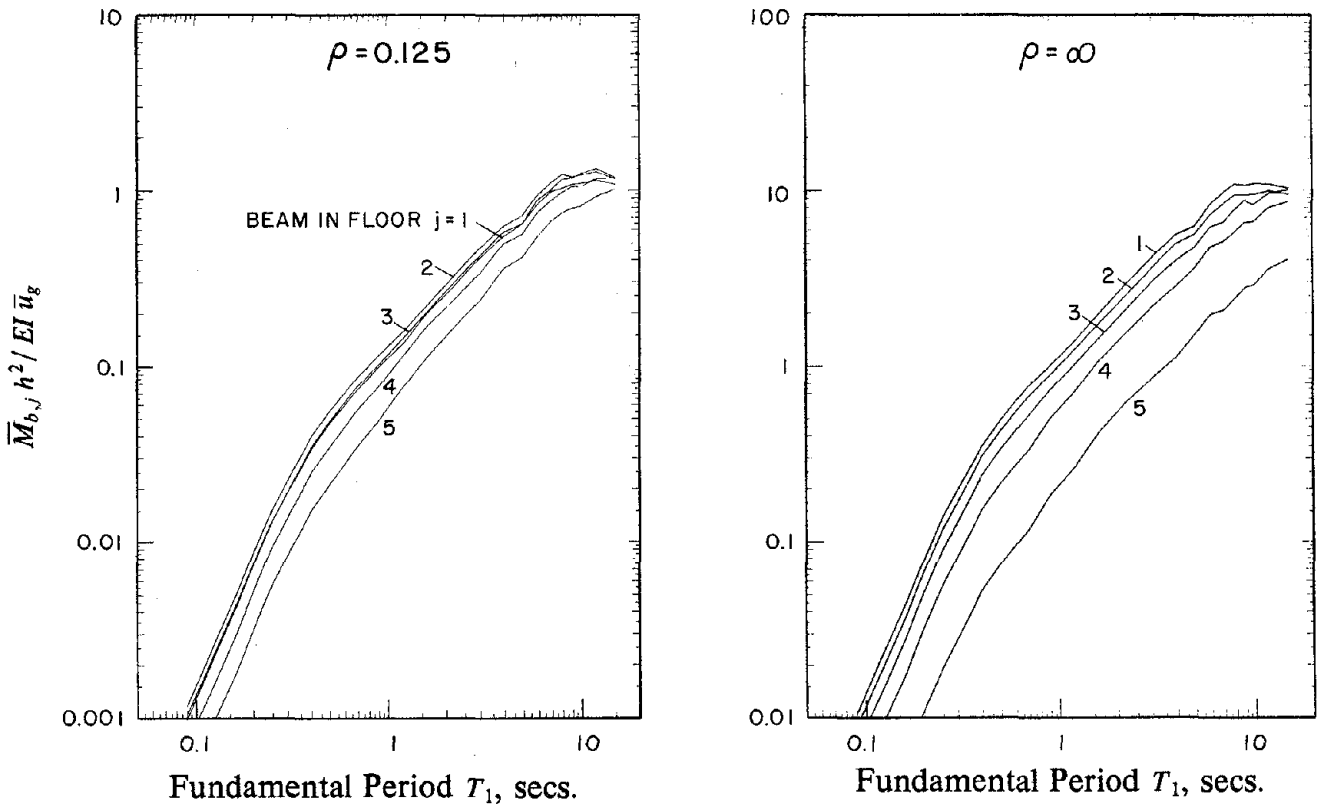

FIGURE 10 Maximum bending moment in individual beams.

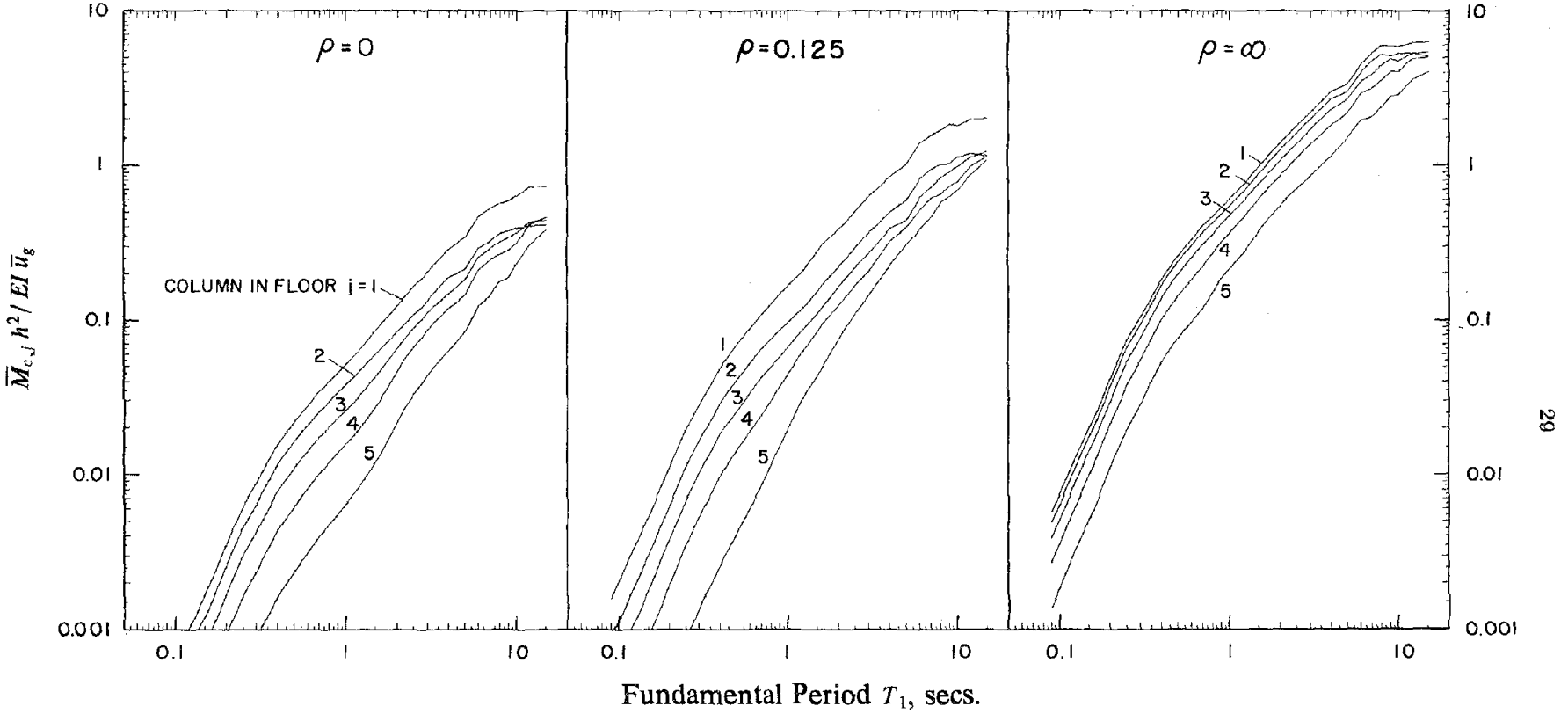

FIGURE 11 Maximum bending moment in individual columns.

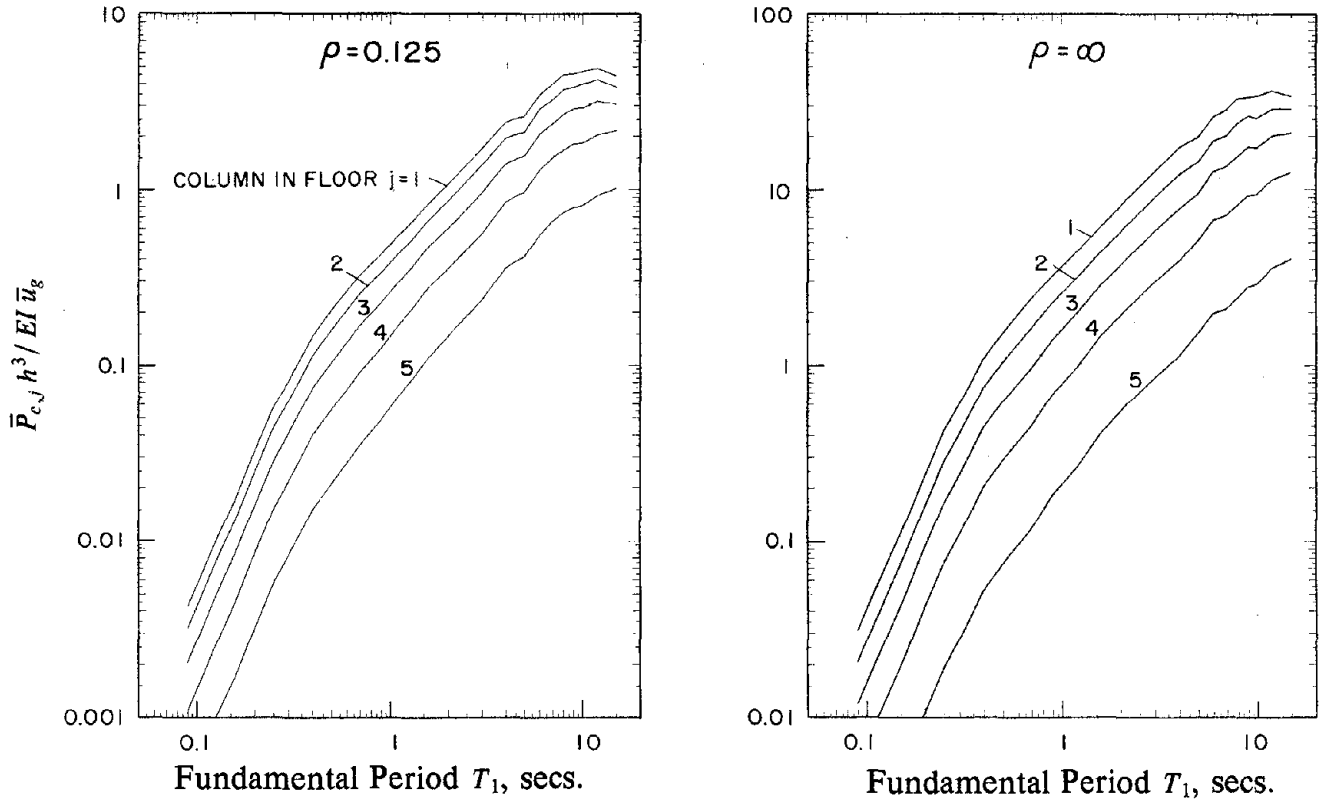

FIGURE 12 Maximum axial force in individual columns.

5. MODAL CONTRIBUTIONS

The ensemble average of the maximum response computed by response history analysis (RHA) is plotted against the fundamental vibration period of the building in the form of a response spectrum. Obtained by considering varying number of vibration modes in RHA, such plots are presented in Figures 13-18 for three values of $\rho = 0$, 0.125, and ∞ and the six normalized response quantities defined in Section 3.

For the subsequent interpretation of the response results it is useful to introduce the concept of unit modal responses. It is the response of the structure in an individual mode of vibration with unit value for the pseudo-acceleration. The unit response in the nth vibration mode is given by equations (9) and (11) with $S_{an} = 1$ for the floor displacements, base shear and base moment. Obviously, the maximum value of any response quantity due to an individual vibration mode is the product of the unit response in that mode and the ordinate S_{an} of the pseudo-acceleration response spectrum corresponding to that mode. In discussing the contributions of various vibration modes to the response, it is useful to normalize the unit response in the nth mode as a fraction of the corresponding value for the first mode. Such normalized unit modal responses for the top floor displacement u_5, base shear V_0, and base moment M_0, presented in Table 5, vary with ρ but not with vibration period or ground motion. The period dependence of the relative modal contributions to a response quantity is all represented by the spectral ordinates for the various modes.

The response contributions of the vibration modes higher than the fundamental mode increase with increasing fundamental vibration period T_1 in the medium- and long-period regions of the earthquake response spectrum. For a fixed ρ, the mode shapes, the normalized unit modal responses, and the ratios of vibration frequencies do not change with T_1. Thus, the increased contribution of the higher modes is due only to the relative values of the response spectrum ordinates, which in turn depend on the spacing of vibration periods and on the shape of the response spectrum. For the selected spectrum, as the fundamental vibration

Table 5: Normalized unit modal responses.

TOP DISPLACEMENT, u_5						
Mode	$\rho = 0$	$\rho = 0.05$	$\rho = 0.125$	$\rho = 0.5$	$\rho = 2$	$\rho = \infty$
1	1.0	1.0	1.0	1.0	1.0	1.0
2	-0.0598	-0.0959	-0.0997	-0.1009	-0.1004	-0.0991
3	0.0082	0.0189	0.0235	0.0278	0.0284	0.0275
4	-0.0017	-0.0043	-0.0060	-0.0084	-0.0090	-0.0085
5	0.0003	0.0008	0.0011	0.0017	0.0019	0.0018
BASE SHEAR, V_0						
Mode	$\rho = 0$	$\rho = 0.05$	$\rho = 0.125$	$\rho = 0.5$	$\rho = 2$	$\rho = \infty$
1	1.0	1.0	1.0	1.0	1.0	1.0
2	0.3040	0.1789	0.1475	0.1223	0.1089	0.0991
3	0.1033	0.0775	0.0647	0.0475	0.0355	0.0275
4	0.0485	0.0385	0.0325	0.0215	0.0132	0.0085
5	0.0176	0.0137	0.0111	0.0063	0.0032	0.0018
BASE OVERTURNING MOMENT, M_0						
Mode	$\rho = 0$	$\rho = 0.05$	$\rho = 0.125$	$\rho = 0.5$	$\rho = 2$	$\rho = \infty$
1	1.0	1.0	1.0	1.0	1.0	1.0
2	0.0873	0.0156	-0.0030	-0.0195	-0.0284	-0.0340
3	0.0182	0.0158	0.0143	0.0111	0.0081	0.0060
4	0.0064	0.0043	0.0028	0.0002	-0.0011	-0.0014
5	0.0020	0.0017	0.0014	0.0009	0.0005	0.0003

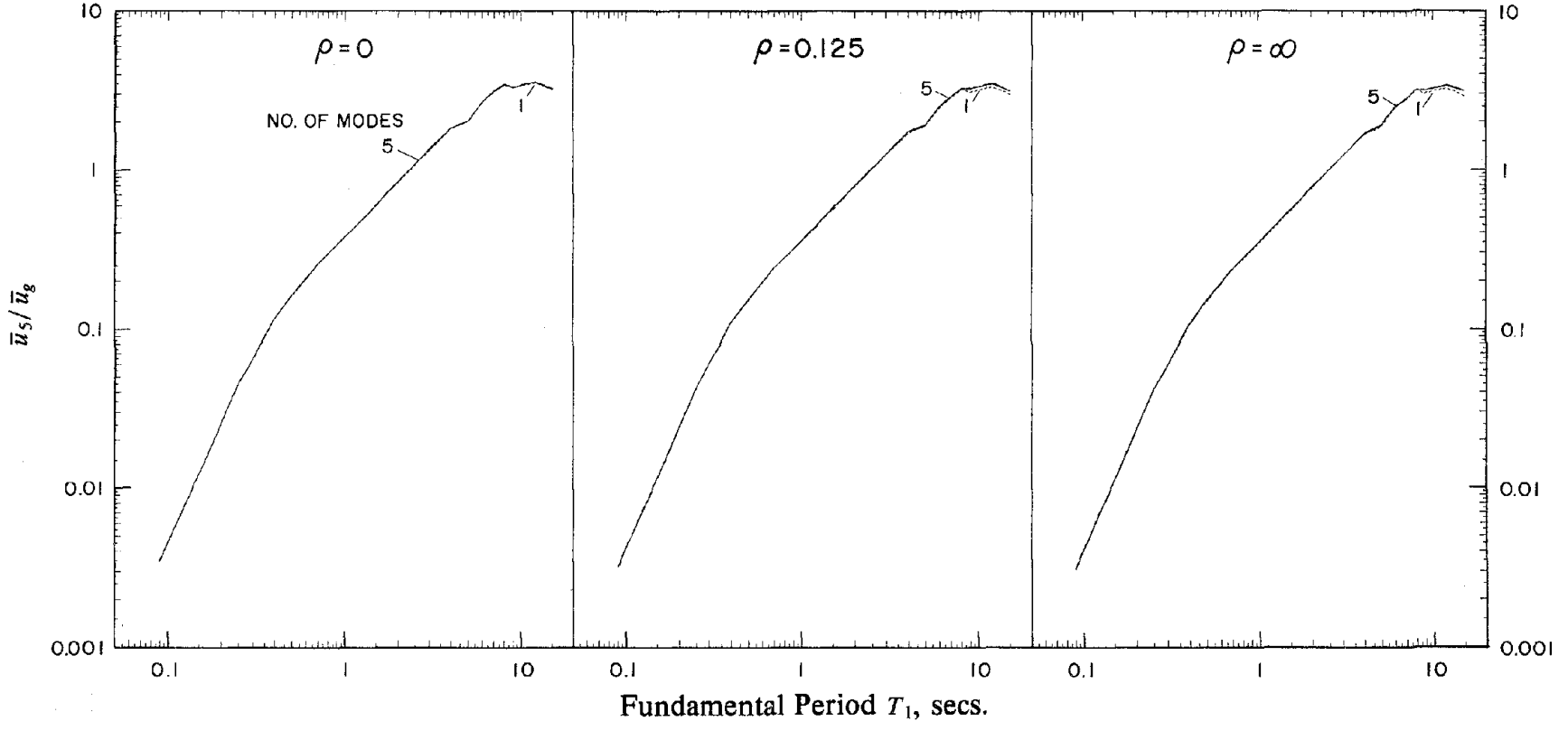

FIGURE 13 Modal contributions to maximum top floor displacement.

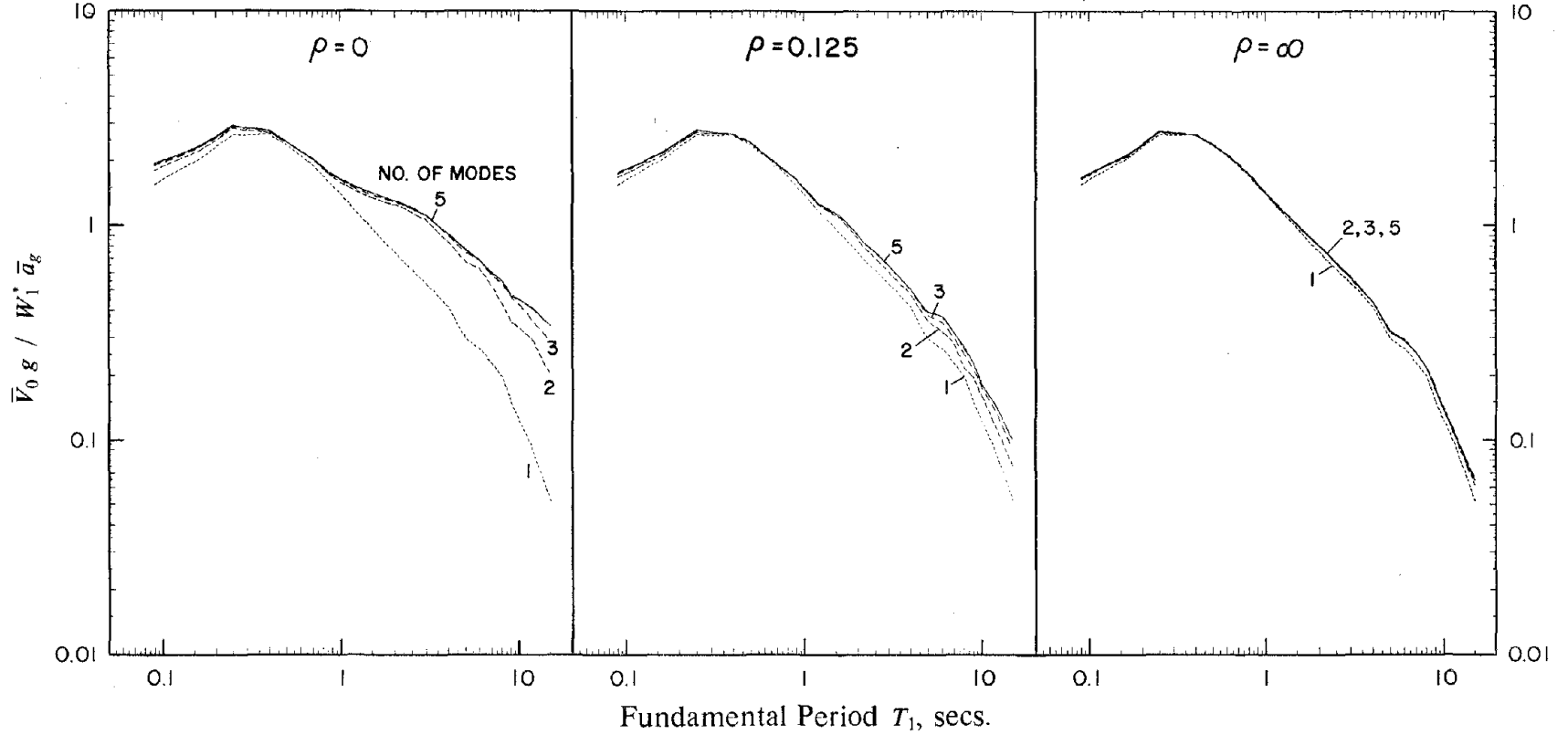

FIGURE 14 Modal contributions to maximum base shear.

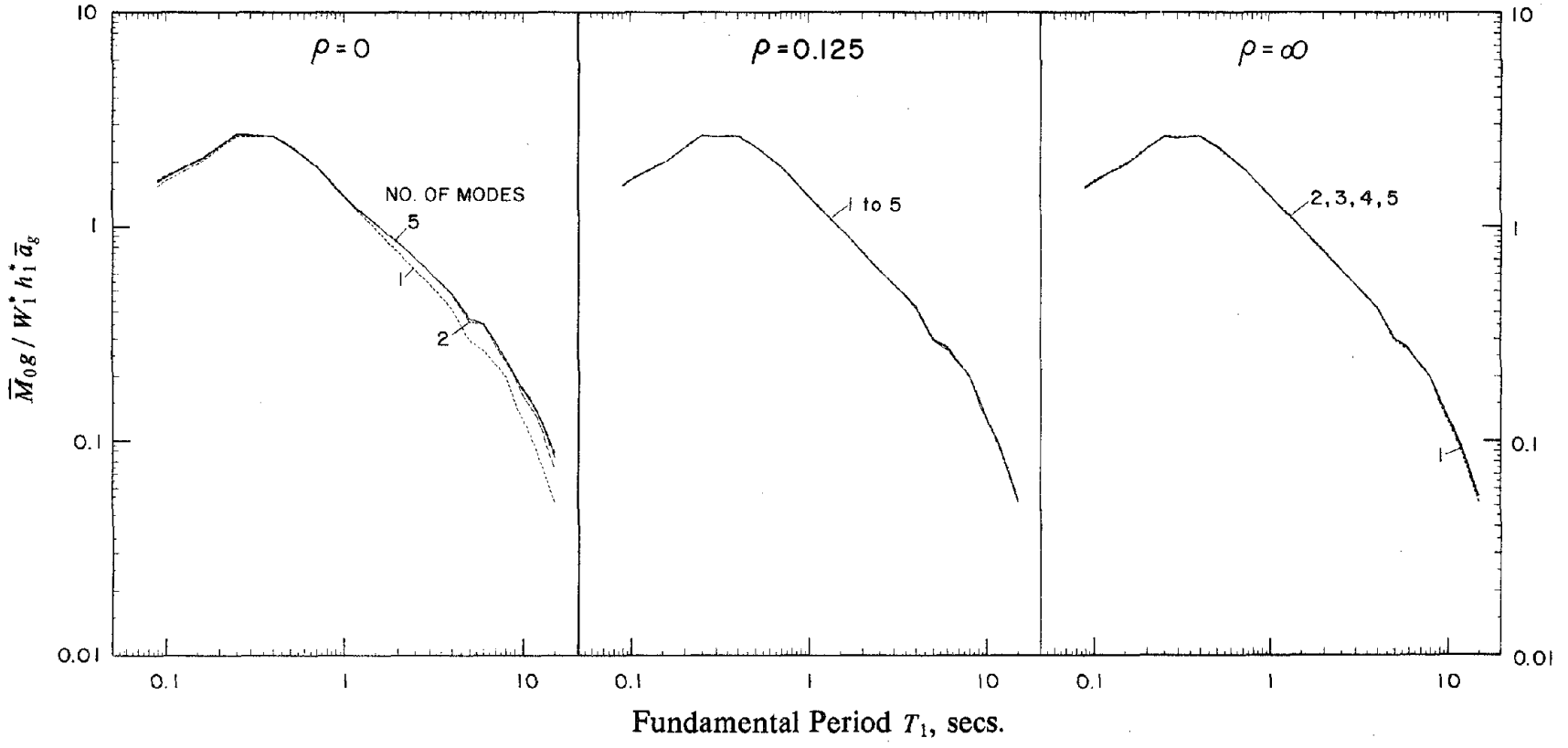

FIGURE 15 Modal contributions to maximum base overturning moment.

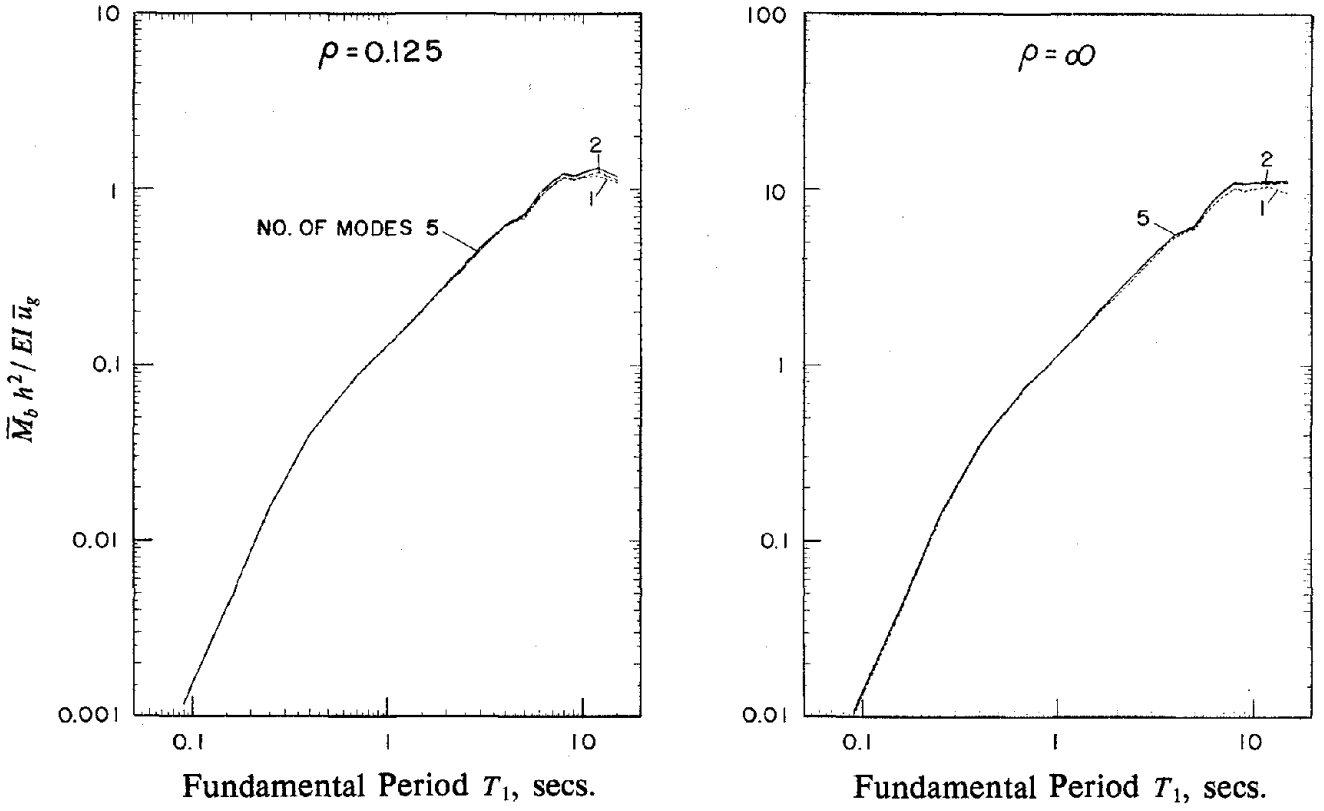

FIGURE 16 Modal contributions to maximum beam bending moment.

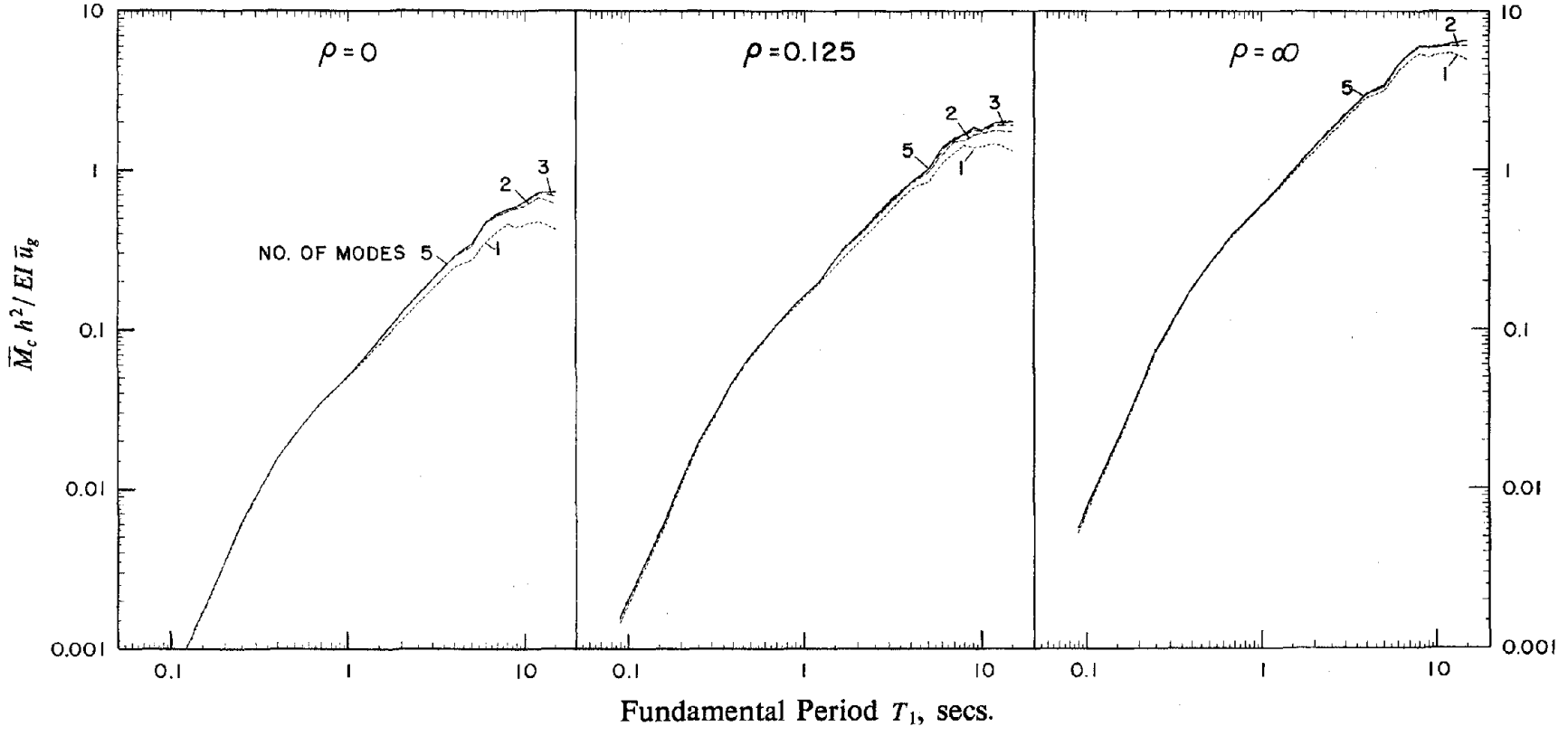

FIGURE 17 Modal contributions to maximum column bending moment.

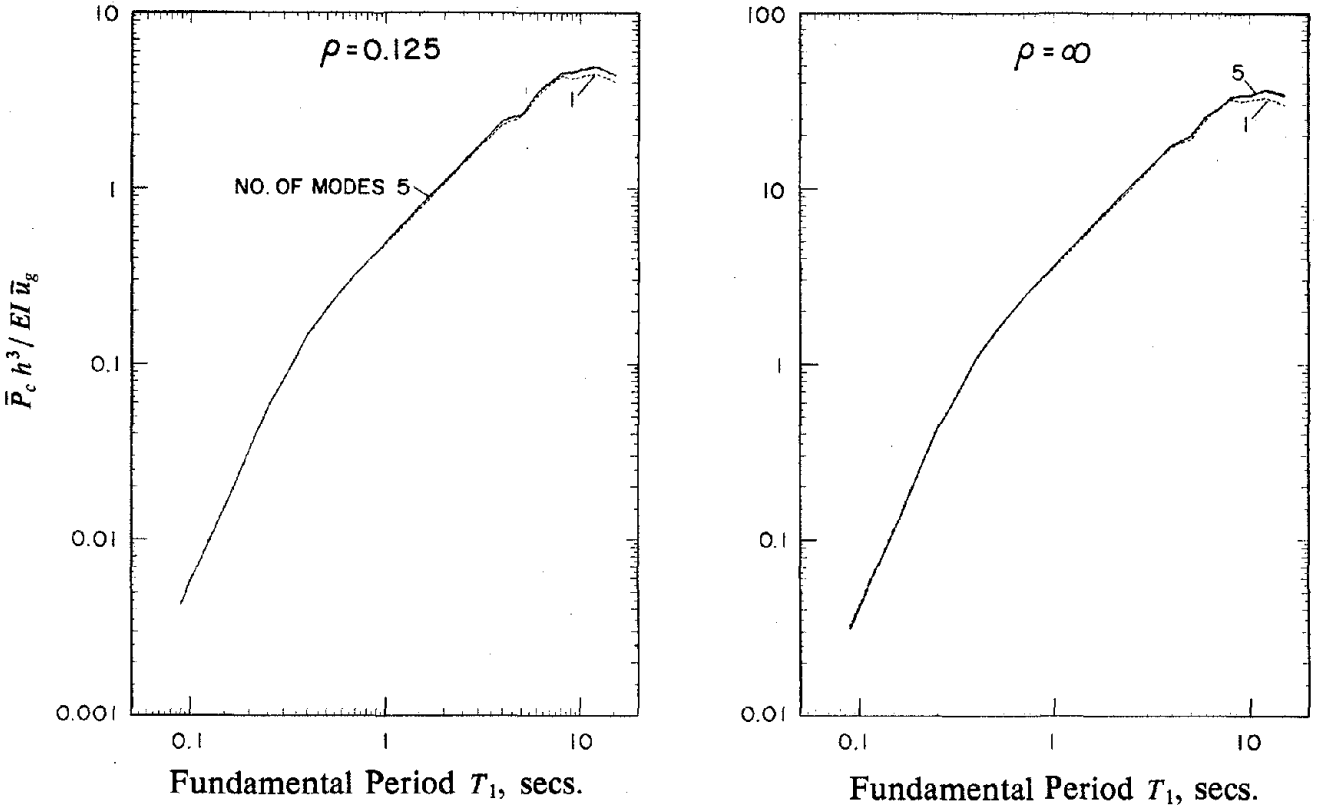

FIGURE 18 Modal contributions to maximum column axial force.

period increases within the above-mentioned spectral regions, the ratio of the pseudo-acceleration spectrum ordinate for a higher vibration mode to that of the fundamental mode generally increases (Figure 19), resulting in increased response contributions of the higher modes.

The increase in response contributions of the higher modes varies with the response quantity. As suggested by the normalized unit modal responses (Table 5), for a fixed value of ρ, Figures 13-15 demonstrate that among the overall response quantities the higher mode contributions are much more significant for the base shear $\overline{V}_0$ than for the top floor displacement $\overline{u}_5$ or base overturning moment $\overline{M}_0$. Similarly Figures 16-18 indicate that, among the local response quantities, the higher mode contributions are more significant for the column moment $\overline{M}_c$ than for the beam moment $\overline{M}_b$ and column axial force $\overline{P}_c$. Column moments are closely related to the story shears which are affected more by higher mode contributions, whereas beam moments and column axial forces are closely related to story overturning moments which are affected less by higher modes.

In addition to the already discussed trends in the results, the base shear and to a lesser degree the base overturning moment, display increasing contributions of higher modes as T_1 decreases in the short-period spectral region (Figures 14 and 15). While this trend can be explained in part by the relative values of the spectral ordinates for the various vibration modes, the more important reason is that the individual modal responses of very short-period structures are essentially all in phase or some are of opposite phase. This is displayed in Figure 20 where the contributions of individual modes to the base shear, normalized to the maximum contribution of the first mode, are presented as a function of time; and the time instants at which modal maxima occur are noted. As a result, almost the full maximum response in a higher mode is directly added to the fundamental mode response, instead of some value less than the maximum if the modal responses were not in phase.

Obviously the higher vibration modes also affect the shear and moments in all stories in addition to the base shear and moment. These effects are summarized in Figures 21 and 22

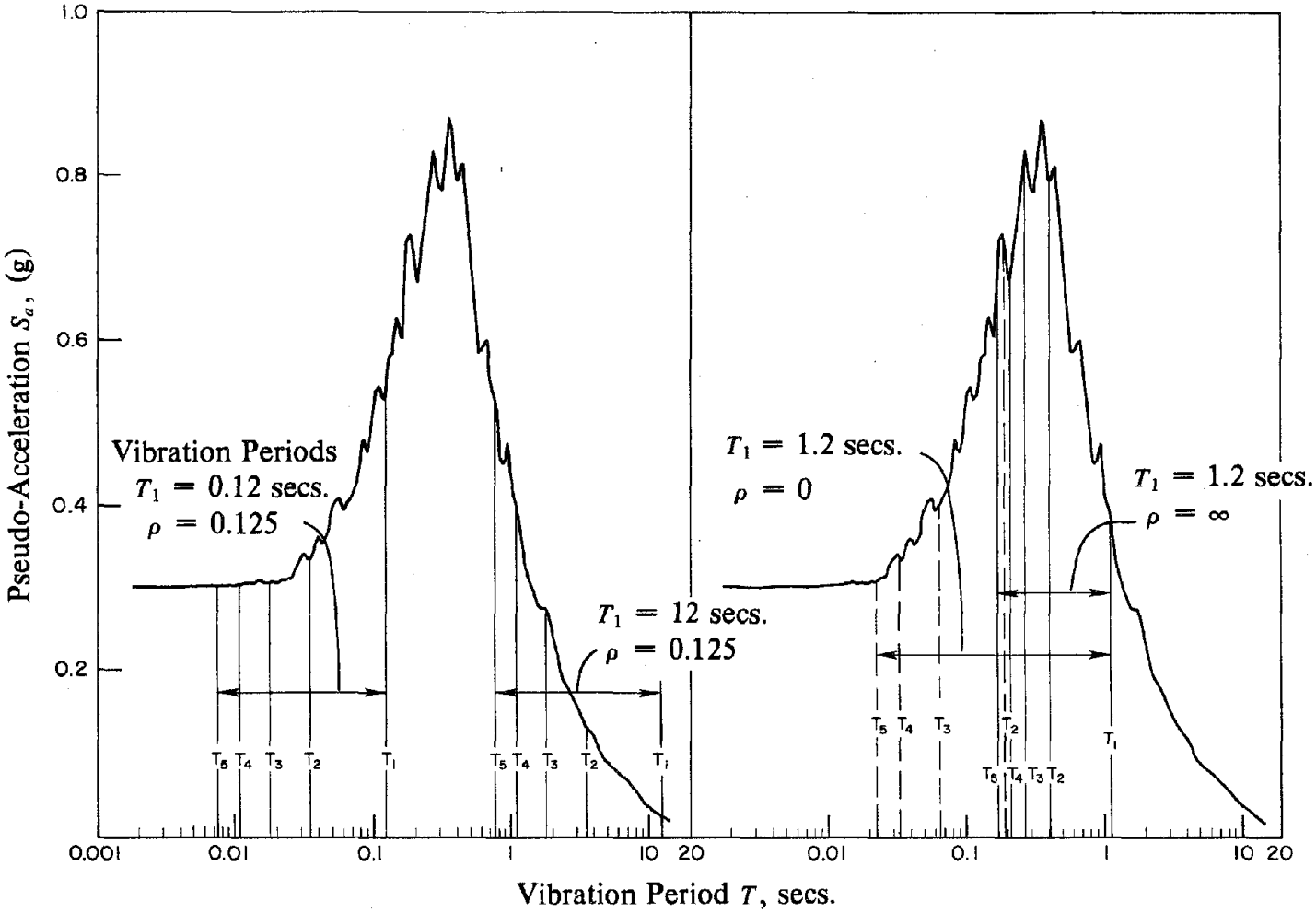

FIGURE 19 Influence of spectrum shape on higher mode contributions to building response.

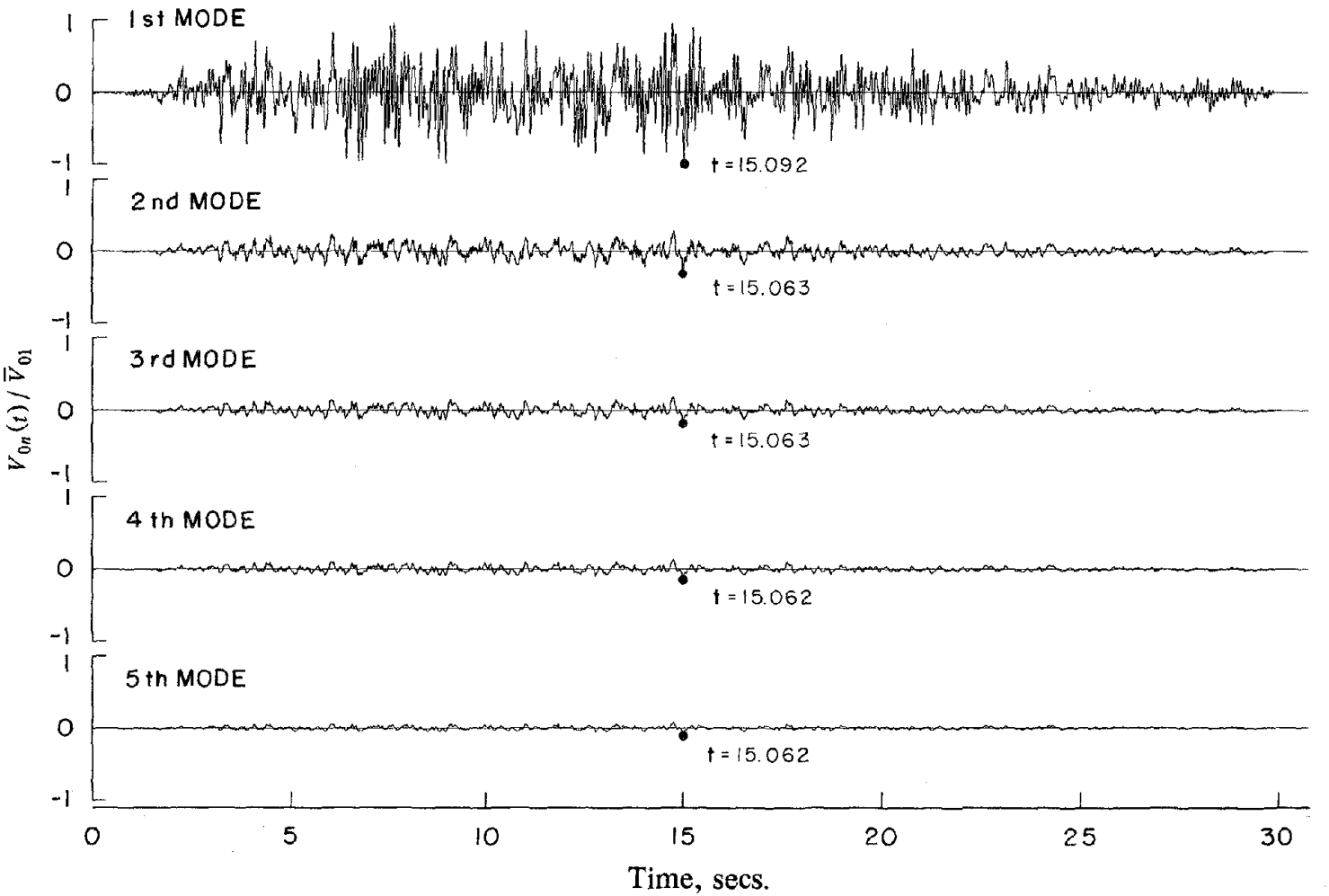

FIGURE 20 Time-variation of modal contributions to base shear response of building with T_1 = 0.09 sec. and ρ = 0.125 to ground motion No. 6.

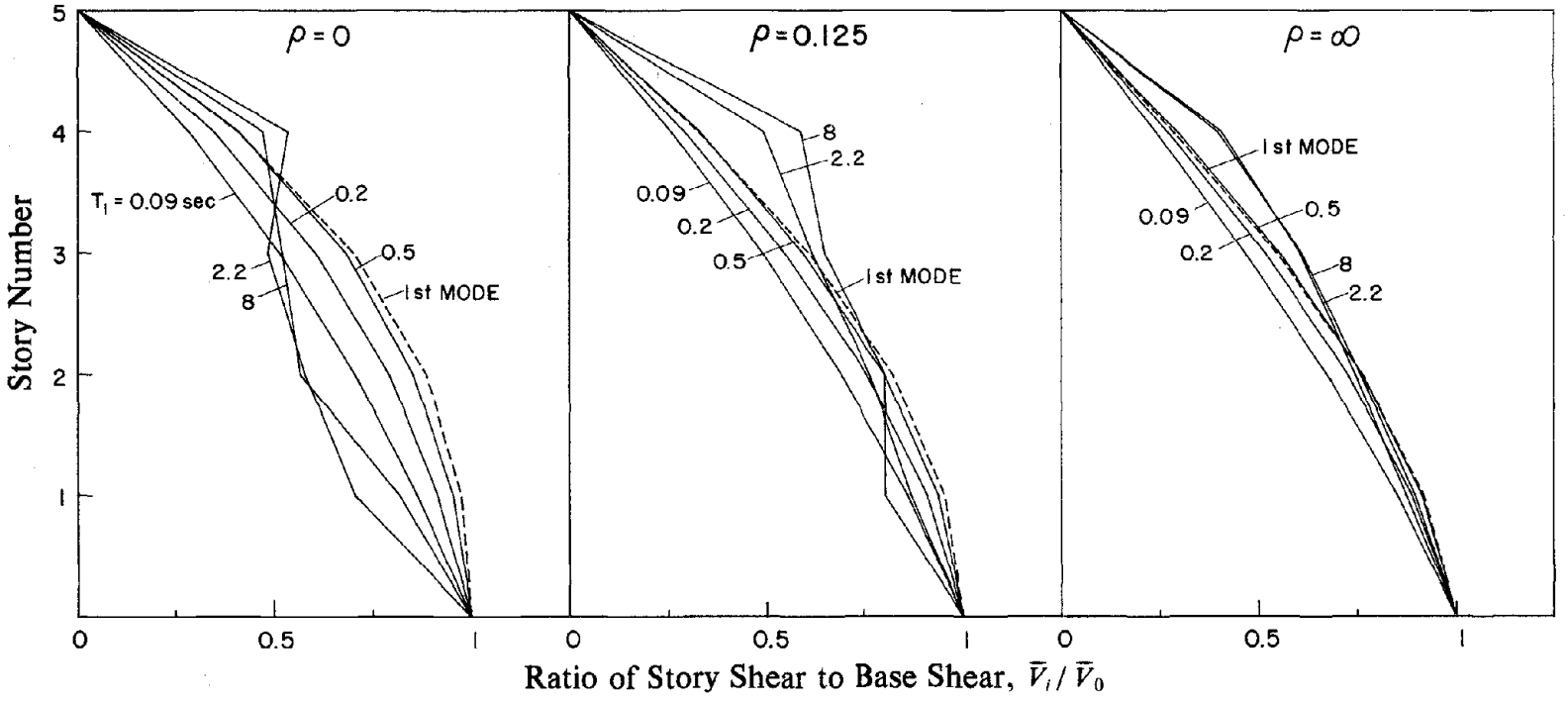

FIGURE 21 Height-wise variation of story shears.

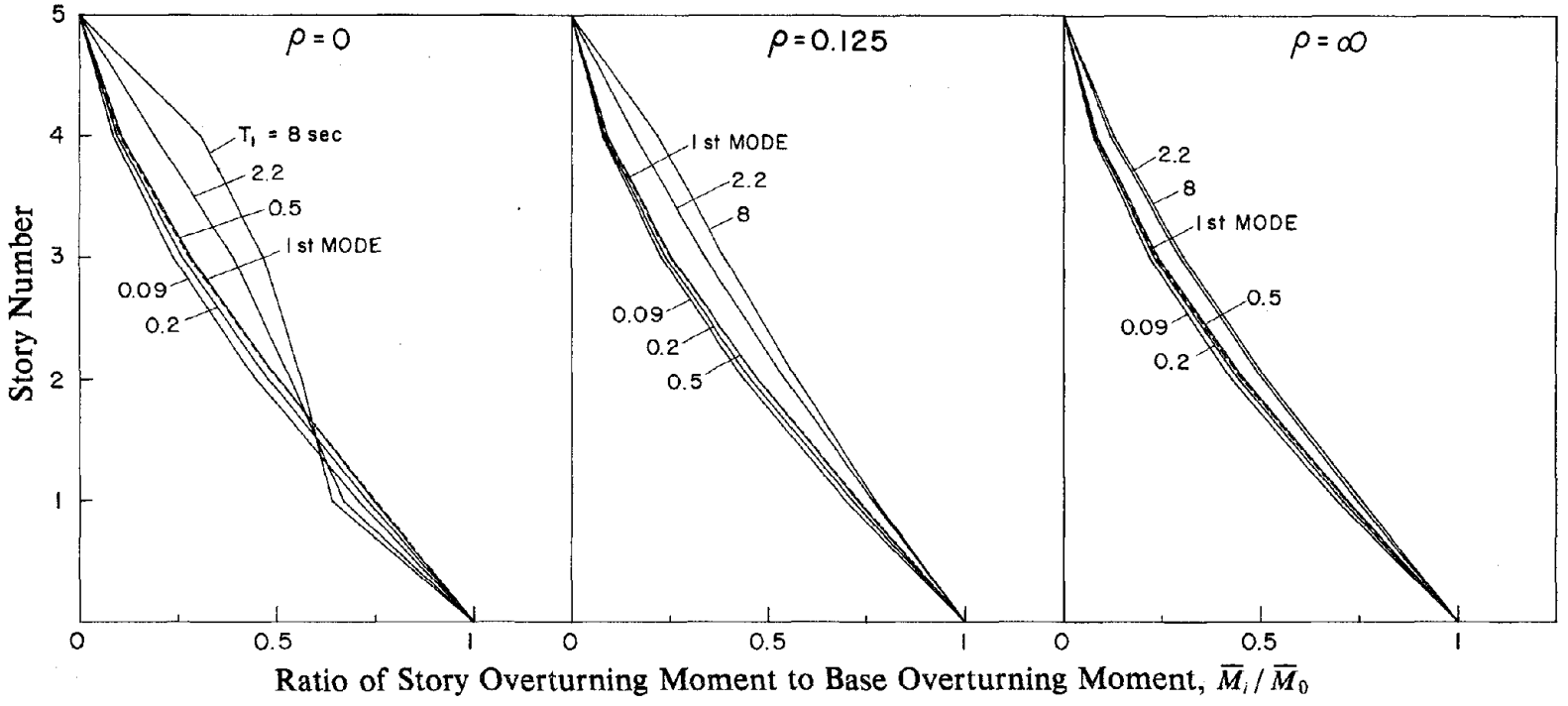

FIGURE 22 Height-wise variation of story overturning moments.

wherein the height-wise variation of story shears and moments, expressed as a ratio of the respective values at the base, are presented for buildings with selected values of T_1. The distribution of only the fundamental mode response, which is the same regardless of T_1, is also included. In a lumped mass system, such as the frame considered here, the shear remains constant in each story with discontinuities at each floor. However, such a plot would not be convenient in displaying the differences among various cases and the alternative presentation with shears varying linearly over story height is used. It is apparent that the higher mode contributions not only influence the magnitude of the story shears and moments but also their distribution because the various vibration modes affect different portions of the building to varying degree. The distribution but not necessarily the actual values of forces in the upper stories is especially affected by the higher mode contributions.

We next examine how the higher mode contributions to earthquake response of the building frame are affected by the stiffness ratio ρ which varies from infinity for a shear beam (with rotation of joints fully restrained) to zero for a bending beam (with no restraint to joint rotation provided by the beams), with intermediate values of ρ representing frames with both beams and columns undergoing flexural deformations. As ρ decreases, the normalized unit modal responses, associated with the higher vibration modes, for the base shear (and base moment) increase, especially for the second mode (Table 5). At the same time the ratios of the modal vibration frequencies increase, spreading the frequencies over a wider portion of the spectrum, thus increasing the effects of the spectrum shape, with these increases depending on the location of T_1 (Figure 19). For the selected spectrum and within the period range considered, the effects of the spectrum shape are especially significant if T_1 is large, with the effects decreasing as T_1 decreases within the moderately long-period region of the spectrum, which explains the trends observed in Figure 14.

The effect of ρ on the contributions of the higher modes varies with the response quantity. As suggested by the normalized unit modal responses (Table 5), Figures 13-15 demonstrate that ρ affects the higher mode contributions in the base shear more than in the top floor

displacement or base overturning moment. The top floor displacement displays trends opposite to base shear and base moment, in the sense that the higher mode contributions decrease with decreasing ρ, but this reverse trend is supported by the normalized unit modal responses (Table 5). However, these contributions are so small that they are of little consequence. The stiffness ratio ρ affects the higher mode contributions in the column moments in the same manner as base shear but to a lesser degree (Figure 17). Finally, the higher mode contributions in the beam moment and column axial force, which are closely related to the story overturning moments, are smaller and affected little by ρ (Figures 16 and 18).

6. ACCURACY OF RESPONSE SPECTRUM ANALYSIS

The ensemble average of the maximum response computed by response history analysis (RHA) and the response computed from the average response spectrum using response spectrum analysis (RSA) procedures, is plotted against the fundamental vibration period of the building in the form of response spectra. The contribution of all five vibration modes were included in these analyses. Also presented in these plots is the maximum response due only to the fundamental vibration mode, which is obviously identical whether computed by RHA or RSA procedures. Response spectra for the six normalized response quantities described in Section 4 are presented in Figures 23-28 for three values of $\rho = 0$, 0.125, and ∞.

The errors in the responses computed by the RSA method, as reflected by the differences in the RHA and RSA results, are closely related to the significance of the response contributions of the vibration modes higher than the fundamental mode. Thus, based on the analysis of results presented in Section 5, the errors in the RSA results generally increase with increasing fundamental vibration period T_1 in the medium- and long-period regions of the spectrum, and with decreasing value of the stiffness ratio ρ. Similarly, these errors increase as T_1 decreases in the short period range of the spectrum but these errors are noticeable primarily in the base shear (Figure 24) and to a lesser degree in the base overturning moment (Figure 25). As mentioned in the preceding section, the individual modal base shear responses of a very short-period structure are essentially in phase, resulting in the combined response being close to the sum of the absolute values of modal responses and larger than the SRSS estimate which is close to the first-mode response.

The errors in the RSA results vary with the response quantity in the same manner as do the significance of the higher mode contributions. Thus, based on the analysis of results presented in Section 5, among the overall response quantities the largest errors occur in the base shear values, with much smaller errors in the base overturning moment, and almost no errors in the top floor displacement. Similarly, among the local response quantities the largest

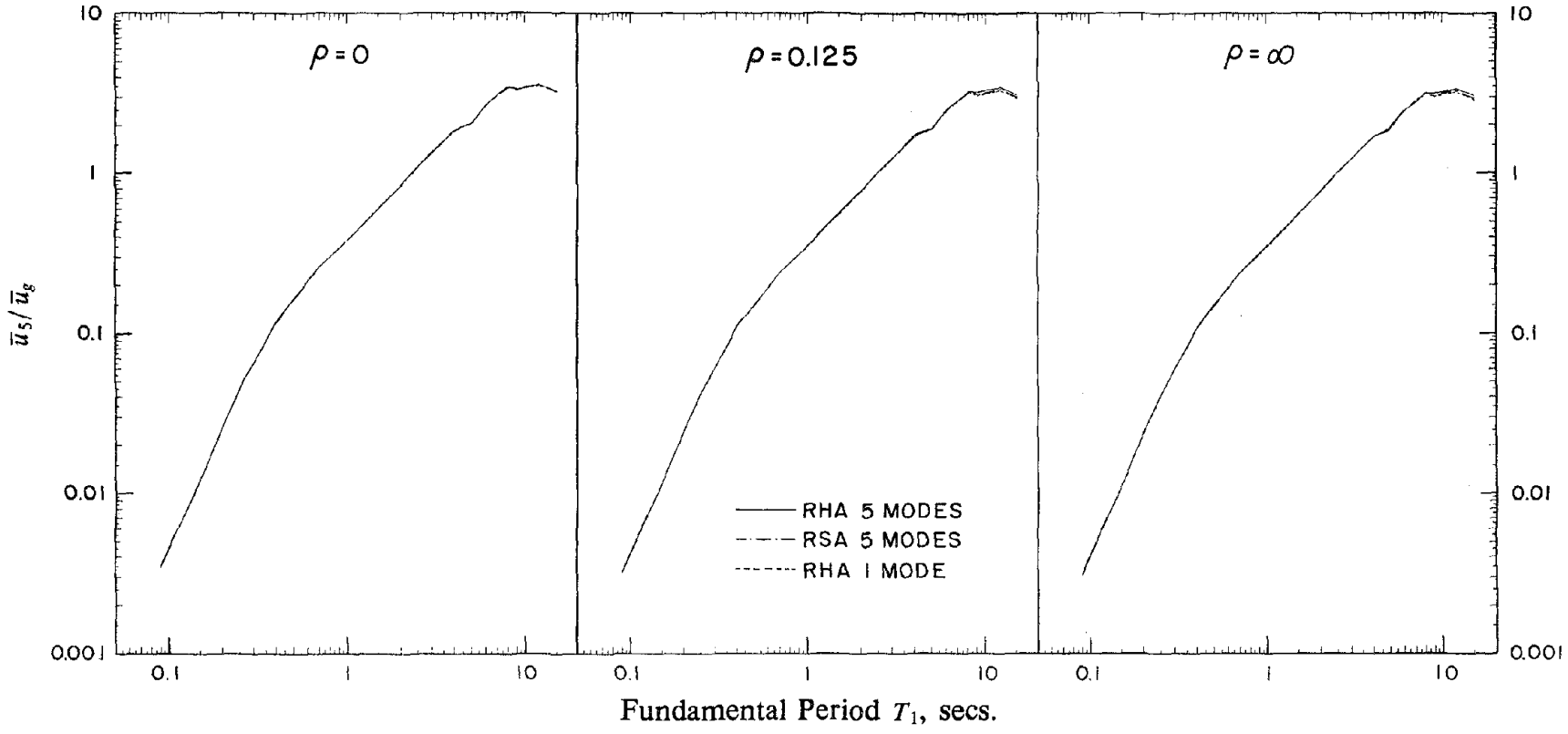

FIGURE 23 Comparison of maximum top floor displacement computed by response history analysis (RHA) and response spectrum analysis (RSA).

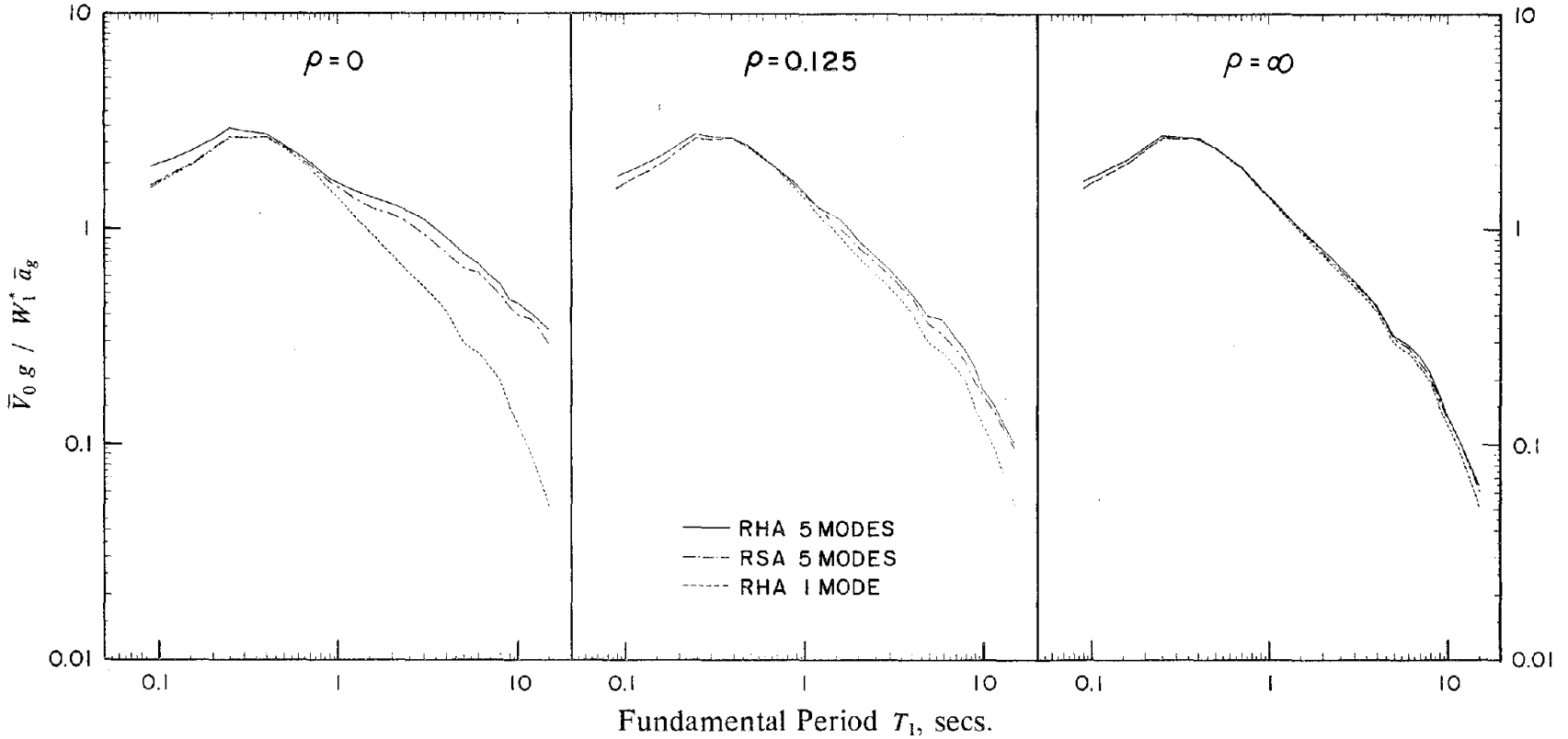

FIGURE 24 Comparison of maximum base shear computed by RHA and RSA.

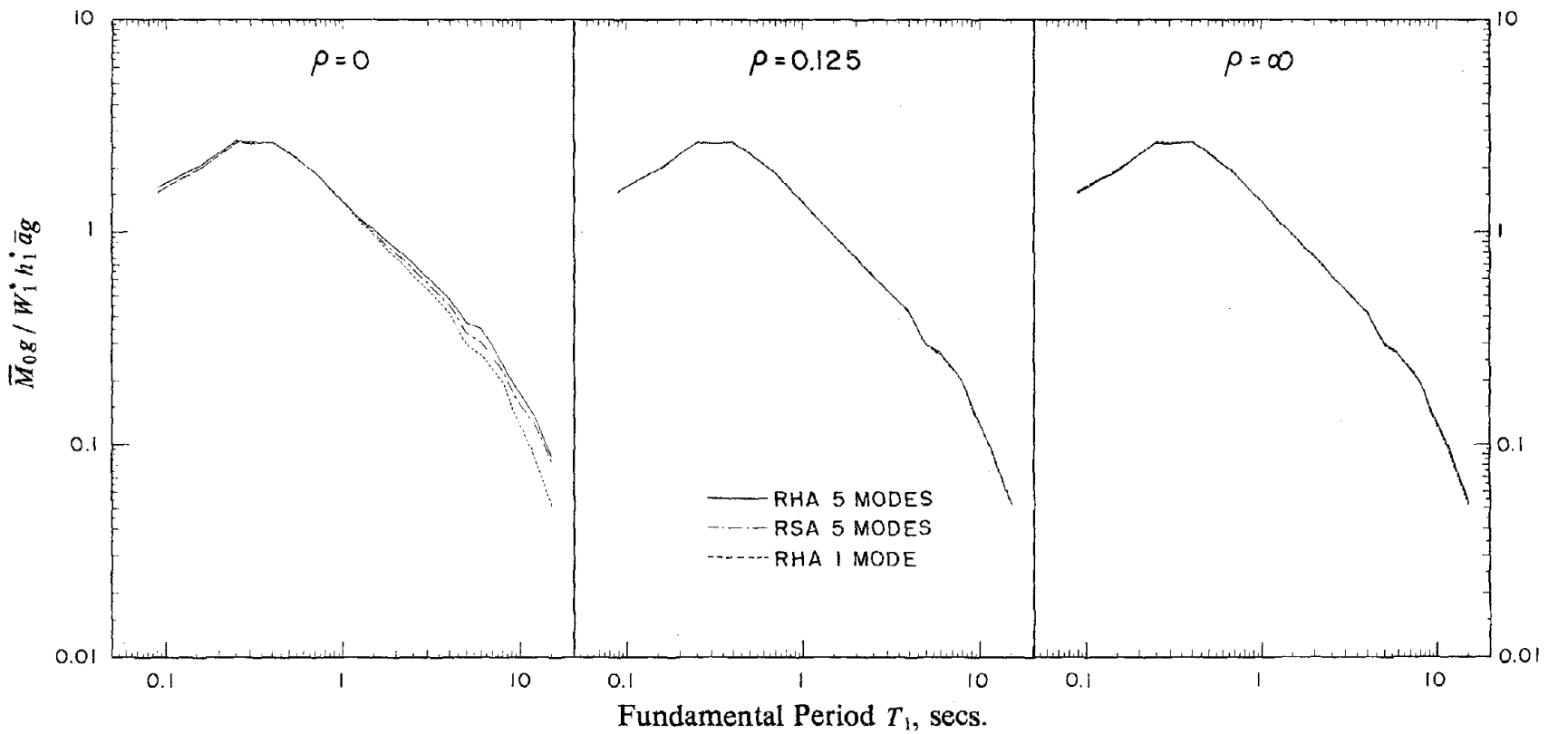

FIGURE 25 Comparison of maximum base overturning moment computed by RHA and RSA.

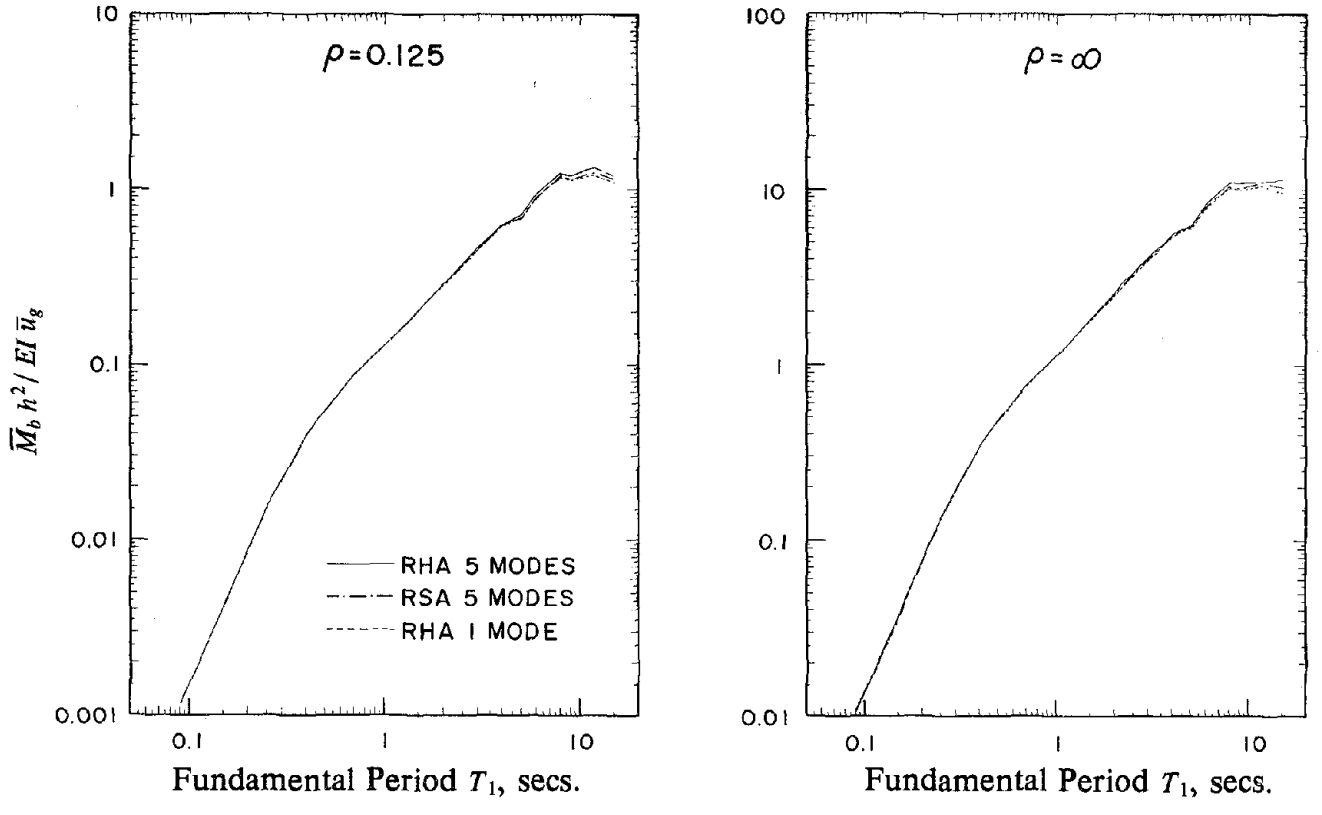

FIGURE 26 Comparison of maximum beam bending moment computed by RHA and RSA.

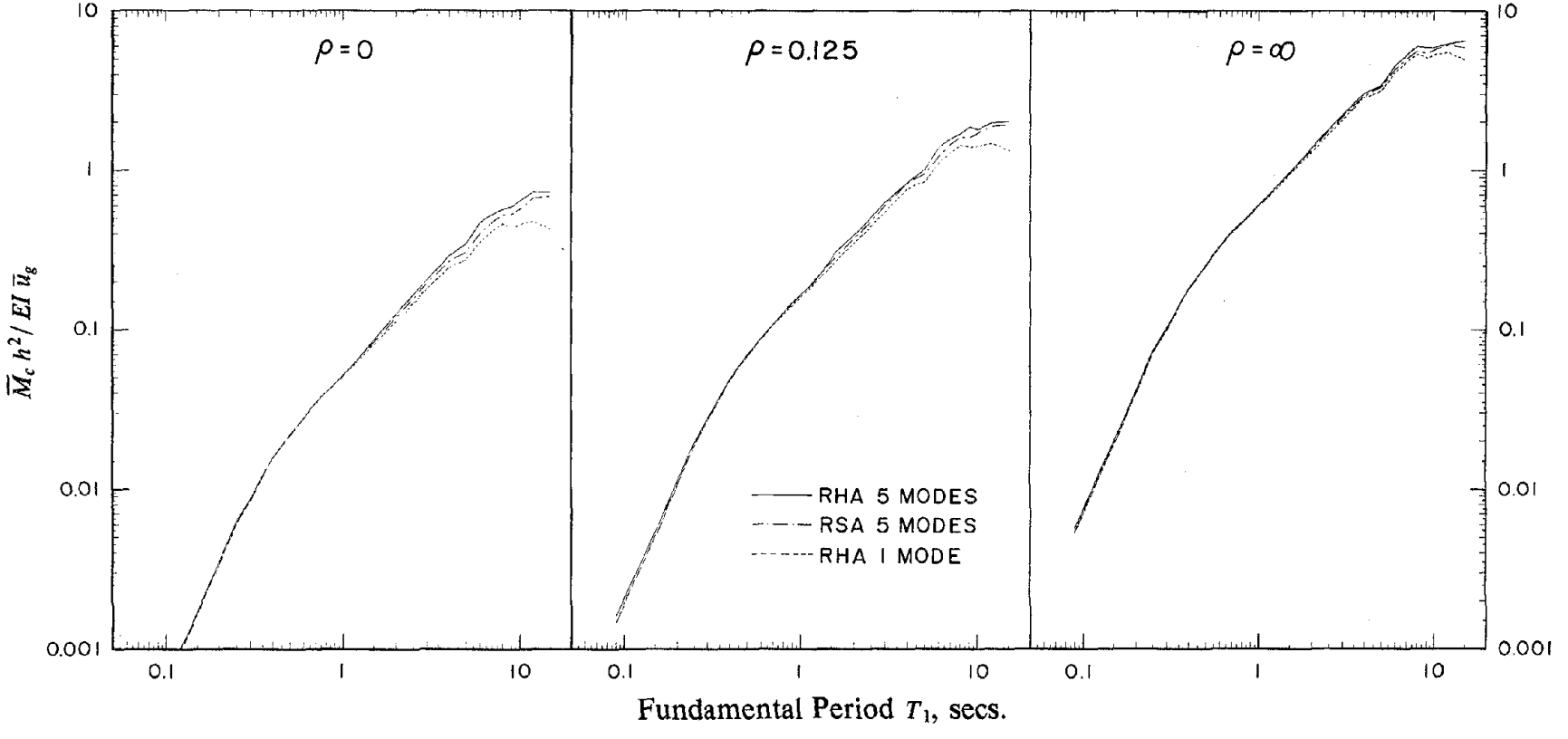

FIGURE 27 Comparison of maximum column bending moment computed by RHA and RSA.

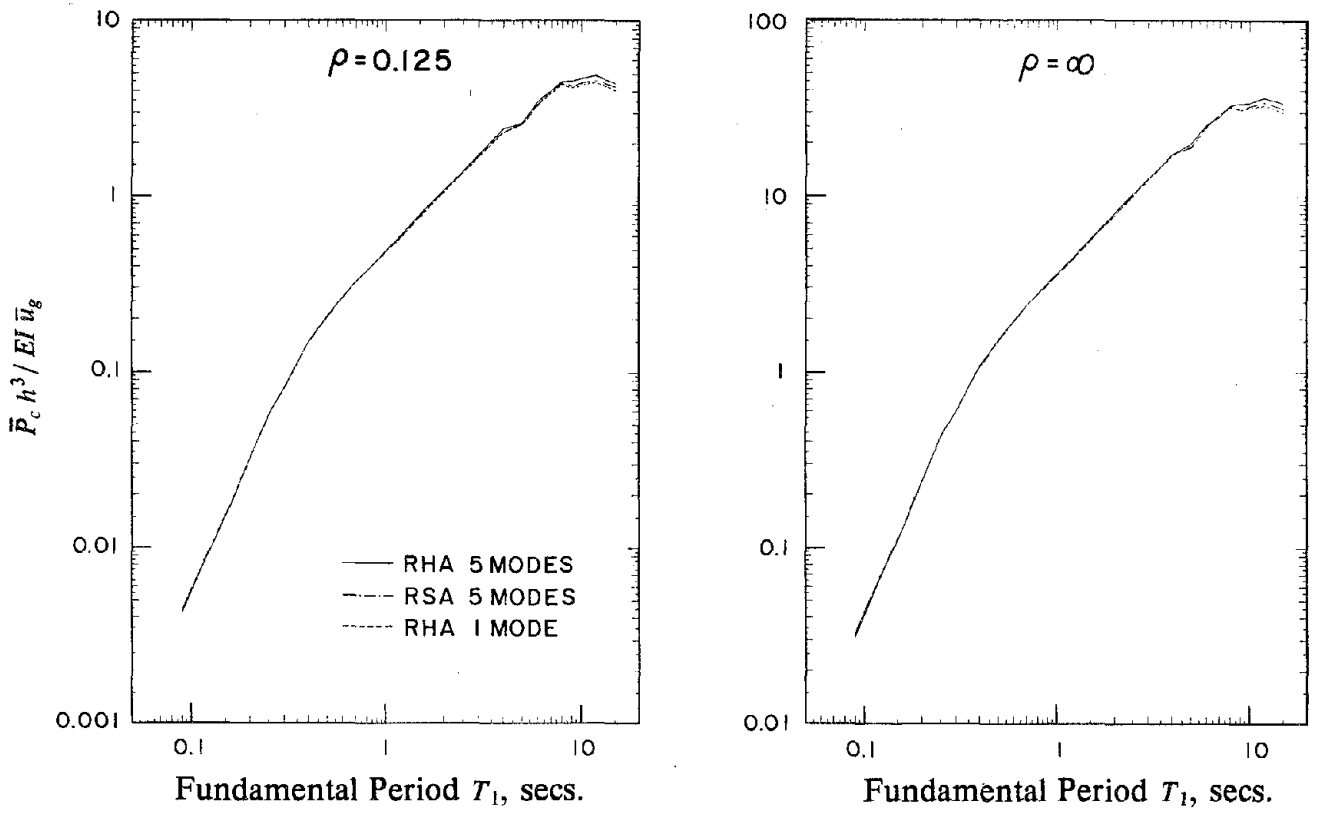

FIGURE 28 Comparison of maximum column axial force computed by RHA and RSA.

errors occur in the column moments, while the errors in the beam moments and column axial forces are smaller and very similar, but these errors are all smaller than in base shear. These errors are summarized in Figures 29 and 30 where they are presented as a function of T_1 for the overall and local response quantities respectively. The errors in the RSA results are expressed as the RSA value minus the RHA value, and presented as a percentage of the RHA value. While the errors in the RSA results depend on the response quantity they are all below 15 percent for structures with fundamental vibration period less than the end of the medium period region, which for the average spectrum of Figure 6 is 8 seconds. Furthermore, the computed responses display some discrepancy between the RHA and the RSA results for very short periods, with the errors tending to increase as T_1 decreases in this range --to around 5 to 20 percent depending on the value of the stiffness ratio ρ.

The story shears and overturning moments have a central role in the design procedures for buildings. The ensemble average of these quantities, computed by the RHA procedure is compared in Figures 31 and 32 with the responses computed for the average response spectrum by the RSA procedure. The percentage errors in the RSA results, although not large for T_1 in the short period region of the spectrum, vary considerably from story to story, especially in the story shears (Table 6). As a result, the distribution of story shears and moments over the height (Figures 33 and 34) estimated by RSA, which is close to the first mode distribution, is different than that from the RHA results, which are close to the summation of the individual modal maxima occurring at almost the same time instant (Figure 20). As T_1 increases in the short-period region, the correlation between the modal responses decreases, the maximum response is essentially due to the fundamental vibration mode, and the distribution of the RHA and RSA forces are almost identical, (Figures 33 and 34) leading to reduced errors (Table 6). As T_1 increases in the medium-period region, the response contributions of the higher modes become increasingly significant and the errors in the story shears and moments computed by RSA increase with a tendency for the larger errors to occur in the upper stories (Table 3).

Table 6: Errors in the RSA results for story shears and overturning moments expressed as percentage of the RHA results.

STORY SHEARS						
ρ	Story	$T_1 = 0.09$	$T_1 = 0.2$	$T_1 = 0.5$	$T_1 = 2.2$	$T_1 = 8$
0	1	-18.72	-9.97	-2.07	-11.03	-11.61
	2	-8.96	-4.49	-0.68	-7.76	-14.48
	3	0.16	-0.30	-0.04	-7.75	-11.54
	4	8.90	3.32	-0.85	-12.23	-15.28
	5	18.44	6.78	-1.36	-9.74	-14.09
0.125	1	-11.91	-6.14	-2.20	-6.96	-11.62
	2	-2.80	-1.86	-1.09	-4.98	-7.36
	3	4.44	1.65	-0.42	-7.09	-17.68
	4	9.66	4.70	0.65	-5.33	-13.02
	5	14.32	6.84	0.52	-15.05	-21.97
∞	1	-6.74	-3.08	-0.43	-3.63	-5.50
	2	0.34	-0.04	-0.44	-3.98	-4.27
	3	5.79	1.79	-0.53	-3.48	-3.44
	4	10.00	2.86	-0.46	-6.11	-4.95
	5	13.11	4.05	0.06	-10.58	-7.08
STORY MOMENTS						
ρ	Story	$T_1 = 0.09$	$T_1 = 0.2$	$T_1 = 0.5$	$T_1 = 2.2$	$T_1 = 8$
0	1	-5.47	-2.85	-0.41	-5.98	-7.57
	2	0.22	-0.26	-0.21	-0.58	-3.53
	3	6.05	2.15	-0.63	-10.29	-14.18
	4	11.81	4.42	-1.24	-12.45	-17.61
	5	18.44	6.78	-1.36	-9.74	-14.09
0.125	1	-0.88	-0.45	-0.35	0.83	-0.90
	2	3.90	1.51	0.04	-2.71	-4.76
	3	7.84	3.67	0.51	-5.28	-9.99
	4	10.88	5.29	0.94	-8.17	-15.68
	5	14.24	6.83	0.53	-15.00	-21.89
∞	1	1.47	0.15	-0.51	-1.47	-0.04
	2	5.23	1.54	-0.71	-3.33	-2.82
	3	8.42	2.48	-0.64	-5.14	-3.64
	4	10.92	3.22	-0.31	-8.24	-5.38
	5	13.11	4.05	0.06	-10.58	-7.08

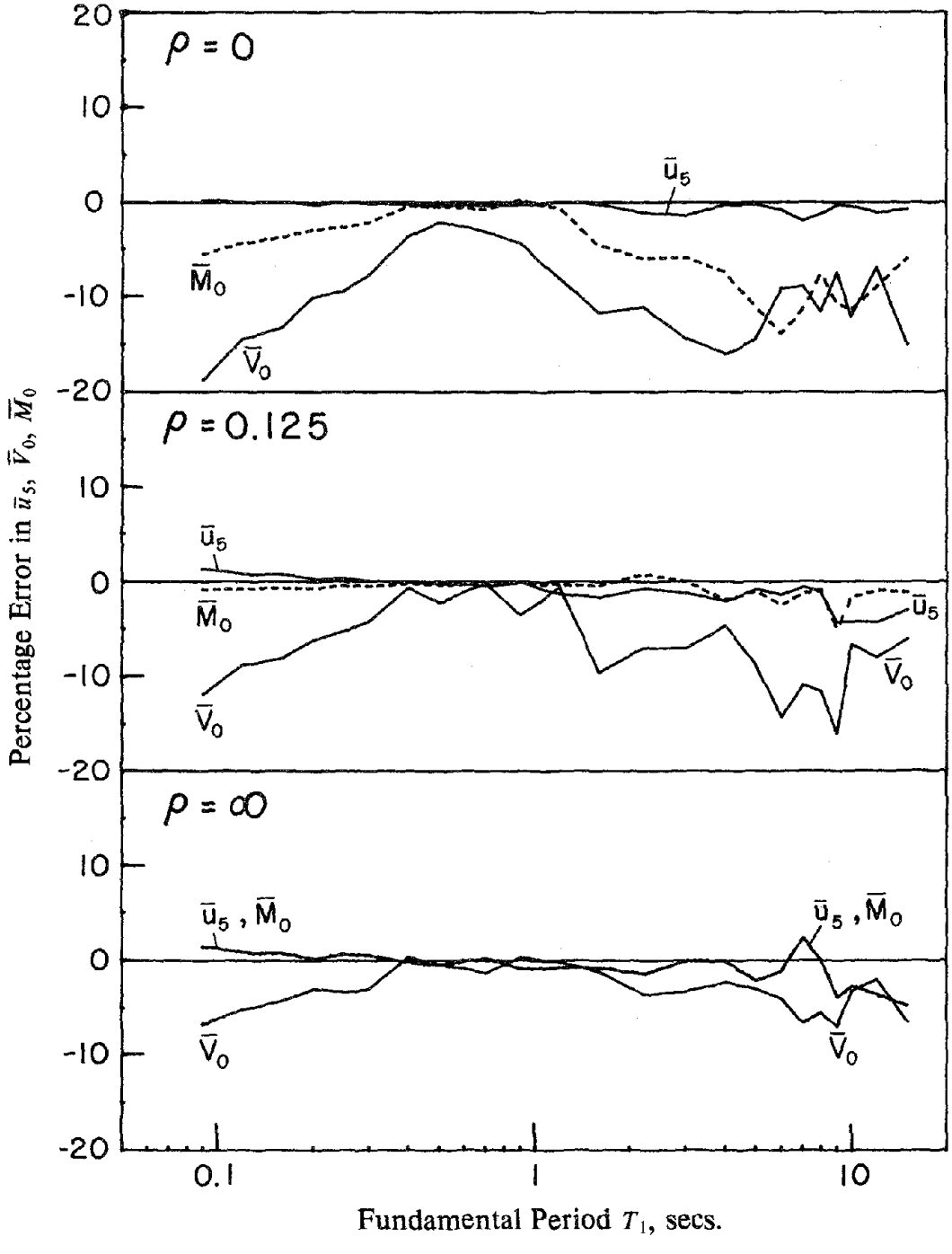

FIGURE 29 Percentage error in overall response quantities computed by RSA, relative to RHA results.

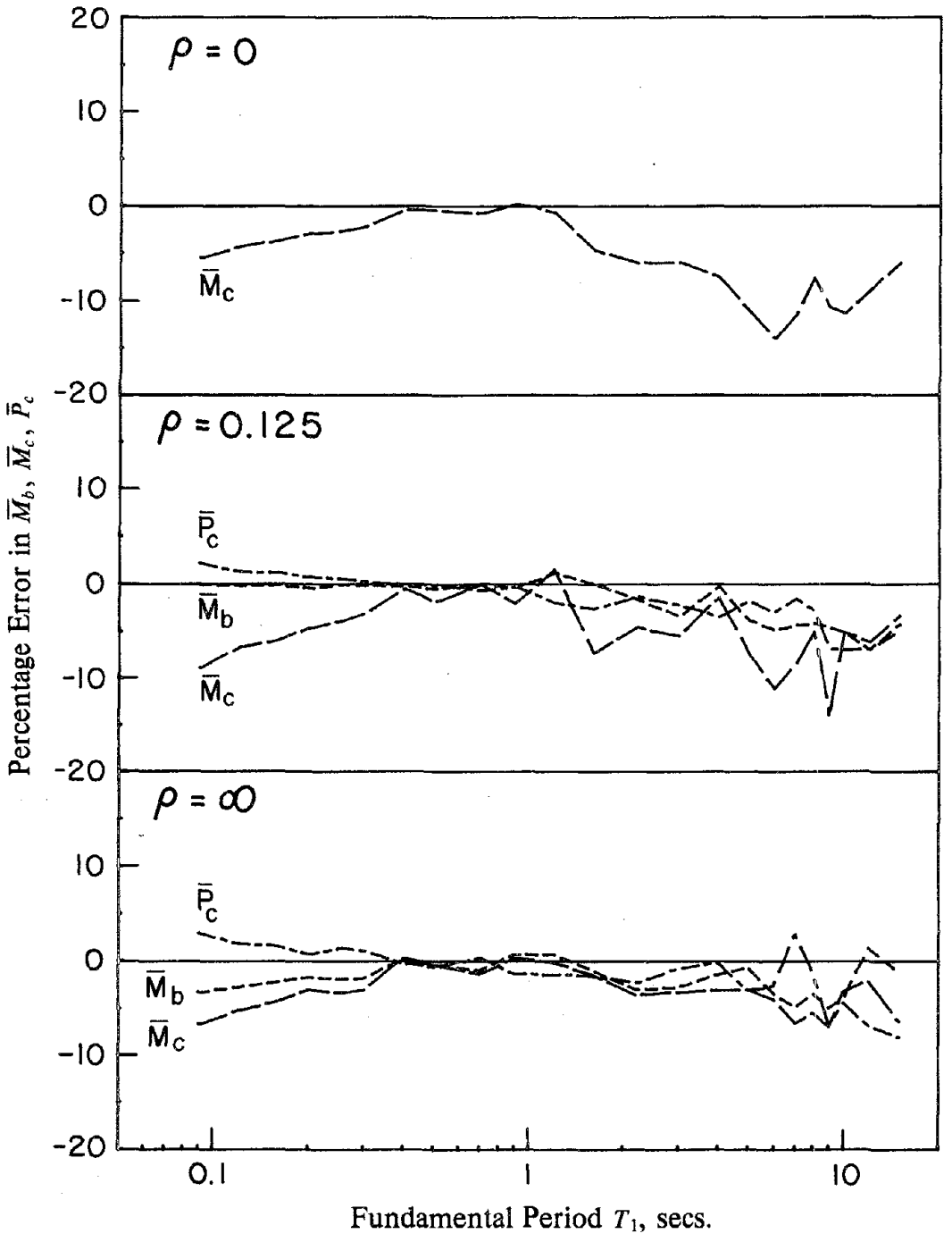

FIGURE 30 Percentage error in local response quantities computed by RSA, relative to RHA results.

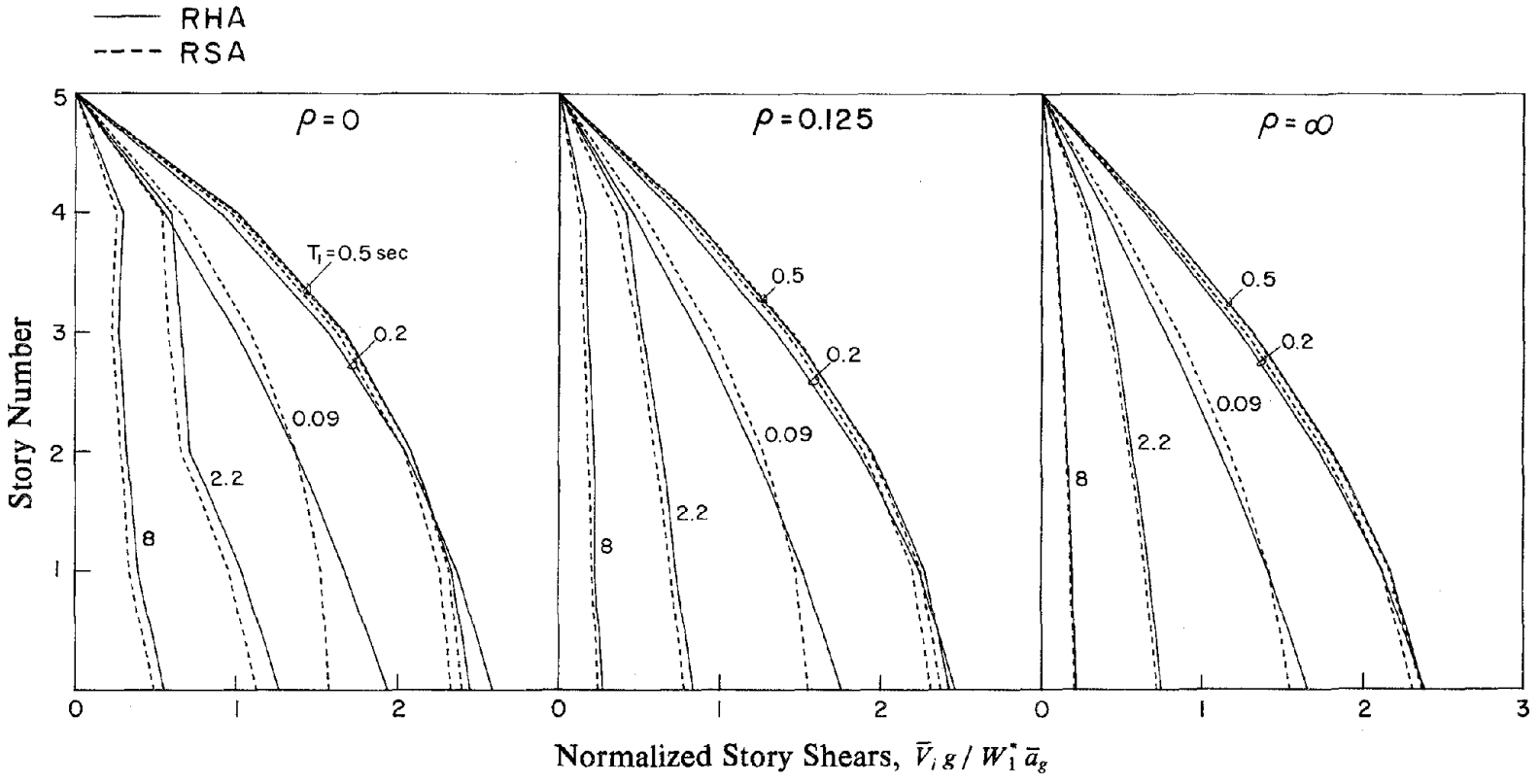

FIGURE 31 Comparison of maximum story shears computed by RHA and RSA.

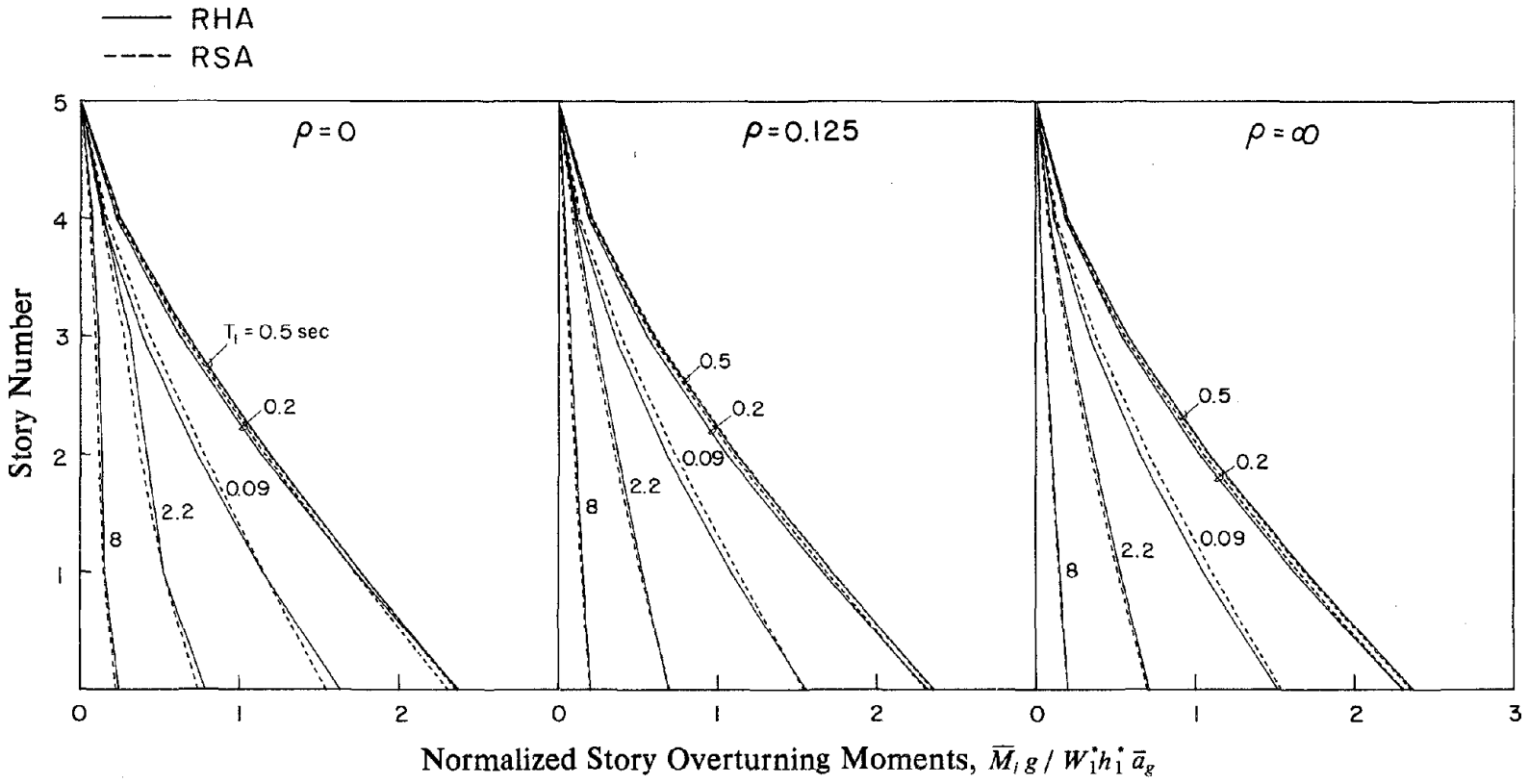

FIGURE 32 Comparison of maximum story overturning moments computed by RHA and RSA.

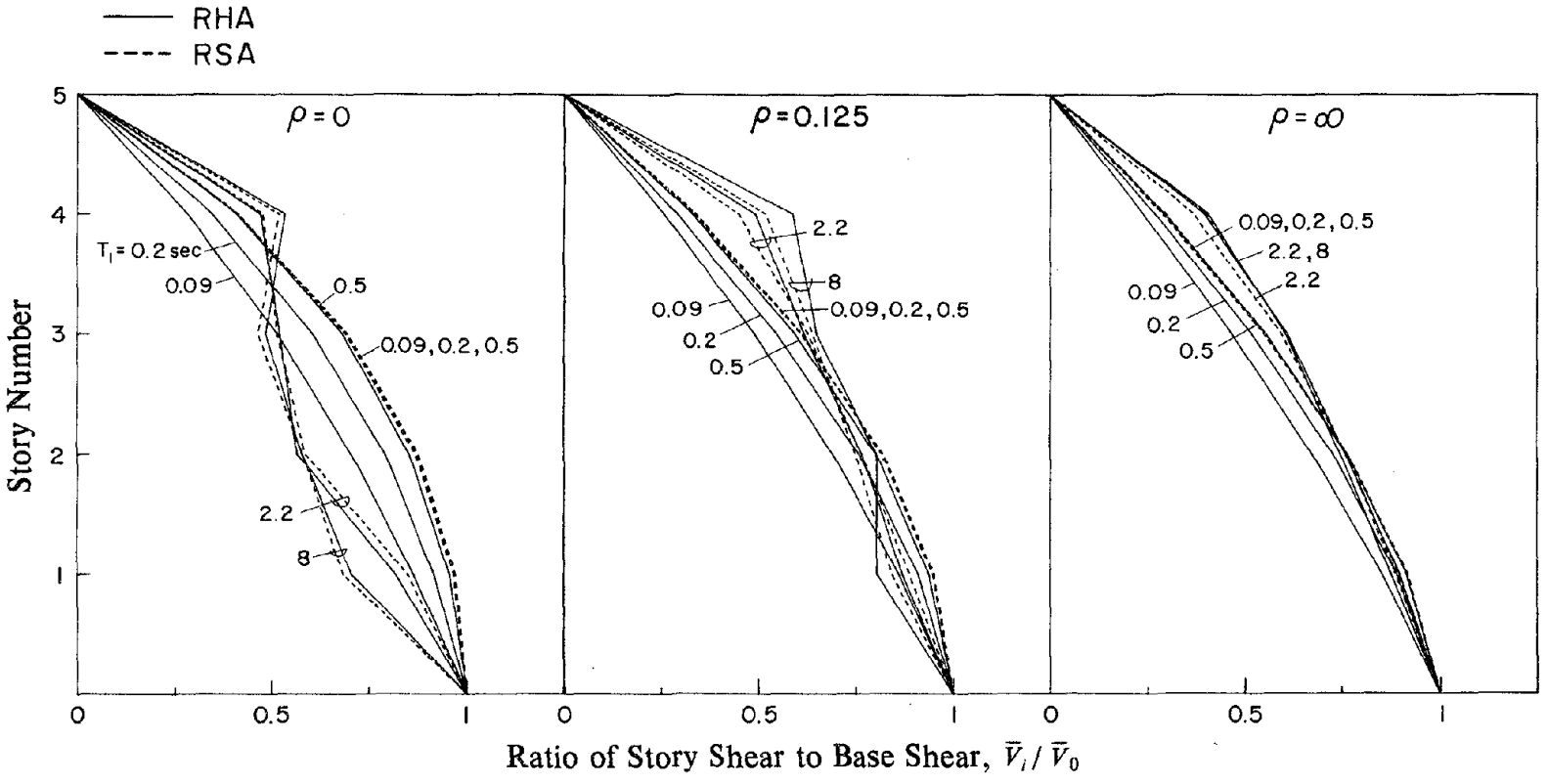

FIGURE 33 Comparison of height-wise variation of story shears computed by RHA and RSA.

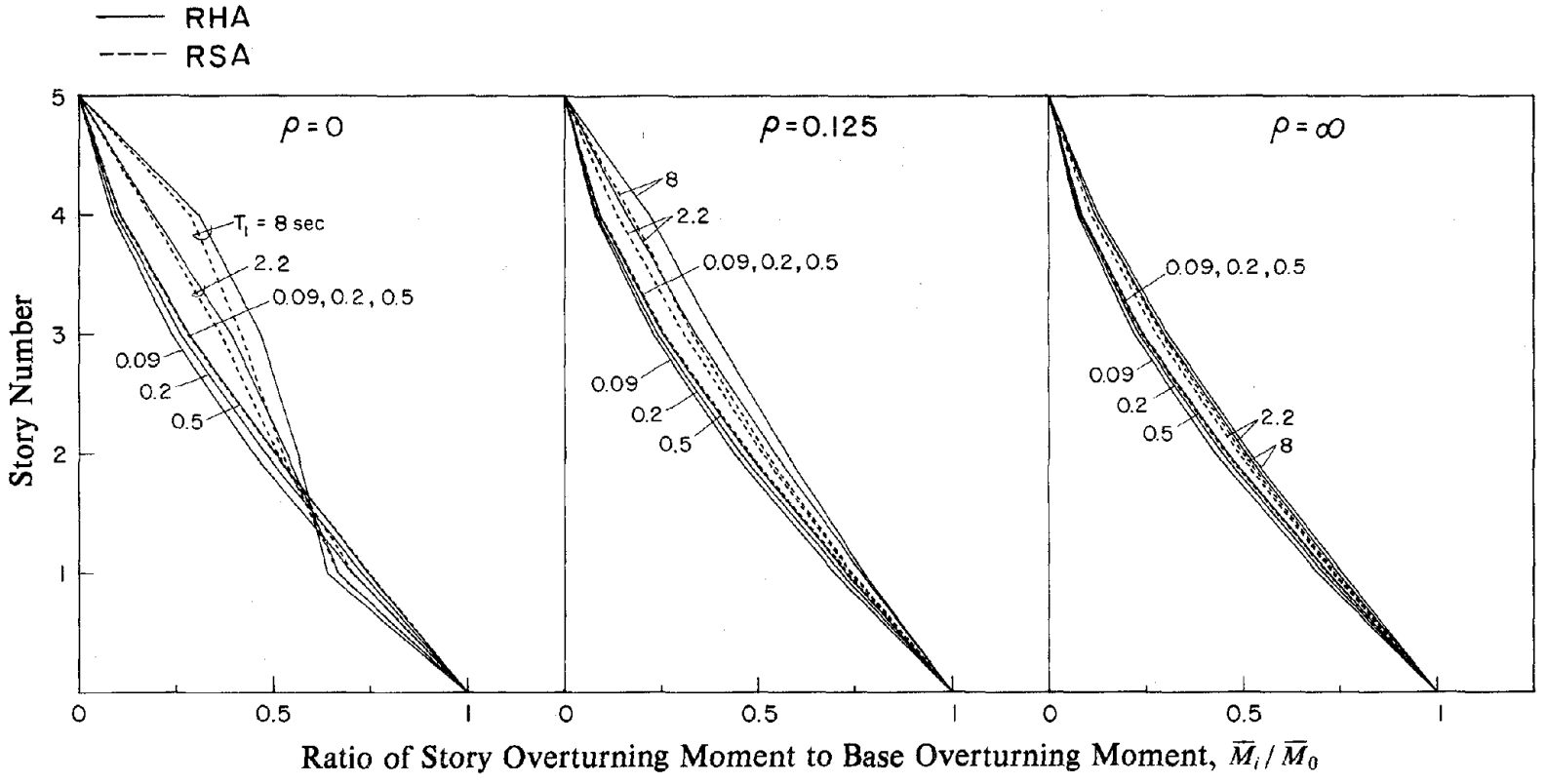

FIGURE 34 Comparison of height-wise variation of story overturning moments computed by RHA and RSA.

7. INFLUENCE OF NUMBER OF BAYS

This entire investigation has so far been based on the earthquake response of one-bay, five story frames with uniform properties. Strictly speaking all the observations presented so far regarding the effect of the stiffness ratio ρ, modal contributions, and errors in results of response spectrum analysis are restricted to this class of frames. However, Roehl [9] has demonstrated that, for a specified ρ, the natural frequencies and mode shapes of vibration practically do not change with the number of bays. The fundamental frequency and mode shape are especially insensitive to the changes in the number of bays. He showed that, consequently, the overall dynamic response --top floor displacement, base shear, and base overturning moment-- of a system having a specified fundamental period and value of ρ is essentially independent of the number of bays in the system. He also demonstrated that, with an appropriate normalization factor which depends on the number of bays, even the local response quantities --beam moment, column moment, and column axial force-- for single-bay and multi-bay frames can be inter-related very well. However, it is generally not possible to estimate the maximum forces in the interior columns of a multi-bay frame from the forces in the columns of a single-bay structure. Based on these valuable results of Roehl's work [9], it appears that the conclusions from this investigation regarding effects of ρ, modal contributions, and errors in RSA results are also applicable to multi-bay frames.

8. CONCLUSIONS

The principal conclusions of this investigation of the earthquake response of uniform five-story frames may be summarized as follows:

1. For a fixed beam-to-column stiffness ratio ρ, the response contributions of the higher vibration modes increase, and consequently the errors in results of response spectrum analysis increase, with increasing fundamental vibration period T_1 in the medium- and long-period regions of the earthquake response spectrum.

2. In addition to the above-mentioned trend, the response contributions of the higher vibration modes increase, and consequently the errors in the results of response spectrum analysis with SRSS combination of modal maxima increase, as T_1 decreases in the short-period region of the earthquake response spectrum.

3. For a fixed T_1, the response contributions of the higher vibration modes increase, and consequently the errors in the results of response spectrum analysis increase, with decreasing value of ρ.

4. The contributions of the higher vibration modes, the errors in the results of response spectrum analysis, and how these errors are affected by T_1 and ρ vary with the response quantity. Among the overall response quantities, the higher mode contributions are much more significant for the base shear than for the top floor displacement or base overturning moment. Among the local response quantities, the higher mode contributions are more significant for the column moments than for the beam moments or column axial forces.

5. While the errors in the results of response spectrum analysis depend on the response quantity they are all below 15 percent for building frames with fundamental vibration period less than the end of the medium-period region of the spectrum. There is a tendency for the errors to be larger in the upper story forces but the trend is not consistent or systematic.

Based on the results presented in this part of the report, improved simplified analysis procedures for preliminary design of buildings are developed in Part II.

REFERENCES

1. Blume, J.A., "Dynamic Characteristics of Multi-story Buildings," *Journal of the Structural Division, ASCE*, Vol. 94, No ST2, Feb., 1968, pp 337-402.

2. Chopra, A.K., "*Dynamics of Structures, A Primer*," Earthquake Engineering Research Institute, Berkeley, California, 1981.

3. Hudson, D.E., "*Reading and Interpreting Accelerograms*," Earthquake Engineering Research Institute, Berkeley, California , 1979.

4. Jennings, P.C., Housner, G.W., and Tsai, N.C., "Simulated Earthquake Ground Motions," *Report No EERL 68-10*, Earthquake Engineering Research Laboratory, California Institute of Technology, Pasadena, California, April, 1968.

5. Lopez, O.A., Chopra, A.K., "Studies of Structural Response to Earthquake Ground Motion," *Report No UCB/EERC-78/07*, Earthquake Engineering Research Center, University of California, Berkeley, California, April, 1978.

6. Murakami, M. and Penzien, J., "Nonlinear Response Spectra for Probabilistic Seismic Design and Damage Assesment of Reinforced Concrete Structures," *Report No UCB/EERC-75/38*, Earthquake Engineering Research Center, University of California, Berkeley, California, Nov., 1975.

7. Newmark, N.M., and Hall, W.J., "Vibration of Structures Induced by Ground Motion," Chapter 29, Part I, in *Shock and Vibration Handbook*, eds. C.M. Harris and C.E. Crede, 2nd Ed., McGraw-Hill Inc., New York, 1976.

8. Nigam, N.C., Jennings, P.C. "*SPECEQ/UQ, Digital Calculation of Response Spectra from Strong-Motion Earthquake Records*," Earthquake Engineering Research Laboratory, California Institute of Technology, Pasadena California, June, 1968.

9. Roehl, J.L., "Dynamic Response of Ground-excited Building Frames," *Ph.D. Thesis*, Rice University, Houston, Texas, Oct., 1971.

10. Ruiz, P., and Penzien, J., "Probabilistic Study of the Behavior of Structures During Earthquakes," *Report No UCB/EERC-69/3*, Earthquake Engineering Research Center, University of California, Berkeley, California, March, 1969.

11. Vanmarcke, E.H., et al., "Comparison of Seismic Analysis Procedures for Elastic Multi-degree Systems", *Report No 76-5*, Department of Civil Engineering, Massachusetts Institute of Technology, Cambridge, Massachusetts, Jan., 1976.

12. Veletsos, A.S., "Maximum Deformations of Certain Nonlinear Systems," *Proceedings of the Fourth World Conference on Earthquake Engineering*, Santiago, Chile, 1969, Vol. I, A-4, pp.156-170.

13. Veletsos, A.S., *Lecture Notes in Structural Dynamics*, Presented at the Department of Civil Engineering, University of California, Berkeley, California, 1977.

APPENDIX A: ANALYSIS PROCEDURE DETAILS

A.1 Model Frame

The systems analyzed are idealized as single-bay, five story moment resisting plane frames with constant story height $= h$, and bay width $= 2h$ (Figure 1). All members are prismatic with constant cross-section. Only flexural deformations are considered in the analysis of these frames. All the beams have the same flexural stiffness (EI_b) and the column stiffness (EI_c) does not vary with height.

A.2 Formulation of Stiffness Matrices.

Element Stiffnesses

For the beams, only two degrees of freedom are considered. The equilibrium equation for each beam can be written as

$$\begin{bmatrix} f_{\theta i} \\ f_{\theta j} \end{bmatrix} = \mathbf{k}_b \begin{bmatrix} \theta_i \\ \theta_j \end{bmatrix} \tag{A-1}$$

where $f_{\theta i}$, θ_i and $f_{\theta j}$, θ_j are the forces (moments) and corresponding rotations at the ends of the beam and $\mathbf{k}_b$ is the beam stiffness matrix which, under the assumptions above and using the definition for ρ given in Section 2 $\rho = I_b / 4\, I_c = I_b / 4\, I$, can be written as

$$\mathbf{k}_b = \frac{EI_b}{2h} \begin{bmatrix} 4 & 2 \\ 2 & 4 \end{bmatrix} = 2\rho \frac{EI}{h} \begin{bmatrix} 4 & 2 \\ 2 & 4 \end{bmatrix} \tag{A-2}$$

For the columns, four degrees of freedom are considered. The equilibrium equations for each column can be written as

$$\begin{bmatrix} f_{\theta i} \\ f_{\theta j} \\ f_{uk} \\ f_{ul} \end{bmatrix} = \mathbf{k}_c \begin{bmatrix} \theta_i \\ \theta_j \\ u_k \\ u_l \end{bmatrix} \tag{A-3}$$

where $f_{\theta i}$, θ_i and $f_{\theta j}$, θ_j are the forces (moments) and corresponding rotations at the ends of

the column; f_k, u_k and f_l, u_l are the forces and lateral displacements at the corresponding floor levels; and $\mathbf{k}_c$ is the column stiffness matrix which, under the assumptions above, can be written as

$$\mathbf{k}_c = \frac{EI_c}{h} \begin{bmatrix} 4 & 2 & \frac{-6}{h} & \frac{6}{h} \\ 2 & 4 & \frac{-6}{h} & \frac{6}{h} \\ \frac{-6}{h} & \frac{-6}{h} & \frac{12}{h^2} & \frac{-12}{h^2} \\ \frac{-6}{h} & \frac{6}{h} & \frac{-12}{h^2} & \frac{12}{h^2} \end{bmatrix} \tag{A-4}$$

This matrix can be rewritten in partitioned form as

$$\mathbf{k}_c = \begin{bmatrix} \mathbf{k}_{c\,\theta\theta} & \mathbf{k}_{c\,\theta u} \\ \mathbf{k}_{c\,u\theta} & \mathbf{k}_{c\,uu} \end{bmatrix} \tag{A-5}$$

and then the equilibrium equation above can be partitioned as

$$\begin{bmatrix} f_{\theta i} \\ f_{\theta j} \end{bmatrix} = \mathbf{k}_{c\,\theta\theta} \begin{bmatrix} \theta_i \\ \theta_j \end{bmatrix} + \mathbf{k}_{c\,\theta u} \begin{bmatrix} u_k \\ u_l \end{bmatrix} \tag{A-6a}$$

$$\begin{bmatrix} f_{uk} \\ f_{ul} \end{bmatrix} = \mathbf{k}_{c\,u\theta} \begin{bmatrix} \theta_i \\ \theta_j \end{bmatrix} + \mathbf{k}_{c\,uu} \begin{bmatrix} u_k \\ u_l \end{bmatrix} \tag{A-6b}$$

Global Stiffness

The global equilibrium equations can also be written in partitioned form, separating the lateral displacements $\mathbf{u}$ from the joint rotations θ, then

$$\begin{bmatrix} \mathbf{f}_u \\ \mathbf{f}_\theta \end{bmatrix} = \mathbf{k}_T \begin{bmatrix} \mathbf{u} \\ \theta \end{bmatrix} = \begin{bmatrix} \mathbf{k}_{uu} & \mathbf{k}_{u\theta} \\ \mathbf{k}_{\theta u} & \mathbf{k}_{\theta\theta} \end{bmatrix} \begin{bmatrix} \mathbf{u} \\ \theta \end{bmatrix} \tag{A-7}$$

where $\mathbf{k}_T$ is the global stiffness matrix.

From the form of equation (A-7) it should be clear that the individual element stiffness matrices ($\mathbf{k}_b$ and $\mathbf{k}_c$) contribute only to some of the submatrices of $\mathbf{k}_T$. The beam stiffness matrices $\mathbf{k}_b$ contribute only to $\mathbf{k}_{\theta\theta}$ and the column stiffness matrices contribute to all the submatrices in $\mathbf{k}_T$ but in a very special form: each of the submatrices of $\mathbf{k}_c$ contributes only to

the corresponding submatrix of $\mathbf{k}_T$, that is, $\mathbf{k}_{c\,\theta\theta}$ into $\mathbf{k}_{\theta\theta}$, $\mathbf{k}_{c\,\theta u}$ into $\mathbf{k}_{\theta u}$ and so on.

Lateral Stiffness

Since there are no forces (moments) applied at the joints, $\mathbf{f}_\theta = 0$ and the second line of the partitioned equilibrium equation yields

$$0 = \mathbf{k}_{\theta u}\ \mathbf{u} + \mathbf{k}_{\theta\theta}\ \theta \tag{A-8a}$$

then

$$\theta = -\mathbf{k}_{\theta\theta}^{-1}\ \mathbf{k}_{\theta u}\ \mathbf{u} = \mathbf{T}\ \mathbf{u} \tag{A-8b}$$

and

$$\mathbf{f}_u = \mathbf{k}_{uu}\ \mathbf{u} + \mathbf{k}_{u\theta}\ \mathbf{T}\ \mathbf{u} = (\mathbf{k}_{uu} + \mathbf{k}_{u\theta}\ \mathbf{T})\ \mathbf{u} = \mathbf{k}\ \mathbf{u} \tag{A-9}$$

thus

$$\mathbf{k} = \mathbf{k}_{uu} + \mathbf{k}_{u\theta}\ \mathbf{T} \tag{A-10}$$

A.3 Formulation of mass matrix

The structure is idealized as a lumped mass system with the same mass m at all the floor levels. Therefore, the mass matrix is diagonal

$$\mathbf{m} = \begin{bmatrix} m & & & & \\ & m & & & \\ & & m & & \\ & & & m & \\ & & & & m \end{bmatrix} \tag{A-11}$$

which only includes the lateral displacements degrees of freedom.

A.4 Formulation of damping matrix

The damping in the structure is approximated by considering it as a fraction of the critical damping for each natural vibration mode of the structure. Therefore, no damping matrix needs to be defined. For completeness,

$$\mathbf{c} = \left[c_{ij} \right] \tag{A-12}$$

where only the lateral displacement degrees of freedom are included.

A.5 Equations of motion

The dynamic equilibrium condition for the frame, under a base excitation defined by ground accelerations $a_g(t)$ is:

$$\mathbf{m}\,\ddot{\mathbf{u}}(t) + \mathbf{c}\,\dot{\mathbf{u}}(t) + \mathbf{k}\,\mathbf{u}(t) = -\mathbf{m}\,\mathbf{1}\,a_g(t) \tag{A-13}$$

where 1 is a vector with as many components as floor levels in the building, all equal to unity. Defining a set of modal coordinates, $Y_1, Y_2, \ldots, Y_5$ such that

$$\mathbf{u}(t) = \sum_{n=1}^{5} \boldsymbol{\phi}_n\, Y_n(t) \tag{A-14}$$

where $\boldsymbol{\phi}_n$ is the nth natural mode of vibration of the frame satisfying the eigen problem equation

$$(\mathbf{k} - \omega_n^2\,\mathbf{m})\,\boldsymbol{\phi}_n = 0 \tag{A-15}$$

with ω_n = the nth mode natural frequency, and the orthogonality conditions

$$\begin{aligned}
\boldsymbol{\phi}_m^T\,\mathbf{m}\,\boldsymbol{\phi}_n &= \begin{cases} 0 & \text{for } m \neq n \\ M_n & \text{for } m = n \end{cases} \\
\boldsymbol{\phi}_m^T\,\mathbf{c}\,\boldsymbol{\phi}_n &= \begin{cases} 0 & \text{for } m \neq n \\ 2\xi_n\,\omega_n\,M_n & \text{for } m = n \end{cases} \\
\boldsymbol{\phi}_m^T\,\mathbf{k}\,\boldsymbol{\phi}_n &= \begin{cases} 0 & \text{for } m \neq n \\ \omega_n^2 M_n & \text{for } m = n \end{cases}
\end{aligned} \tag{A-16}$$

where ξ_n is the damping ratio on the nth mode. Using the modal coordinates the equation of motion can be reduced to a set of uncoupled equations of the form

$$\ddot{Y}_n(t) + 2\xi_n \omega_n \dot{Y}_n(t) + \omega_n^2 Y_n(t) = -\frac{L_n}{M_n} a_g(t) \tag{A-17}$$

where $L_n = \phi_n^T \mathbf{m}\, 1$ and $M_n = \phi_n^T \mathbf{m}\, \phi_n$.

The damping ratio for all the natural modes of vibration is assumed to be 5 percent so ξ_n is set to 0.05.

A.6 Response history analysis

The solution of the modal equations of motion can be written as:

$$Y_n(t) = -\frac{L_n}{M_n} \frac{1}{\omega_{nD}} \int_0^t a_g(\tau) e^{-\xi_n \omega_n (t-\tau)} \sin\omega_{nD}(t-\tau)\, d\tau \tag{A-18}$$

where $\omega_{nD} = \omega_n \sqrt{1-\xi_n^2}$. By defining $C_n = \frac{L_n}{M_n}$ and $Y_n(t) = C_n\ u_n^*(t)$ the expressions for the response quantities, that are presented next, will be simplified considerably.

Modal Responses

The different response quantities, for each mode, can be computed from the following expressions:

- Story displacements

$$\mathbf{u}_n(t) = Y_n(t)\, \phi_n = C_n\ \phi_n\ u_n^*(t) \tag{A-19}$$

- Equivalent lateral forces

$$\mathbf{f}_n(t) = \mathbf{k}\, \mathbf{u}_n(t) = Y_n(t)\, \mathbf{k}\, \phi_n = C_n\ \mathbf{k}\, \phi_n\ u_n^*(t) \tag{A-20a}$$

or in terms of the mass matrix

$$\mathbf{f}_n(t) = C_n\, \omega_n^2\, \mathbf{m}\, \phi_n\ u_n^*(t) = C_n\ \mathbf{m}\, \phi_n\ \ddot{u}_n^*(t) \tag{A-20b}$$

- Story shears: at the ith floor level

$$V_{in}(t) = \sum_{k=i}^{5} f_{kn}(t) \tag{A-21a}$$

or in matrix form

$$\mathbf{V}_n(t) = \mathbf{S}\,\mathbf{f}_n(t) \tag{A-21b}$$

where

$$\mathbf{S} = \begin{bmatrix} 1 & 1 & 1 & 1 & 1 \\ & 1 & 1 & 1 & 1 \\ & & 1 & 1 & 1 \\ & & & 1 & 1 \\ & & & & 1 \end{bmatrix} \tag{A-21c}$$

is a summation matrix which is nondimensional. The base shear, in particular, can be computed from

$$V_{0n}(t) = C_n\ \mathbf{1}^T\ \mathbf{m}\ \boldsymbol{\phi}_n\ \ddot{u}_n^*(t) \tag{A-22}$$

- Story overturning moments: at the ith floor level

$$M_{in}(t) = \sum_{k=i}^{5} (h_k - h_{i-1})\ f_{kn}(t) \tag{A-23a}$$

where h_i is the height from the base to floor level i. In matrix form

$$\mathbf{M}_n(t) = \mathbf{H}\,\mathbf{f}_n(t) \tag{A-23b}$$

where

$$\mathbf{H} = h \begin{bmatrix} 1 & 2 & 3 & 4 & 5 \\ & 1 & 2 & 3 & 4 \\ & & 1 & 2 & 3 \\ & & & 1 & 2 \\ & & & & 1 \end{bmatrix} \tag{A-23c}$$

is a summation matrix which has dimensions of length. The base overturning moment, in particular, can be computed from

$$M_{0n}(t) = C_n\ \mathbf{h}^T\ \mathbf{m}\ \boldsymbol{\phi}_n\ \ddot{u}_n^*(t) \tag{A-24}$$

- Joint rotations: from equation (A-8)

$$\theta_n(t) = \mathbf{T}\,\mathbf{u}_n(t) = Y_n(t)\,\mathbf{T}\,\boldsymbol{\phi}_n = C_n\,\mathbf{T}\,\boldsymbol{\phi}_n\,u_n^*(t) \tag{A-25}$$

-Beam moments: for each beam, apply equation (A-1), then

$$\begin{bmatrix} M_{bin}(t) \\ M_{bjn}(t) \end{bmatrix} = \mathbf{k}_b \begin{bmatrix} \theta_{in}(t) \\ \theta_{jn}(t) \end{bmatrix} \tag{A-26}$$

-Column moments: for each column, apply equation (A-6a), then

$$\begin{bmatrix} M_{cin}(t) \\ M_{cjn}(t) \end{bmatrix} = \mathbf{k}_{c\,\theta\theta} \begin{bmatrix} \theta_{in}(t) \\ \theta_{jn}(t) \end{bmatrix} + \mathbf{k}_{c\,\theta u} \begin{bmatrix} u_{kn}(t) \\ u_{ln}(t) \end{bmatrix} \tag{A-27}$$

For the first story columns $\theta_{jn}(t) = u_{ln}(t) = 0$.

- Column axial forces

Using statics, compute $P_{ci}(t) =$ axial force on the ith story column from the moments on the end of the beams on the stories above.

On the kth story:

$$P_{ckn}(t) = \frac{1}{2h}\left(M_{bin}(t) + M_{bjn}(t) \right) + P_{c\,k+1\,n}(t) \tag{A-28}$$

where $M_{bin}(t)$ and $M_{bjn}(t)$ are the end moments of the beam on the kth story.

Total response

The total response $r(t)$ for any response quantity r is obtained by adding the individual mode responses $r_n(t)$

$$r(t) = \sum_{n=1}^{N} r_n(t) \tag{A-29}$$

where N is the total number of modes considered.

Maxima of the responses

For each response quantity of interest $r(t)$ the maximum throughout the complete time-history $\bar{r}$ is determined by monitoring the response as it is being computed.

A.7 Response spectrum analysis

Modal coordinates maxima

The maximum $\overline{Y}_n$ of the modal coordinates $Y_n(t)$ can be obtained directly from the displacement response spectrum as

$$\overline{Y}_n = \max_t | Y_n(t) | = | -\frac{L_n}{M_n} | S_{dn}(\omega_n, \xi_n) \tag{A-30}$$

where $S_{dn}(\omega_n, \xi_n)$ is the ordinate of the displacement response spectrum for damping $\xi_n = 0.05$ at frequency ω_n corresponding to the ground acceleration $a_g(t)$.

Modal response maxima

After the values for $\overline{Y}_n$ are known, the maxima of the modal responses can be obtained from equations (A-19) through (A-28) by substituting $\overline{Y}_n$ for $Y_n(t)$ to obtain $\overline{r}_n$ rather than $r_n(t)$.

Total response maxima

An estimate of the total response maxima is obtained using the square-root-of-the-sum-of-the-squares (SRSS) combination rule. Then,

$$\overline{r} = \left[\sum_{n=1}^{N} \overline{r}_n^2 \right]^{1/2} \tag{A-31}$$

Although more sophisticated modal combination formulas are available they are not needed in this case because the vibration frequencies are well separated and the estimates from SRSS will be almost identical to the estimates of the other combination rules.

APPENDIX B: IMPLEMENTATION OF ANALYSIS PROCEDURE

Based on the definition of the problem in Section 2.1 and the details of the analysis provided in Appendix A it is possible to formulate the problem in terms of nondimensional response quantities taking advantage of the particular characteristics of the model frame used. Furthermore, using this new formulation it will be shown that the natural vibration mode shapes and the ratios of the natural vibration frequencies depend only on the geometric characteristics of the frame and the value of the stiffness parameter rho.

B.1 Formulation of stiffness matrices

Element stiffness

For the beams,

$$\mathbf{k}_b = 2\rho\frac{EI}{h}\begin{bmatrix} 4 & 2 \\ 2 & 4 \end{bmatrix} = \frac{EI}{h}\,\mathbf{k}_b^0 \tag{B-1}$$

For the columns,

$$\mathbf{k}_c = \begin{bmatrix} \mathbf{k}_{c\,\theta\theta} & \mathbf{k}_{c\,\theta u} \\ \mathbf{k}_{c\,u\theta} & \mathbf{k}_{c\,uu} \end{bmatrix} = \begin{bmatrix} \frac{EI}{h}\,\mathbf{k}_{c\,\theta\theta}^0 & \frac{EI}{h^2}\,\mathbf{k}_{c\,\theta u}^0 \\ \frac{EI}{h^2}\,\mathbf{k}_{c\,u\theta}^0 & \frac{EI}{h^3}\,\mathbf{k}_{c\,uu}^0 \end{bmatrix} \tag{B-2}$$

Note that among the above matrices only $\mathbf{k}_b^0$ depends on the stiffness ratio ρ.

Global stiffness

Since the individual element stiffness matrices contribute only to parts of the global stiffness matrix $\mathbf{k}_T$, we can write:

$$\mathbf{k}_t = \begin{bmatrix} \frac{EI}{h^3}\,\mathbf{k}_{uu}^0 & \frac{EI}{h^2}\,\mathbf{k}_{u\theta}^0 \\ \frac{EI}{h^2}\,\mathbf{k}_{\theta u}^0 & \frac{EI}{h}\,\mathbf{k}_{\theta\theta}^0 \end{bmatrix} \tag{B-3}$$

Note that only $\mathbf{k}^0_{\theta\theta}$ depends on ρ, through the contributions of the beam stiffness matrices $\mathbf{k}^0_b$.

Lateral Stiffness

From equation (A-8) in Appendix A,

$$\theta = -\mathbf{k}_{\theta\theta}^{-1}\,\mathbf{k}_{\theta u}\,\mathbf{u} = \mathbf{T}\,\mathbf{u} = \frac{h}{EI}\,\mathbf{k}_{\theta\theta}^{0-1}\,\frac{EI}{h^2}\,\mathbf{k}^0_{\theta u}\,\mathbf{u} \tag{B-4}$$

$$= -\frac{1}{h}\,\mathbf{k}_{\theta\theta}^{0-1}\,\mathbf{k}^0_{\theta u}\,\mathbf{u} = \frac{1}{h}\,\mathbf{T}^0\,\mathbf{u}$$

Then equation (A-9) changes to

$$\mathbf{f}_u = \frac{EI}{h^3}\,\mathbf{k}^0_{uu} + \frac{EI}{h}\,\mathbf{k}^0_{u\theta}\,\frac{1}{h}\,\mathbf{T}^0\,\mathbf{u} = \frac{EI}{h^3}\,\mathbf{k}^0\,\mathbf{u} \tag{B-5a}$$

and

$$\mathbf{k}^0 = \mathbf{k}^0_{uu} + \mathbf{k}^0_{u\theta}\,\mathbf{T}^0 \tag{B-5b}$$

Note that $\mathbf{T}^0$ and therefore $\mathbf{k}^0$ depend on ρ.

B.2 Formulation of mass matrix

Clearly, the mass matrix can be written as

$$\mathbf{m} = m\ \mathbf{I} = m\ \mathbf{m}^0 \tag{B-6}$$

where $\mathbf{I}$ is a diagonal matrix with all its elements equal to 1.

B.3 Formulation of damping matrix

Although it is not needed since damping is being included at the modal equations level it can be presented for the sake of completeness as

$$\mathbf{c} = c\ \mathbf{c}^0 \tag{B-7}$$

B.4 Equations of motion

The equation of motion in Appendix A [equation (A-13)] can be written

$$m\ \mathbf{m}^o\ \ddot{\mathbf{u}}(t) + c\ \mathbf{c}^o\ \dot{\mathbf{u}}(t) + \frac{EI}{h^3}\ \mathbf{k}^o\ \mathbf{u}(t) = -m\ \mathbf{m}^o\ \mathbf{1}\ a_g(t) \tag{B-8}$$

using the definition of modal coordinates, $Y_1, Y_2, \ldots, Y_5$

$$\mathbf{u}(t) = \sum_{n=1}^{5} \boldsymbol{\phi}_n\ Y_n(t) \tag{B-9}$$

the eigen problem equation can be written as

$$\left(\frac{EI}{h^3}\ \mathbf{k}^0 - \omega_n^2\ m\ \mathbf{m}^0\right)\ \boldsymbol{\phi}_n = 0 \tag{B-10}$$

which is equivalent to

$$\left(\mathbf{k}^0 - \alpha_n^2\ \mathbf{m}^0\right)\ \boldsymbol{\psi}_n = 0 \tag{B-11}$$

where

$$\omega_n^2 = \alpha_n^2\ \frac{EI}{m\ h^3} \qquad \text{and} \qquad \boldsymbol{\phi}_n = \boldsymbol{\psi}_n$$

Clearly, the eigen vectors of the new problem $\boldsymbol{\psi}_n$ satisfy the orthogonality conditions

$$\begin{aligned}
\boldsymbol{\psi}_m^T\ \mathbf{m}^0\ \boldsymbol{\psi}_n &= \begin{cases} 0 & \text{for } m \neq n \\ M_n^0 & \text{for } m = n \end{cases} \\
\boldsymbol{\psi}_m^T\ \mathbf{c}^0\ \boldsymbol{\psi}_n &= \begin{cases} 0 & \text{for } m \neq n \\ 2\xi_n\ \alpha_n\ M_n^0 & \text{for } m = n \end{cases} \\
\boldsymbol{\psi}_m^T\ \mathbf{k}^0\ \boldsymbol{\psi}_n &= \begin{cases} 0 & \text{for } m \neq n \\ \alpha_n^2 M_n^0 & \text{for } m = n \end{cases}
\end{aligned} \tag{B-12}$$

where ξ_n is the damping ratio on the nth mode.

From the equations above it should be clear that the mode shapes ($\boldsymbol{\phi}_n$ or $\boldsymbol{\psi}_n$) and the ratios between the natural frequencies of vibration (α_n/α_1 or ω_n/ω_1) do not change as the fundamental period $T_1 = 2\pi/\omega_1$ changes. In fact, the fundamental period can be computed from

$$T_1 = \frac{2\pi}{\omega_1} = \frac{2\pi}{\alpha_1}\sqrt{\frac{mh^3}{EI}} \tag{B-13}$$

therefore, any value of T_1 can be obtained by adequately adjusting the values of E, I, h, and m.

The modal equations of motion [equation (A-17)] will still be different for each fundamental period case, but all the terms in them can be directly computed from the invariant quantities (under T_1 changes).

$$L_n = \boldsymbol{\phi}_n^T \mathbf{m}\, 1 = \boldsymbol{\psi}_n\ m\ \mathbf{m}^0 1 = m\ \boldsymbol{\psi}_n^T \mathbf{m}^0 1 = m\ L_n^0 \tag{B-14a}$$

$$M_n = \boldsymbol{\phi}_n^T \mathbf{m}\, \boldsymbol{\phi}_n = m\ \boldsymbol{\psi}_n^T \mathbf{m}^0\, \boldsymbol{\psi}_n = m\ M_n^0 \tag{B-14b}$$

but L_n and M_n always occur together as $C_n = L_n / M_n$ thus

$$C_n = \frac{m\ L_n^0}{m\ M_n^0} = \frac{L_n^0}{M_n^0} = C_n^0 \tag{B-15}$$

B.5 Response history analysis

Solution of modal equations

Rather than evaluating the Duhamel integral in equation (A-18), the solution of the modal equations can be obtained through direct numerical integration using the Newmark β-method with $\beta = 1/6$, which corresponds to assuming linearly varying acceleration within each integration step [B.1]. The basic equations of the integration scheme, written for time t, are:

$$\ddot{x}_t + 2\xi\omega\dot{x}_t + \omega^2 x_t = \ddot{y}_t \tag{B-16}$$

which corresponds to the equation of motion, and

$$\dot{x}_{t+\Delta t} = \dot{x}_t + \frac{1}{2}\left(\ddot{x}_t + \ddot{x}_{t+\Delta t}\right)\Delta t \tag{B-17a}$$

$$x_{t+\Delta t} = x_t + \dot{x}_t\ \Delta t + \ddot{x}_t\ \frac{\Delta t^2}{3} + \ddot{x}_{t+\Delta t}\ \frac{\Delta t^2}{6} \tag{B-17b}$$

Writing these expressions in incremental form

$$\Delta\ddot{x} + 2\xi\omega\Delta\dot{x} + \omega^2\Delta x = \Delta\ddot{y} \tag{B-18}$$

and

$$\Delta\dot{x} = \ddot{x}_t\,\Delta t + \Delta\ddot{x}\,\frac{\Delta t}{2} \tag{B-19a}$$

$$\Delta x = \dot{x}_t\,\Delta t + \ddot{x}_t\,\frac{\Delta t^2}{2} + \Delta\ddot{x}\,\frac{\Delta t^2}{6} \tag{B-19b}$$

where Δx, $\Delta\dot{x}$, $\Delta\ddot{x}$, and $\Delta\ddot{y}$ are the changes in the quantities x, $\dot{x}$, $\ddot{x}$, and $\ddot{y}$ going from time t to time $t + \Delta t$ (one integration step of duration Δt).

The third equation necessary to compute the change $\Delta\ddot{x}$ in the accelerations $\ddot{x}$ after one integration time step can be obtained by substitution of equations (B-19) in equation (B-18), then

$$\Delta\ddot{x} = \frac{\Delta\ddot{y} - 2\xi\omega\ddot{x}_t\,\Delta t - \omega^2\left(\dot{x}_t\,\Delta t + \ddot{x}_t\,\dfrac{\Delta t^2}{2}\right)}{1 + 2\xi\omega\dfrac{\Delta t}{2} + \omega^2\dfrac{\Delta t^2}{6}} \tag{B-20}$$

Equations (B-19) and (B-20) allow to compute the increments in the state variables x, $\dot{x}$, and $\ddot{x}$ if the increments in the excitation $\ddot{y}$ are known. The integration algorithm can be summarized as:

1. Initialization

$$x_0 = 0\,, \quad \dot{x}_0 = 0\,, \quad \ddot{x}_0 = -\ddot{y}_0$$

2. For $t = 0,\ \Delta t,\ 2\Delta t,\ 3\Delta t,\ \ldots$, until satisfied

   (a) Compute increments in excitation $\ddot{y}$ and in state variables x, $\dot{x}$, and $\ddot{x}$

$$\Delta\ddot{y} = \ddot{y}_{t+\Delta t} - \ddot{y}_t$$

$\Delta\ddot{x}$ from equation (B-20)

$\Delta\dot{x}$ from equation (B-19a)

Δx from equation (B-19b)

   (b) Compute new state variables at time $t + \Delta t$

$$\ddot{x}_{t+\Delta t} = \ddot{x}_t + \Delta\ddot{x}$$

$$\dot{x}_{t+\Delta t} = \dot{x}_t + \Delta\dot{x}$$

$$x_{t+\Delta t} = x_t + \Delta x$$

The integration was carried out using a constant value of the time step Δt. The same value was used for all the modal equations and it was selected as the smallest of $T_1/50$, $T_5/5$, and 0.01 but rounded so that an exact number of steps occur between two consecutive data points in the input ground motions (digitized at 0.02 secs.). The actual expression for the computation of the time step is

$$\Delta t = \frac{0.02}{1 + \dfrac{0.02}{\min\left\{\dfrac{T_1}{50}, \dfrac{T_5}{5}, 0.02\right\}}} \tag{B-21}$$

T_1 and T_5 are the periods of the first and last mode respectively. This time-step guarantees the convergence and stability of the integration scheme for all the modes while providing enough accuracy even for the highest mode. The integration was carried along after the end of the excitation for a duration of 1.5 T_1 to include the possibility of maxima occurring during that time.

Modal responses

Taking advantage of the invariance of the mode shapes and the frequency ratios, the responses on each mode can be computed in terms of the unit modal responses defined in Section 5. Then the response quantities of interest can be computed from equations (A-19) through (A-28) as

- Floor displacements

$$\mathbf{u}_n(t) = Y_n(t)\,\boldsymbol{\phi}_n = Y_n(t)\,\mathbf{u}_n^0 \tag{B-22}$$

-Equivalent lateral forces

$$\mathbf{f}_n = Y_n(t)\omega_n^2\,\mathbf{m}\,\boldsymbol{\phi}_n = m\;Y_n(t)\,\mathbf{m}^0\,\boldsymbol{\psi}_n = \omega_n^2\,m\;Y_n(t)\,\mathbf{f}_n^0 \tag{B-23}$$

- Story shears

$$\mathbf{V}_n(t) = \omega_n^2\,m\;Y_n(t)\,\mathbf{V}_n^0 \tag{B-24}$$

-Story overturning moments

$$\mathbf{M}_n(t) = \omega_n^2\, mh\;\; Y_n(t)\,\mathbf{M}_n^0 \tag{B-25}$$

- Joint rotations

$$\boldsymbol{\theta}_n(t) = \frac{1}{h}\; Y_n(t)\boldsymbol{\theta}_n^0 \tag{B-26}$$

- Beam moments

$$\begin{bmatrix} M_{bin}(t) \\ M_{bjn}(t) \end{bmatrix} = \frac{EI}{h}\,\mathbf{k}_b^0 \begin{bmatrix} \theta_{in}(t) \\ \theta_{jn}(t) \end{bmatrix} = \frac{EI}{h}\,\mathbf{k}_b^0\; Y_n(t)\;\frac{1}{h}\begin{bmatrix} \theta_{in}^0 \\ \theta_{jn}^0 \end{bmatrix} \tag{B-27}$$

$$= \frac{EI}{h^2}\; Y_n(t)\begin{bmatrix} M_{bin}^0 \\ M_{bjn}^0 \end{bmatrix}$$

-Column moments

$$\begin{bmatrix} M_{cin}(t) \\ M_{cjn}(t) \end{bmatrix} = \frac{EI}{h}\,\mathbf{k}_{c\,\theta\theta}^0 \begin{bmatrix} \theta_{in}(t) \\ \theta_{jn}(t) \end{bmatrix} + \frac{EI}{h^2}\,\mathbf{k}_{c\,\theta u}^0 \begin{bmatrix} u_{kn}(t) \\ u_{ln}(t) \end{bmatrix}$$

$$= \frac{EI}{h}\,\mathbf{k}_{c\,\theta\theta}^0\; Y_n(t)\;\frac{1}{h}\begin{bmatrix} \theta_{in}^0 \\ \theta_{jn}^0 \end{bmatrix} + \frac{EI}{h^2}\,\mathbf{k}_{c\,\theta u}^0\;\; Y_n(t)\begin{bmatrix} u_{kn}^0 \\ u_{ln}^0 \end{bmatrix} \tag{B-28}$$

$$= \frac{EI}{h^2}\; Y_n(t)\begin{bmatrix} M_{cin}^0 \\ M_{cjn}^0 \end{bmatrix}$$

For the first story columns $\theta_{jn}(t) = u_{ln}(t) = 0$.

- Column axial forces

Using statics, compute $P_{ci}(t) =$ axial force on the ith story column from the moments on the end of the beams on the stories above.

On the kth story:

$$P_{ckn}(t) = \frac{1}{2h}\left(M_{bin}(t) + M_{bjn}(t) \right) + P_{c\;\,k+1\;n}(t)$$

$$= \frac{1}{2h}\,\frac{EI}{h^2}\; Y_n(t)\left(M_{bin}^0 + M_{bjn}^0 \right) + P_c{}^0{}_{k+1\;n} \tag{B-29}$$

$$= \frac{EI}{h^3}\; Y_n(t)\left(P_{ckn}^0 + P_c{}^0{}_{k+1\;n} \right)$$

where M^{0}_{bin} and M^{0}_{bjn} are the end moments of the beam on the kth story.

Equations (B-22) through (B-29) define each of the unit modal responses r^{0} in terms of the original nondimensional stiffness and mass matrices and the invariant mode shapes. The values of $Y_n(t)$ were computed as described before (Section B.5) and since the structure characteristics (E, I, h, m) were not included in the formulation the actual responses computed were just $Y_n(t)\, r^{0}$ which automatically includes part of the normalization used for the response quantities.

Taking advantage of the invariance of the unit modal responses r_n^{0} when the fundamental period T_1 changes, they were computed in advance for each ρ case and then used for each of the different fundamental period cases considered, avoiding in this form a considerable amount of numerical computations. To include the rather special normalization used for story shears and overturning moments the values of the first mode effective weight and height W_1^{*} and h_1^{*} were also compute --only once for each ρ case-- and included in the corresponding unit modal responses. From the definitions of W_1^{*} and h_1^{*}

$$W_1^{*} = g\ \frac{L_1^{2}}{M_1} = g\ \frac{m^{2}\, L_1^{0\,2}}{m\ M_n^{0}} = m\ g\ W_1^{*0} \tag{B-30}$$

$$h_1^{*} = \frac{\mathbf{h}^{T}\ \mathbf{m}\ \boldsymbol{\phi}_1}{M_1} = \frac{h\ m\ \mathbf{h}^{0T}\ \mathbf{m}^{0}\ \boldsymbol{\psi}_1}{m\ M_1^{0}} = h\ h_1^{*0} \tag{B-31}$$

These quantities are incorporated in the definitions of $\mathbf{V}_n^{0}$ and $\mathbf{M}_n^{0}$ so that the only extra normalization needed to arrive at the response quantities presented in the results is to divide by $\bar{a}_g$ or $\bar{u}_g$, the maximum of the ground acceleration or the ground displacement, respectively.

Total response

The total response $r(t)$ for any response quantity r is obtained by adding the individual mode responses $r_n(t)$, then

$$r(t) = \sum_{n=1}^{N} r_n(t) \tag{B-32}$$

where N is the total number of modes considered. The values of $r(t)$ were computed at each step of te integration of the modal coordinates $Y_n(t)$.

Maxima of the responses

After each step in the numerical integration the values of the responses were checked against the previous maximum for the corresponding response and if necessary the maximum was updated.

B.6 Response spectrum analysis

Modal coordinates maxima

The maximum of the modal coordinates are computed directly from the accelerations response spectrum. The ordinates of which are considered known for the adequate values of period (frequency) and damping (5 percent in all cases). Then,

$$\overline{Y}_n = \left| -\frac{L_n}{M_n} \right| S_{dn}(\omega_n, \xi_n) = \left| -C_n \right| \frac{1}{\omega_n^2} S_{an}(\omega_n, \xi_n) \tag{B-33}$$

Modal response maxima

After the values for $\overline{Y}_n$ are known, the maxima of the modal responses can be obtained using the unit modal responses as defined in equations (B-22) through (B-29) in the corresponding expressions of the form

$$\overline{r}_n = \overline{Y}_n \; r_n^0$$

for each of the response quantities of interest.

Total response maxima

An estimate of the total response maxima can be obtained using the square-root-of-the-sum-of-the-squares (SRSS) combination rule. Then,

$$\bar{r} = \left[\sum_{n=1}^{N} \bar{r}_n^2 \right]^{1/2} \tag{B-34}$$

B.7 Computer program outline

A complete, although not very detailed, flow chart of the computer program developed to carry out the computations described before is given in the following paragraphs. The program is written in FORTRAN (1966 standard) and is actually implemented on the CDC 7600 computer at the Lawrence Berkeley Laboratory Computer Center.

PROGRAM SPRPSTN

Read ρ parameter value

Form total stiffness matrix $\mathbf{k}_T^0$

Compute lateral stiffness matrix $\mathbf{k}^0$

Form mass matrix $\mathbf{m}^0$

Compute frequencies α_n^2 and mode shapes ψ_n

Compute unit modal responses r^0

Perform response history analysis (details follow)

Perform response spectrum analysis (details follow)

Go back for a new ρ case

RESPONSE HISTORY ANALYSIS PROCEDURE

Read number of ground motions to use

For each ground motion

Read ground acceleration time-history $a_g(t)$

Read number of fundamental period cases

Read array with fundamental period values T_1

For each fundamental period case

Compute actual mode frequencies $\omega_n = \omega_1(\alpha_n/\alpha_1)$

Select integration time step Δt

Perform numerical integration procedure (details follow)

Print results

NUMERICAL INTEGRATION PROCEDURE

Initialize state variables $Y_n(0)$, $\dot{Y}_n(0)$, $\ddot{Y}_n(0)$, $n = 1,\ldots,5$

Compute number of steps during the excitation

For each integration step

Compute increments ΔY_n, $\Delta \dot{Y}_n$, $\Delta \ddot{Y}_n$

Compute new state variables (at time $t + \Delta t$)

Compute modal responses $r_n(t)$

Compute total responses $r(t)$

Check for maxima of total responses $\bar{r}$

Compute number of steps after excitation ends

For each integration step

Compute increments (with zero excitation) ΔY_n, $\Delta \dot{Y}_n$, $\Delta \ddot{Y}_n$

Compute new state variables (at time $t + \Delta t$)

Compute modal responses $r_n(t)$

Compute total responses $r(t)$

Check for maxima of total responses $\bar{r}$

RESPONSE SPECTRUM ANALYSIS PROCEDURE

Read number of response spectra to use

For each response spectrum

Read number of fundamental period cases

Read array with fundamental period values T_1

For each fundamental period case

Compute actual mode frequencies $\omega_n = \omega_1 (\alpha_n / \alpha_1)$

Read spectral acceleration ordinates S_{an}

Compute modal maxima of responses $\bar{r}_n$

Estimate maxima of total response $\bar{r}$ by SRSS

Print results

REFERENCES

B.1 Newmark, N.M., "A Method of Computation for Structural Dynamics," *Journal of the Engineering Mechanics Division, ASCE,* Vol 85, No EM3, July, 1959, pp 67-94.

APPENDIX C: NOTATION

$\bar{a}_g$	maximum ground acceleration due to earthquake ground motion
$a_g(t)$	time-history of ground acceleration due to earthquake ground motion
E	modulus of elasticity
$f_{jn}(t)$	equivalent lateral force at jth floor level in nth natural vibration mode
$\mathbf{f}_n(t)$	time-history of vector of equivalent lateral forces $f_{jn}(t)$
$\bar{\mathbf{f}}_n$	vector of maximum equivalent lateral forces in the nth vibration mode
g	acceleration of gravity
h	story height
h_j	height from base to floor level j
h_n^*	effective height in the nth natural vibration mode
I_b	moment of inertia of beams
I_c	moment of inertia of columns
$\mathbf{k}$	stiffness matrix
L_b	length of beam
L_c	length of column
L_n	participation factor for the nth natural vibration mode
m_j	lumped mass at jth floor level
$\mathbf{m}$	mass matrix
M_n	modal mass in the nth natural vibration mode
M_0	base overturning moment
$\bar{M}_0$	maximum base overturning moment

$M_{on}(t)$	time-history of base overturning moment in nth mode
$\overline{M}_{on}$	maximum base overturning moment in nth mode
$\overline{M}_b$	maximum moment among all beams
$\overline{M}_c$	maximum moment among all columns
$\overline{M}_i$	maximum overturning moment at story i
N	total number of stories in the structure
$\overline{P}_c$	maximum axial force among all columns
$r(t)$	time-history of response quantity r
$\overline{r}$	maximum of response quantity r
$r_n(t)$	time-history of nth vibration mode contribution to response quantity r
$\overline{r}_n$	maximum of nth vibration mode component of response quantity r
S_a	pseudo-acceleration response spectrum
S_{an}	spectral pseudo-acceleration ordinate for nth natural vibration mode
S_d	displacement response spectrum
S_v	pseudo-velocity response spectrum
t	time variable
T_1	fundamental vibration period of a multi-degree of freedom system
T_n	natural vibration period in the nth mode
$\overline{u}_g$	maximum ground displacement due to earthquake ground motion
u_5	lateral displacement at fifth (top) floor level
$\overline{u}_5$	maximum lateral displacement at fifth (top) floor level
$\mathbf{u}_n(t)$	time-history of lateral displacements vector in nth vibration mode
$\overline{\mathbf{u}}_n$	vector of maximum lateral displacements in nth vibration mode

$\bar{v}_g$ maximum ground velocity due to earthquake ground motion

V_0 base shear

$\bar{V}_0$ maximum of base shear

$V_{0n}(t)$ time-history of base shear in nth mode

$\bar{V}_{0n}$ maximum of base shear in nth mode

$\bar{V}_i$ maximum of story shear at story i

W_n^* effective weight associated with the nth natural vibration mode

$Y_n(t)$, $\dot{Y}_n(t)$, $\ddot{Y}_n(t)$ time-history of nth modal coordinate and its time derivatives

1 vector with all components equal to 1

ξ_n damping ratio in the nth natural vibration mode

ρ beam-to-column stiffness ratio

ϕ natural vibration mode shape

ϕ_n nth natural vibration mode shape

ω natural vibration frequency in radians per second

ω_n nth natural vibration frequency

PART II

SIMPLIFIED PROCEDURES FOR ELASTIC ANALYSIS OF BUILDINGS

1. INTRODUCTION

While dynamic analysis procedures have been available for many years, the earthquake forces considered in the design of most buildings are computed by the Equivalent Lateral Force Method specified in the governing building code. However, the codes recommend dynamic analysis for unusual buildings, but generally do not provide enough guidance on when the code formulas should be abandoned in favor of dynamic analysis, whether the dynamic response should be determined by response history or response spectrum analysis, and how such analyses should be implemented. This is perhaps one of the major reasons why many building designers refrain from dynamic analyses, making them increasingly dependent on code formulas, thus perpetuating them further.

Another reason why dynamic analyses find only limited use in building design is that such analyses are much complicated in concept as well as implementation compared to the simple and readily usable code formulas. It should therefore be useful to develop simplified versions of dynamic analyses which are easier to implement than standard methods and provide results that are sufficiently accurate for the design of many buildings. With the availability of such a method, dynamic analysis could be conveniently used in the design of many buildings.

The objectives of Part II of this investigation are: (1) to review briefly the accuracy of response spectrum analysis (RSA) in comparison to response history analysis (RHA); (2) to present a simplified response spectrum analysis (SRSA) method and evaluate its accuracy; (3) to identify a hierarchy of four analysis methods: code-type formulas, SRSA, RSA, and RHA methods; and (4) to present criteria to decide the least complicated of these methods which would provide sufficiently accurate results for a particular design application.

This investigation is restricted to elastic analysis of planar vibration of buildings without any torsional effects. The SRSA method may however be applied to approximate, inelastic analyses in which the design forces and deformations are obtained by response spectrum

analysis of the structure based on an inelastic design spectrum instead of the elastic spectrum.

2. EVALUATION OF RESPONSE SPECTRUM ANALYSIS

In order to examine the contributions of various vibration modes of a building to its response and to evaluate the accuracy of the response spectrum analysis method, the maximum earthquake response of a class of multistory buildings is presented. The buildings analyzed are idealized as single-bay, five-story moment-resisting plane frames with mass and stiffness properties uniform over the height. The response of these idealized frames to eight simulated ground motions, for which the average response spectrum is presented in Figure 1, is determined. Standard procedures were employed for both the response history analysis (RHA) and the response spectrum analysis (RSA) of the dynamic response of the idealized frame to the simulated ground motions. The RHA was carried out by the mode superposition method, and the maximum of each of the response quantities of interest during each simulated motion was determined. The ensemble average of the maximum response was obtained by averaging the maximum values corresponding to each of the eight simulated motions. In the RSA the maximum value of each of the response quantities of interest was estimated as the square-root-of-the-sum-of-the squares (SRSS) combination of individual modal maxima, computed directly from the response spectrum of Figure 1.

The ensemble average of the maximum base shear, computed by the RHA method is plotted against the fundamental vibration period of the building in the form of response spectra. Four sets of plots obtained by considering 1,2,3 and all 5 modes, respectively, are presented in Figure 2. Response results are presented for three values of the beam-to-column stiffness ratio parameter ρ, representing a bending beam ($\rho = 0$), shear beam ($\rho = \infty$) and a frame. It is apparent that the significance of the responses contributions of the vibration modes higher than the fundamental mode increase with increasing fundamental vibration period T_1, and with decreasing value of the parameter ρ. However, over a useful range of fundamental vibration period T_1 and the stiffness ratio ρ, two vibration modes are sufficient to predict the earthquake response of the frame; over a restricted but still useful range of

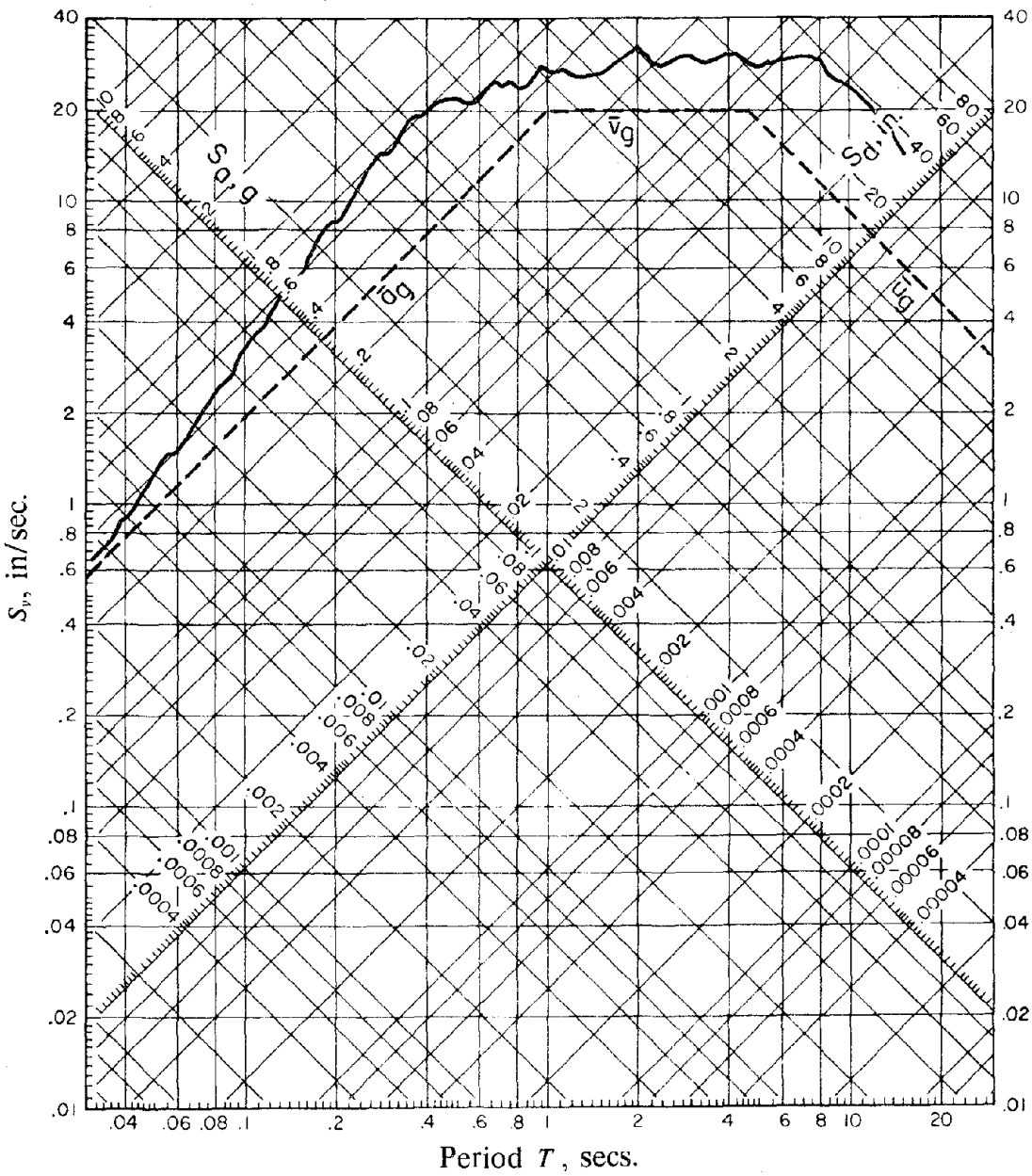

FIGURE 1 Average response spectrum (5% damping) for eight simulated earthquakes.

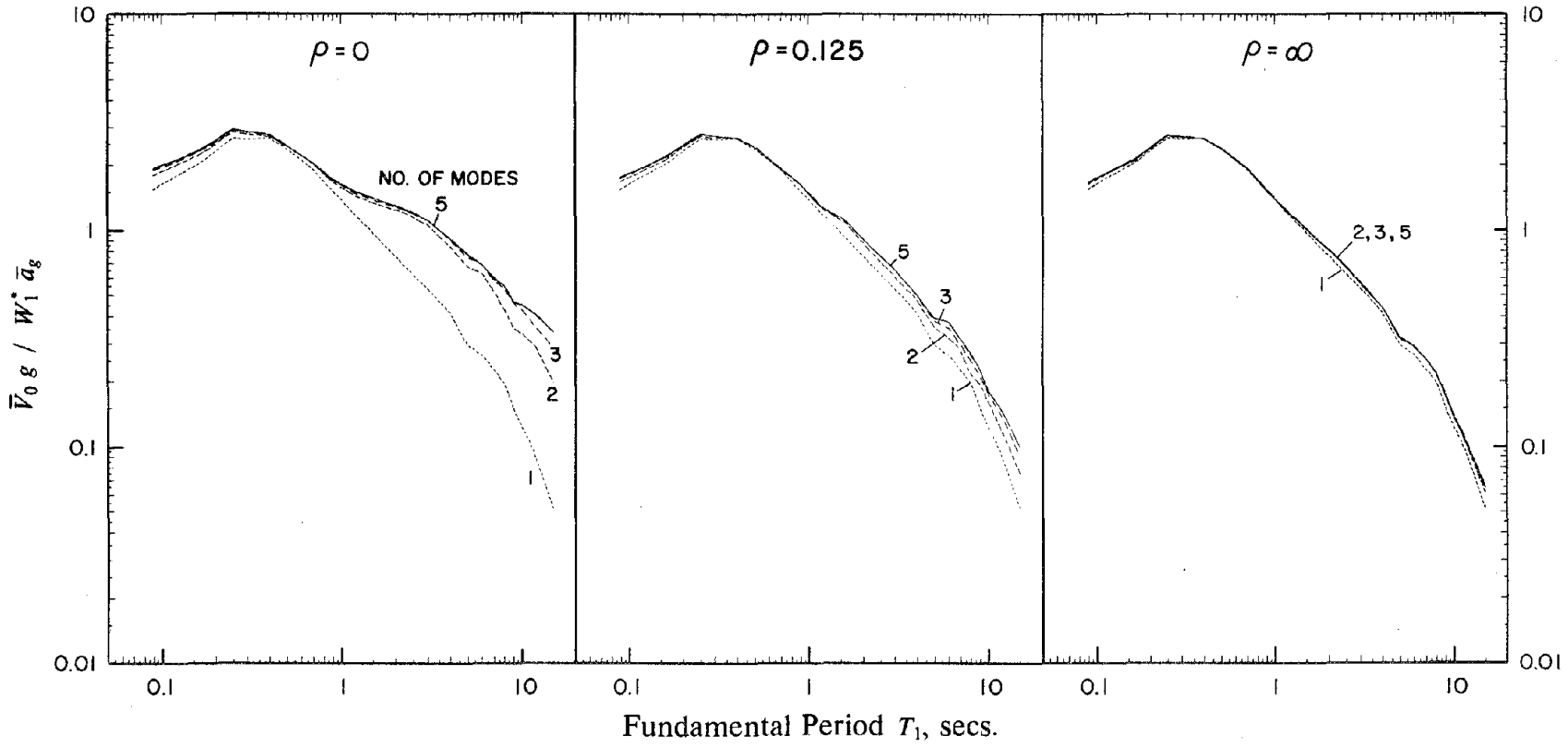

FIGURE 2 Ensemble average of base shear computed by response history analysis (RHA) considering 1, 2, 3, and 5 modes. Results are for Case 1: uniform 5-story frame.

parameters even one mode is adequate. These observations, based here on the response results for the base shear in the building, are also supported by the results for the other response quantities presented in Part I of this report.

The ensemble average of the maximum base shear, computed by including the contribution of all five vibration modes in the response history analysis (RHA) and in the response spectrum analysis (RSA) procedures is plotted against the fundamental vibration period of the building in the form of response spectra in Figure 3; also included in these plots is the maximum response due only to the fundamental vibration mode, which is obviously identical whether computed by RHA or RSA procedures. It is apparent that the differences between the RSA and the RHA results are closely related to the contributions of the higher vibration modes. These differences increase with increasing fundamental vibration period T_1 and with decreasing value of ρ.

The response spectrum for the base shear in the uniform five-story building frame computed by RHA and RSA methods was presented in Figure 2. The error response spectra showing the percentage error in the RSA results as a function of the vibration period for the six response quantities considered are presented in Figure 4. As indicated by these results and discussed in Part I, the response contributions of the vibration modes higher than the fundamental mode increase, and consequently the differences between the RHA and RSA results increase, with increasing fundamental period T_1 and with decreasing value of the stiffness ratio ρ. While the errors in the RSA results depend on the response quantity they are all below 15 percent for structures with vibration period less than the end of the velocity controlled region, which for the average spectrum of Figure 1 is eight seconds. Furthermore, the computed responses display some discrepancy between the RHA and the RSA results for very short periods, with the errors tending to increase as T_1 decreases in this range --to around 5 to 20 percent depending on the value of the ρ parameter.

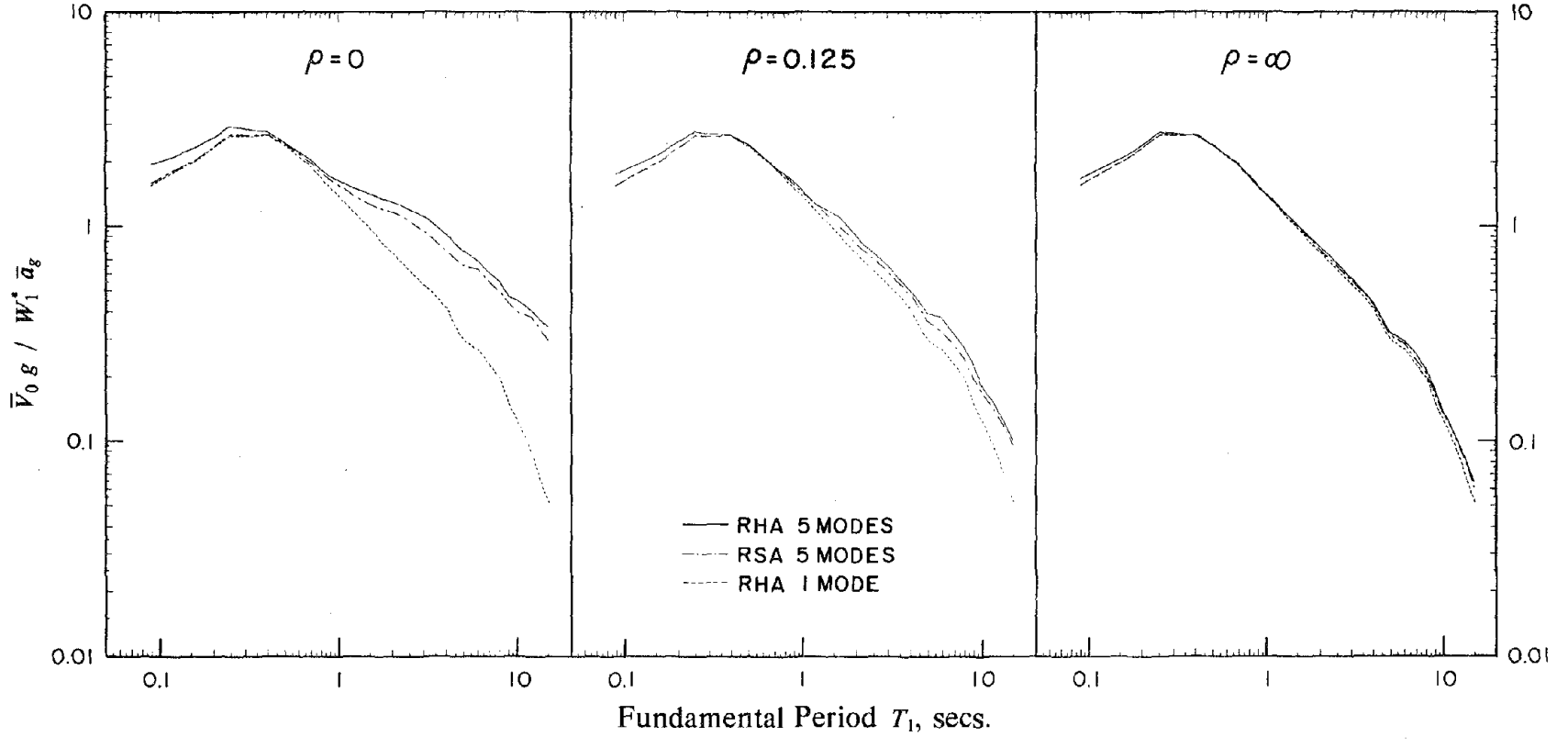

FIGURE 3 Comparison of ensemble average of base shear computed by RHA considering 1 and 5 modes and by response spectrum analysis (RSA) from average response spectrum. Results are for Case 1: uniform 5-story frame.

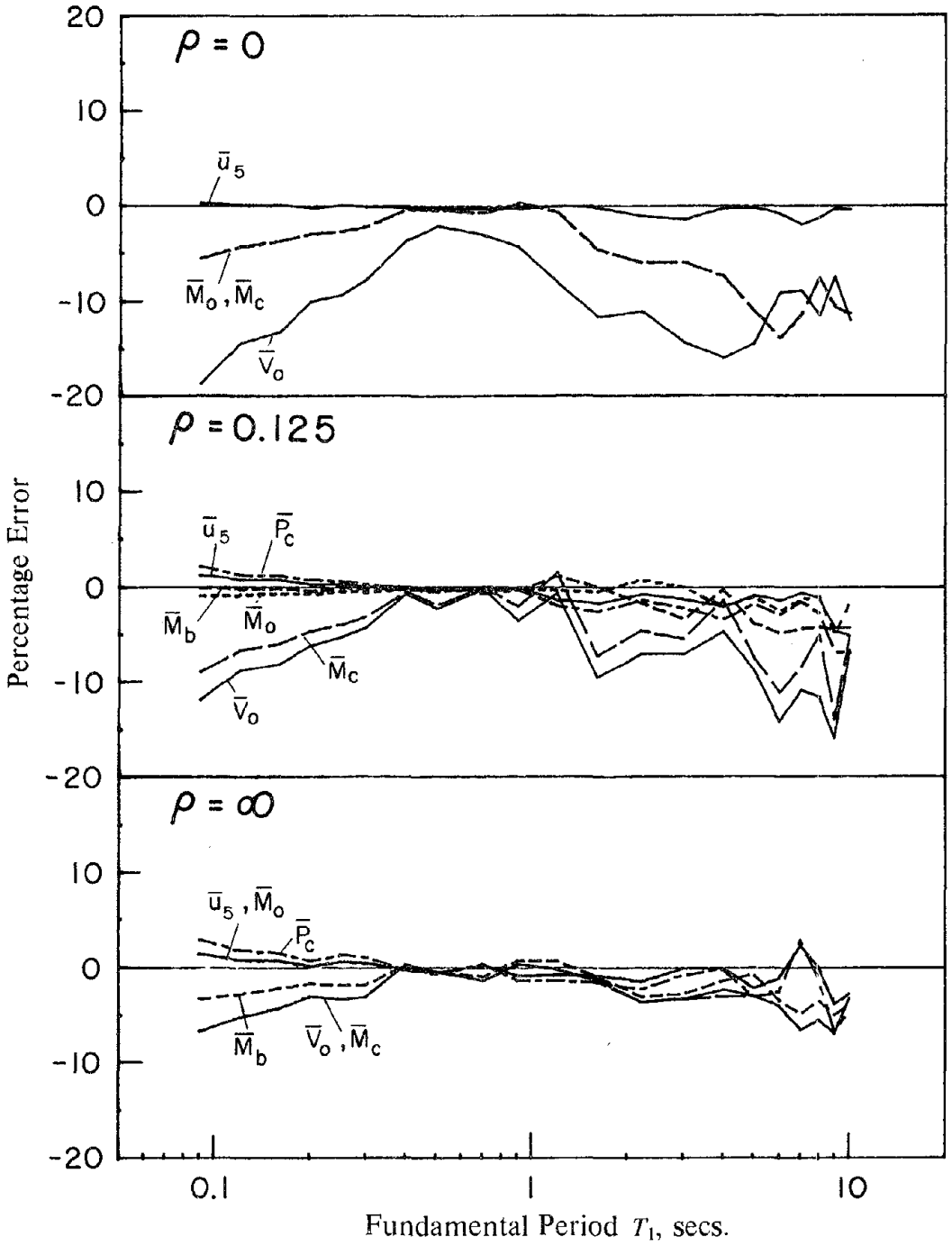

FIGURE 4 Percentage error in the responses computed by the response spectrum analysis (RSA) method, relative to ensemble average of response history analysis (RHA) results, for Case 1: uniform 5-story frame.

3. SIMPLIFIED RESPONSE SPECTRUM ANALYSIS

3.1 Response Spectrum Analysis

It is apparent from the preceding discussion that, over a useful range of fundamental vibration periods, the earthquake response of building frames may be satisfactorily estimated from the earthquake response spectrum by considering the contributions of only the first two modes of vibration; even the first mode alone is sufficient in many cases. The response spectrum analysis (RSA) procedure to estimate the maximum response is well known [5]. It is summarized here from [4] for convenient reference and to provide a basis for presenting the simplified version of the procedure:

1. Define the smooth elastic design spectrum for the structure at the particular site.
2. Define structural properties:
   (a) Compute mass matrix **m** for the building with its mass appropriately lumped at floor levels,
   (b) Compute the lateral stiffness matrix **k** of the building frame from the complete stiffness matrix by condensing out the vertical and rotational degrees of freedom at the joints,
   (c) Estimate modal damping ratios ξ_n.
3. Determine the first one or two, as necessary, natural frequencies ω_n (natural periods $T_n = 2\pi/\omega_n$) and the modes ϕ_n of vibration.
4. Compute the maximum response in individual modes of vibration by repeating the following steps for the first one or two, as necessary, modes of vibration:
   (a) Corresponding to period T_n and damping ratio ξ_n, read the pseudo-acceleration ordinate S_{an} of the elastic design spectrum of the earthquake ground motion,
   (b) Compute the effective weight W_n^* (or portion of the weight) of the building that participates in the nth mode of vibration from

$$W_n^* = \frac{\left[\sum_{j=1}^{N} w_j \ \phi_{jn}\right]^2}{\sum_{j=1}^{N} w_j \ \phi_{jn}^2} \tag{1}$$

where $w_j = m_j \ g$ is the weight at the jth floor level, ϕ_{jn} is the modal displacement of the jth floor, and N is the total number of floor levels. Also compute the effective height h_n^* from

$$h_n^* = \frac{\sum_{j=1}^{N} h_j \ w_j \ \phi_{jn}}{\sum_{j=1}^{N} w_j \ \phi_{jn}} \tag{2}$$

where h_j is the height from the base to the jth floor level.

(c) Compute the maximum values $\overline{V}_{0n}$ and $\overline{M}_{0n}$ of the base shear $V_{0n}(t)$ and base overturning moment $M_{0n}(t)$ from

$$\overline{V}_{0n} = \frac{S_{an}}{g} \ W_n^* \tag{3}$$

and

$$\overline{M}_{0n} = h_n^* \ \overline{V}_{0n} \tag{4}$$

(d) Compute the maximum value of the equivalent lateral force at the jth floor level from

$$\overline{f}_{jn} = \overline{V}_{0n} \ \frac{w_j \ \phi_{jn}}{\sum_{i=1}^{N} w_i \ \phi_{in}} \tag{5}$$

and repeat this computation for all floors.

(e) Compute the floor displacements, or deflections, due to the lateral forces $\overline{f}_{jn}$ from

$$\overline{u}_{jn} = \frac{1}{\omega_n^2} \ \frac{g}{w_j} \ \overline{f}_{jn} \tag{6}$$

and repeat this computation for all floors.

(f) Compute the maximum deformation (or drift) in the jth story from the floor displacements using

$$\overline{\Delta}_{jn} = \overline{u}_{jn} - \overline{u}_{j-1,n} \tag{7}$$

and repeat this computation for all stories.

(g) Compute internal forces (story shears, story overturning moments and member forces) by static analysis of the structure subjected to equivalent lateral forces $\overline{f}_{jn}$.

5. Determine an estimate of the maximum $\overline{r}$ of any response quantity (displacement of a floor, deformation in a story, shear or moment in a story, etc) by combining the modal maxima $\overline{r}_n$ for the response quantity in accordance with the square-root-of-the-sum-of-the-squares (SRSS) formula:

$$\overline{r} = \left[\sum_{n=1}^{N} \overline{r}_n^2 \right]^{1/2} \tag{8}$$

in which only the lower modes that contribute significantly to the total response need to be included in the summation.

The SRSS formula generally provides a good estimate of the maximum response for systems with well separated natural periods of vibration, a property typically valid for planar motion of a building. For structures with this property, the SRSS method provides results essentially identical to the CQC method [7]. However for very short fundamental periods --periods in the first third of the acceleration controlled region of the spectrum-- the maximum value of a response quantity is better estimated by the absolute sum combination of the modal maxima:

$$\overline{r} = \sum_{n=1}^{N} | \overline{r}_n | \tag{9}$$

since in that range of periods the modal responses are in phase and their maxima occur almost simultaneously (see Part I).

3.2 Computation of Natural Frequencies and Modes of Vibration

Among all the computational steps in the response spectrum analysis (RSA) procedure, the evaluation of the natural frequencies and modes of vibration of the structure is one of the most, if not the most, time consuming steps; analytically and conceptually it is the most complicated step. Computation of the vibration properties requires a solution of the matrix equation

$$\mathbf{k}\,\boldsymbol{\phi} = \omega^2\,\mathbf{m}\,\boldsymbol{\phi} \tag{10}$$

which in mathematical terminology defines an eigen-problem. For a N-DOF system, such as the idealized N-story building with mass lumped at floor levels, the mass and stiffness matrices are of order N. Solution of the eigen-problem leads to the N natural frequencies and modes of vibration: ω_n, $\boldsymbol{\phi}_n$, $n = 1,2, \cdots N$.

Many methods have been developed for computer analysis of the eigen-problem for complex structures such as multistory buildings. For many applications these procedures are overly complicated in the early stages of the structural design process. Furthermore computer programs may not be readily available, or the structural designer may not be experienced in their proper use. Thus there is a need for simplified procedures which are conceptually simple and can be implemented by the non-specialist in dynamics of structures on a pocket calculator. The Stodola and Rayleigh methods [2,5] are especially convenient for this purpose.

3.2.1 Fundamental Mode

The fundamental frequency and mode of vibration may be determined by the Stodola method, which is presented here in a form especially suited for multi-story buildings with masses lumped at the floor levels:

1. Compute the earthquake forces specified by the governing building code, e.g. the Uniform Building Code [9], or by appropriate design recommendations, e.g. the equivalent lateral force procedure in the ATC-3 design provisions [1]. The earthquake force at the jth floor

level is F_j.

2. Develop a preliminary design of the building to resist the forces computed in step 1, along with dead and live loads specified by the code.

3. By static structural analysis, compute lateral displacements $\hat{U}_j$ at all floors due to the code earthquake forces F_j acting simultaneously at all the floor levels. This requires solution of the static equilibrium equations

$$\mathbf{k}\,\hat{\mathbf{U}} = \mathbf{F} \tag{11}$$

Normalize the computed displacements by dividing them by the top (Nth) floor displacement:

$$U_j = \hat{U}_j / \hat{U}_N \tag{12}$$

The displacement at any other floor or any convenient reference value, such as the largest of all floor displacements, may be used to normalize the computed displacements.

4. Compute the distribution of inertia forces associated with the deflected shape from step 3:

$$f_j = m_j U_j \tag{13}$$

5. Compute lateral displacements $\hat{u}_j$ at all floors by static analysis of the building subjected to forces f_j applied simultaneously at all floor levels. Normalize the computed displacements by dividing them by the top (Nth) floor displacement

$$u_j = \hat{u}_j / \hat{u}_N \tag{14}$$

6. Compare displacement vectors $\mathbf{U}$ (consisting of floor displacements U_j) used in step 4 and $\mathbf{u}$ (consisting of floor displacements u_j) computed in step 5. If they do not agree to a desired degree of accuracy, repeat steps 4 and 5 with previous values of U_j replaced by u_j computed in step 5. After a few such iterative repetitions, the two vectors will agree to a sufficient degree of accuracy. Then proceed to the next step.

7. The fundamental mode shape $\boldsymbol{\phi}_1$ is given by the displacement vector $\mathbf{u}$ computed in the final iteration cycle.

8. Compute the fundamental frequency ω_1 from

$$\omega_1^2 = 1/\hat{u}_N \tag{15}$$

or preferably from the Rayleigh quotient for $\boldsymbol{\phi}_1$

$$\omega_1^2 = \frac{\boldsymbol{\phi}_1^T \mathbf{k}\, \boldsymbol{\phi}_1}{\boldsymbol{\phi}_1^T \mathbf{m}\, \boldsymbol{\phi}_1} \tag{16}$$

At the expense of additional computational effort, the latter equation is more accurate and is consistent with the usage for the second mode to be described later.

3.2.2 Second Mode

As is well known and described in text books [2,5] the Stodola method can be modified to include a sweeping matrix to eliminate the first mode contribution in the deflected shape. With this modification introduced in each iteration cycle, the iterative process will converge to the second mode, leading to its vibration properties in a manner analogous to that described above for the fundamental mode. However, the contributions of the second vibration mode to building response are relatively small compared to those of the fundamental mode. Thus, it seems unnecessary to compute the vibration properties of the second mode to a high degree of accuracy. Therefore we avoid the Stodola method with iteration in computing the vibration properties of the second mode. Instead we develop a simple procedure which directly -- without iteration-- provides a good approximation to the second vibration mode.

The deformation response $\mathbf{u}(t)$ of a multistory building with mass lumped at the floor levels subjected to ground motion will be identical to the response of the structure on fixed base subjected to external forces at each floor level equal to floor mass times the ground acceleration, acting opposite to the sense of ground acceleration ([4], page 61). The ground motion can therefore be replaced by effective forces $-m_j\, a_g(t)$, j = 1,2, ... N. Expressed in vector form these effective forces are:

$$\mathbf{p}(t) = -\mathbf{m}\, \mathbf{1}\, a_g(t) \tag{17}$$

where $\mathbf{1}$ is a vector with as many components as floor levels in the building, all equal to unity. The vector $-\mathbf{m}\,\mathbf{1}$ defines the spatial variation of the forces and the ground acceleration $a_g(t)$ defines their time variation. The effective forces can be expressed in terms of their modal components:

$$\mathbf{p}(t) = -\mathbf{m}\,\mathbf{1}\,a_g(t) = -a_g(t)\sum_{n=1}^{N}\frac{L_n}{M_n}\,\mathbf{m}\,\boldsymbol{\phi}_n \tag{18}$$

where

$$L_n = \boldsymbol{\phi}_n^T\,\mathbf{m}\,\mathbf{1} = \sum_{j=1}^{N} m_j\,\phi_{jn} \tag{19}$$

and the nth modal mass

$$M_n = \boldsymbol{\phi}_n^T\,\mathbf{m}\,\boldsymbol{\phi}_n = \sum_{j=1}^{N} m_j\,\phi_{jn}^2 \tag{20}$$

Because of orthogonality properties of the modes, dynamic forces defined by the nth term in the series of equation (18) cause response only in the nth mode and no other modes are excited. In particular, having determined the exact frequency and shape of the fundamental vibration mode, the response due to the fundamental mode accounts for the first term in the series. The spatial variation of remainder of the effective forces

$$\mathbf{p}_r = -\mathbf{m}\left(\mathbf{1}-\frac{L_1}{M_1}\,\boldsymbol{\phi}_1\right) \tag{21}$$

then provide an effective means to determine an approximation to ω_2 and $\boldsymbol{\phi}_2$, the frequency and shape of the second natural mode of vibration of the structure.

These approximate results $\widetilde{\omega}_2$ and $\widetilde{\boldsymbol{\phi}}_2$ can be determined by the following procedure:

1. By static structural analysis, compute lateral displacements u_{rj} at all floors due to the forces p_{rj} defined by equation (21) acting simultaneously at all the floor levels. This requires solution of the static equilibrium equations

$$\mathbf{k}\,\mathbf{u}_r = \mathbf{p}_r \tag{22}$$

2. Determine the approximate second mode shape $\widetilde{\phi}_2$ by normalizing the computed displacements by dividing them by a convenient reference value, say the top floor displacement u_{rN}: Thus the modal displacement at the jth floor is given by

$$\widetilde{\phi}_{j2} = u_{rj} / u_{rN} \tag{23}$$

3. Compute the second mode frequency from the mode shape using the Rayleigh quotient

$$\widetilde{\omega}_2^2 = \frac{\widetilde{\phi}_2^T \mathbf{k} \widetilde{\phi}_2}{\widetilde{\phi}_2^T \mathbf{m} \widetilde{\phi}_2} \tag{24}$$

Two useful properties of the approximate frequency $\widetilde{\omega}_2$ and mode $\widetilde{\phi}_2$ can be demonstrated (Appendix A): Firstly, the approximate frequency $\widetilde{\omega}_2$ is always larger than the exact value ω_2. Secondly, the approximate second mode shape $\widetilde{\phi}_2$ is orthogonal to the exact fundamental mode shape ϕ_1; and is a linear combination of the higher vibration modes ϕ_2, ϕ_3, ... ϕ_N with this combination dominated by the second mode.

The simplified procedure presented to determine an approximation to the second natural frequency and mode of vibration is closely related to the well known Rayleigh and Stodola methods. Traditionally, the Rayleigh method is applied to determine the fundamental vibration frequency from an assumed shape which is an approximation to the fundamental natural mode of vibration. In contrast, the Rayleigh method has been utilized here to determine the second natural frequency from an approximation $\widetilde{\phi}_2$ to the second mode shape determined as described above, an idea that has been mentioned earlier [2]. Alternatively, the simplified procedure may be viewed as a single iteration in the Stodola method to determine the second mode with the starting vector equal to unit value at all floors [2]. Both of these observations are further discussed in Appendix A.

The simplified procedure described above to determine $\widetilde{\phi}_2$ is similar (see Appendix A) to the recent procedure to develop a series of Ritz vectors for dynamic analysis [15]. However, the two procedures differ in the selection of the first vector. In this work it is selected as the exact first mode shape but as the static deflected shape due to lateral forces equal to the floor

masses in the Ritz method [15]. As a result, orthogonalization of the subsequent vectors through the stiffness matrix, which requires solution of a reduced eigen-problem, necessary in the Ritz Method is avoided in this work.

3.3 Simplified Response Spectrum Analysis

Procedures, which are conceptually simple and can be conveniently implemented on a pocket calculator, to determine the first two natural frequencies and modes of vibration of a building have been presented. Furthermore, as noted earlier the earthquake response of building frames over a useful range of periods can be estimated from the response spectrum for the ground motion by considering only the first two modes of vibration; even the first mode alone is sufficient in many cases. Combining these two ideas provides the basis for a simplified response spectrum analysis (SRSA) method. This method is the same as the RSA method for one or two modes presented in Section 3.1; wherein the vibration frequencies and modes are computed by procedures presented in Section 3.2.

Because the second mode shape is not computed exactly, equation (6) provides only an approximate relationship between lateral forces $\tilde{f}_{j2}$ and displacements $\tilde{u}_{j2}$. Thus the displacements computed contain the approximations inherent in the mode shape. In fact, $\tilde{\mathbf{f}}_2$ and $\tilde{\mathbf{u}}_2$ do not satisfy the equilibrium equation

$$\mathbf{k}\,\tilde{\mathbf{u}}_2 = \tilde{\mathbf{f}}_2 \tag{25}$$

but instead they satisfy the quadratic form

$$\tilde{\mathbf{u}}_2^T\,\mathbf{k}\,\tilde{\mathbf{u}}_2 = \tilde{\mathbf{u}}_2^T\,\tilde{\mathbf{f}}_2 \tag{26}$$

a result of computing $\tilde{\omega}_2$ from equation (24).

4. EVALUATION OF THE SRSA METHOD

4.1 Systems Considered

The rectangular plane frames analyzed in this study are idealized as single-bay, moment-resisting plane frames with constant story height $= h$, and bay width $= 2h$ (Figure 5). Only flexural deformations are considered in the members which are assumed to be prismatic. The modulus of elasticity E is the same for all members but the moments of inertia of beams I_b and columns I_c --same for both columns in any story-- may vary over the height, as in cases 3 to 5 of Figure 5, with the ratio of the two same in all stories. The mass of the structure is assumed to be concentrated at the floor levels and the rotational inertia is neglected. The damping ratio for all the natural modes of vibration is assumed to be 5 percent.

Each building frame shown in Figure 5 is completely characterized by two additional parameters: the period of the fundamental mode of vibration T_1 and a stiffness ratio ρ. The latter was originally [3] defined as the ratio of the sum of the stiffness of all the beams at the mid-height story of the frame to the summation of the stiffnesses of all the columns at the same story, i.e.

$$\rho = \frac{\sum_{beams} EI_b / L_b}{\sum_{columns} EI_c / L_c} \tag{27}$$

For the one-bay frames considered in this study, this parameter reduces to

$$\rho = I_b \ / \ 4 \, I_c \tag{28}$$

and it has the same value for all stories.

This parameter is a measure of the relative beam-to-column stiffness and hence indicates the degree of frame action. The extreme values of ρ, 0 and ∞, represent the following limiting cases of a frame respectively: flexural beam with the beams imposing no restraint to joint rotations; and a shear beam in which the joint rotations are completely restrained and deformations occur only through double curvature bending of columns. An intermediate value of ρ

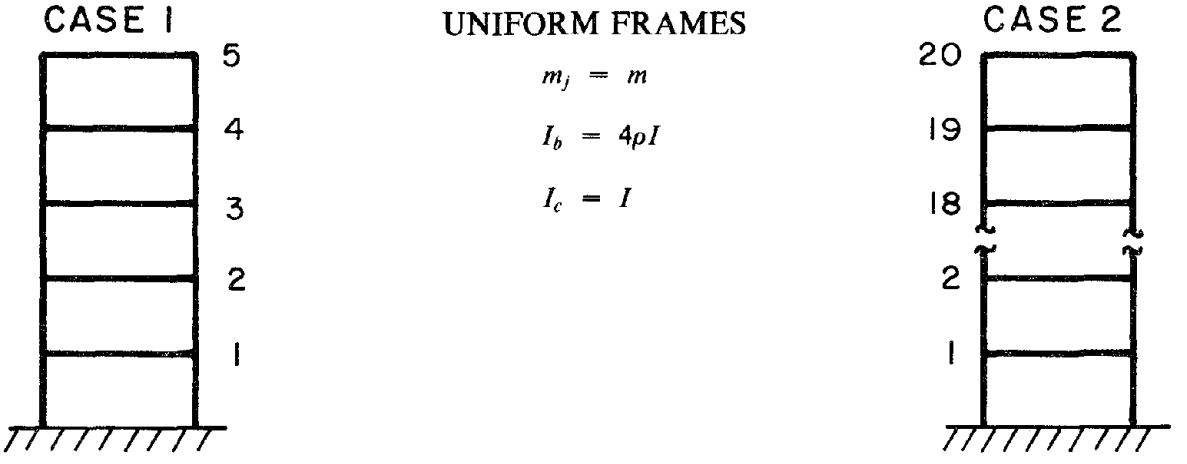

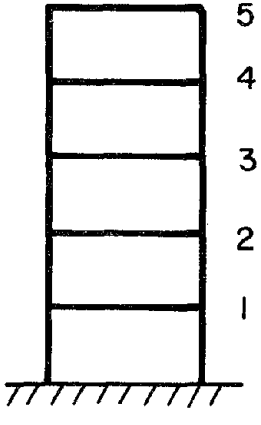

CASE 3			CASE 4			CASE 5		
m_j	I_b	I_c	m_j	I_b	I_c	m_j	I_b	I_c
m	$2\rho I$		$0.5m$	$2\rho I$		$0.3m$	$1.2\rho I$	
		$0.5I$			$0.5I$			$0.3I$
m	$3\rho I$		$0.75m$	$3\rho I$		$0.3m$	$1.2\rho I$	
		$0.75I$			$0.75I$			$0.3I$
m	$4\rho I$		m	$4\rho I$		$0.3m$	$1.2\rho I$	
		I			I			$0.3I$
m	$5\rho I$		$1.25m$	$5\rho I$		m	$4\rho I$	
		$1.25I$			$1.25I$			I
m	$6\rho I$		$1.5m$	$6\rho I$		m	$4\rho I$	
		$1.5I$			$1.5I$			I

FIGURE 5 Stiffness and mass characteristics for 5 one-bay frame cases. All frames have constant story height h and bay width $2h$.

represents a frame in which beams and columns undergo bending deformations with joint rotation.

The effective weights W_1^* and W_2^* for the first two vibration modes ([4], page 84), expressed as fraction of the total weight of the building are presented in Table 1. Both exact and approximate values, W_2^* and $\widetilde{W}_2^*$, for the second mode are included.

4.2 Earthquake Design Spectrum

All the building frames are analyzed for the earthquake input characterized by the smooth design spectrum of Figure 6. This spectrum is developed by well established procedures [10] for excitations with maximum ground acceleration $\bar{a}_g$, velocity $\bar{v}_g$, and displacement $\bar{u}_g$ of 1g, 48 in/sec, and 36 in, respectively. With this data and from the shape of the design spectrum it is apparent that the maximum response of short period structures is controlled by the ground acceleration, that of long-period structures by the ground displacement, and that of medium period structures by the ground velocity [13,14]. Thus the spectrum can be subdivided into acceleration-controlled or short-period, velocity-controlled or medium-period, and displacement-controlled or long-period regions as shown in Figure 6 [14]. Amplification factors for the acceleration-, velocity- and displacement-controlled regions were taken from [10] for 84.1 percentile response and 5 percent damping ratio to construct the spectrum shown in Figure 6. It will be shown in later sections of this part of the study that the quality of the results from the approximate methods of analysis can be correlated to the relative position of the fundamental period of the structure with respect to the different regions of the spectrum just defined.

4.3 Vibration Frequencies and Mode Shapes

In the SRSA method, the natural frequency and shape of the fundamental mode of vibration are computed by the Stodola method. By performing a sufficient number of iterations, these vibration properties can be computed almost exactly. On the other hand, no attempt is

Table 1: Modal effective weights for different frame models.

Frame Case	ρ	$\frac{W_1^*}{W}$	$\frac{W_2^*}{W}$	$\frac{\tilde{W}_2^*}{W_2^*}$	$\frac{W_1^* + \tilde{W}_2^*}{W}$
1	0	0.6787	0.2063	1.0936	0.9043
	0.125	0.7963	0.1175	1.2409	0.9422
	∞	0.8795	0.0872	1.2282	0.9866
2	0	0.6287	0.1930	1.0990	0.8408
	0.125	0.7998	0.0918	1.3366	0.9225
	∞	0.8300	0.0915	1.3311	0.9518
3	0	0.6557	0.2034	1.1160	0.8827
	0.125	0.7405	0.1420	1.2500	0.9180
	∞	0.8043	0.1213	1.3347	0.9665
4	0	0.5786	0.2468	1.1410	0.8602
	0.125	0.7005	0.1654	1.2910	0.9141
	∞	0.8056	0.1343	1.2800	0.9775
5	0	0.4568	0.3621	1.0665	0.8430
	0.125	0.5600	0.3122	1.0980	0.9028
	∞	0.6583	0.2983	1.0609	0.9728

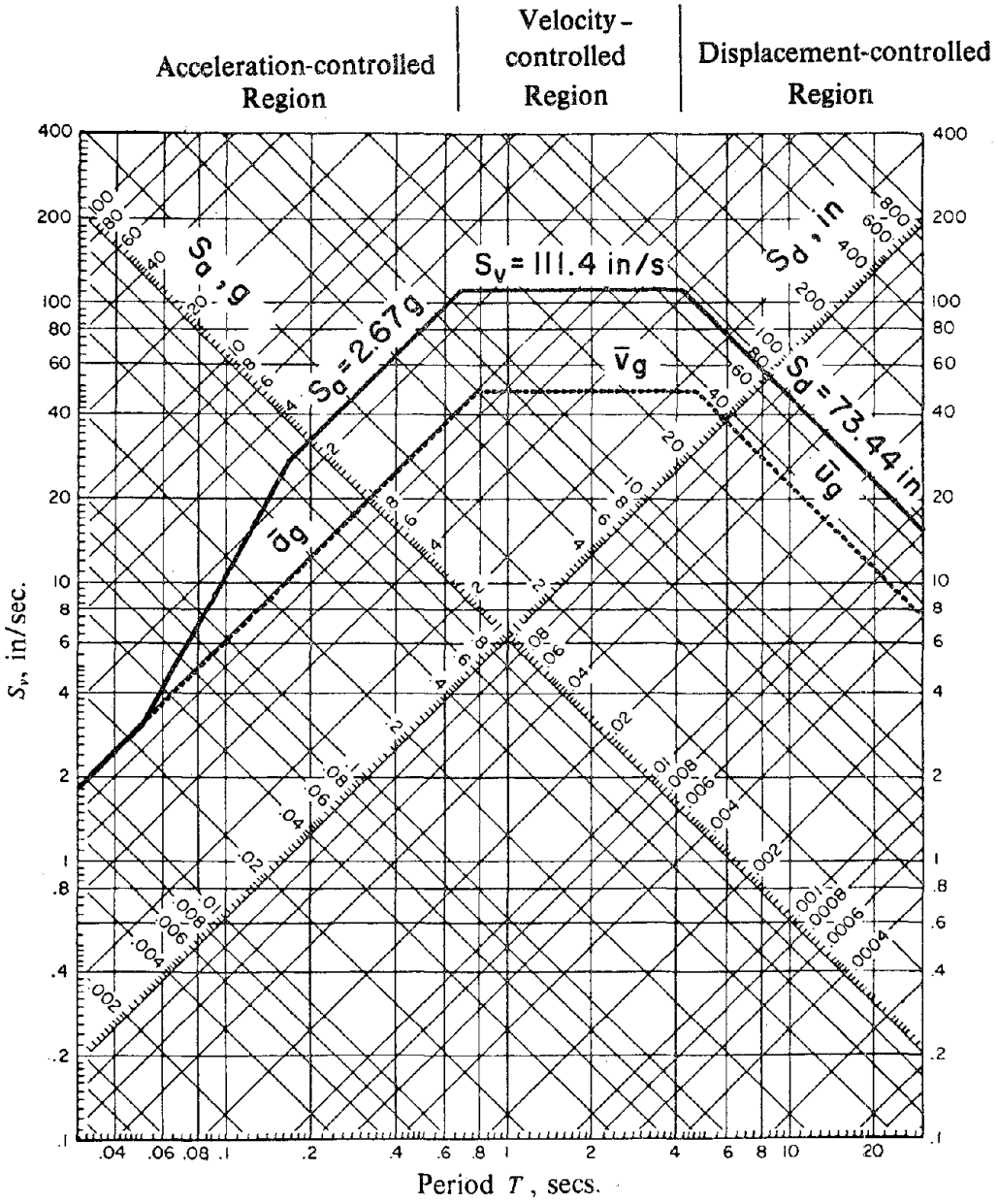

FIGURE 6 Design spectrum for ground motions with maximum ground acceleration $\bar{a}_g$ = 1g, velocity $\bar{v}_g$ = 48 in/sec, and displacement $\bar{u}_g$ = 36 in; damping = 5%.

made in the SRSA method to exactly compute the natural vibration frequency and shape of the second vibration mode. The approximate results obtained by this procedure are compared in Figure 7 with the exact frequency and shape of the second vibration mode obtained by computer analysis of the eigen-problem. Considering the simplicity of the SRSA procedure, the quality of the approximate results is surprisingly good, which indicates that the SRSA procedure should be very useful in practical application

4.4 Earthquake Responses

4.4.1 Overall and Local Response Quantities

The maximum response, computed by the RSA procedure --wherein the contribution of all the natural vibration modes of the frame are included-- and by the SRSA procedure, is plotted against the fundamental vibration period of the frame in the form of response spectra. Such plots are presented in Figures 8 to 13 for the uniform five-story frame (Case 1) for three values of $\rho = 0$, 0.125, and ∞ and six response quantities: top floor displacement $\overline{u}_N$, base shear $\overline{V}_0$, base overturning moment $\overline{M}_0$, the largest moment $\overline{M}_b$ among all the beams, the largest moment $\overline{M}_c$ among all the columns, and the largest axial force $\overline{P}_c$ among all the columns. The response quantities are presented in dimensionless form as defined in Figures 8 to 13, where $\overline{u}_g$ and $\overline{a}_g$ are the maximum ground displacement and acceleration, respectively; W_1^* and h_1^* are the effective weight and height, respectively, for the first vibration mode of the building (Section 3.1, see also [4]). The values chosen to non-dimensionalize $\overline{V}_0$ and $\overline{M}_0$ are the base shear and moment for a rigid single-degree-of-freedom system with lumped weight W_1^* and height h_1^*.

It is obvious from Figures 8 to 13 that the responses of the uniform five-story frame (Case 1) computed by the SRSA method are very close to those from the RSA method. For purposes of evaluating the SRSA method, the response results obtained by the RSA are treated as exact, because that is the best that can be expected from the SRSA method. As discussed later the RSA results themselves contain errors in the sense that they are not

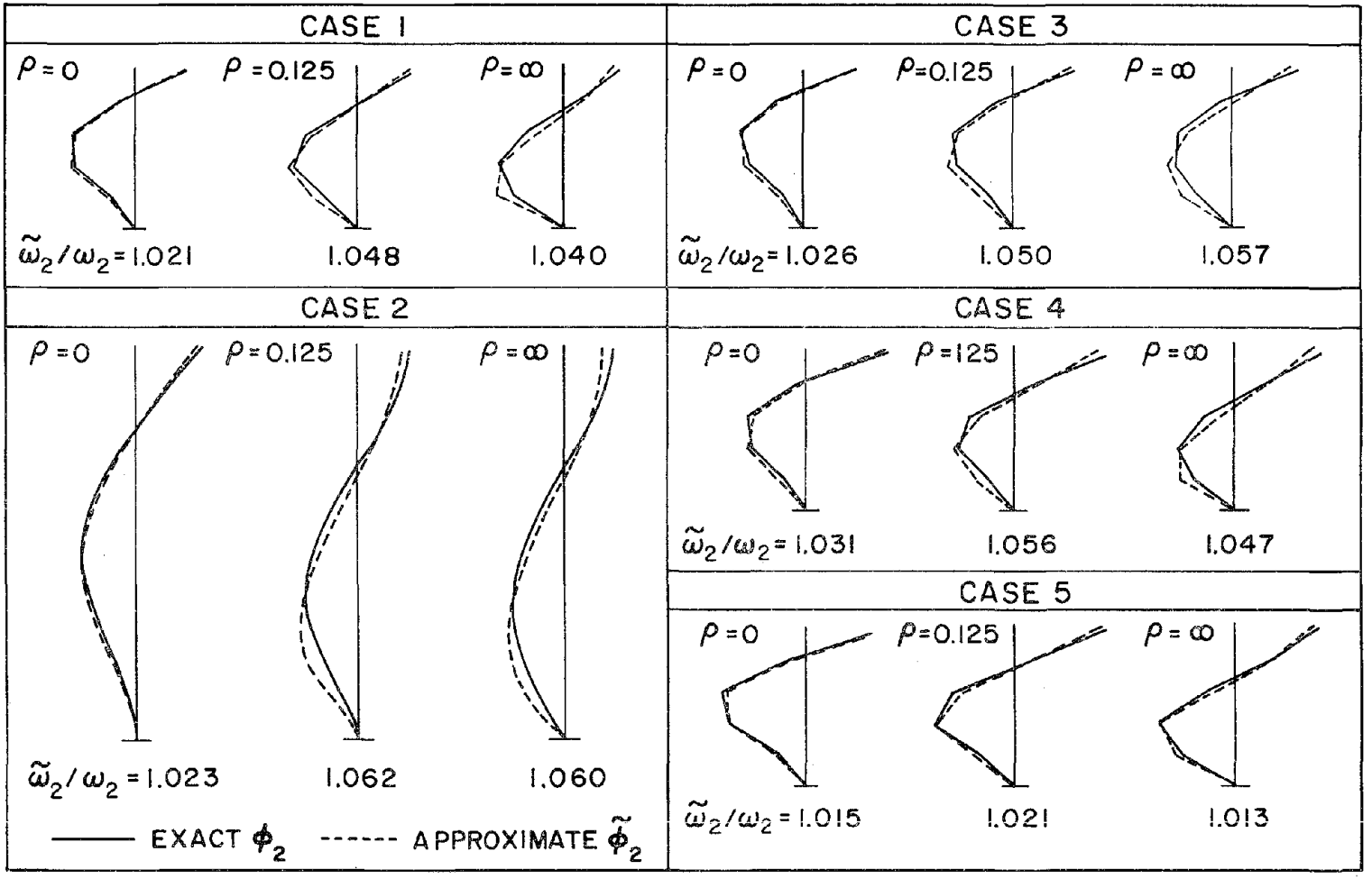

FIGURE 7 Comparison of exact and approximate values for the frequency (ω_2 and $\tilde{\omega}_2$) and shape (ϕ_2 and $\tilde{\phi}_2$) for the second vibration mode.

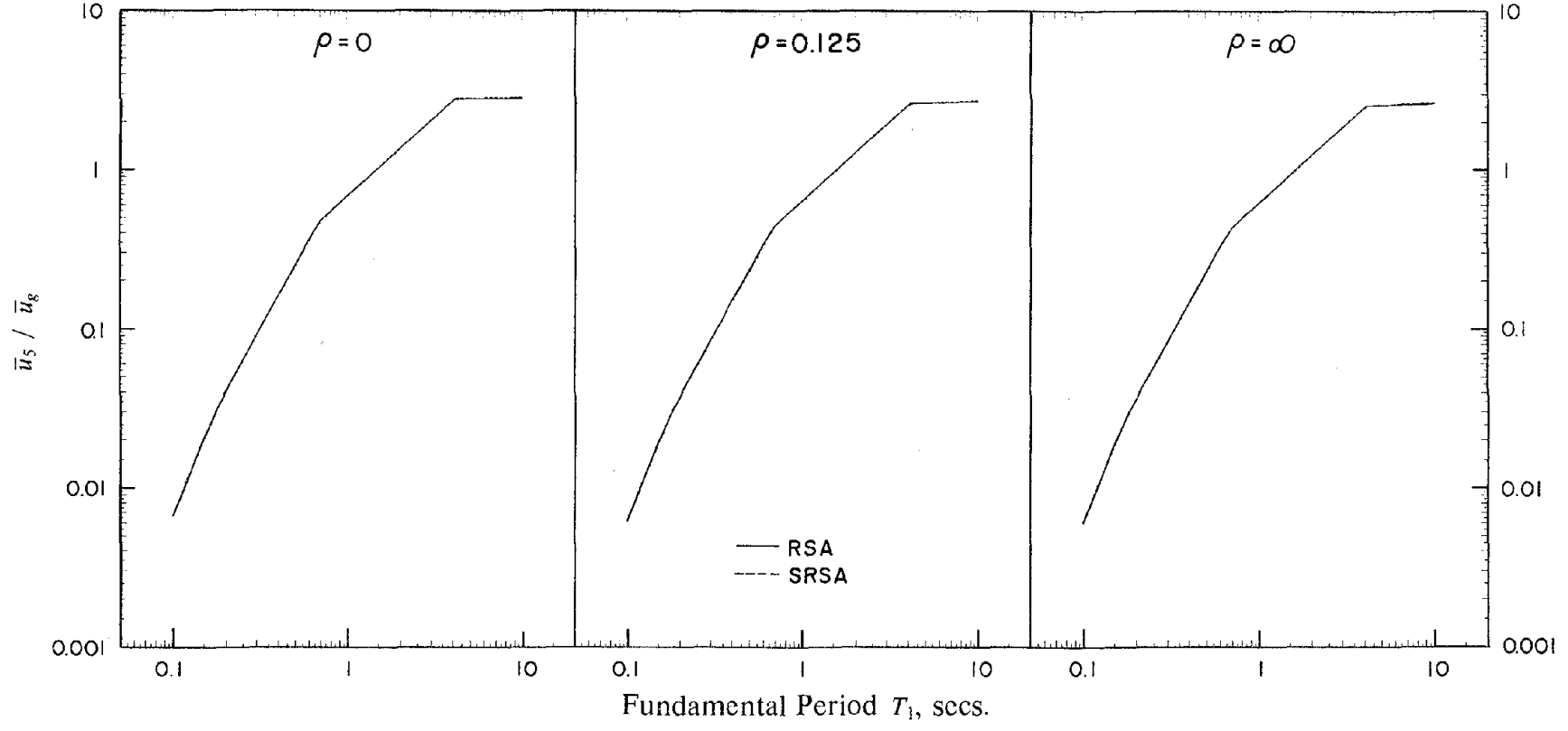

FIGURE 8 Comparison of maximum top-story displacement values computed by response spectrum analysis (RSA) and simplified response spectrum analysis (SRSA) methods. Results are for Case 1: uniform 5-story frame.

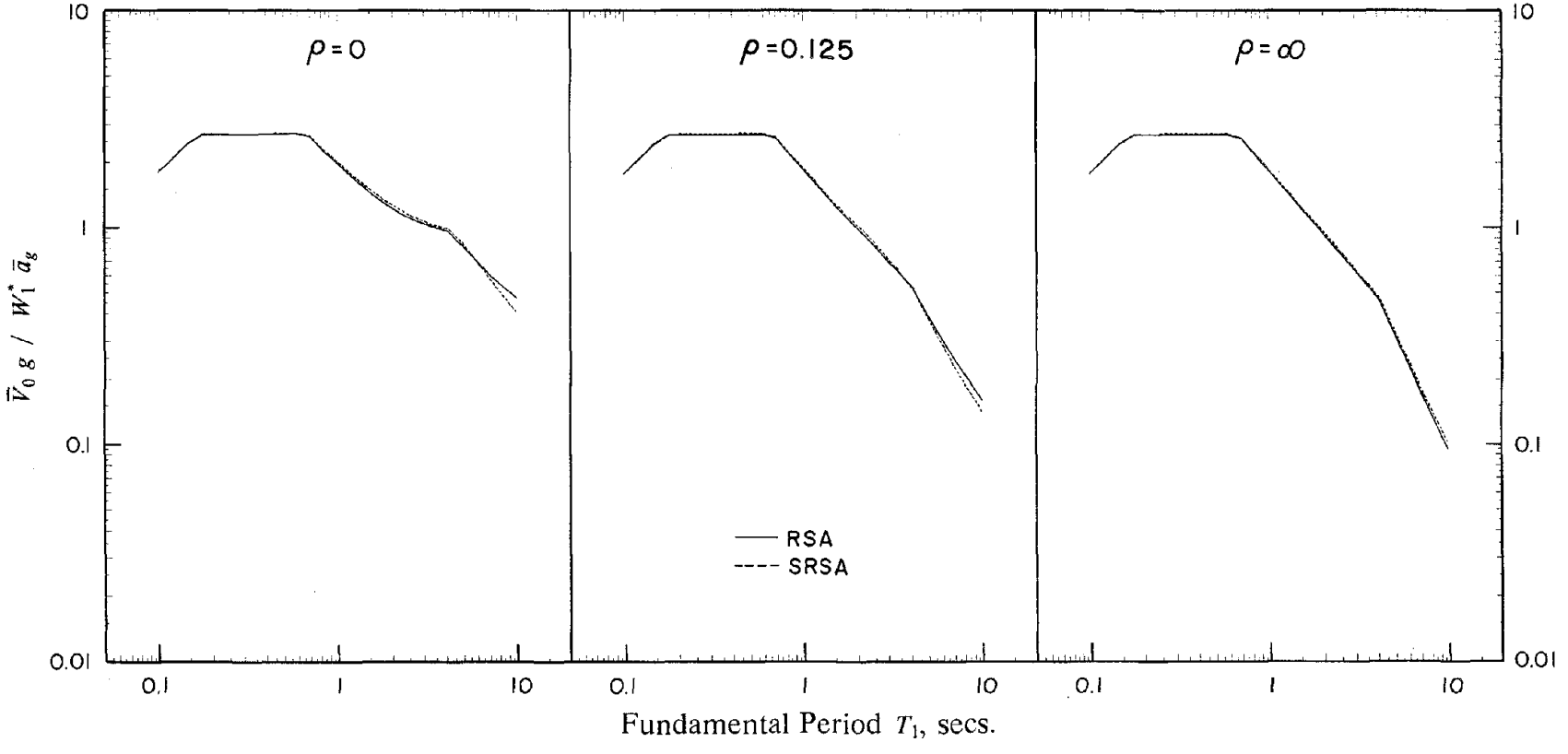

FIGURE 9 Comparison of maximum base shear values computed by RSA and SRSA methods.

Results are for Case 1: uniform 5-story frame.

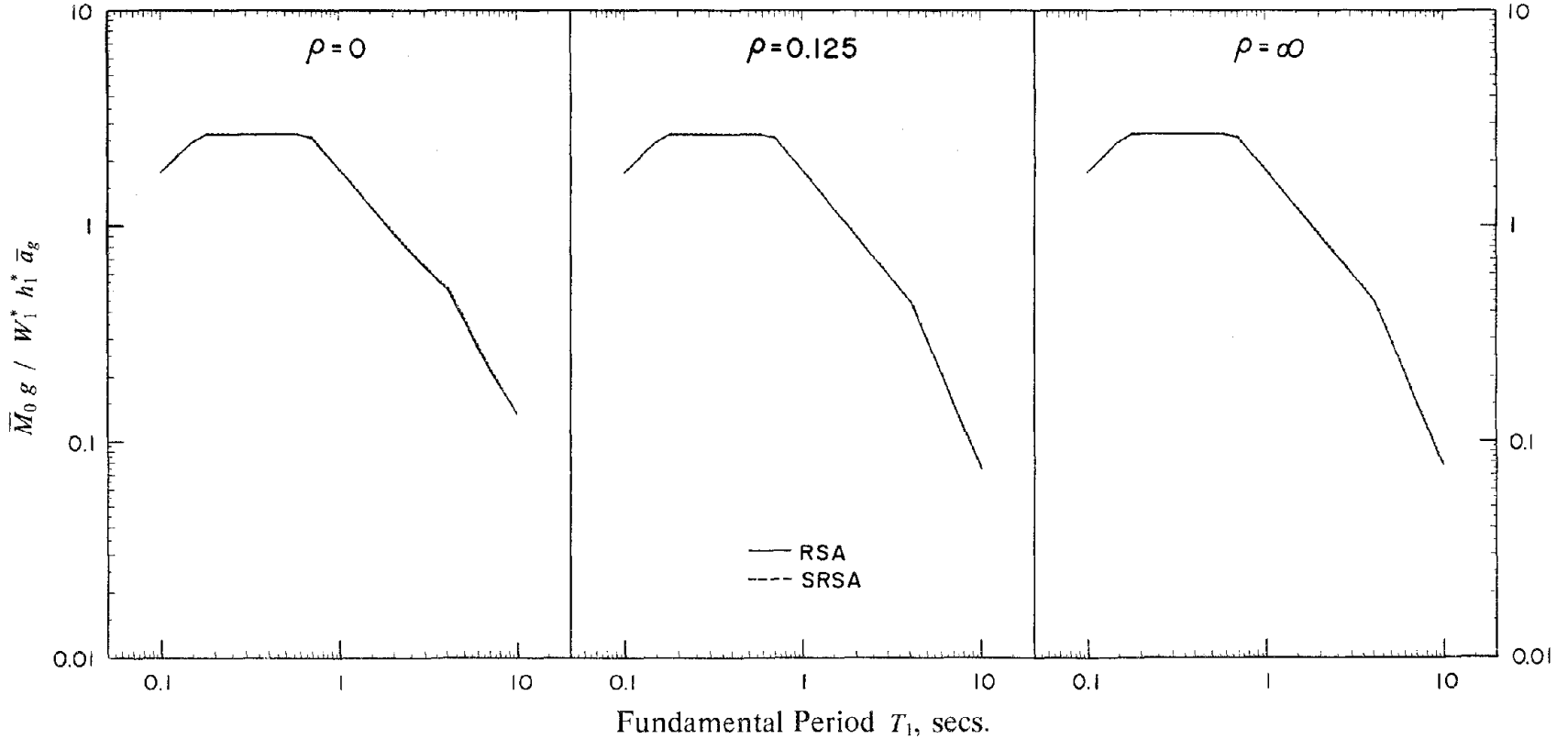

FIGURE 10 Comparison of maximum base overturning moment values computed by RSA and SRSA methods. Results are for Case 1: uniform 5-story frame.

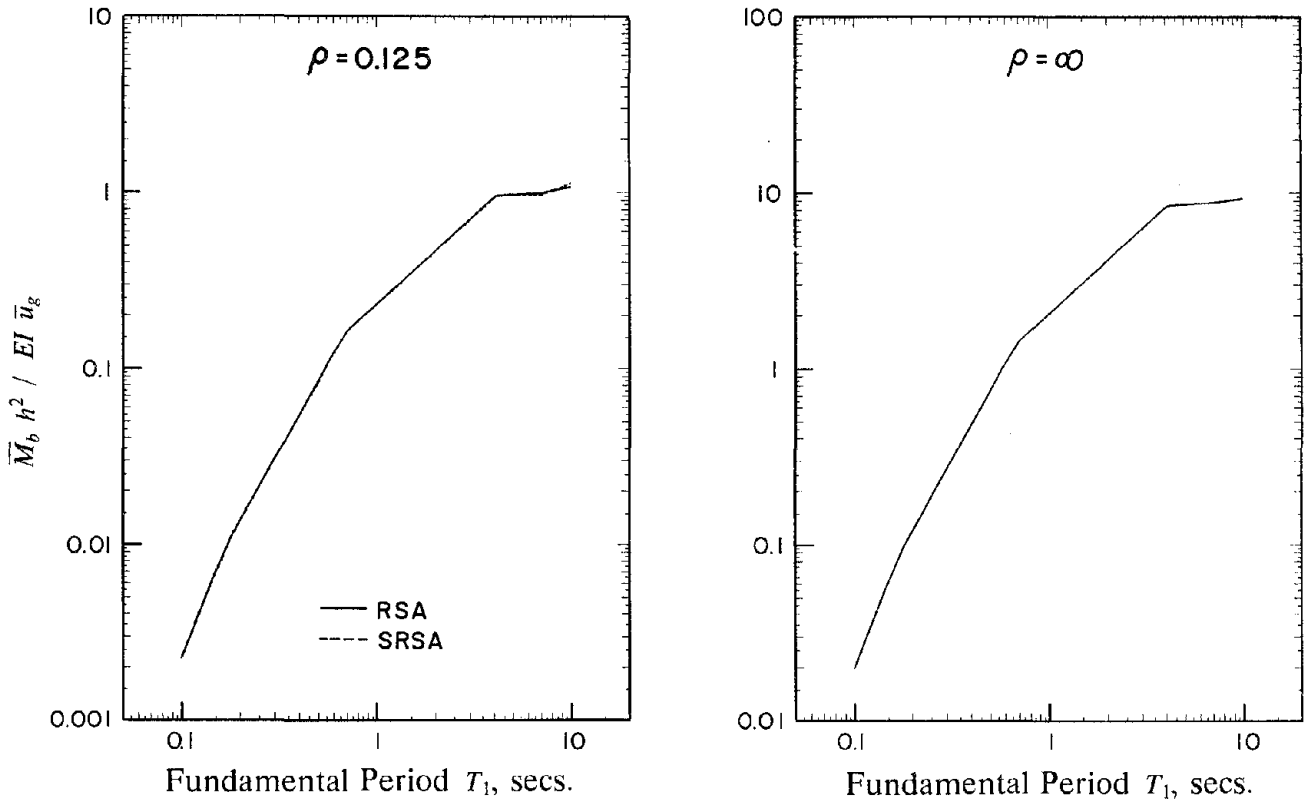

FIGURE 11 Comparison of maximum beam moment values computed by RSA and SRSA methods. Results are for Case 1: uniform 5-story frame.

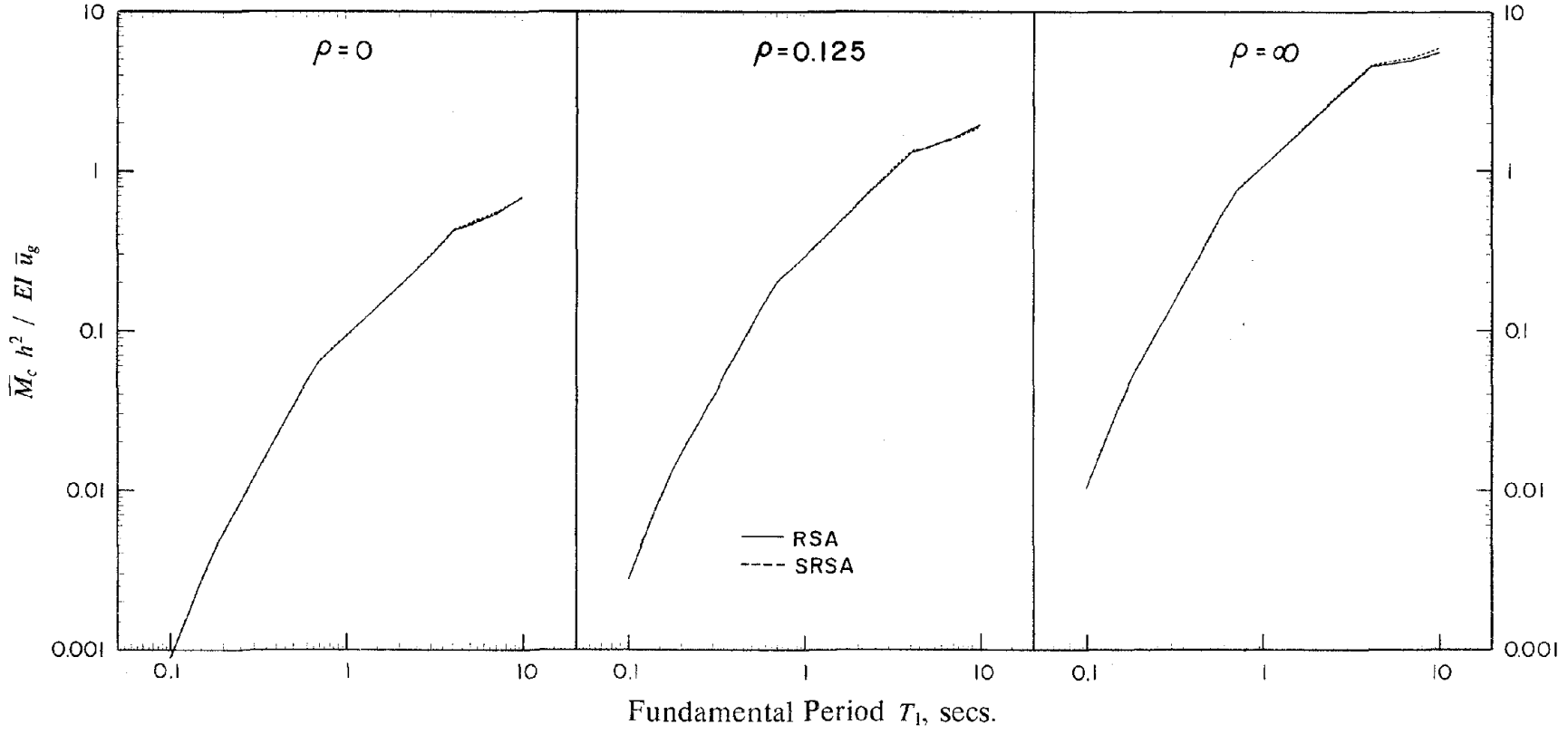

FIGURE 12 Comparison of maximum column moment values computed by RSA and SRSA methods. Results are for Case 1: uniform 5-story frame.

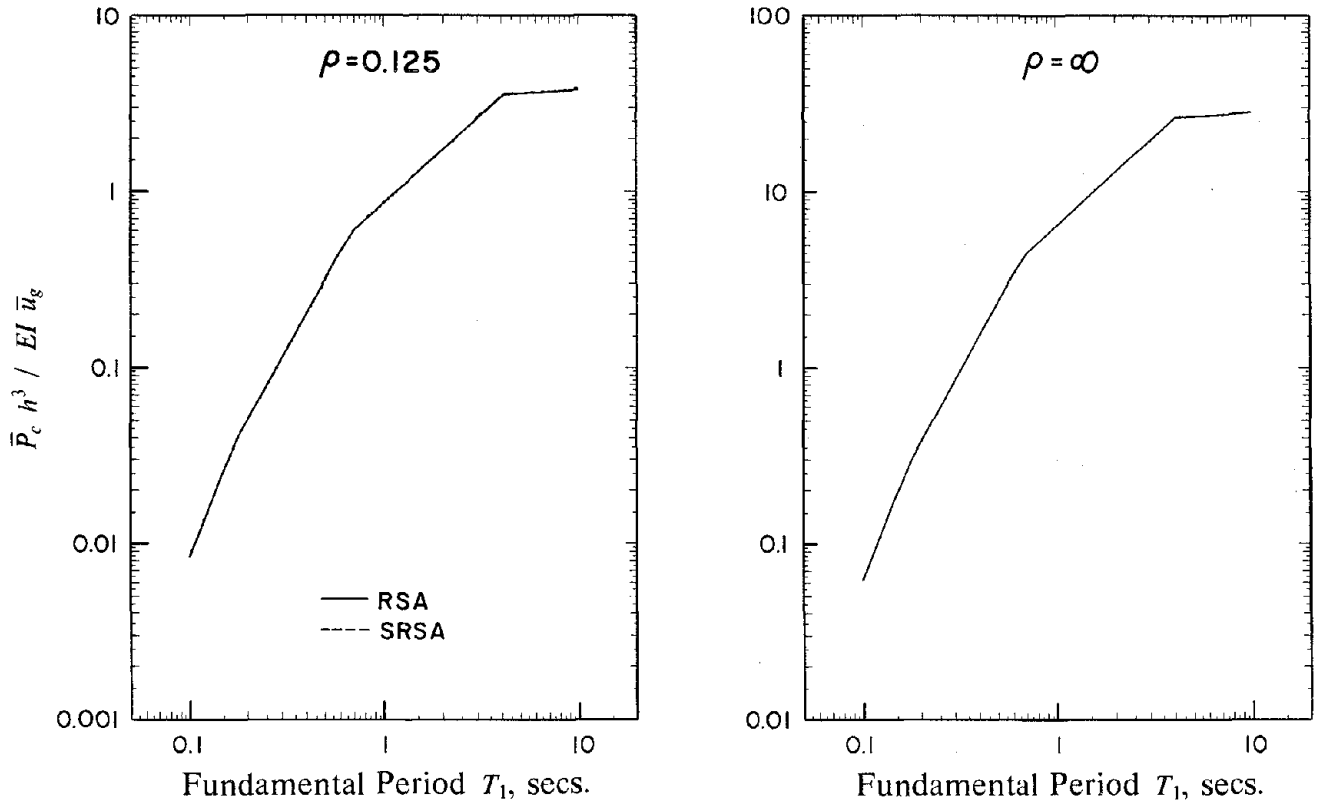

FIGURE 13 Comparison of maximum column axial force values computed by RSA and SRSA methods. Results are for Case 1: uniform 5-story frame.

identical to the exact, response history analysis results. The percentage error, defined as the difference in the responses computed by the two methods and divided by the RSA response value, is presented in Figures 14 to 19, along with similar results for the other cases presented in Figure 5. Positive error indicates that the response computed by the SRSA method exceeds that computed by the RSA method.

Figures 14 to 19 lead to the following observations: The errors in the SRSA results tend to increase with increasing fundamental vibration period T_1, and with decreasing stiffness ratio ρ. This increase in error is closely related to the contributions of the vibration modes higher than the fundamental mode, which as shown in Part I and in [11], increase with increase in T_1 and decrease in ρ. The errors in the SRSA results tend to be larger in buildings with nonuniform variation of mass or stiffness or both over height (Cases 3, 4, and 5) compared to uniform buildings (Cases 1 and 2). As indicated by comparison of Cases 1 and 2, the errors in the SRSA results tend to be larger for the taller buildings. While the errors in the SRSA results depend on the response quantity and on the height-wise distribution of the mass and stiffness and on the height of the frame, the errors are all below about 5 percent for frames with fundamental vibration period T_1 shorter than about 4 seconds, the value corresponding to the end of the velocity-controlled region on the response spectrum (Figure 6). However, the errors can increase to more than 20 percent for T_1 around 10 seconds (Figure 15) but for most cases and response quantities they are less than 5 percent even at this very long period. Among the overall response quantities, the largest errors occur in the base shear values, with much smaller errors in the base overturning moment, and almost no errors in the top floor displacement. Among the local response quantities, the errors in the column axial forces are very small; the larger errors in column moments and beam moments are similar in magnitude but are smaller than in base shear.

The SRSA method may lead to responses smaller or larger than those from the RSA method, depending on T_1, ρ, and the response quantity. This behavior is related to the relative importance of the modes higher than the second mode which are not considered in the

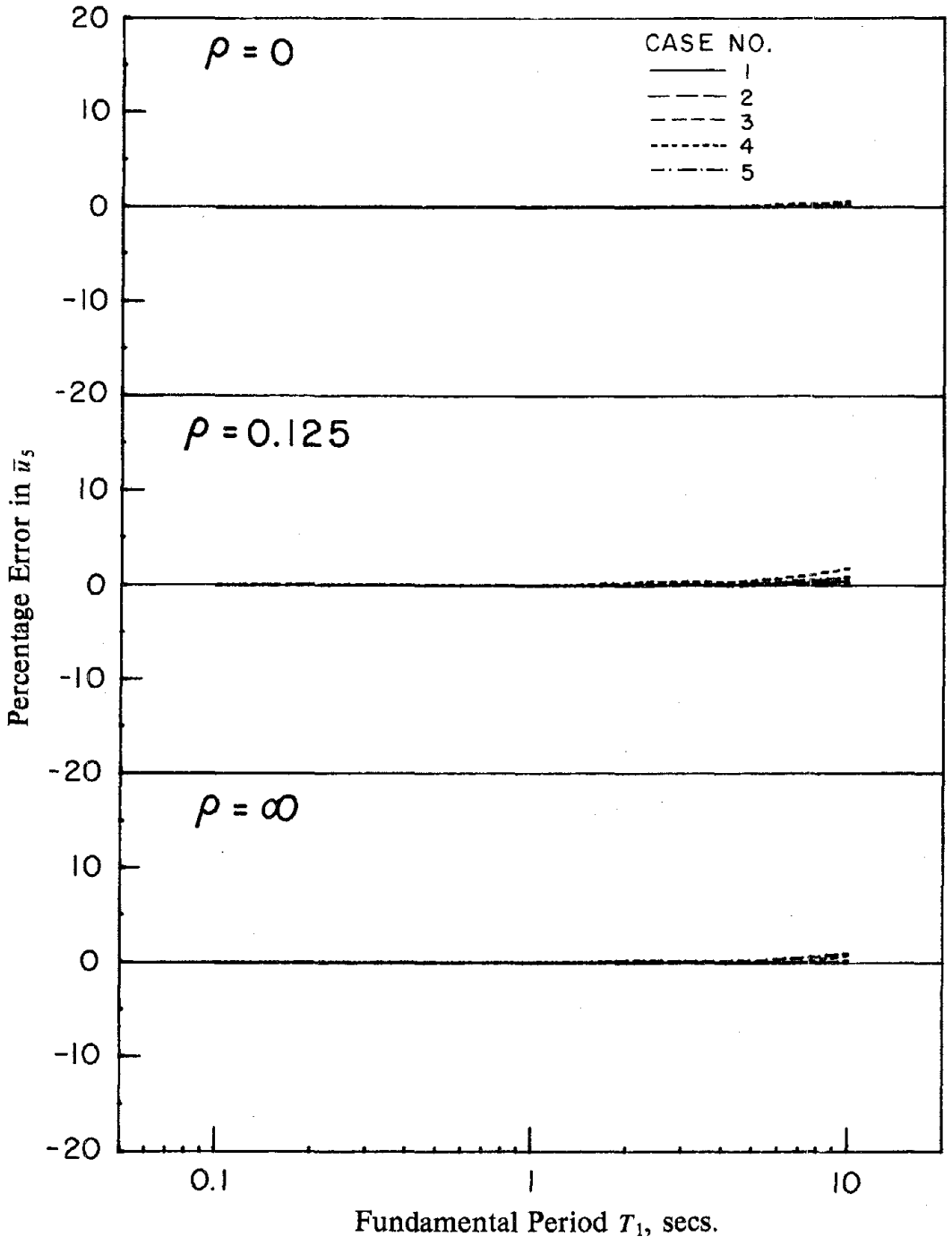

FIGURE 14 Percentage error in top-story displacements computed by simplified response spectrum analysis (SRSA) method, relative to response spectrum analysis (RSA) results, for 5 frame cases.

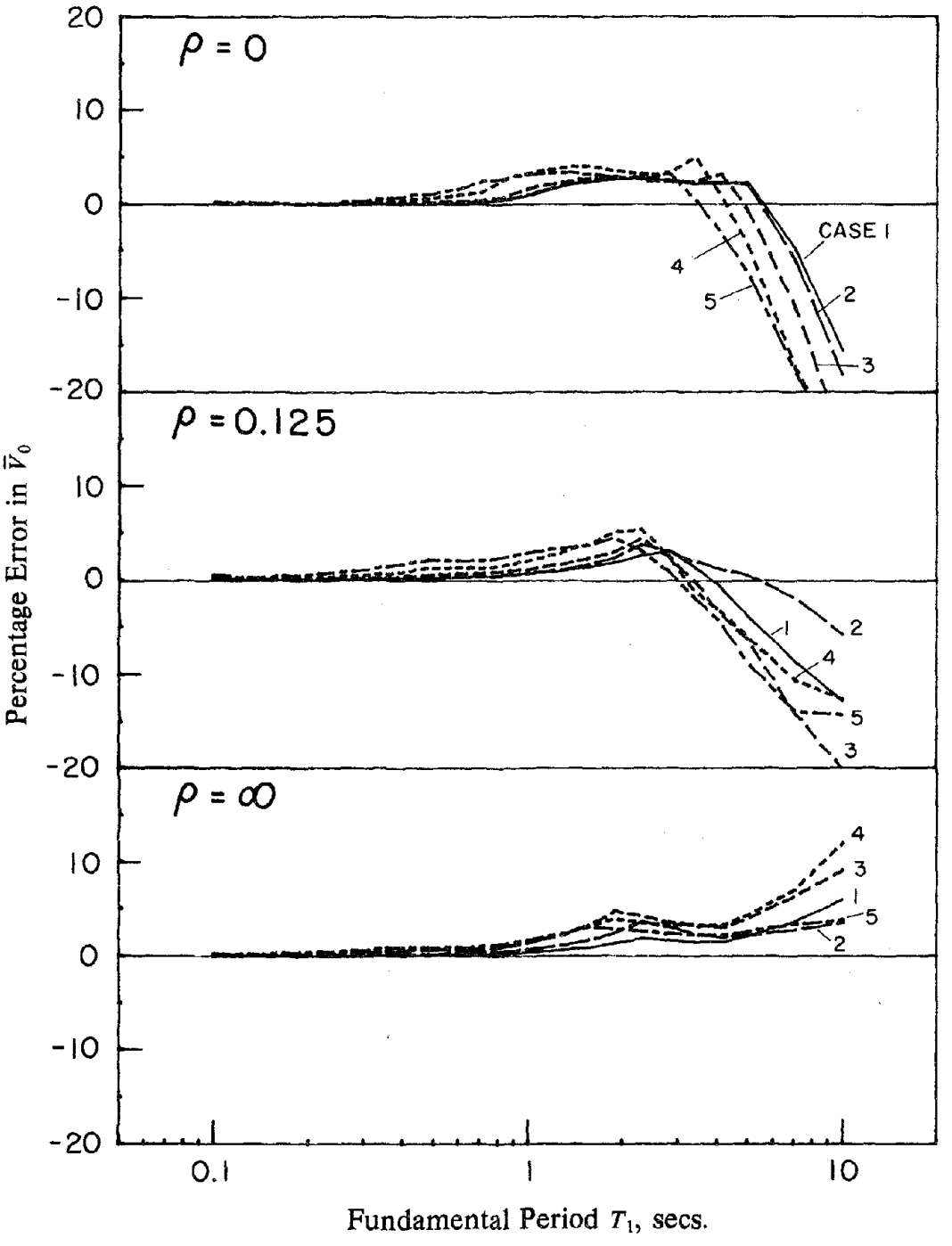

FIGURE 15 Percentage error in base shear computed by SRSA method, relative to RSA results, for 5 frame cases.

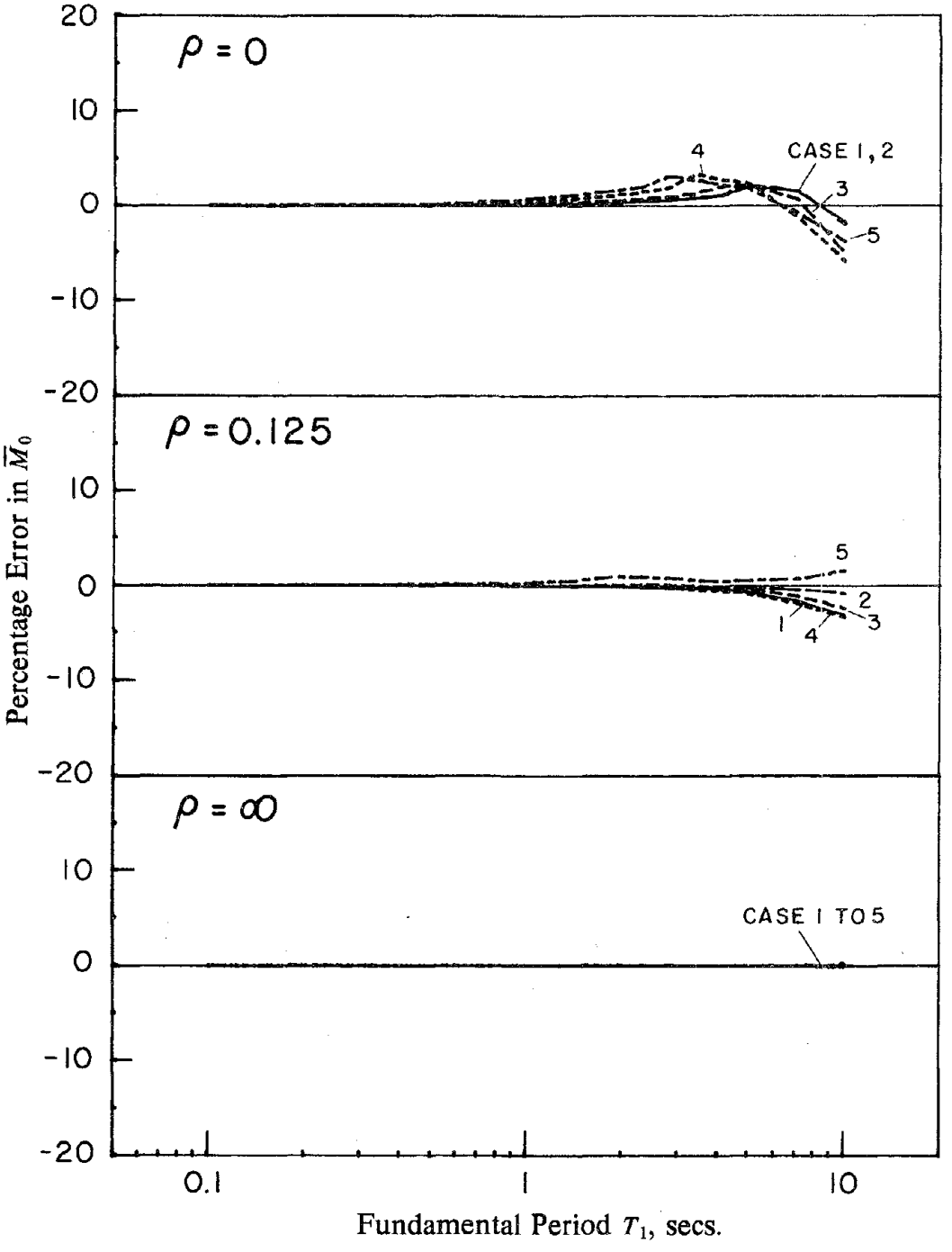

FIGURE 16 Percentage error in base overturning moment computed by SRSA method, relative to RSA results, for 5 frame cases.

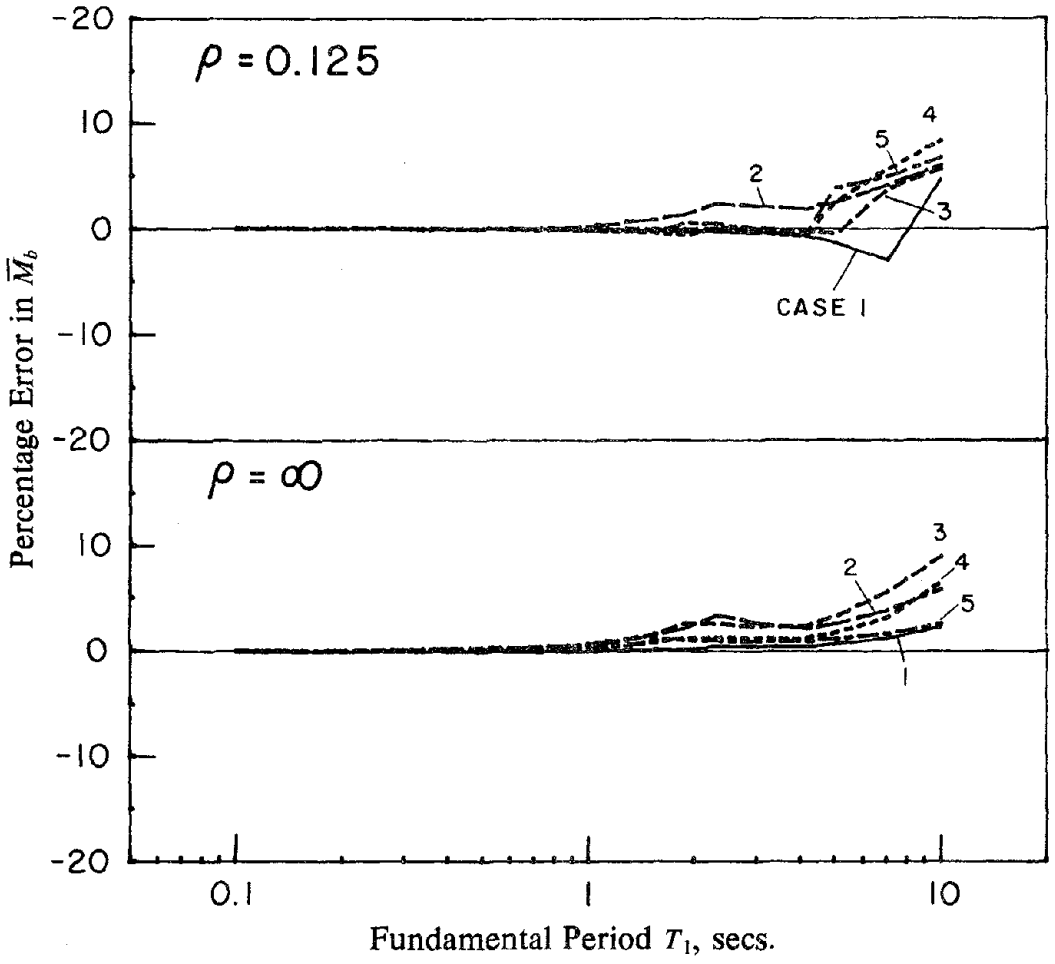

FIGURE 17 Percentage error in maximum beam moment computed by SRSA method, relative to RSA results, for 5 frame cases.

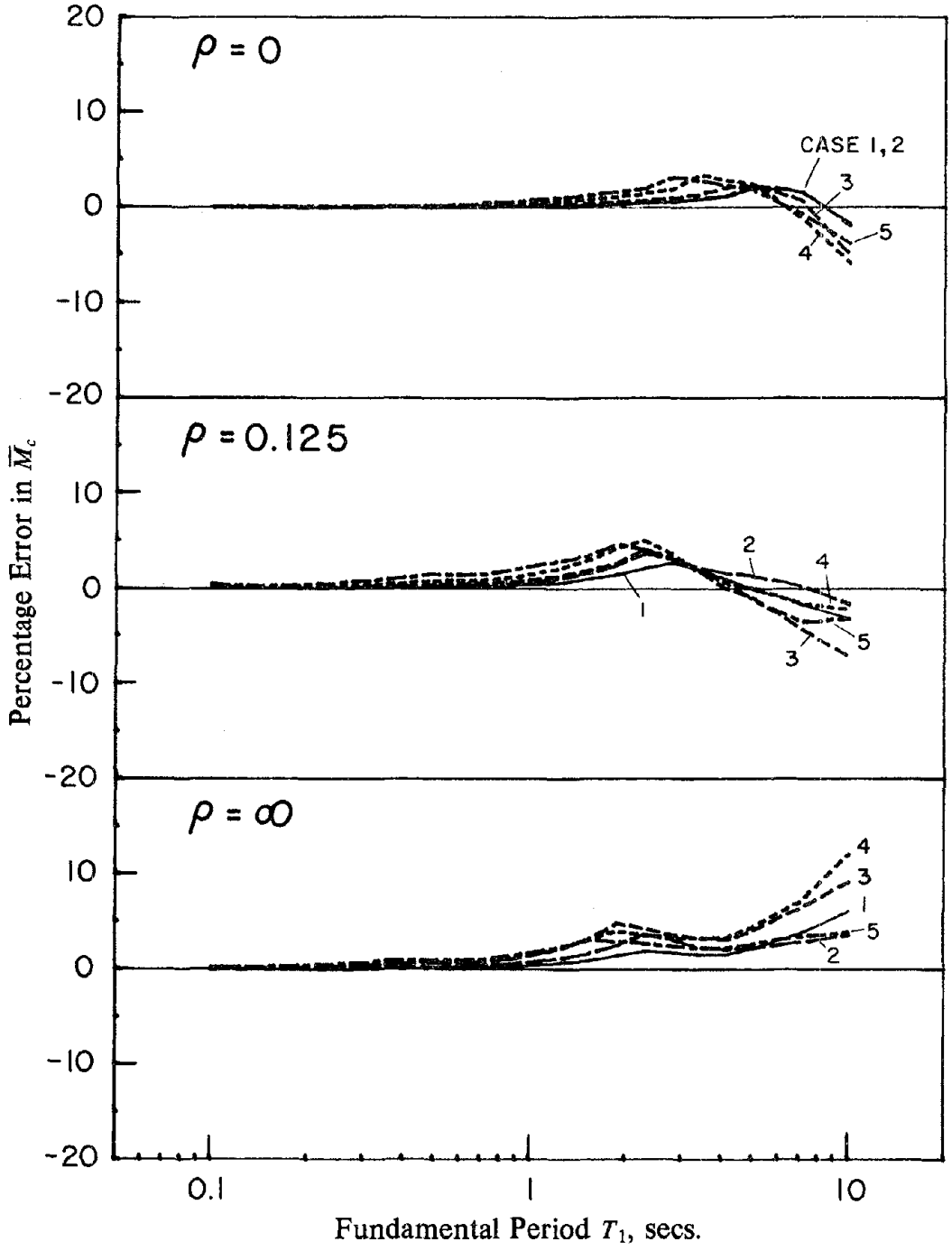

FIGURE 18 Percentage error in maximum column moment computed by SRSA method, relative to RSA results, for 5 frame cases.

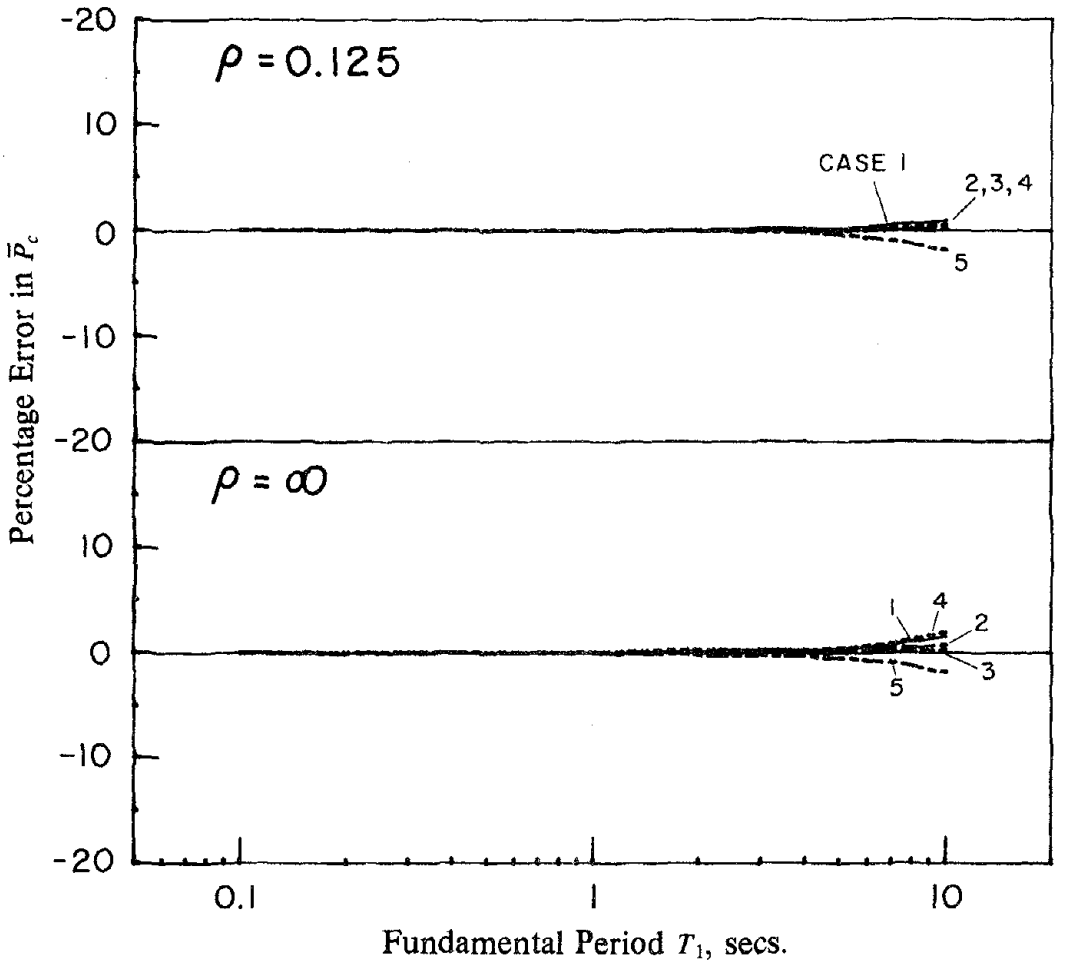

FIGURE 19 Percentage error in maximum column axial force computed by SRSA method, relative to RSA results, for 5 frame cases.

SRSA method and to the nature of the approximation introduced in the computation of second mode response by the SRSA method. For example, if the stiffness ratio ρ is small, the SRSA method overestimates the base shear value for frames with shorter vibration periods but underestimates it for frames with long vibration periods. As seen in Figure 2, the response of the uniform 5-story frame computed by response history analysis including the contribution of the first two vibration modes is essentially equal to the response considering all the five modes if the fundamental vibration period T_1 is within the acceleration-controlled region of the spectrum, because the contributions of the 3rd, 4th and 5th modes are very small. On the other hand, as T_1 increases the contributions of these higher modes become increasingly significant and the two-mode response is smaller than the five-mode response. Because the SRSA method overestimates the effective weight W_2^* of the second mode (Table 1) and underestimates the vibration period T_2 (because it overestimates the frequency ω_2, Figure 7), which for the selected response spectrum leads to a larger spectral ordinate, the contribution of the second mode as computed by the SRSA method tends to be larger than in the RSA method. Thus the SRSA method will overestimate the response if it is essentially given by the combination of the first two modes, which is the case for shorter T_1; but will tend to underestimate the response at longer periods where it ignores the significant higher mode contributions although this is partially compensated by overestimation of the second mode response.

Thus, the SRSA method, considering the contributions of the first two vibration modes, provides overall and local response values that are within five percent of the RSA values for all the frame cases studied (Figure 5), over the entire range of ρ, provided the fundamental period T_1 is below the end of the velocity-controlled region of the spectrum. If T_1 is within the acceleration-controlled region of the spectrum, only the fundamental vibration mode needs to be considered in the SRSA method.

4.4.2 Height-wise Distribution of Story Shears and Overturning Moments

The height-wise variation of story shears and story moments computed by the RSA and SRSA methods is presented in Figures 20 to 23 for the uniform 5-story frame (Case 1). In a lumped mass system, such as the frames considered here, the shear remains constant in each story with discontinuities at each floor. However, such a plot would not be convenient in displaying the differences among various cases and the alternative presentation with shears varying linearly over story height is used. Results are presented for four values of T_1, chosen to be representative of the different period regions of the response spectrum. The height-wise variation is presented in two forms: actual values, (Figures 20 and 22) and the ratio of story shears (and moments) to base shear (and moment) (Figures 21 and 23). The percentage error in the results computed by the SRSA method, defined in the same manner as for the overall and local response quantities is presented in Tables 2 to 7 for all the frame cases (Figure 5). Consistent with the earlier observations from errors in overall and local response quantities computed by the SRSA method, the errors in the story shears and moments also tend to increase with increasing fundamental vibration period T_1 and with decreasing ρ; and are larger for the taller frames and for frames with non-uniform distribution of mass, stiffness, or both, over height. The magnitudes of errors vary over the height of the frame, being larger in the upper stories where the contributions of the higher vibration modes are shown to be more significant (see Part I, also [6,8,11]).

However, even for the frame with highly-irregular mass and stiffness distributions over the height (Case 5) and for the taller frame (Case 2), the errors are within 10 percent provided the fundamental vibration period T_1 is below the midpoint of the velocity controlled region of the spectrum (on a logarithmic scale), which is 1.6 sec. for the spectrum of Figure 6. The response of the 5-story frame with uniform distributions of mass and stiffness (Case 1) is accurate over a wider range of T_1, up to the end of the velocity controlled region of the spectrum (Tables 2 to 7). Therefore, the errors in the height-wise distribution of story shears and moments impose a stricter limit on the range of fundamental periods in which the SRSA

Table 2: Percentage error in story shears computed by the simplified response spectrum analysis (SRSA) method, with respect to response spectrum analysis (RSA) results. ρ=0

Frame Case	Story	$T_1 = 0.22$	$T_1 = 1.27$	$T_1 = 4.11$	$T_1 = 10.0$
1	1	0.03	1.96	2.24	-15.63
	2	0.03	0.78	2.65	-0.47
	3	-0.07	-0.54	-11.71	-59.05
	4	-0.02	0.36	-0.98	-28.20
	5	-0.18	-0.77	-6.44	-26.20
2	1	0.	2.10	2.30	-18.20
	5	0.	1.70	3.40	-7.40
	10	-0.10	-0.50	-10.80	-58.20
	15	0.	0.50	1.30	-11.30
	20	-1.00	-3.40	-15.40	-48.30
3	1	0.03	2.35	3.16	-25.13
	2	0.04	1.29	5.20	-5.99
	3	-0.07	-0.65	-9.82	-53.68
	4	-0.05	0.21	-5.64	-48.86
	5	-0.15	-0.69	-4.29	-27.97
4	1	0.10	3.94	0.84	-26.90
	2	0.07	1.78	4.86	-7.55
	3	-0.17	-1.95	-24.14	-73.05
	4	-0.03	1.04	-3.69	-36.91
	5	-0.51	-2.66	-11.43	-36.85
5	1	0.11	3.38	-3.06	-27.44
	2	0.03	1.64	0.36	-14.69
	3	-0.20	-2.59	-29.43	-78.35
	4	-0.06	0.39	-8.42	-44.13
	5	-0.46	-2.78	-14.00	-38.14

Table 3: Percentage error in story shears

computed by the SRSA method, with respect to RSA results. $\rho = 0.125$

Frame Case	Story	$T_1 = 0.22$	$T_1 = 1.27$	$T_1 = 4.11$	$T_1 = 10.0$
1	1	0.06	1.12	-0.74	-12.82
	2	0.	0.13	-0.36	-14.94
	3	-0.02	-0.56	-7.21	-35.76
	4	0.02	0.89	0.77	-15.35
	5	-0.33	-3.77	-16.47	-31.77
2	1	0.10	1.30	1.30	-5.80
	5	0.	0.10	0.	-7.60
	10	0.	0.30	-1.70	-13.70
	15	-0.10	-0.10	-1.40	-10.40
	20	-1.00	-10.70	-39.90	-67.10
3	1	0.14	1.82	-3.52	-20.03
	2	0.03	0.76	0.36	-17.40
	3	-0.06	-1.13	-10.76	-48.13
	4	0.03	0.58	-5.03	-26.83
	5	-0.28	-2.59	-12.98	-21.48
4	1	0.32	3.03	-3.32	-12.66
	2	0.	0.25	-1.94	-18.78
	3	-0.03	-1.41	-13.49	-43.41
	4	-0.10	1.70	-1.85	-16.28
	5	-1.01	-7.74	-24.75	-33.73
5	1	0.73	3.50	-4.47	-14.27
	2	-0.04	-0.16	-6.80	-20.89
	3	0.03	-0.72	-10.12	-32.80
	4	0.04	0.46	-4.28	-18.18
	5	-0.78	-5.75	-20.74	-31.47

Table 4: Percentage error in story shears

computed by the SRSA Method, with respect to RSA results. $\rho = \infty$.

Frame Case	Story	$T_1 = 0.22$	$T_1 = 1.27$	$T_1 = 4.11$	$T_1 = 10.0$
1	1	0.05	0.70	1.54	6.05
	2	-0.01	-0.25	-1.28	-6.76
	3	0.03	0.32	-0.17	-0.82
	4	-0.02	0.12	0.53	1.25
	5	-0.34	-4.00	-11.96	-20.41
2	1	0.10	1.20	2.00	3.60
	5	0.	-0.10	-0.80	-7.20
	10	0.	0.40	-0.50	-5.30
	15	-0.10	-0.40	-1.80	-7.00
	20	-0.80	-9.40	-34.10	-57.80
3	1	0.22	2.27	3.08	9.18
	2	-0.01	-0.02	-1.03	-5.23
	3	-0.01	-0.55	-3.86	-17.38
	4	0.12	1.18	-0.20	0.50
	5	-0.43	-2.81	-5.52	-9.32
4	1	0.26	2.31	3.26	12.03
	2	-0.06	-0.73	-2.19	-10.25
	3	0.12	0.75	-0.57	-1.35
	4	-0.03	0.50	0.93	4.59
	5	-1.40	-8.69	-16.20	-21.77
5	1	0.43	2.36	2.24	3.86
	2	-0.26	-2.10	-6.18	-17.59
	3	0.14	0.82	0.33	0.08
	4	-0.11	-0.35	-0.54	-0.87
	5	-0.73	-4.06	-8.56	-16.70

Table 5: Percentage error in story overturning moments computed by the SRSA method, with respect to RSA results. $\rho = 0$.

Frame Case	Story	$T_1 = 0.22$	$T_1 = 1.27$	$T_1 = 4.11$	$T_1 = 10.0$
1	1	0.01	0.18	1.12	-1.77
	2	0.	-0.01	-0.32	-9.59
	3	0.01	0.22	1.09	-4.69
	4	0.01	0.42	1.33	0.18
	5	-0.18	-0.77	-6.44	-26.20
2	1	0.	0.20	1.20	-2.00
	5	0.	0.	-0.20	-7.70
	10	0.	0.40	2.10	3.20
	15	0.	0.	-2.30	-14.00
	20	-1.00	-3.40	-15.40	-48.30
3	1	0.01	0.30	2.12	-5.01
	2	0.	0.	-0.10	-7.13
	3	0.	0.17	0.57	-17.66
	4	0.03	0.66	4.04	1.93
	5	-0.15	-0.69	-4.29	-27.97
4	1	0.02	0.64	2.75	-5.86
	2	-0.01	-0.06	-1.14	-20.97
	3	0.02	0.58	1.70	-12.84
	4	0.05	1.14	4.04	-1.75
	5	-0.51	-2.66	-11.43	-36.89
5	1	0.04	1.04	2.20	-3.78
	2	-0.01	-0.08	-2.19	-27.54
	3	0.01	0.47	-0.22	-12.79
	4	-0.01	0.40	0.78	-4.85
	5	-0.46	-2.78	-14.00	-38.14

Table 6: Percentage Error in story overturning moments computed by the SRSA Method, with respect to RSA results. $\rho = 0.125$.

Frame Case	Story	$T_1 = 0.22$	$T_1 = 1.27$	$T_1 = 4.11$	$T_1 = 10.0$
1	1	0.	-0.04	-0.40	-3.15
	2	0.01	0.16	0.63	1.30
	3	0.03	0.75	3.17	0.03
	4	-0.01	0.40	1.20	0.03
	5	-0.33	-3.77	-16.47	-31.77
2	1	0.	0.	-0.10	-0.80
	5	0.	0.40	1.40	5.50
	10	0.	0.80	3.00	7.30
	15	-0.20	-2.30	-7.80	-16.60
	20	-1.00	-10.70	-34.20	-67.10
3	1	0.	0.05	-0.22	-2.34
	2	0.	0.04	-0.09	-3.46
	3	0.04	0.66	1.57	3.45
	4	0.04	1.19	3.62	4.62
	5	-0.28	-2.59	-12.98	-21.68
4	1	0.01	0.03	-0.53	-3.44
	2	0.02	0.24	0.20	-1.45
	3	0.11	1.76	4.39	10.21
	4	-0.01	1.06	1.68	1.22
	5	-1.01	-7.74	-24.75	-33.73
5	1	0.05	0.54	0.54	1.59
	2	-0.01	-0.15	-2.20	-19.12
	3	0.09	1.00	1.95	5.03
	4	-0.10	-0.34	-1.78	-2.80
	5	-0.78	-5.75	-20.74	-31.47

Table 7: Percentage error in story overturning moments computed by the SRSA method, with respect to RSA results. $\rho = \infty$.

Frame Case	Story	$T_1 = 0.22$	$T_1 = 1.27$	$T_1 = 4.11$	$T_1 = 10.0$
1	1	0.	0.	0.01	0.07
	2	0.02	0.30	0.95	4.22
	3	0.01	0.42	1.62	5.06
	4	-0.09	-0.75	-1.60	-3.58
	5	-0.34	-4.00	-11.96	-20.41
2	1	0.	0.	0.	0.20
	5	0.	0.40	1.60	6.40
	10	0.	0.60	2.40	6.00
	15	-0.20	-2.50	-9.00	-16.30
	20	-0.80	-9.40	-34.10	-57.80
3	1	0.	0.	-0.01	-0.04
	2	0.02	0.26	0.42	2.16
	3	0.09	1.12	2.46	9.11
	4	0.06	1.26	3.38	8.34
	5	-0.43	-2.81	-5.52	-9.32
4	1	0.	-0.02	-0.03	-0.14
	2	0.07	0.74	1.36	6.98
	3	0.10	1.38	3.10	11.11
	4	-0.29	-1.17	-1.07	0.65
	5	-1.40	-8.69	-16.20	-21.77
5	1	0.01	0.06	0.02	0.02
	2	0.03	0.10	-0.58	-3.27
	3	-0.01	0.21	0.54	1.88
	4	-0.28	-1.27	-1.89	-3.74
	5	-0.73	-4.06	-8.59	-16.70

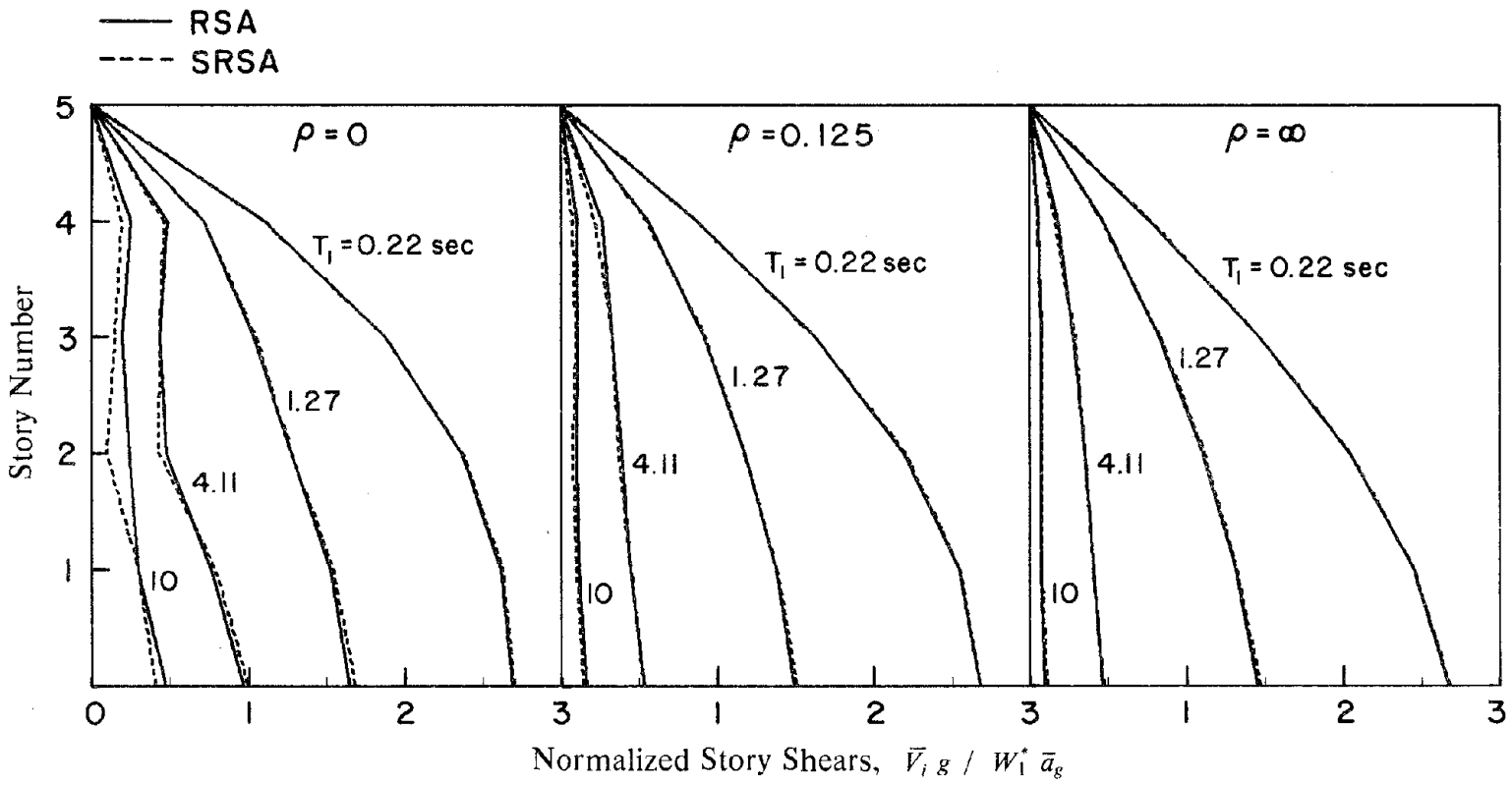

FIGURE 20 Comparison of story shears computed by simplified response spectrum analysis (SRSA) and response spectrum analysis (RSA) methods for 4 values of the fundamental period T_1. Results are for Case 1: uniform 5-story frame.

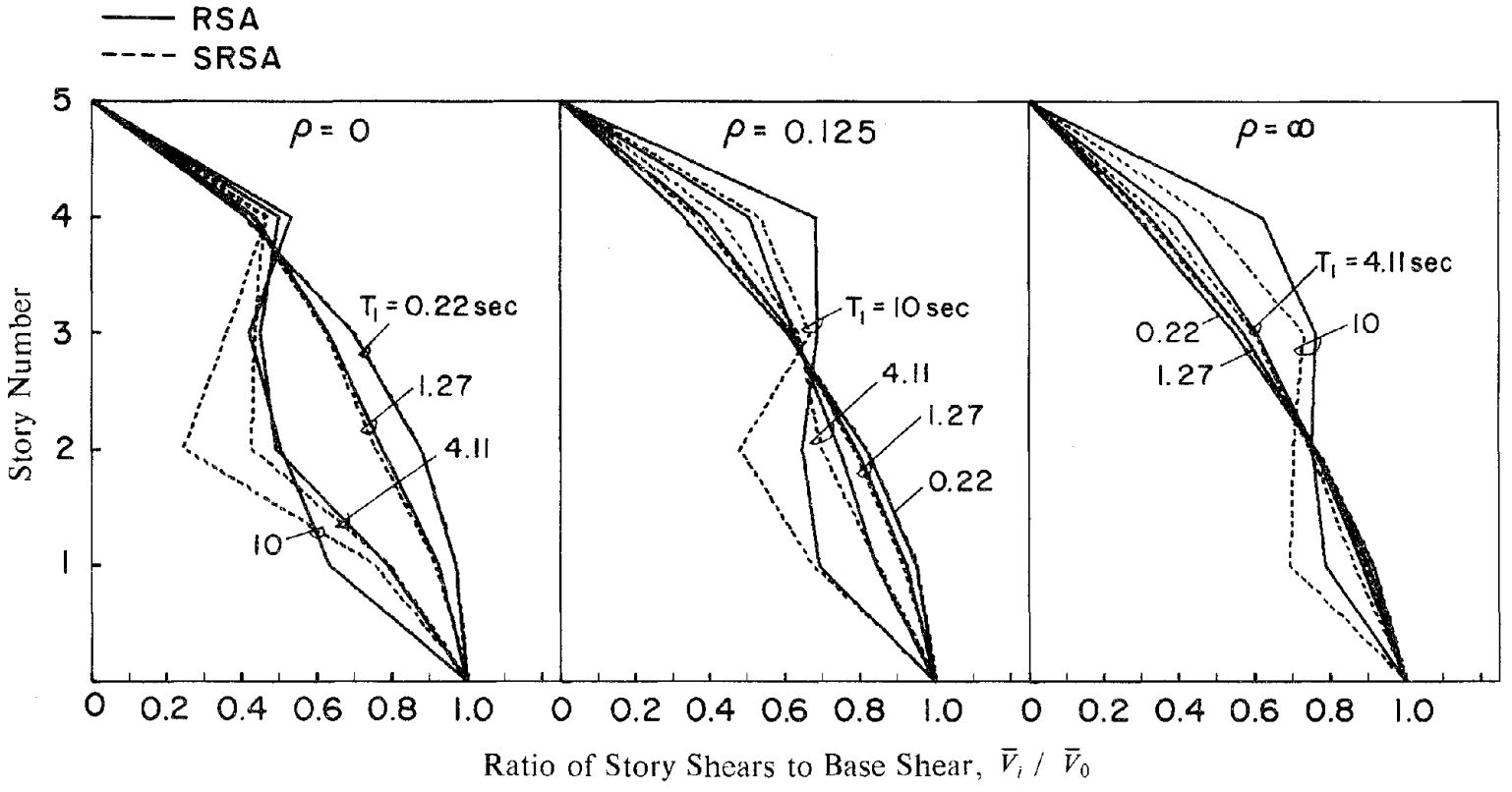

FIGURE 21 Comparison of distributions of story shears computed by SRSA and RSA methods for 4 values of the fundamental period T_1. Results are for Case 1: uniform 5-story frame.

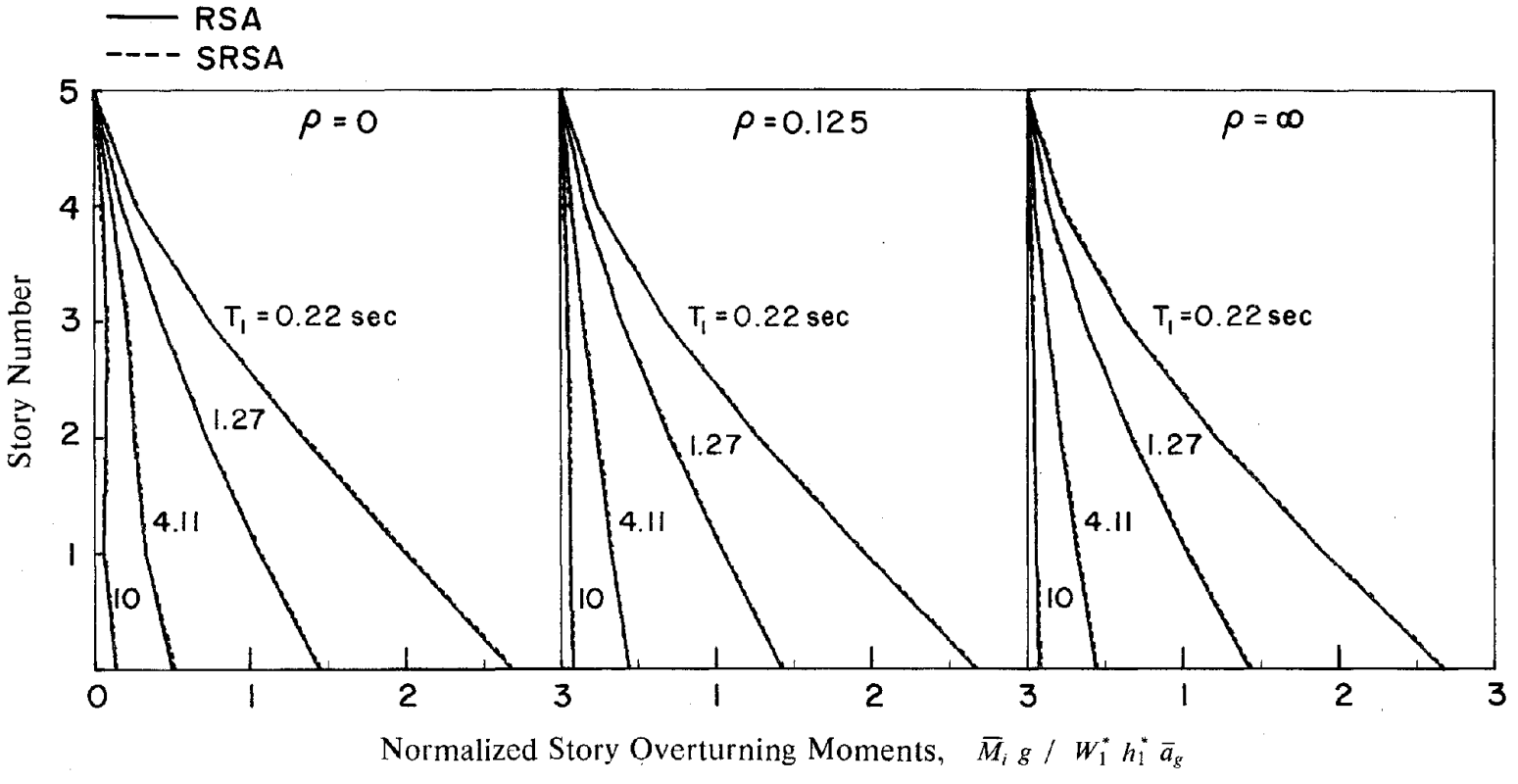

FIGURE 22 Comparison of story overturning moments computed by SRSA and RSA methods for 4 values of the fundamental period T_1. Results are for Case 1: uniform 5-story frame.

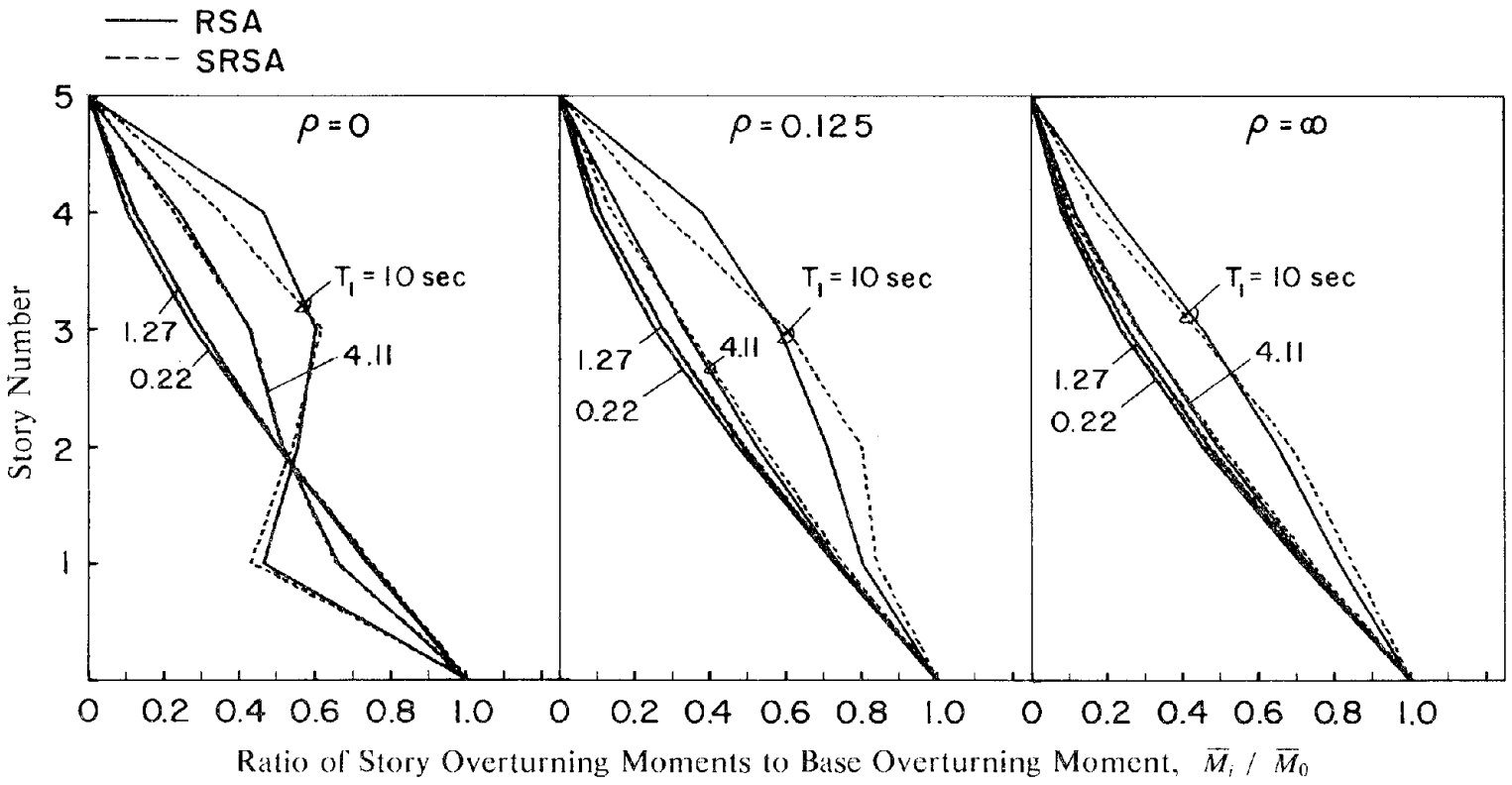

FIGURE 23 Comparison of distributions of story overturning moments computed by SRSA and RSA methods for 4 values of the fundamental period T_1. Results are for Case 1: uniform 5-story frame.

method considering the first two modes contributions will provide satisfactory results than the limit obtained from the errors in the overall and local response quantities.

4.4.3 Extrapolation of Observations on SRSA Method

The simplified response spectrum analysis (SRSA) procedure includes the contributions of only the first two vibration modes of the structure, whereas all the modes can be recognized in response spectrum analysis (RSA). In particular, the effective weight of the building frame included in computing the base shear by the SRSA method is only a portion of the total weight of the building, whereas the entire weight is accounted for when all the vibration modes are included in the RSA method. The effective weights W_1^* and $\widetilde{W}_2^*$ for the first two modes and the combined value computed in the SRSA method depend on the vibration mode shapes and therefore on ρ. On the other hand, the significance of the contributions of the higher vibration modes vary with the fundamental vibration period T_1 in addition to their dependence on ρ. Thus it would seem that the effective weight included in the SRSA method would provide an indication of the accuracy of the responses computed by the method, but only a partial indication because the additional dependence of higher mode contributions on T_1 is not recognized in the effective weight values. This expectation is confirmed by comparing the effective weight values presented in Table 1 with the errors in responses computed by the SRSA procedure presented in Figures 14 to 19 and Tables 2 to 7. In general, the larger the portion of the effective weight considered, the smaller the errors in the SRSA results. The aforementioned observations regarding the accuracy of the SRSA results, which were based on results for the five frame cases of Figure 5, may therefore be extrapolated to other frames with different number of stories or dissimilar variation of mass and stiffness over height. This seems reasonable provided the total effective weight included in the SRSA method exceeds 85 percent of the total weight, a value exceeded in all the cases and ρ values considered in this study.

4.4.4 Fundamental Mode Analysis

As shown in Figure 3, for buildings with fundamental vibration period T_1 within the acceleration-controlled region of the earthquake response spectrum, the fundamental mode alone provides essentially the same results as those obtained by including all the modes in the RSA method. Thus, in this range of vibration periods, only the first mode needs to be considered in the SRSA method. In order to ensure that the errors in the results from one-mode analysis are within reasonable limits it is recommended that this simplification may be employed only if the effective weight in the fundamental vibration mode of the building exceeds 75 percent of the total weight (Appendix B).

5. HIERARCHY OF ANALYSIS PROCEDURES

5.1 Analysis Procedures

With the development of the simplified response spectrum analysis (SRSA), four analysis procedures to determine the earthquake forces are available to the building designer. Listed in order of increasing complexity these procedures are:

- Code-type Procedure, such as the lateral forces specified in the building codes [9,12], the equivalent lateral force procedure developed in the ATC-3 design provisions [1], or the improved code-type analysis procedure developed in Part III of this Report.
- SRSA --Simplified Response Spectrum Analysis.
- RSA --Response Spectrum Analysis [4].
- RHA --Response History Analysis [4].

With the increasing complexity in these analysis procedures comes improved accuracy in the analysis of the structure. The computation of base shear in the Uniform Building Code (UBC) uses a fundamental vibration period obtained from an empirical formula based on overall building dimensions. Except for the additional force F_t assigned to the top of the building the UBC lateral forces are distributed over the height of the building under the assumption of linearly varying floor displacements in the fundamental mode shape [4]. Assignment of an additional force F_t at the top of the building is intended by the code to roughly and implicitly account for the contributions of the higher vibration modes to building response. The SRSA method will obviously lead to better values of base shear, lateral forces and member forces because it is based on exact analysis of the fundamental mode period and shape, and the contribution of the second vibration mode to building response is explicitly computed from a very good approximation to the frequency and shape of this mode. The RSA method will obviously lead to even improved accuracy in the computed earthquake forces because the period, shape, and earthquake response in each of the modes are analyzed exactly.

As demonstrated in the preceding section, this improvement over the SRSA method is of little consequence if only two vibration modes provide a sufficiently accurate description of the response, but becomes substantial if the higher modes contribute significantly to building response. Finally, response history analysis (RHA) provides exact response of the idealized building because it avoids the errors in the RSA method arising from combining the modal maxima without the benefit of knowing the time-variation of the modal responses. These errors, which were examined in Section 2, would exist no matter which of the available combination rules, SRSS (equation (8) with all modal terms), or CQC [7] are used; because for the frames with well-separated vibration periods considered herein the two combinations rules lead to essentially identical results.

Because the four analysis procedures listed earlier in increasing order of complexity provide increasingly accurate results for the structure, they should be considered in sequence, proceeding no farther than the least complex method that leads to sufficiently accurate results. What remains to be developed are the criteria for transition from one procedure to the next.

5.2 Transition from Code Analysis to SRSA Method

Initially, before the building has been designed only the code-type analysis procedures can be used to compute the earthquake forces, because the other three analysis procedures mentioned above require building properties that are not available at this stage of design. Because the code-type analysis procedures are based on an assumed shape for the fundamental mode and implicit, indirect recognition of the higher vibration mode contributions, they may not always provide sufficiently accurate results. Thus, a procedure should be developed to evaluate the quality of the results from a code analysis and, if necessary, to improve the results by proceeding to the SRSA method, which is next in the hierarchy of analysis procedures.

One such procedure, which was included in the seismic provisions prepared by ATC-3, the Applied Technology Council [1], is quoted with minor editorial changes:

1. Compute lateral forces and story shears using the code procedure.
2. Approximately dimension structural members.
3. Compute lateral displacements of the structure, as designed in step 2, due to lateral forces from step 1.
4. Compute a new set of lateral forces, with the base shear from step 1 distributed in accordance with the displacements computed in step 3; in computing the lateral force at any floor this involves replacing the story height in the UBC or story height to the power k in the ATC-3 equivalent lateral forces formulas by the displacement at the particular floor computed in step 3. Compute the story shears from this new set of lateral forces.
5. If at any story the shear computed in step 4 differs from that computed in step 1 by more than 30 percent the structure should be reanalyzed using response spectrum analysis (RSA) procedure. If the difference is less than this value the RSA procedure is unnecessary, and the structure should be designed using the story shears obtained in step 4; they represent an improvement over the results of step 1.

In evaluating the effectiveness of this method, we will focus our attention on the underlying concepts; whether the 30 percent limit in step 4 is appropriate is of secondary concern because it can be modified if necessary, provided the basic procedure is conceptually correct. Steps 3 and 4 of this method are equivalent to one cycle in an iterative procedure, based on the Stodola method, for calculating the fundamental mode of vibration. Thus, the lateral displacements computed in step 3 represent an improved shape for the fundamental vibration mode compared to that implied in the code formula for lateral forces, e.g. the linear shape implied in the UBC formula. Thus, the method described above will provide an improved approximation to the lateral forces associated with the fundamental mode of vibration, but it does not consider the contribution of the higher modes of vibration.

This expectation is confirmed by the results presented in Tables 8 to 10, wherein for each selected structure the percentage difference in story shear values computed in steps 1 and 4 of the procedure described above --starting from the equivalent lateral forces distribution

provided by the ATC-3 design provisions-- are presented, along with the percentage error in the story shear from step 4 relative to the value computed from the response spectrum analysis (RSA) method. Each table, corresponding to a particular value of ρ contains results for four fundamental periods selected to be representative of different regions of the response spectra for all the five stories of buildings of cases 1, 3, 4, and 5 and for five selected stories of the 20-story building of case 2 (Figure 5).

These results lead to the following observations: For short-period buildings ($T_1 = 0.15$ or 0.48 secs., i.e. within the acceleration-controlled region of the spectrum), whose response is almost entirely due to the fundamental mode of vibration, the equivalent lateral force (ELF) procedure of ATC-3 provisions [1] or UBC [9] provides very accurate results if the implied linear shape of the fundamental vibration mode is an excellent approximation to the actual shape of the fundamental mode (e.g. Case 1, $\rho = 0.125$, Table 9); the results are in considerable error if the fundamental mode shape is much different (e.g. Case 5, $\rho = 0$, Table 8) but in these cases the results from step 4 of the above-described procedure are very close to the RSA values. For long-period buildings ($T_1 = 1.55$ or 5.0 sec., i.e. within the velocity- or displacement-controlled regions of the response spectrum) whose response contains significant contributions from the higher modes of vibration, the results from step 4 of the above-described procedure may be only slightly different than those from the ELF procedure (e.g. Case 5, $\rho = 0$, $T_1 = 5.0$ sec., Table 8) indicating that the latter provided a good approximation to the fundamental mode response; but because the higher-mode contributions are not reflected in the step 4 results, they may contain large errors, exceeding 100 percent in the selected example.

It is therefore concluded that the preceding procedure from ATC-3 provisions is effective in identifying the errors in the ELF procedure and providing an improved set of design forces only if the building response is almost entirely due to the fundamental mode of vibration. For such cases, any large differences in the story shears computed in steps 1 and 4 simply indicate that the first mode response was not well represented by the code formulas, but they provide

Table 8: Percentage difference in story shears values computed in steps 1 and 4 of the ATC-3 procedure and percentage error in the step 4 value; $\rho = 0$.

Frame Case	Story	$T_1 = 0.15$		$T_1 = 0.48$		$T_1 = 1.55$		$T_1 = 5.0$	
		$\frac{\text{Step 4 - Step 1}}{\text{Step 1}}$	$\frac{\text{Step 4 - RSA}}{\text{RSA}}$	$\frac{\text{Step 4 - Step 1}}{\text{Step 1}}$	$\frac{\text{Step 4 - RSA}}{\text{RSA}}$	$\frac{\text{Step 4 - Step 1}}{\text{Step 1}}$	$\frac{\text{Step 4 - RSA}}{\text{RSA}}$	$\frac{\text{Step 4 - Step 1}}{\text{Step 1}}$	$\frac{\text{Step 4 - RSA}}{\text{RSA}}$
1	1	0.	0.	0.	0.	0.	0.	0.	0.
	2	4.4	0.3	4.4	0.5	1.0	7.3	-0.7	28.2
	3	10.4	0.6	10.4	1.0	2.0	19.9	-2.6	94.5
	4	16.4	0.3	16.4	0.7	2.5	15.5	-5.9	65.0
	5	21.8	-1.0	21.8	-1.3	2.1	-8.7	-10.0	-19.4
2	1	0.	0.	0.	0.	0.	0.	0.	0.
	5	3.4	0.3	3.4	0.4	0.7	4.5	-0.4	17.5
	10	11.2	0.6	11.2	1.1	2.1	20.5	-2.8	99.5
	15	19.1	0.1	19.1	0.3	2.5	9.3	-7.3	35.3
	20	25.7	-2.9	25.7	-3.6	1.5	22.7	-13.3	-41.5
3	1	0.	0.	0.	0.	0.	0.	0.	0.
	2	4.7	0.3	4.7	0.5	1.3	6.5	-0.4	26.2
	3	11.6	0.6	11.6	1.3	3.2	19.2	-1.5	75.2
	4	19.1	0.3	19.1	1.0	5.0	18.3	-3.5	64.5
	5	26.3	-1.2	26.3	-1.6	6.1	-8.5	-6.5	-15.6
4	1	0.	0.	0.	0.	0.	0.	0.	0.
	2	8.3	0.8	8.3	1.7	2.2	14.9	-0.8	44.7
	3	18.7	1.1	18.7	3.3	4.9	36.8	-2.9	88.7
	4	28.9	0.2	28.9	1.8	6.8	24.0	-6.2	56.8
	5	37.6	-2.7	37.6	-4.1	7.5	-15.0	-10.2	-22.4
5	1	0.	0.	0.	0.	0.	0.	0.	0.
	2	11.0	1.9	11.0	5.5	3.4	20.2	-0.5	36.6
	3	34.8	3.6	34.8	15.4	12.5	98.3	-0.1	151.6
	4	46.2	2.5	46.2	12.7	16.5	79.2	-0.2	138.5
	5	56.9	-0.3	56.9	5.3	19.4	28.2	-1.8	34.4

Table 9: Percentage difference in story shears values computed in steps 1 and 4 of the ATC-3 procedure and percentage error in the step 4 value; $\rho = 0.125$.

Frame Case	Story	$T_1 = 0.15$		$T_1 = 0.48$		$T_1 = 1.55$		$T_1 = 5.0$	
		Step 4 - Step 1 / Step 1	Step 4 - RSA / RSA	Step 4 - Step 1 / Step 1	Step 4 - RSA / RSA	Step 4 - Step 1 / Step 1	Step 4 - RSA / RSA	Step 4 - Step 1 / Step 1	Step 4 - RSA / RSA
1	1	0.	0.	0.	0.	0.	0.	0.	0.
	2	2.2	0.1	2.2	0.5	-1.1	4.3	-2.6	19.9
	3	2.8	0.2	2.8	0.8	-4.5	5.8	-8.6	14.0
	4	1.3	-0.1	1.3	-0.5	-10.1	-1.4	-16.9	-0.8
	5	-2.2	-0.9	-2.2	-3.5	-17.0	-18.1	-26.3	-40.3
2	1	0.	0.	0.	0.	0.	0.	0.	0.
	5	0.4	0.2	0.4	0.5	-2.1	2.7	-3.0	10.2
	10	-1.8	0.5	-1.8	0.8	-9.1	3.3	-13.0	7.1
	15	-7.0	0.5	-7.0	-1.1	-18.8	-7.4	-25.9	-16.2
	20	-15.0	1.1	-15.0	-4.2	-30.2	-25.5	-39.6	-61.0
3	1	0.	0.	0.	0.	0.	0.	0.	0.
	2	3.2	0.1	3.2	0.7	-0.1	5.3	-1.6	21.8
	3	6.3	0.	6.3	1.3	-1.3	9.6	-5.4	22.6
	4	8.3	-0.7	8.3	-0.1	-3.7	3.7	-11.0	8.9
	5	8.4	-1.9	8.4	-5.1	-7.8	-17.0	-17.8	-27.9
4	1	0.	0.	0.	0.	0.	0.	0.	0.
	2	4.9	0.2	4.9	1.6	-0.6	10.5	-3.3	29.6
	3	8.2	-0.1	8.2	2.1	-3.5	13.8	-10.1	24.3
	4	8.7	-1.1	8.7	-2.0	-8.4	-2.1	-18.5	0.1
	5	6.4	-3.6	6.4	-10.6	-14.9	-29.1	-27.7	-42.8
5	1	0.	0.	0.	0.	0.	0.	0.	0.
	2	7.3	1.1	7.3	5.7	0.5	21.2	-2.9	28.9
	3	20.9	0.3	20.9	10.1	2.9	56.1	-7.3	83.9
	4	24.7	-1.8	24.7	4.3	2.0	30.6	-11.0	49.5
	5	24.5	-4.6	24.5	-3.7	-2.3	1.6	-17.9	-0.7

Table 10: Percentage difference in story shears values computed in steps 1 and 4 of the ATC-3 procedure and percentage error in the step 4 value; $\rho = \infty$.

Frame Case	Story	$T_1 = 0.15$		$T_1 = 0.48$		$T_1 = 1.55$		$T_1 = 5.0$	
		Step 4 - Step 1 / Step 1	Step 4 - RSA / RSA	Step 4 - Step 1 / Step 1	Step 4 - RSA / RSA	Step 4 - Step 1 / Step 1	Step 4 - RSA / RSA	Step 4 - Step 1 / Step 1	Step 4 - RSA / RSA
1	1	0.	0.	0.	0.	0.	0.	0.	0.
	2	-1.3	0.3	-1.3	0.7	-4.3	2.8	-5.6	5.7
	3	-3.9	0.7	-3.9	0.8	-10.5	2.3	-14.1	2.7
	4	-7.9	0.9	-7.9	-0.2	-17.8	-3.9	-23.8	-9.7
	5	-13.2	0.9	-13.2	-2.1	-25.9	-13.7	-33.8	-30.7
2	1	0.	0.	0.	0.	0.	0.	0.	0.
	5	-1.0	0.3	-1.0	0.6	-3.3	3.0	-4.3	8.3
	10	-4.3	0.7	-4.3	0.9	-11.3	2.7	-15.1	4.4
	15	-10.0	0.9	-10.0	-0.9	-21.4	-7.6	-28.2	-17.5
	20	-18.1	0.3	-18.1	-3.4	-32.7	-22.9	-41.7	-55.5
3	1	0.	0.	0.	0.	0.	0.	0.	0.
	2	0.6	0.1	0.6	0.7	-2.4	4.0	-3.8	7.2
	3	1.3	0.1	1.3	1.0	-5.5	6.2	-9.3	8.8
	4	1.5	-0.3	1.5	-0.5	-9.1	0.1	-15.5	-0.9
	5	0.5	-1.4	0.5	-5.3	-13.6	-17.5	-22.5	-25.3
4	1	0.	0.	0.	0.	0.	0.	0.	0.
	2	-0.1	0.5	-0.1	1.4	-5.0	7.1	-7.3	10.3
	3	-1.2	0.7	-1.2	1.2	-11.1	5.8	-16.7	7.1
	4	-3.8	0.2	-3.8	-2.0	-17.9	-7.8	-26.3	-9.7
	5	-8.1	-1.2	-8.1	-8.1	-25.3	-26.4	-35.7	-36.3
5	1	0.	0.	0.	0.	0.	0.	0.	0.
	2	1.5	1.4	1.5	5.5	-4.2	20.3	-7.0	22.1
	3	10.7	-0.5	10.7	4.1	-4.1	25.9	-12.6	37.8
	4	10.3	-2.3	10.3	-0.3	-8.1	12.1	-18.8	19.7
	5	6.2	-3.7	6.2	-4.2	-15.0	0.3	-27.6	0.3

no insight into the significance of higher mode contributions. Thus, it is inappropriate to use the differences between results of steps 1 and 4 as a basis for deciding whether the structure should be reanalyzed by the RSA method, which better accounts for higher mode contributions.

In light of these comments, the preceding procedure from ATC-3 provisions should be modified as follows to evaluate the quality of results from a code-type analysis and to identify the need to employ the SRSA method, which is next in the hierarchy of analysis procedures:

1. Estimate the fundamental vibration period T_1 of the building. If T_1 is within the acceleration-controlled region of the earthquake design spectrum, proceed to the next step; otherwise the higher mode effects may be significant and analyze the structure by the SRSA method.
2. Compute the effective weight W_1^* for the approximation to the fundamental mode of vibration of the building implicit in the lateral force distribution specified by the building code. If W_1^* exceeds 75 percent of the total weight of the building (Section 4.4.4), proceed to the next step; otherwise the higher mode effects may be significant and analyze the structure by the SRSA method.
3. If T_1 is within the acceleration-controlled region of the earthquake design spectrum and the effective weight W_1^* exceeds 75 percent of the total weight, use the preceding ATC-3 procedure, with one change: The 30 percent limit in step 4 should be deleted as a condition for requiring reanalysis by the RSA method, but an appropriate practical limit may be introduced to decide if the changes in the story shears from steps 1 and 4 make it necessary to re-dimension the structural members.

5.3 Transition from SRSA to RSA Method

Based on the preceding results and their interpretation, the SRSA method would provide a sufficiently accurate estimate of building response for purposes of its design provided two conditions are satisfied: Firstly, the fundamental vibration period T_1 of the building is below

the midpoint of the velocity-controlled region of the spectrum. This acceptable region may be extended to the end of the velocity-controlled region of the spectrum for buildings with a large ρ value, resulting in close to shear beam behavior. Secondly, the effective weights W_1^* and W_2^* for the first two vibration modes combine to account for more than 85 percent of the total weight of the building. Thus, if either of these two requirements are not satisfied, a response spectrum analysis (RSA) of the building should be performed before its design is finalized.

5.4 Transition from RSA to RHA Method

As seen earlier the errors in results of a response spectrum analysis (RSA) tend to increase with the fundamental vibration period T_1 of the building, reaching as much as 15 percent for uniform 5-story buildings with T_1 at the end of the velocity controlled region of the selected spectrum. Thus, it may be necessary to go beyond the RSA method to response history analysis of earthquake forces for tall buildings with fundamental period in the displacement-controlled region of the spectrum, T_1 exceeding 4 seconds for the earthquakes considered here, and for buildings with unusual distributions of mass and stiffness over height, for which sufficient experience or rational basis is not readily available to predict the accuracy of the RSA method. In some cases, such as a soft-first story building, although the stiffness of the soft story is much less than the stiffnesses of the other stories, the RSA method may still be good enough because the response of such building is dominated by the first natural vibration mode.

If the response history analysis is considered necessary in a particular situation, it should be carried out not for only one ground motion but several design ground motions and the statistics of the response should be examined. This is necessary for two reasons: Firstly, the response spectrum of a single ground motion with all its irregularities is not compatible with the smooth design spectrum specified in design criteria for actual projects. Secondly, the way in which individual modal responses of some buildings combine may be sensitive to the details of the ground motion and it would obviously be inappropriate to base the design decisions on a single ground motion.

6. CONCLUSIONS

Recognizing that the earthquake response of many buildings can be estimated by considering only the first two modes of vibration in the response spectrum analysis (RSA) procedure, a simplified response spectrum analysis (SRSA) procedure has been developed. The simplification is achieved mainly in evaluating the natural frequencies and modes of vibration of the structure, which is one of the most time consuming steps in the RSA procedure; analytically and conceptually it is the most complicated step. Procedures based on the Rayleigh and Stodola methods, which are conceptually simple and can be conveniently implemented on a pocket calculator, have been presented to determine the first two natural frequencies and modes of vibration of a building. Over a wide range of values for the fundamental vibration period T_1 and the stiffness ratio ρ, the SRSA method is shown to provide responses that are accurate enough for purposes of design. If T_1 is within the acceleration-controlled region of the spectrum, only the fundamental vibration mode response needs to be considered in the SRSA method.

With the development of the simplified response spectrum analysis (SRSA), a hierarchy of four analysis procedures to determine the earthquake forces are available to the building designer. Listed in order of increasing complexity and improving accuracy these procedures are: code-type procedure, SRSA --simplified response spectrum analysis, RSA --response spectrum analysis, and RHA --response history analysis. These four procedures should be considered in sequence proceeding no farther than the least complex method that leads to sufficiently accurate results. The criteria presented to evaluate the accuracy of the response results from each procedure, and to decide whether it is necessary to improve results by using the next procedure, utilize all the preceding computations and are therefore convenient.

In particular, a procedure is developed to evaluate the quality of results from a code-type analysis and, if necessary, to improve the results by proceeding to the SRSA method. It is shown that one such procedure, which was included in the ATC-3 seismic provisions, is

conceptually deficient. A rational procedure is presented, which recognizes all the important parameters: the shape of the design spectrum, the fundamental vibration period T_1, the stiffness ratio ρ, and the effective weights for the first two vibration modes.

It is believed that the simplified response spectrum analysis (SRSA) will provide results for earthquake-induced forces and deformations that are sufficiently accurate for the final design of many buildings. In all cases, it will provide the basis for a very good preliminary design. Thus the SRSA method should be very useful in practical design applications because, although much simpler than the RSA method, it provides very similar estimates of design forces for many buildings.

Buildings are usually designed to deform beyond the yield limit during moderate to intense ground shaking. In many cases, the effects of inelastic behavior on the design forces and deformations can be considered by response spectrum analysis based on the design spectrum for inelastic systems associated with an allowable ductility factor instead of the elastic design spectrum. The SRSA method presented herein would also be convenient for such simplified inelastic analyses.

REFERENCES

1. Applied Technology Council, "Tentative Provisions for the Development of Seismic Regulations for Buildings," *Report ATC 3-06,* NBS Special Publication 510, NSF Publication 78-08, June 1978.

2. Biggs, J.M., "*Introduction to Structural Dynamics,*" McGraw-Hill Inc., New York, 1964.

3. Blume, J.A., "Dynamic Characteristics of Multi-story Buildings," *Journal of the Structural Division, ASCE,* Vol 94, No ST2, Feb., 1968, pp 337-402.

4. Chopra, A.K., "*Dynamics of Structures, A Primer,*" Earthquake Engineering Research Institute, Berkeley, California, 1981.

5. Clough, R.W., and Penzien, J., "*Dynamics of Structures,*" McGraw-Hill Inc., New York, 1975.

6. Cruz, M.F., Lopez, O.A., "Numero de Modos para el Analisis Sismico de Edificios," *Boletin IMME,* Universidad Central de Venezuela, Caracas, Venezuela, Ano 18, No. 67, Jul.-Dec., 1980, pp. 19-43, (in Spanish).

7. Der Kiureghian, A., "A Response Spectrum Method for Random Vibrations," *Report No. UCB/EERC-80/15,* Earthquake Engineering Research Center, University of California, Berkeley, California, June, 1980.

8. Fenves, S.J., and Newmark, N.M., "Seismic Forces and Overturning Moments in Buildings, Towers, and Chimneys," *Proceedings of the Fourth World Conference on Earthquake Engineering,* Santiago, Chile, 1969, Vol I, B-5, pp. 1-12.

9. International Conference of Building Officials, *Uniform Buiding Code,* 1982.

10. Newmark, N.M., and Hall, W.J., "Vibration of Structures Induced by Ground Motion," Chapter 29, Part I, in *Shock and Vibration Handbook,* eds. C.M. Harris and C.E. Crede, 2nd Ed., McGraw-Hill Inc., New York, 1976.

11. Roehl, J.L., "Dynamic Response of Ground-excited Building Frames," *Ph.D. Thesis*, Rice University, Houston, Texas, Oct., 1971.

12. Rosenblueth, E., "Seismic Design Requirements in a Mexican 1976 Code," *Earthquake Engineering and Structural Dynamics*, Vol. 7, 1979, pp. 49-61.

13. Veletsos, A.S., Newmark, N.M., and Chelapati, C.V., "Deformation Spectra for Elastic and Elasto-Plastic Systems subjected to Ground Shock and Earthquake Motions," *Proceedings of the Third World Conference on Earthquake Engineering*, Wellington, New Zealand, 1965, Vol II, pp. 663-682.

14. Veletsos, A.S., "Maximum Deformation of Certain Nonlinear Systems," *Proceedings of the Fourth World Conference on Earthquake Engineering*, Santiago, Chile, 1969, Vol I, A-4, pp. 156-170.

15. Wilson, E.L., Yuan, M.W., Dickens, J.M., "Dynamic Analysis by Direct Superposition of Ritz Vectors," *Earthquake Engineering and Structural Dynamics*, Vol 10, No 6, Nov.-Dec., 1982.

APPENDIX A:

APPROXIMATE SECOND VIBRATION MODE SHAPE AND FREQUENCY

Several useful properties of the approximate second mode shape $\widetilde{\phi}_2$ and the approximate second mode frequency $\widetilde{\omega}_2$ can be easily shown by expressing $\widetilde{\phi}_2$ and $\widetilde{\omega}_2$ in terms of the exact mode shapes ϕ_n and frequencies ω_n of the structure using the orthogonality conditions satisfied by the exact vibration modes of the structure

$$\begin{aligned} \phi_n^T \mathbf{m}\, \phi_m &= 0 \\ \phi_n^T \mathbf{k}\, \phi_m &= 0 \end{aligned} \qquad \text{for } n \neq m \tag{A.1}$$

and

$$\begin{aligned} \phi_n^T \mathbf{m}\, \phi_m &= M_n \\ \phi_n^T \mathbf{k}\, \phi_m &= \omega_n^2 M_n \end{aligned} \qquad \text{for } n = m \tag{A.2}$$

From equations (21) to (23) in Section 3.2.2

$$\widetilde{\phi}_2 = \mathbf{k}^{-1}\, \mathbf{m}\, (1 - \frac{L_1}{M_1}\, \phi_1) \tag{A.3}$$

where 1 is a vector with all components equal to unity. But, since the mode shapes ϕ_n are orthogonal through $\mathbf{m}$

$$1 = \sum_{n=1}^{N} \frac{L_n}{M_n}\, \phi_n \tag{A.4}$$

then

$$\widetilde{\phi}_2 = \mathbf{k}^{-1}\, \mathbf{m} \left(\sum_{n=2}^{N} \frac{L_n}{M_n}\, \phi_n \right) = \sum_{n=2}^{N} \frac{L_n}{M_n} \frac{1}{\omega_n^2}\, \phi_n \tag{A.5}$$

Therefore, the approximate second mode shape ϕ_2 is orthogonal, through the mass and the stiffness matrices $\mathbf{m}$ and $\mathbf{k}$ to the exact first mode shape ϕ_1, because

$$\widetilde{\phi}_2^T\, \mathbf{m}\, \phi_1 = \sum_{n=2}^{N} \frac{L_n}{M_n} \frac{1}{\omega_n^2}\, \phi_n^T\, \mathbf{m}\, \phi_1 = 0 \tag{A.6}$$

and

$$\widetilde{\phi}_2^T \mathbf{k}\, \phi_1 = \sum_{n=2}^{N} \frac{L_n}{M_n} \frac{1}{\omega_n^2}\, \phi_n^T \mathbf{k}\, \phi_1 = 0 \tag{A.7}$$

That ϕ_2 is in fact an approximation to the exact second vibration mode shape can be shown by considering the following expression

$$\widetilde{\phi}_2 = \sum_{n=2}^{N} \frac{L_n}{M_n} \frac{1}{\omega_n^2}\, \phi_n = \frac{1}{\omega_2^2} \sum_{n=2}^{N} \frac{L_n}{M_n} \left(\frac{\omega_2}{\omega_n} \right)^2 \phi_n \tag{A.8}$$

and recognizing that the frequency ratios (ω_2/ω_n), by definition, are always less or equal to 1 and decrease as n increases. For example, for a uniform cantilever shear beam $(\omega_2/\omega_n) = 3/(2n-1)$ and for a uniform cantilever bending beam $(\omega_2/\omega_n) = 6.27, 1.0, 0.36, 0.18, 0.11, 0.07, \ldots, 2.23/(n-1/2)$. Also, the values of the participation factors (L_n/M_n) for the type of structures considered in this study (plane frames) normally decrease as the mode number n increases, but this is not necessarily so for other types of structures, especially three dimensional structures.

From equation (24) in Section 3.2.2 the approximate second vibration mode frequency is computed from

$$\widetilde{\omega}_2^2 = \frac{\widetilde{\phi}_2^T \mathbf{k}\, \widetilde{\phi}_2}{\widetilde{\phi}_2^T \mathbf{m}\, \widetilde{\phi}_2} \tag{A.9}$$

but, using equation (A.5)

$$\widetilde{\phi}_2^T \mathbf{k}\, \widetilde{\phi}_2 = \sum_{n=2}^{N} \left(\frac{L_n}{M_n} \right)^2 \frac{1}{\omega_n^4}\, \phi_n^T \mathbf{k}\, \phi_n \tag{A.10}$$

and

$$\widetilde{\phi}_2^T \mathbf{m}\, \widetilde{\phi}_2 = \sum_{n=2}^{N} \left(\frac{L_n}{M_n} \right)^2 \frac{1}{\omega_n^4}\, \phi_n^T \mathbf{m}\, \phi_n \tag{A.11}$$

then

$$\widetilde{\phi}_2^T \mathbf{k}\, \widetilde{\phi}_2 = \sum_{n=2}^{N} \left(\frac{L_n}{M_n} \right)^2 \frac{1}{\omega_n^4}\, \omega_n^2 M_n = \sum_{n=2}^{N} \frac{L_n^2}{M_n} \frac{1}{\omega_n^2} \tag{A.12}$$

and

$$\tilde{\phi}_2^T \mathbf{m} \tilde{\phi}_2 = \sum_{n=2}^{N} \left(\frac{L_n}{M_n} \right)^2 \frac{1}{\omega_n^4} M_n = \sum_{n=2}^{N} \frac{L_n^2}{M_n} \frac{1}{\omega_n^4} \tag{A.13}$$

Therefore,

$$\tilde{\omega}_2^2 = \frac{\sum_{n=2}^{N} \frac{W_n^*}{g} \frac{1}{\omega_n^2}}{\sum_{n=2}^{N} \frac{W_n^*}{g} \frac{1}{\omega_n^4}} \tag{A.14}$$

From the equation above, by re-arranging the terms can write

$$\tilde{\omega}_2^2 = \omega_2^2 \frac{\sum_{n=2}^{N} \frac{W_n^*}{g} \left(\frac{\omega_2}{\omega_n} \right)^2}{\sum_{n=2}^{N} \frac{W_n^*}{g} \left(\frac{\omega_2}{\omega_n} \right)^4} \tag{A.15}$$

then, clearly ω_2 is an approximation to the second mode frequency because the frequency ratios (ω_2/ω_n) are always less or equal to 1 and the effective weights W_n^* normally decrease as the mode number n increases making the ratio of the two sums above close to 1.0, but always larger. For example, for the uniform cantilever shear beam $(\tilde{\omega}_2/\omega_2) = 1.0616$, and for the uniform cantilever bending beam $(\tilde{\omega}_2/\omega_2) = 1.0226$. In Figure 6 the exact and approximate second vibration mode shapes (ϕ_2 and $\tilde{\phi}_2$) and frequencies (ω_2 and $\tilde{\omega}_2$) for the five frame cases considered in this part of the study are compared.

From a strictly mathematical perspective $\tilde{\phi}_2$ is the vector that results from making the initial vector $\mathbf{x}_2^* = \mathbf{k}^{-1} \mathbf{m} \mathbf{1}$ orthogonal (through the mass matrix $\mathbf{m}$) to the exact first mode shape ϕ_1 using the Gram-Schmidt orthogonalization procedure [2], which can be summarized as:

Given two vectors $\mathbf{x}_1$ and $\mathbf{x}_2^*$, want to obtain a third vector $\mathbf{x}_2$ such that $\mathbf{x}_1^T \mathbf{m} \mathbf{x}_2 = 0$, that is $\mathbf{x}_1$ and $\mathbf{x}_2$ are orthogonal through the matrix $\mathbf{m}$. Consider $\mathbf{x}_2 = \mathbf{x}_2^* - \alpha \mathbf{x}_1$, to satisfy the orthogonality condition α must be

$$\alpha = \frac{\mathbf{x}_1^T \mathbf{m} \mathbf{x}_2^*}{\mathbf{x}_1^T \mathbf{m} \mathbf{x}_1} \tag{A.16}$$

For our case $\mathbf{x}_1 = \boldsymbol{\phi}_1$, and $\mathbf{x}_2^* = \mathbf{k}^{-1}\,\mathbf{m}\,\mathbf{1}$ so that, using equation (A.4),

$$\mathbf{x}_2^* = \sum_{n=1}^{N} \frac{L_n}{M_n} \frac{1}{\omega_n^2}\,\boldsymbol{\phi}_n \tag{A.17}$$

Therefore,

$$\alpha = \frac{1}{M_1} \sum_{n=1}^{N} \frac{L_n}{M_n} \frac{1}{\omega_n^2}\,\boldsymbol{\phi}_1^T\,\mathbf{m}\,\boldsymbol{\phi}_n = \frac{L_1}{M_1} \frac{1}{\omega_1^2} \tag{A.18}$$

and

$$\mathbf{x}_2 = \sum_{n=1}^{N} \frac{L_n}{M_n} \frac{1}{\omega_n^2}\,\boldsymbol{\phi}_n - \frac{L_1}{M_1} \frac{1}{\omega_1^2}\,\boldsymbol{\phi}_1 = \mathbf{k}^{-1}\,\mathbf{m}\,(1 - \frac{L_1}{M_1}\,\boldsymbol{\phi}_1) = \tilde{\boldsymbol{\phi}}_2 \tag{A.19}$$

The procedure to compute $\tilde{\boldsymbol{\phi}}_2$, as presented in Section 3.2.2, is also equivalent to performing one iteration of the Rayleigh Method for the computation of higher modes frequencies and mode shapes [2] starting from the vector 1. The Rayleigh Method can be summarized as:
Given a starting vector $\mathbf{x}_2^{**}$ and the known first mode shape $\boldsymbol{\phi}_1$, take

$$\mathbf{x}_2^* = \mathbf{x}_2^{**} - \frac{\boldsymbol{\phi}_1^T\,\mathbf{m}\,\mathbf{x}_2^{**}}{M_1}\,\boldsymbol{\phi}_1 \qquad \text{and} \qquad \mathbf{x}_2 = \mathbf{k}^{-1}\,\mathbf{m}\,\mathbf{x}_2^* \tag{A.20}$$

The resulting vector $\mathbf{x}_2$ will be orthogonal to the first mode shape $\boldsymbol{\phi}_1$ through $\mathbf{m}$ and $\mathbf{k}$ and also a better approximation to the second mode shape $\boldsymbol{\phi}_2$ than the starting vector $\mathbf{x}_2^{**}$.
For our case, $\mathbf{x}_2^{**} = \mathbf{1}$ therefore $\boldsymbol{\phi}_1^T\,\mathbf{m}\,\mathbf{x}_2^{**} = L_1$ so that, from equation (A.20)

$$\mathbf{x}_2 = \mathbf{k}^{-1}\,\mathbf{m}\,(1 - \frac{L_1}{M_1}\,\boldsymbol{\phi}_1) = \tilde{\boldsymbol{\phi}}_2 \tag{A.21}$$

This sequence of steps corresponds exactly to using one iteration of the Stodola Iteration procedure for computing the second mode shape described in [2]:
Given a starting vector $\mathbf{x}_0$ and the known first mode shape $\boldsymbol{\phi}_1$ compute the approximation $\mathbf{x}_1^*$ to the exact second mode shape $\boldsymbol{\phi}_2$ from

$$\mathbf{x}_1^* = \mathbf{D}_2 \, \mathbf{x}_0 \tag{A.22}$$

where

$$\mathbf{D}_2 = \mathbf{D} \, \mathbf{S} \tag{A.23}$$

$$\mathbf{D} = \mathbf{k}^{-1} \, \mathbf{m} \tag{A.24}$$

$$\mathbf{S} = \left(\mathbf{I} - \frac{1}{M_1} \boldsymbol{\phi}_1 \, \boldsymbol{\phi}_1^T \, \mathbf{m} \right) \tag{A.25}$$

For our case $\mathbf{x}_o = 1$ then

$$\mathbf{x}_1^* = \mathbf{D}_2 \, 1 = \mathbf{D} \, \mathbf{S} \, 1 = \mathbf{k}^{-1} \, \mathbf{m} \left(\mathbf{I} - \frac{1}{M_1} \boldsymbol{\phi}_1 \, \boldsymbol{\phi}_1^T \, \mathbf{m} \right) 1$$

$$= \mathbf{k}^{-1} \, \mathbf{m} \left[1 - \frac{1}{M_1} (\boldsymbol{\phi}_1^T \, \mathbf{m} \, 1) \, \boldsymbol{\phi}_1 \right] = \mathbf{k}^{-1} \, \mathbf{m} \left(1 - \frac{L_1}{M_1} \boldsymbol{\phi}_1 \right) = \widetilde{\boldsymbol{\phi}}_2 \tag{A.26}$$

The approximate second mode shape $\widetilde{\boldsymbol{\phi}}_2$ corresponds to the first of the set of Ritz vectors proposed by Wilson *et al.* [15] to represent the loading $\mathbf{p}_r(t) = \mathbf{p}(t) - \mathbf{p}_1(t)$ (Section 3.2.2). This approximate second mode shape $\widetilde{\boldsymbol{\phi}}_2$ together with the exact first mode shape $\boldsymbol{\phi}_1$ form an alternative basis to solve the problem to the one produced by the procedure proposed by Wilson *et al.* using only the first two Ritz vectors. Because the two bases span different subspaces (of the N-dimensional vector space spanned by the N exact vibration mode shapes) the solutions obtained by the two procedures are in general different. For very special cases, when the static spatial distribution of the loading is proportional to a linear combination of two of the exact vibration mode shapes, both procedures produce exactly the two natural vibration modes of the system represented in the loading. It can be easily shown that the final Ritz vectors in the procedure proposed by Wilson *et al.* [15] correspond to the approximation to the exact vibration mode shapes computed after one iteration of the Subspace Iteration algorithm for the computation of vibration frequencies and mode shapes for the system with mass and stiffness matrices **m** and **k** (starting the iteration with a very special set of vectors, orthogonal through the mass matrix **m**) [A1], and since it is known that the convergence of this algorithm is good only for the first half of the vectors considered it can be expected that the second

mode shape approximation obtained by the Ritz vectors from Wilson's approach using only two vectors will be poor and can introduce rather large errors in the computed response.

REFERENCES

A1. Bathe, K-J, and E.L. Wilson, "*Numerical Methods in Finite Element Analysis,*" Prentice-Hall Inc., Englewood Cliffs, New Jersey, 1976.

APPENDIX B:

ERRORS IN BASE SHEAR FROM ONE MODE ANALYSIS BY SRSA METHOD

In the response spectrum analysis (RSA) method the maximum of the base shear $\overline{V}_0$ is computed from equations 3 and 8 in Section 3.1 as

$$\overline{V}_0 = \left[\sum_{n=1}^{N} \left(\frac{S_{an}}{g} W_n^* \right)^2 \right]^{1/2} \tag{B.1}$$

If the fundamental vibration period of the structure T_1 is within the accelcration-controlled region of the spectrum, then the acceleration response spectrum ordinates for the higher modes S_{an} are always smaller, or at best equal, than that of the first mode S_{a1}, that is $S_{an} \leq S_{a1}$ for n $= 2, 3, \ldots N$, and the maximum of the base shear can be written as

$$\overline{V}_0 \leq \frac{S_{a1}}{g} \left[\sum_{n=1}^{N} W_n^{*2} \right]^{1/2} \leq \frac{S_{a1}}{g} \left[W_1^{*2} + \sum_{n=2}^{N} W_n^{*2} \right]^{1/2} \tag{B.2}$$

$$\leq \frac{S_{a1}}{g} \left[W_1^{*2} + \left(\sum_{n=2}^{N} W_n^* \right)^2 \right]^{1/2}$$

For the type of structures considered in this study the effective weights of the individual vibration modes W_n^* add up to the total weight of the structure W, that is $W = \sum_{n=1}^{N} W_n^*$, and therefore the maximum base shear can be expressed as

$$\overline{V}_0 \leq \frac{S_{a1}}{g} \left[W_1^{*2} + (W - W_1^*)^2 \right]^{1/2} \tag{B.3}$$

The maximum base shear computed considering only the first mode contribution is given directly by

$$\overline{V}_{01} = \frac{S_{a1}}{g} W_1^* \tag{B.4}$$

To estimate the error in the single mode approximation value for the base shear $\overline{V}_{01}$ computed by SRSA we can compare it to the base shear $\overline{V}_0$ computed from RSA considering the contributions of all the vibration modes to the response using the ratio $\overline{V}_{01}/\overline{V}_0$. For structures with fundamental vibration period within the acceleration-controlled region can use the bound for $\overline{V}_0$ computed above (Equation B.3), then

$$\frac{\overline{V}_{01}}{\overline{V}_0} \geq \frac{W_1^*}{\left[W_1^{*2} + (W - W_1^*)^2\right]^{1/2}} \tag{B.5}$$

Defining $\eta = W_1^*/W$, the ratio of the first mode effective weight to the total weight of the structure, the equation above can be written as

$$\frac{\overline{V}_{01}}{\overline{V}_0} \geq \frac{\eta}{\left[\eta^2 + (1-\eta)^2\right]^{1/2}} \tag{B.6}$$

where $0 < \eta \leq 1$. The variation with η of this lower bound for the ratio $\overline{V}_{01}/\overline{V}_0$ is shown in Figure B1. For values of η larger than about 0.60, that is when the first mode effective weight W_1^* is larger than 60 percent of the total weight of the structure W, the bound for the ratio $\overline{V}_{01}/\overline{V}_0$ is not sensitive to changes in η and is always larger than about 0.85. For η below 0.6 the variation of $\overline{V}_{01}/\overline{V}_0$ is almost linear with η so the quality of the approximation to $\overline{V}_0$ obtained from $\overline{V}_{01}$ deteriorates rapidly.

If the errors in the single mode approximation to the maximum base shear $\overline{V}_{01}$ are to be kept within 5 percent of the maximum base shear values computed by RSA $\overline{V}_0$, the lower bound for the ratio $\overline{V}_{01}/\overline{V}_0$ should be 0.95. Therefore need to solve for η from

$$\frac{\eta}{\left[\eta^2 + (1-\eta)^2\right]^{1/2}} \geq 0.95 \tag{B.7}$$

with $0 < \eta \leq 1$ which gives $\eta \geq 0.753$. Thus if $W_1^*/W \geq 0.75$, that is the first mode effective weight is larger than 75 percent of the total weight of the structure, then $\overline{V}_{01}/\overline{V}_0$ will always be larger than 0.95, that is the error in the approximation for the maximum base shear obtained by considering only the first mode contribution is less than 5 percent, provided the

fundamental vibration period of the structure T_1 is within the acceleration-controlled region of the spectrum.

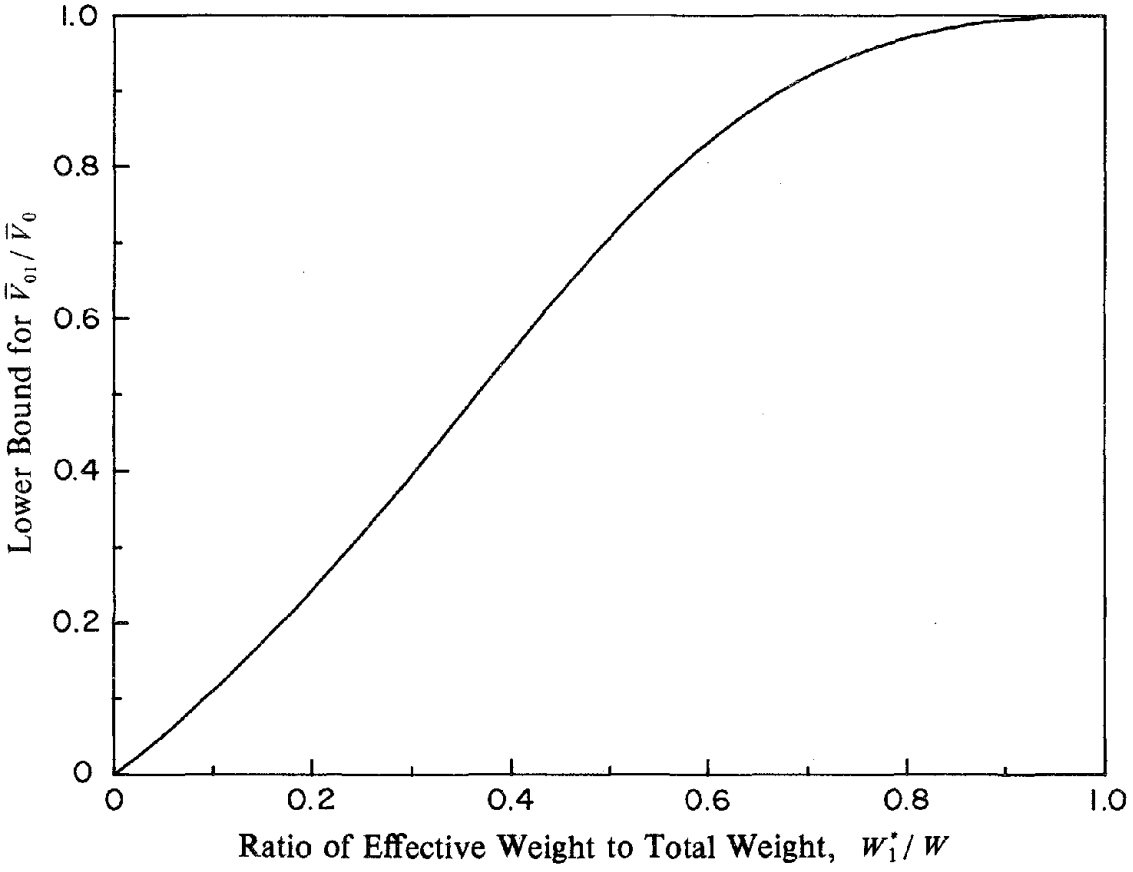

FIGURE B.1 Dependence of bound for first mode contribution to base shear on fundamental mode effective weight.

APPENDIX C: NOTATION

$a_g(t)$	time-history of ground acceleration due to earthquake ground motion
$\overline{a}_g$	maximum ground acceleration due to earthquake ground motion
E	modulus of elasticity
f_j	inertia force at floor level j due to displacements U_j
$\widetilde{f}_{j2}$	approximate equivalent lateral force at jth floor level in second natural vibration mode
$\widetilde{f}_{jn}$	maximum equivalent lateral force at jth floor level in nth natural vibration mode
$\widetilde{\mathbf{f}}_2$	vector of approximate equivalent lateral forces in the second vibration mode $\widetilde{f}_{j2}$
F_j	lateral force at jth floor level specified by the code formula
F_t	added lateral force at top floor level specified by the code formula
$\mathbf{F}$	vector of code lateral forces F_j
g	acceleration of gravity
h	story height
h_j	height from base to floor level j
h_n^*	effective height in the nth natural vibration mode
I_b	moment of inertia of beams
I_c	moment of inertia of columns
$\mathbf{k}$	stiffness matrix
L_b	length of beam
L_c	length of column
L_n	participation factor for the nth natural vibration mode

m_j	lumped mass at jth floor level
$\mathbf{m}$	mass matrix
M_n	modal mass in the nth natural vibration mode
$M_{0n}(t)$	time-history of base overturning moment in nth mode
$\overline{M}_{0n}$	maximum base overturning moment in nth mode
$\overline{M}_0$	maximum base overturning moment
$\overline{M}_b$	maximum bending moment among all beams
$\overline{M}_c$	maximum bending moment among all columns
$\overline{M}_i$	maximum overturning moment at story i
N	total number of floor levels in frame
p_{rj}	spatial distribution of lateral effective forces in higher modes, jth floor level, used to compute $\widetilde{\phi}_2$
$\mathbf{p}(t)$	time-history of lateral effective forces due to earthquake excitation
$\mathbf{p}_r$	vector of lateral effective forces p_{rj}
$\overline{P}_c$	maximum axial force among all columns
$\overline{r}$	maximum of response quantity r
$\overline{r}_n$	maximum of nth vibration mode component of response quantity r
S_a	pseudo-acceleration response (design) spectrum
S_{an}	spectral pseudo-acceleration ordinate for nth natural vibration mode
S_d	displacement response (design) spectrum
S_v	pseudo-velocity response (design) spectrum
t	time variable
T_1	fundamental vibration period of a multi-degree of freedom system

T_n	natural vibration period in the nth mode
u_j	normalized lateral displacement at jth floor level
$\hat{u}_j$	lateral displacement at jth floor level due to lateral forces f_j
$\overline{u}_g$	maximum ground displacement due to earthquake ground motion
$\overline{u}_N$	maximum top floor displacement
u_{rj}	lateral displacement at jth floor level due to lateral forces p_{rj}
$\widetilde{u}_{j2}$	approximate displacement at jth floor level in second mode
$\overline{u}_{jn}$	maximum lateral displacement at jth floor level on the nth vibration mode
$\mathbf{u}$	vector of lateral displacements u_j
$\mathbf{u}_r$	vector of lateral displacements u_{rj}
$\widetilde{\mathbf{u}}_2$	vector of approximate lateral displacements in second mode $\widetilde{u}_{j2}$
$\mathbf{u}(t)$	time-history of lateral displacements vector
U_j	normalized lateral displacement at jth floor level
$\hat{U}_j$	lateral displacement at jth floor level due to lateral forces F_j
$\mathbf{U}$	vector of normalized lateral displacements U_j
$\hat{\mathbf{U}}$	vector of lateral displacements $\hat{U}_j$
$\overline{v}_g$	maximum of ground velocity due to earthquake ground motion
$\overline{V}_0$	*maximum* of base shear
$\overline{V}_i$	maximum of story shear at story i
$V_{0n}(t)$	time-history of base shear in nth mode
$\overline{V}_{0n}$	maximum of base shear in nth mode
w_j	weight lumped at the jth floor level
W	total weight of the structure

$\widetilde{W}_1^*$	effective weight in the approximate first mode of vibration
$\widetilde{W}_2^*$	effective weight in the approximate second mode of vibration
W_n^*	effective weight in the nth natural vibration mode
1	vector with all components equal to 1
$\overline{\Delta}_{jn}$	maximum inter-story drift at jth story in the nth natural vibration mode
ξ_n	damping ratio in the nth natural vibration mode
ρ	beam-to-column stiffness ratio
ϕ_{jn}	jth component of the nth natural vibration mode
$\widetilde{\phi}_{j2}$	jth component of the approximate second vibration mode
ϕ	natural vibration mode shape
ϕ_n	nth natural vibration mode shape
$\widetilde{\phi}_2$	approximate second vibration mode shape
ω	natural vibration frequency
ω_n	nth natural vibration frequency
$\widetilde{\omega}_2$	approximate second vibration frequency

PART III

AN IMPROVED CODE-TYPE ANALYSIS PROCEDURE FOR PRELIMINARY DESIGN

1. INTRODUCTION

Since the early 1960's, the earthquake response of multistory buildings has been one of the most extensively researched subjects in earthquake engineering. Analytical procedures and computer programs have been developed to determine the earthquake response of structures; static, cyclic tests have been conducted on building components; dynamic tests on full-scale models of small buildings and medium-scale models of larger buildings have been conducted on shaking tables; experimental data has been correlated with analytical results and advanced analytical techniques have been applied to investigate the performance of buildings affected by past earthquakes. Hundreds of publications reporting the results of such research have appeared.

However very few of the advances in analytical structural dynamics have found their way into building codes in the United States or many other countries. Although the code formulas for base shear and lateral forces have gone through changes every few years, the underlying concepts in the Uniform Building Code are still based on the 1959 recommendations of the Structural Engineers Association of California [13]. Several years ago it became apparent that the analysis and design provisions should be comprehensively reviewed, the current state of knowledge should be evaluated, and a coordinate set of provisions should be developed. In response to this need the ATC-3 design provisions were published in 1978 [1], but so far they have not been incorporated in building codes. However, at about the same time a new version of Mexico's Federal District Building Code, which incorporated many recent research results, was developed [6,11].

The principal procedure specified in most building codes to estimate earthquake forces is an Equivalent Lateral Force Procedure. Formulas for base shear, height-wise distribution of lateral forces, and computation of overturning moments are the key elements of this procedure. Such formulas contained in the three design documents mentioned above are evaluated here in light of the results of dynamic analysis of buildings. It is demonstrated that

these formulas do not properly recognize the effects of some of the most significant building parameters. An improved procedure to compute the earthquake forces for the initial, preliminary design of buildings is presented.

Buildings designed for code forces are expected to deform beyond the yield limit during moderate to intense ground shaking. However, inelastic response history analysis, especially three-dimensional analysis, is an impractical requirement in the design of most buildings. It is believed that for many buildings satisfactory approximations to the design forces and deformations can be obtained by response spectrum analysis based on the design spectrum for inelastic systems associated with an allowable ductility factor instead of the elastic design spectrum. This is the concept underlying simplified, inelastic analysis procedures in building codes, e.g. the ATC-3 seismic design provisions or Mexico's Federal District Building Code [6,11]. It is therefore appropriate to base this study on elastic analysis and response of buildings. Furthermore, at this stage, this investigation is restricted to planar vibration of buildings without any torsional effects.

2. ANALYSIS PROCEDURES

2.1 Response Spectrum Analysis Procedure

The maximum response of a multistory building to horizontal earthquake ground motion can be estimated from the earthquake design spectrum by the following procedure [4]:

1. Define the smooth, elastic design spectrum for the structure at the particular site.
2. Define structural properties:
   (a) Compute the mass matrix $\mathbf{m}$ of the building with its mass appropriately lumped at floor levels.
   (b) Compute the lateral stiffness matrix $\mathbf{k}$ of the building from the complete stiffness matrix by condensing out the vertical and rotational degrees of freedom at the joints.
   (c) Estimate modal damping ratios ξ_n.
3. Solve the eigen problem

$$\mathbf{k}\,\boldsymbol{\phi} = \omega^2\,\mathbf{m}\,\boldsymbol{\phi} \tag{1}$$

   to determine the natural frequencies ω_n (natural periods $T_n = 2\pi/\omega_n$) and the modes $\boldsymbol{\phi}_n$ of vibration.
4. Compute the maximum response in individual modes of vibration by repeating the following steps for each mode of vibration:
   (a) Corresponding to period T_n and damping ratio ξ_n, read the ordinate S_{an} of the pseudo-acceleration design spectrum
   (b) Compute the effective weight W_n^* (or portion of the weight) of the building that participates in the nth mode of vibration from

$$W_n^* = \frac{\left[\sum_{j=1}^{N} w_j \ \phi_{jn}\right]^2}{\sum_{j=1}^{N} w_j \ \phi_{jn}^2} \tag{2}$$

where $w_j = m_j g$ is the weight at the jth floor level, ϕ_{jn} is the modal displacement of the jth floor, and N is the total number of floor levels. Also compute the effective height h_n^* from

$$h_n^* = \frac{\sum_{j=1}^{N} h_j \ w_j \ \phi_{jn}}{\sum_{j=1}^{N} w_j \ \phi_{jn}} \tag{3}$$

where h_j is the height from the base to the jth floor level.

(c) Compute the maximum values $\overline{V}_{0n}$ and $\overline{M}_{0n}$ of the base shear $V_{0n}(t)$ and base overturning moment $M_{0n}(t)$ from

$$\overline{V}_{0n} = \frac{S_{an}}{g} \ W_n^* \tag{4}$$

and

$$\overline{M}_{0n} = h_n^* \ \overline{V}_{0n} \tag{5}$$

(d) Compute the maximum value of the equivalent lateral force at the jth floor level from

$$\overline{f}_{jn} = \overline{V}_{0n} \ \frac{w_j \ \phi_{jn}}{\sum_{i=1}^{N} w_i \ \phi_{in}} \tag{6}$$

and repeat this computation for all floors.

(e) Compute the floor displacements, or deflections, due to the lateral forces $\overline{f}_{jn}$ from

$$\overline{u}_{jn} = \frac{1}{\omega_n^2} \ \frac{g}{w_j} \ \overline{f}_{jn} \tag{7}$$

and repeat this computation for all floors.

(f) Compute the maximum deformation (or drift) in the jth story from the floor displacements using

$$\overline{\Delta}_{jn} = \overline{u}_{jn} - \overline{u}_{j-1,n} \tag{8}$$

and repeat this computation for all stories.

(g) Compute internal forces (story shears, story overturning moments and member forces) by static analysis of the structure subjected to equivalent lateral forces $\overline{f}_{jn}$.

5. Determine an estimate of the maximum $\overline{r}$ of any response quantity (displacement of a floor, deformation in a story, shear or moment in a story, etc) by combining the modal maxima $\overline{r}_n$ for the response quantity in accordance with the square-root-of-the-sum-of-the-squares (SRSS) formula:

$$\overline{r} = \left[\sum_{n=1}^{N} \overline{r}_n^2 \right]^{1/2} \tag{9}$$

The SRSS formula generally provides a good estimate of the maximum response for systems with well separated natural periods of vibration, a property typically valid for planar motion of a building. For structures with this property, the SRSS method provides results essentially identical to the CQC method [5]. However for very short fundamental periods --periods in the first third of the acceleration-controlled region of the spectrum (see Section 3.2)-- the maximum value of a response quantity is better estimated by the absolute sum combination of the modal maxima:

$$\overline{r} = \sum_{n=1}^{N} | \overline{r}_n | \tag{10}$$

since in that range of periods the modal responses are in phase and their maxima occur almost simultaneously (see Part I).

2.2 Building Code Analysis

The principal procedure to estimate earthquake forces, specified in the Uniform Building Code [7], ATC-3 design recommendations [1], and Mexico's Federal District Code [6,11] is an Equivalent Lateral Force procedure. Based on an estimate of the fundamental vibration period, formulas are specified in these building codes (for convenience in writing, at times, we refer to ATC-3 recommendations as a building code although they have not been adopted in a code) for the base shear and distribution of lateral forces over the height of the building. The design shears and moments for the various stories of the building are determined from static analysis of the building subjected to the lateral forces, with some codes permitting reductions in the resulting story moments. The formulas for base shear and equivalent lateral forces are presented in this section along with some observations on their relation to corresponding formulas in the response spectrum analysis procedure.

2.2.1 Base Shear

For the present purposes the formula for the design base shear in the above mentioned building codes and design recommendations can be expressed as

$$V_0 = C\ W \tag{11}$$

where W is the total weight and the seismic coefficient C depends on the fundamental vibration period T. The seismic coefficient specified in three codes are displayed in Figure 1 and may be expressed as follows:

Uniform Building Code (UBC):

$$C = \begin{cases} 0.12 & T \leq 0.31 \text{ sec.} \\ \dfrac{1}{15\sqrt{T}} & T \geq 0.31 \text{ sec.} \end{cases} \tag{12}$$

wherein the seismic zone coefficient Z, and the structural-type coefficient K have been selected as 1.

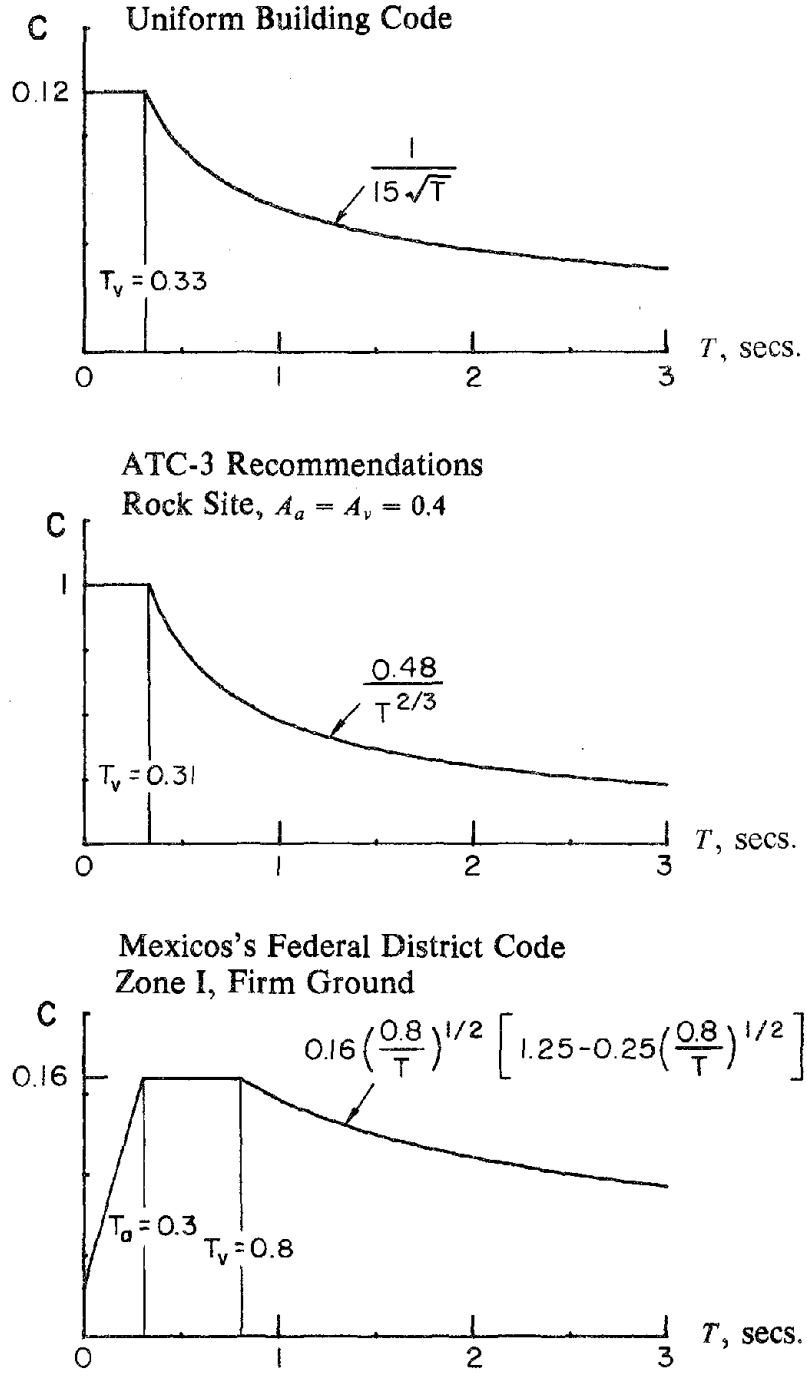

FIGURE 1 Seismic coefficient in building codes.

ATC-3 Recommendations:

$$C = \begin{cases} \dfrac{2.5\,A_a}{R} & T \leq 0.33 \text{ sec.} \\ \dfrac{1.2\,A_v}{R\,T^{2/3}} & T \geq 0.33 \text{ sec.} \end{cases} \tag{13}$$

for rock site. In equation (13), A_v and A_a are the seismic coefficients representing effective peak velocity-related acceleration and the effective peak acceleration, respectively, and R is the reduction factor to account for effects of inelastic behavior.

Mexico's Federal District Code (MFDC):

$$C = \begin{cases} \dfrac{S_a}{g} & T \leq T_v \\ \dfrac{S_a}{g}\left\{1 + 0.5\,r\,\left[1 - \left(\dfrac{T_v}{T}\right)^r\right]\right\} & T \geq T_v \end{cases} \tag{14}$$

where the pseudo-acceleration design spectrum S_a is given by

$$\frac{S_a}{g} = \begin{cases} a_0 + (A - a_0)\dfrac{T}{T_a} & T \leq T_a \\ A & T_a \leq T \leq T_v \\ A\left(\dfrac{T_v}{T}\right)^r & T \geq T_v \end{cases} \tag{15}$$

For Zone I, firm ground: $a_0 = 0.03$, $A = 0.16$, $T_a = 0.3$ sec., $T_v = 0.8$ sec., $r = 1/2$. To evaluate the base shear, the seismic coefficient is divided by the factor μ' which is related to the allowable ductility factor μ as follows

$$\mu' = \begin{cases} 1 + \dfrac{T}{T_a}(\mu - 1) & T \leq T_a \\ \mu & T \geq T_a \end{cases} \tag{16}$$

The seismic coefficients displayed in Figure 1 are for Uniform Building Code, ATC-3 recommendations with $A_v = A_a = 0.4$ and $R = 1$, and Mexico's Federal District Code with $\mu = 1$. Because the seismic coefficient is determined after reduction by R or μ' in ATC-3 recommendations and Mexico's Federal District Code respectively, the ordinates of the seismic

coefficient spectrum for these two codes are not directly comparable to the Uniform Building Code. However the comparison of the spectral shapes, especially for T greater than T_v will be useful. Each of the above design codes include variations in the above formulas to account for soil conditions, importance of the structure, but these factors are not considered in the present evaluation.

Among the three building codes considered, only the MFDC explicitly specifies the pseudo-acceleration design spectrum and recognizes that the base shear in buildings with fundamental vibration period larger than T_v, especially in "flexural" structures, exceeds the product of (S_a / g) and the total weight. The ATC-3 recommendations start with a design spectrum and raise its descending branch in the velocity- and displacement-controlled regions to decay at a slower rate with increasing T.

2.2.2 Distribution of Lateral Forces

The distribution of lateral forces over the height of the building is to be determined from the base shear in accordance with the formulas for the lateral force at the jth floor:

Uniform Building Code (UBC):

$$F_j = (V_0 - F_t) \frac{w_j \, h_j}{\sum_{i=1}^{N} w_i \, h_i} \tag{17}$$

with the exception that the force at the top floor computed from equation (17) is increased by an additional force

$$F_t = \begin{cases} 0 & T \leq 0.7 \text{ secs.} \\ 0.07 \; T \; V_0 & 0.7 < T < 3.6 \text{ secs.} \\ 0.25 \; V_0 & T \geq 3.6 \text{ secs.} \end{cases} \tag{18}$$

where w_i is the weight at the ith floor and h_i is the height of the ith floor above the base. Except for the additional force F_t assigned to the top of the building the UBC lateral forces are distributed over the height of the building under the assumption of linearly varying floor

displacement in the fundamental mode shape. Assignment of an additional force F_t at the top of the building is intended by the code to roughly and implicitly account for the contributions of the higher vibration modes to building response.

ATC-3 Recommendations:

$$F_j = V_0 \frac{w_j \; h_j^k}{\sum_{i=1}^{N} w_i \; h_i^k} \tag{19}$$

in which k is a coefficient related to the vibration period T as follows:

$$k = \begin{cases} 1 & T \leq 0.5 \text{ secs.} \\ (T + 1.5)/2 & 0.5 \leq T \leq 2.5 \text{ secs.} \\ 2 & T \geq 2.5 \text{ secs.} \end{cases} \tag{20}$$

The height-wise distribution of lateral forces is based on the assumption that the horizontal accelerations of floor masses are proportional to the elevation above ground for buildings with $T_1 \leq 0.5$ sec., to the square of this elevation for $T_1 \geq 2.5$ sec.; and to an intermediate power of this elevation for intermediate values of T_1. These force distributions are intended to recognize the changing fundamental mode shape and increasing higher mode contributions to response with increasing T_1 [3].

Mexico's Federal District Code (MFDC):

$$F_j = V_0^{(1)} \frac{w_j \; h_j}{\sum_{i=1}^{N} w_i \; h_i} + V_0^{(2)} \frac{w_j \; h_j^2}{\sum_{i=1}^{N} w_i \; h_i^2} \tag{21}$$

where the base shear V_0 of equation (11) has been separated into two parts: $V_0^{(1)}$ and $V_0^{(2)}$, distributed over the height assuming that the accelerations of floor masses are proportional to their elevation above ground, and to square of this elevation, respectively. These base shear components are

$$V_0^{(1)} = W \frac{S_a}{g} \left\{ 1 - r \left[1 - \left(\frac{T_v}{T} \right)^r \right] \right\} \tag{22}$$

$$V_0^{(2)} = W \frac{S_a}{g} \left\{ 1.5 \, r \left[1 - \left(\frac{T_v}{T} \right)^r \right] \right\} \tag{23}$$

The height-wise distribution of lateral forces is approximated by specifying horizontal accelerations proportional to elevation above ground, to the square of this elevation, or intermediate between these. The acceleration distribution implied in equation (21) passes smoothly from a straight line when $T = T_s$ to a parabola as T tends to infinity. This variation in acceleration distribution with fundamental vibration period T is intended to recognize the changing fundamental mode shape and increasing higher mode contributions to response with increasing T_1 [11].

2.2.3 Story Shears and Moments

The design shears for the various stories of the building are determined from static analysis of the building subjected to the lateral forces computed from the above equations.

The story moments can be similarly determined from the lateral forces by methods of statics. However, as will be seen in Section 4.3, there is a rationale for reducing the statically computed overturning moments to obtain the design values. The design value of moment in any story may then be expressed as a reduction factor multiplied by the statically computed moment. This reduction factor is specified in ATC-3 recommendations as 1.0 for the top 10 stories; between 1.0 and 0.8 for the next 10 stories from the top, linearly varying with height; 0.8 for the remaining stories. In Mexico's Federal District Code it is specified as varying linearly from 1.0 for the top story to 0.8 for the bottom story, with the additional requirement that even after modifying the computed moments at any story by the reduction factor, it should not be less than the product of the story shear at that elevation and the distance to the center of gravity of the portion of the building above the elevation being considered. This reduction factor is specified as 1.0 in the UBC, implying no reduction in the statically computed moments.

3. SYSTEMS AND DESIGN SPECTRUM

3.1 Systems Considered

The rectangular plane frames analyzed in this study are idealized as single-bay, moment-resisting plane frames with constant story height $= h$, and bay width $= 2h$ (Figure 2). Only flexural deformations are considered in the members which are assumed to be prismatic. The modulus of elasticity E is the same for all members but the moments of inertia of beams I_b and columns I_c --same for both columns in any story-- may vary over the height, as in cases 3 to 5 of Figure 2, with the ratio of the two same in all stories. The mass of the structure is assumed to be concentrated at the floor levels and the rotational inertia is neglected. The damping ratio for all the natural modes of vibration is assumed to be 5 percent.

Each building frame shown in Figure 2 is completely characterized by two additional parameters: the period of the fundamental mode of vibration T_1 and a stiffness ratio ρ. The latter was originally [2] defined as the ratio of the sum of the stiffness of all the beams at the mid-height story of the frame to the summation of the stiffnesses of all the columns at the same story, i.e.

$$\rho = \frac{\sum_{beams} EI_b / L_b}{\sum_{columns} EI_c / L_c} \tag{24}$$

For the one-bay frames considered in this study, this parameter reduces to

$$\rho = I_b \ / \ 4 \ I_c \tag{25}$$

and it has the same value for all stories.

This parameter is a measure of the relative beam-to-column stiffness and hence indicates the degree of frame action. The extreme values of ρ, 0 and ∞, represent the following limiting cases of a frame respectively: vertical cantilever with the beams imposing no restraint to joint rotations; and a shear building in which the joint rotations are completely restrained and deformations occur only through double curvature bending of columns. An intermediate value

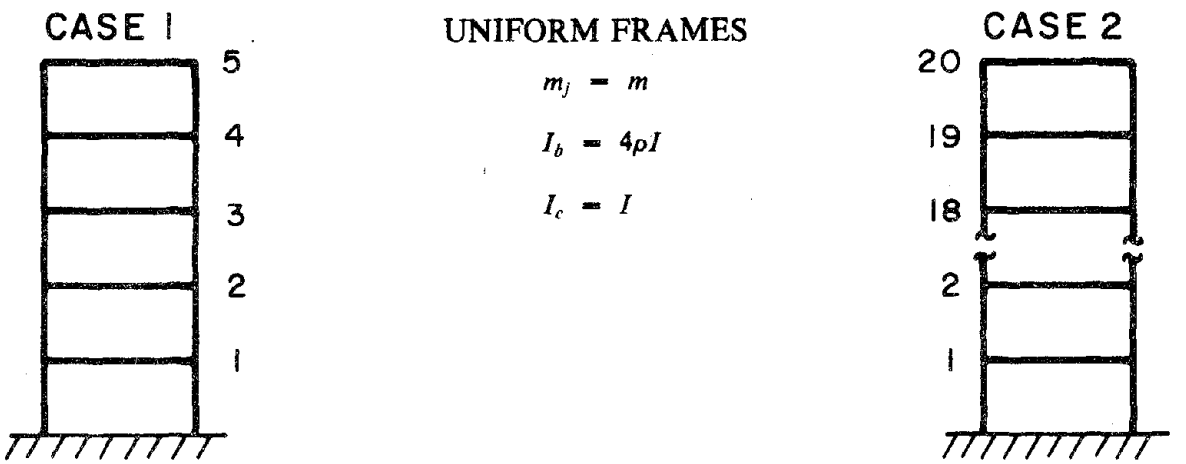

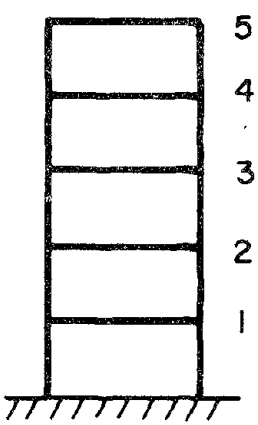

	CASE 3			CASE 4			CASE 5		
	m_j	I_b	I_c	m_j	I_b	I_c	m_j	I_b	I_c
5	m	$2\rho I$		$0.5m$	$2\rho I$		$0.3m$	$1.2\rho I$	
			$0.5I$			$0.5I$			$0.3I$
4	m	$3\rho I$		$0.75m$	$3\rho I$		$0.3m$	$1.2\rho I$	
			$0.75I$			$0.75I$			$0.3I$
3	m	$4\rho I$		m	$4\rho I$		$0.3m$	$1.2\rho I$	
			I			I			$0.3I$
2	m	$5\rho I$		$1.25m$	$5\rho I$		m	$4\rho I$	
			$1.25I$			$1.25I$			I
1	m	$6\rho I$		$1.5m$	$6\rho I$		m	$4\rho I$	
			$1.5I$			$1.5I$			I

FIGURE 2 Idealized building frames.

of ρ represents a frame in which beams and columns undergo bending deformations with joint rotation.

3.2 Earthquake Design Spectrum

The earthquake excitation is characterized by the smooth design spectrum of Figure 3 which is constructed by the well known procedures proposed by Newmark and Hall. This spectrum is for ground motions with maximum acceleration $\bar{a}_g$, velocity $\bar{v}_g$, and displacement $\bar{u}_g$ equal to $1g$, 48 in/sec, and 36 in, respectively. With this data and from the shape of the design spectrum, it is apparent that the maximum response of short period structures is controlled by the ground acceleration, that of long period structures by the ground displacement, and that of intermediate period structures by the ground velocity. The spectrum can thus be divided , as shown, into acceleration-controlled, velocity-controlled, and displacement-controlled regions. Amplification factors for these regions were selected from [8] for 84.1 percentile response and 5 percent damping ratio to construct the spectrum.

The design spectrum of Figure 3 is replotted in Figure 4 as a normalized pseudo-acceleration spectrum to emphasize that the spectral acceleration is constant in part of the acceleration-controlled region, varies as $1/T$ in the velocity-controlled region, and as $1/T^2$ in the displacement-controlled region.

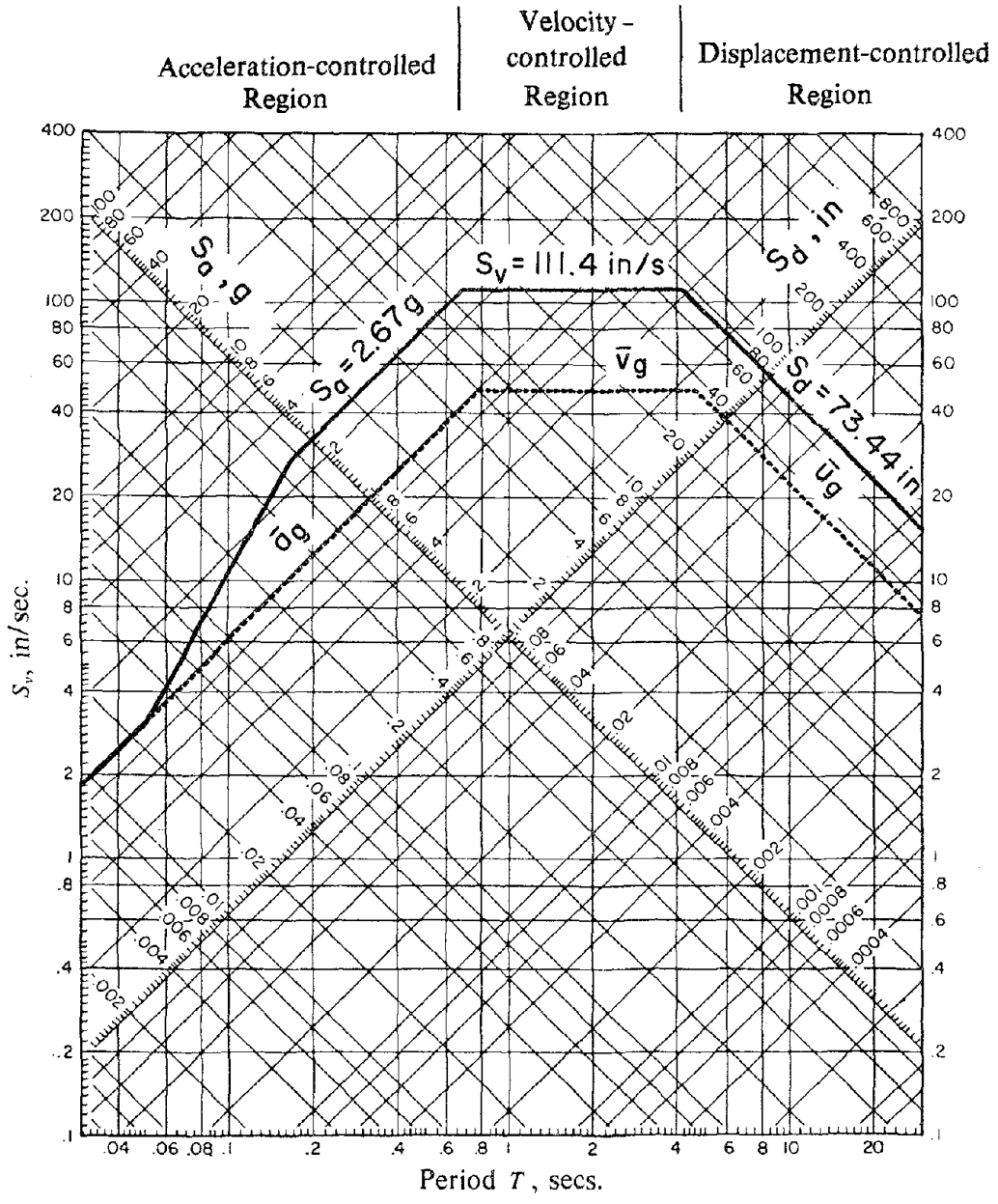

FIGURE 3 Design spectrum for ground motions with maximum ground acceleration $\bar{a}_g = 1g$, velocity $\bar{v}_g = 48$ in/sec, and displacement $\bar{u}_g = 36$ in; 84.1 percentile response and damping = 5%.

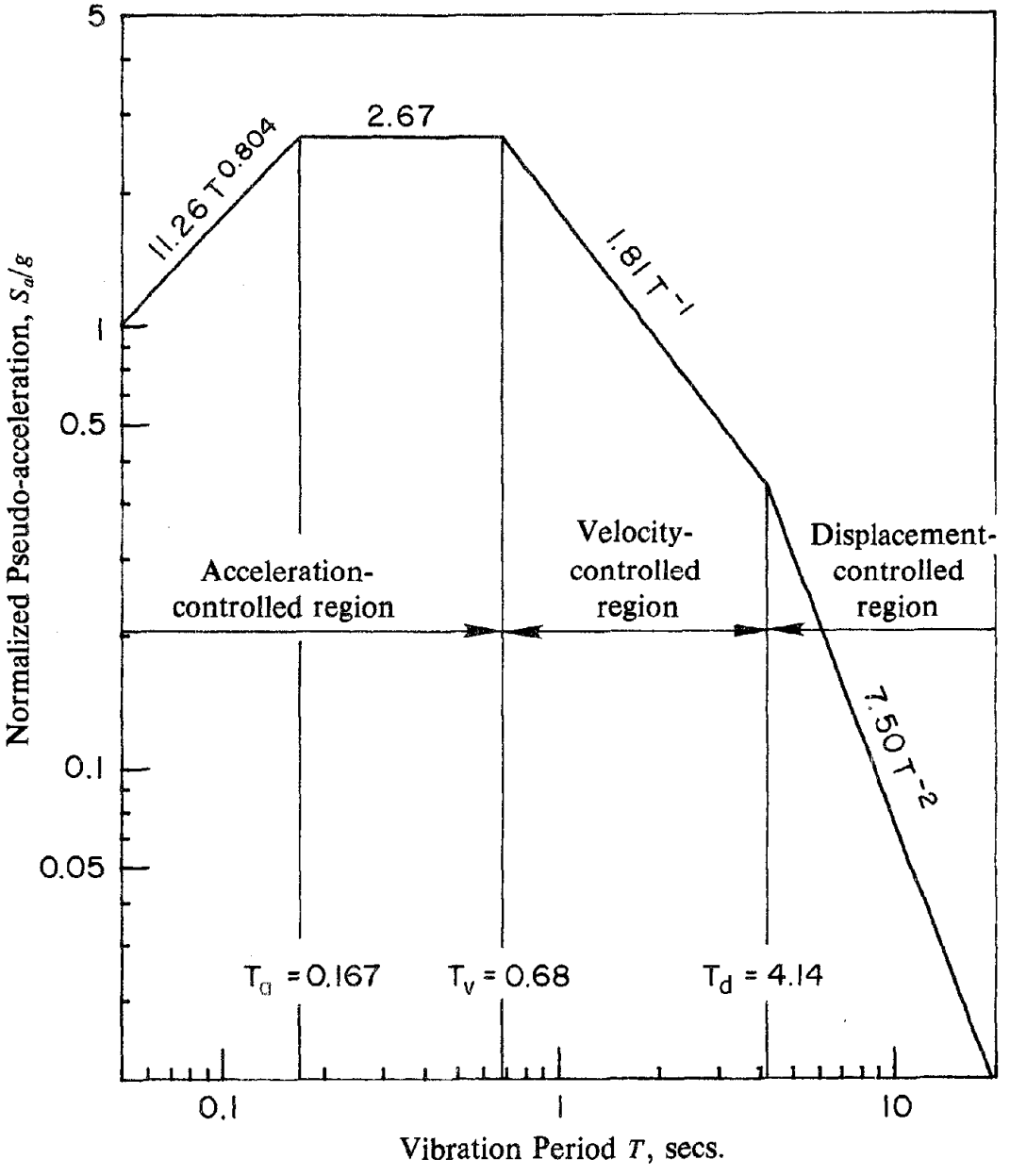

FIGURE 4 Normalized pseudo-acceleration design spectrum.

4. EVALUATION OF BUILDING CODE ANALYSIS PROCEDURES

4.1 Base Shear

The maximum response associated with the selected design spectrum, computed by the RSA procedure --wherein the contribution of all the natural vibration modes of the frame are included-- is plotted against the fundamental vibration period T_1 in the form of response spectra. Such a plot is presented in Figure 5 for the base shear in the uniform five-story frame (Case 1) for three values of $\rho = 0$, 0.125, and ∞. The base shear is presented in dimensionless form, having been normalized with respect to the effective weight W_1^* participating in the first vibration mode of the building. Also presented is the base shear considering the contribution of only the fundamental mode of vibration, which in the normalized form of Figure 5 is the same for all ρ values and is identical to the design spectrum of Figure 4.

It is apparent from Figure 5 that the normalized base shear for buildings with fundamental vibration period T_1 within the acceleration-controlled region of the spectrum is essentially identical to the contribution of only the fundamental vibration mode. However, for buildings with T_1 in the velocity- or the displacement-controlled regions of the spectrum, the response contributions of the vibration modes higher than the fundamental mode can be significant. They increase with increasing T_1 and decreasing ρ for reasons discussed elsewhere (see Roehl [10] and Part I of this report).

If the seismic coefficient C in building codes was defined as S_{a1}/g, the pseudo-acceleration ordinate at T_1 normalized with respect to the acceleration of gravity, the code formulas -- equation (11)-- would accurately predict the base shear for buildings with T_1 within the acceleration-controlled region of the spectrum provided the effective weight W_1^* was used instead of the total weight W in computing the code shear. However, the base shear formula in building codes is based on the total weight W, which obviously is always larger than W_1^*, resulting in a larger base shear. This is confirmed by replotting the results of Figure 5 in the form of a seismic coefficient spectrum as shown in Figure 6 wherein the base shear is

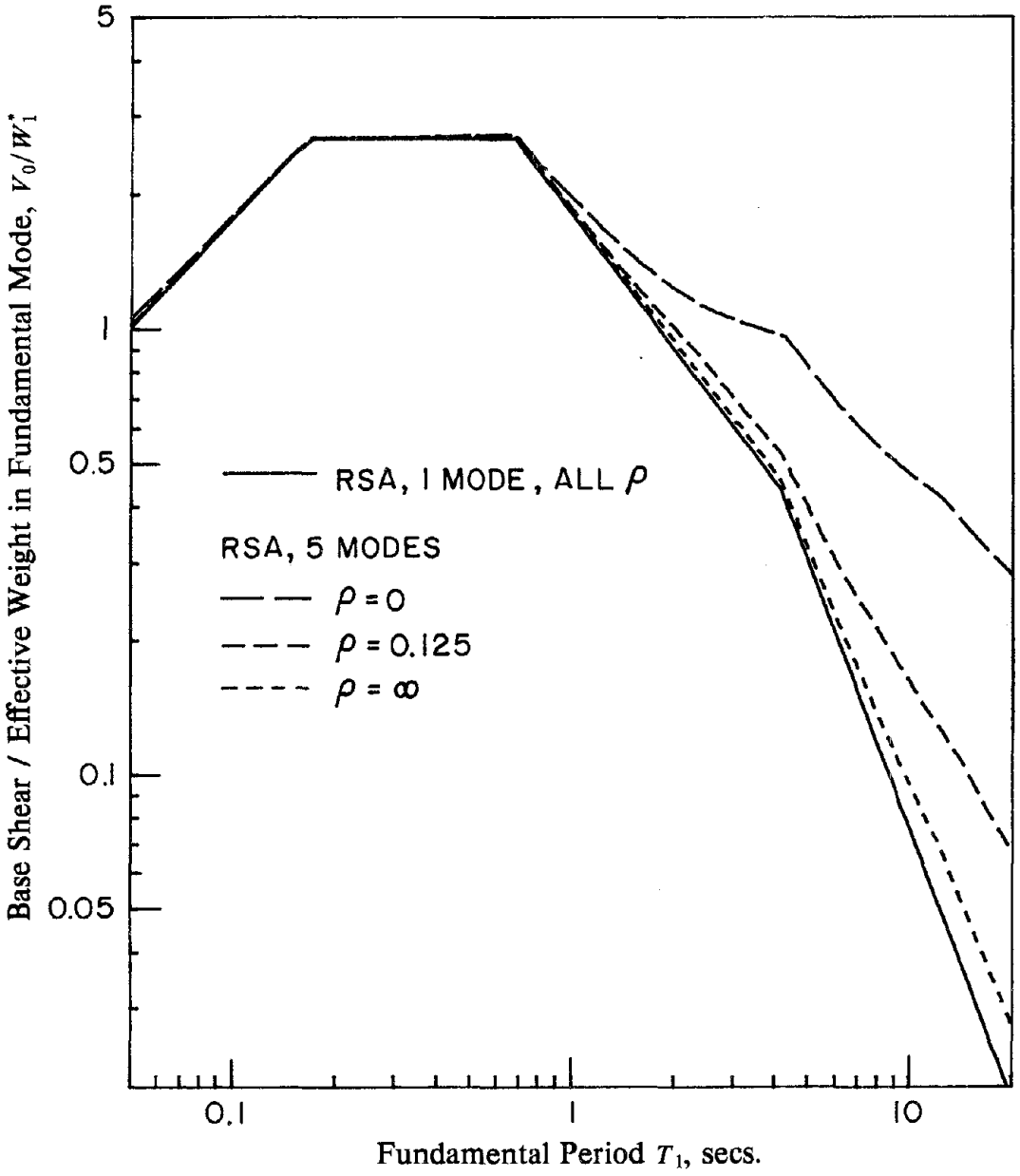

FIGURE 5 Normalized base shear in uniform five-story frame computed by response spectrum analysis (RSA) for three values of ρ.

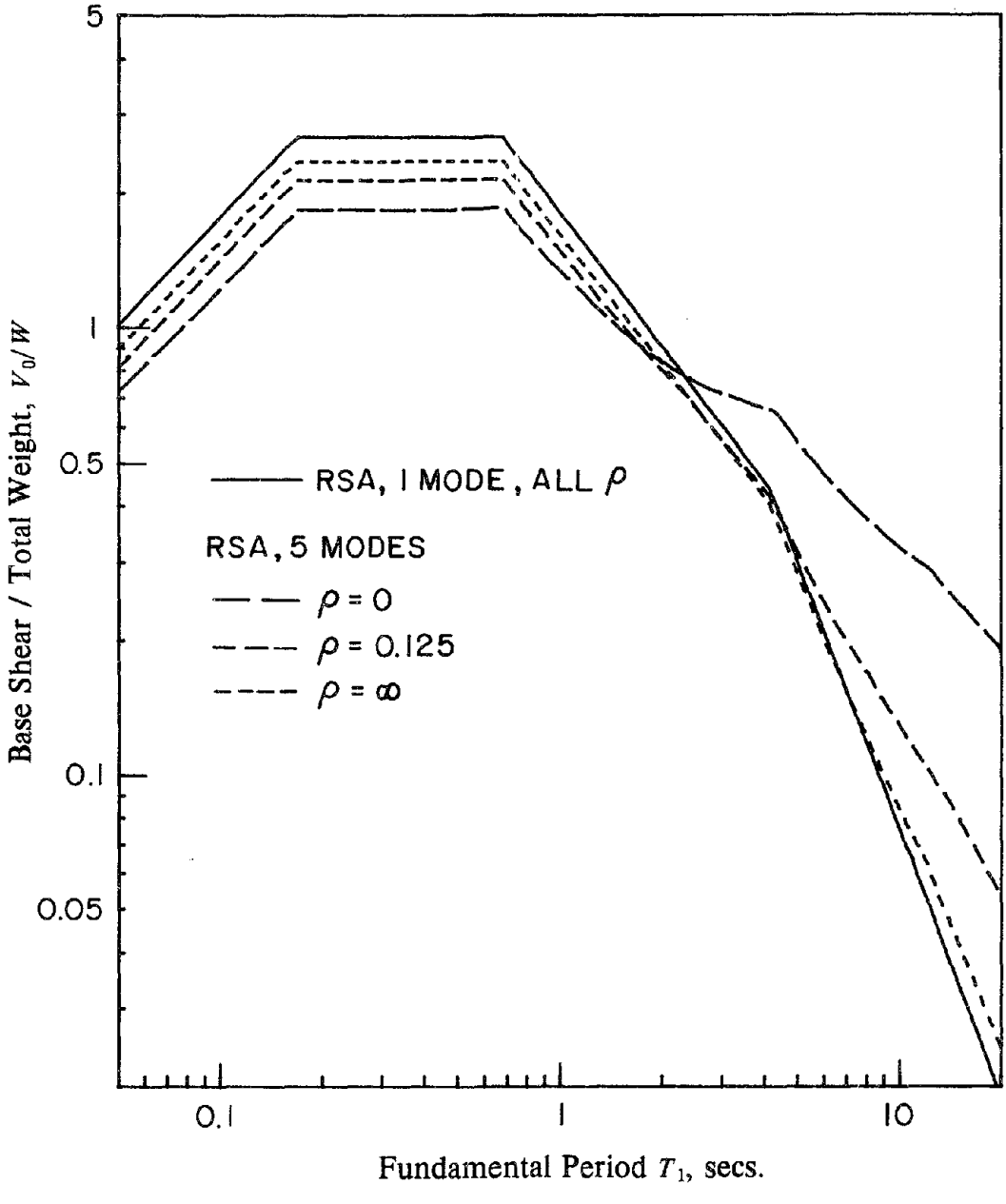

FIGURE 6 Seismic coefficient spectrum for uniform five-story frame computed by RSA for three values of ρ.

normalized with respect to the total weight. Within the acceleration-controlled region of the spectrum, for buildings with the same total weight the base shear decreases with decreasing ρ because W_1^* decreases with ρ (Table 1); and the code value for base shear exceeds the RSA value for all ρ values. However in the velocity- or displacement-controlled regions the higher mode contributions can be significant enough for the RSA value of base shear to exceed the code value. The code formula is inadequate for longer period buildings because it does not properly recognize the contributions of higher vibration modes and their dependence on the building parameters T_1 and ρ.

In order to further evaluate the response behavior in this period range, the curve $\alpha T^{-\beta}$ is fitted to the normalized base shear response spectrum of Figure 5. The parameters α and β, for each of the velocity- and displacement-controlled regions of the spectrum are evaluated by a least-squared error fit --that minimizes the error defined as the sum, over the range of periods considered, of the squares of the differences between the ordinates of the "exact" and the fitted curve on a logarithmic scale-- to the computed response with the following constraints: Firstly, the ordinate of the fitted curve at $T = T_v$ is equal to the "exact" value computed by RSA procedure, which for all values of ρ can be replaced by the ordinate of the flat part of the normalized pseudo-acceleration spectrum. Secondly, the curves fitted to the velocity- and displacement-controlled spectral regions have the same ordinates at $T = T_d$, the period value at the junction between the two regions. Comparison of the "exact" response spectra of Figure 5 with the fitted curves (Figure 7) indicates that the selected functions provide a satisfactory approximation to the computed response. The correlation coefficient presented in Table 2 indicates how closely the "exact" response can be approximated by the function $\alpha T^{-\beta}$ in each of the two spectral regions considered; a correlation coefficient = 1 represents a perfect fit, decreasing as the fit becomes poorer. This process of fitting curves $\alpha T^{-\beta}$ to the normalized base shear spectrum computed by the RSA procedure was repeated for all the frame cases of Figure 2, and the resulting values of β are presented in Table 3.

Table 1: Ratio of first mode effective weight W_1^* to total weight W for different frame models.

Frame Case	$\rho = 0$	$\rho = 0.05$	$\rho = 0.125$	$\rho = 0.5$	$\rho = 2$	$\rho = \infty$
1	0.679	0.764	0.796	0.835	0.862	0.880
2	0.629	0.785	0.800	0.814	0.824	0.830
3	0.656	0.714	0.741	0.773	0.792	0.804
4	0.579	0.662	0.701	0.750	0.784	0.806
5	0.457	0.531	0.560	0.601	0.634	0.658

Table 2: Correlation coefficients for least-squared error fit of functions $\alpha T^{-\beta}$ to the exact normalized base shear in uniform 5-story frames.

ρ	Spectral Regions		
	Acceleration–controlled	Velocity–controlled	Displacement–controlled
0	1.	0.971	0.999
0.125	1.	0.987	0.999
∞	1.	0.972	0.984

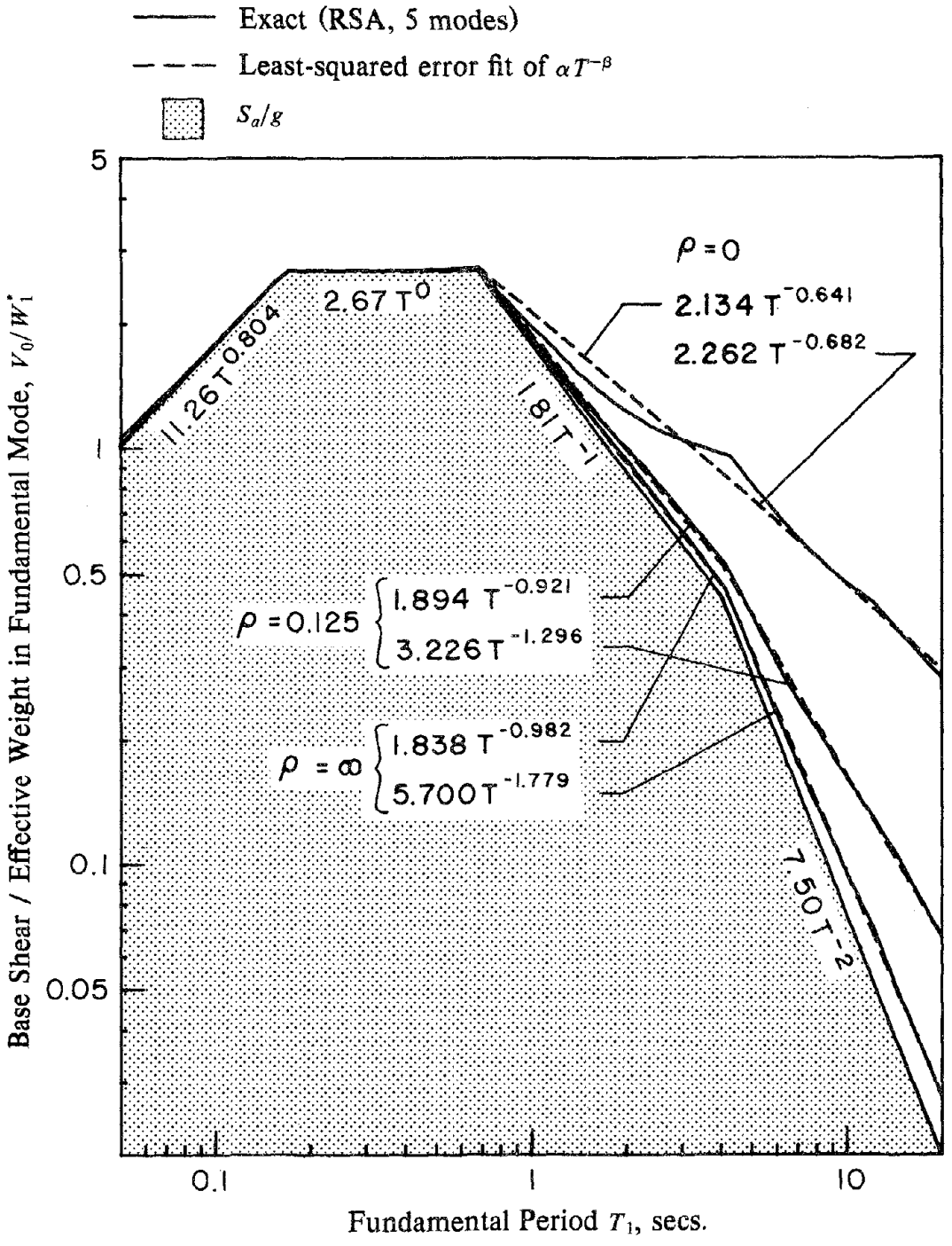

FIGURE 7 Least-squared error fit of functions αT^{β} to the exact base shear response spectrum for long periods. Uniform five-story frame.

Recalling that the difference between the normalized pseudo-acceleration response spectrum and the normalized base shear represents the contributions of the vibration modes higher than the fundamental mode, it is apparent from Figure 7 that these contributions can be approximately represented by raising the spectrum curve by changing the exponent $-\beta$ for T. The degree to which the spectrum needs to be raised for the velocity- and displacement-controlled spectral regions depends on the stiffness ratio ρ; the spectrum need be raised very little for shear buildings ($\rho = \infty$), but to an increasing degree with increasing frame action, i.e. decreasing ρ (Figure 7). The spectral modifications also depend on the number of stories, and mass and stiffness distributions of the building (Table 3).

Presented in Figure 8 are the fitted curves for normalized base shear from Figure 7 along with the seismic coefficients specified by UBC and MFDC codes and ATC-3 design recommendations [equations (12)-(16)]. All the curves presented in Figure 8 have been normalized to a unit maximum value. It is apparent that the seismic coefficient in building codes decreases with increase in period at a rate slower than demonstrated by dynamic analyses; but this does not necessarily imply that the codes are actually conservative. Furthermore none of the codes recognize that the normalized base shear, as predicted by dynamic analysis, in the long-period range depends significantly on the stiffness ratio ρ. However Mexico's Federal District code recognizes that, for long-period buildings, the base shear computed from $V_0 = (S_a/g)\,W$ should be increased to recognize that, in general, the longer the fundamental period of vibration the more important will flexural deformations tend to be relative to shear deformations and the more significant will the contributions of higher modes tend to be relative to the fundamental. But, even the MFDC code does not explicitly recognize that this increase in base shear depends not only on the fundamental period T_1 but also on the stiffness ratio ρ.

In summary, building codes attempt to account for the contributions of the higher modes of vibration to the base shear in a simple, empirical manner by increasing each of the two factors that are multiplied. The total weight W is used instead of the first mode effective weight W_1^*; and, for long-period buildings, the seismic coefficient used is increased above the design

Table 3: Exponents β_v and β_d in $T^{-\beta}$

for the decaying portion of the base shear response spectrum.

Frame Case	Spectral Regions	$\rho = 0$	$\rho = 0.125$	$\rho = \infty$
1	Velocity	-0.641	-0.921	-0.982
	Displacement	-0.682	-1.296	-1.779
2	Velocity	-0.600	-0.957	-0.964
	Displacement	-0.710	-1.570	-1.692
3	Velocity	-0.616	-0.866	-0.951
	Displacement	-0.702	-1.220	-1.688
4	Velocity	-0.487	-0.823	-0.954
	Displacement	-0.690	-1.258	-1.722
5	Velocity	-0.242	-0.613	-0.801
	Displacement	-0.875	-1.148	-1.525

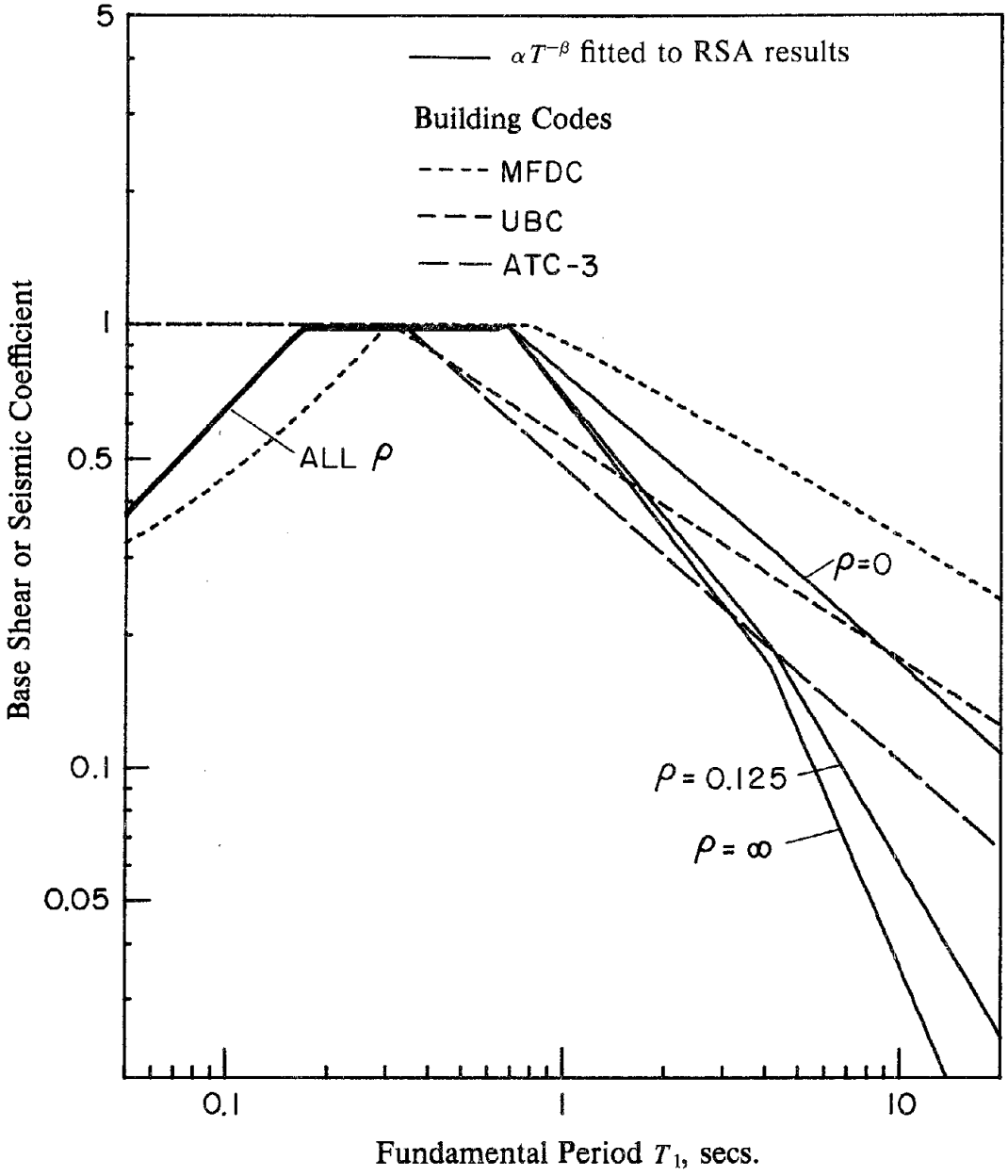

FIGURE 8 Comparison of seismic coefficient spectrum shapes in building codes with base shear spectrum shape computed by RSA for uniform five-story frame.

spectrum by raising its descending branch. Both of these concepts lead to the desired result of increasing the design base shear but the increases are not handled rationally because their dependence on building parameters T_1 and ρ is not recognized.

The above investigation has been concerned with the velocity- and displacement-controlled regions of the spectrum. In defining the seismic coefficient in the very-short period range, the MFDC recognizes the decrease in pseudo-accelerations as the period decreases, but the UBC or ATC-3 do not. In the later two, the flat part of the spectrum extends to zero period. The periods T_a and T_v at which the flat part of the spectrum begins and ends, respectively, vary from code to code.

4.2 Story Shears

Having examined the base shear computed by response spectrum analysis (RSA) procedure and compared it with code formulas, we next extend our investigation to story shears. The distribution of story shears over the height of the uniform 5-story frame (Case 1), computed by the RSA procedure including the contribution of all five modes of vibration, is presented in Figure 9 for three values of ρ, and four values of the fundamental period chosen to be representative of different period regions of the spectrum. Also presented are RSA results considering only the fundamental mode of vibration. The distribution of lateral forces, computed from the story shears of Figure 9 as the differences between the shears in consecutive stories, is presented in Figure 10. In a lumped mass system, such as the frames considered here, the lateral forces are concentrated at the floor levels and the shear remains constant in each story with discontinuities at each floor. However, such plots of lateral forces and story shears would not be convenient in displaying the differences among various cases and the alternative presentation with lateral forces and shears varying linearly over story height is used.

It is apparent from both these figures that, for the entire range of ρ, the contributions of the vibration modes higher than the fundamental mode are negligible in the response of buildings with short fundamental vibration period. Results generated for many more T_1 values

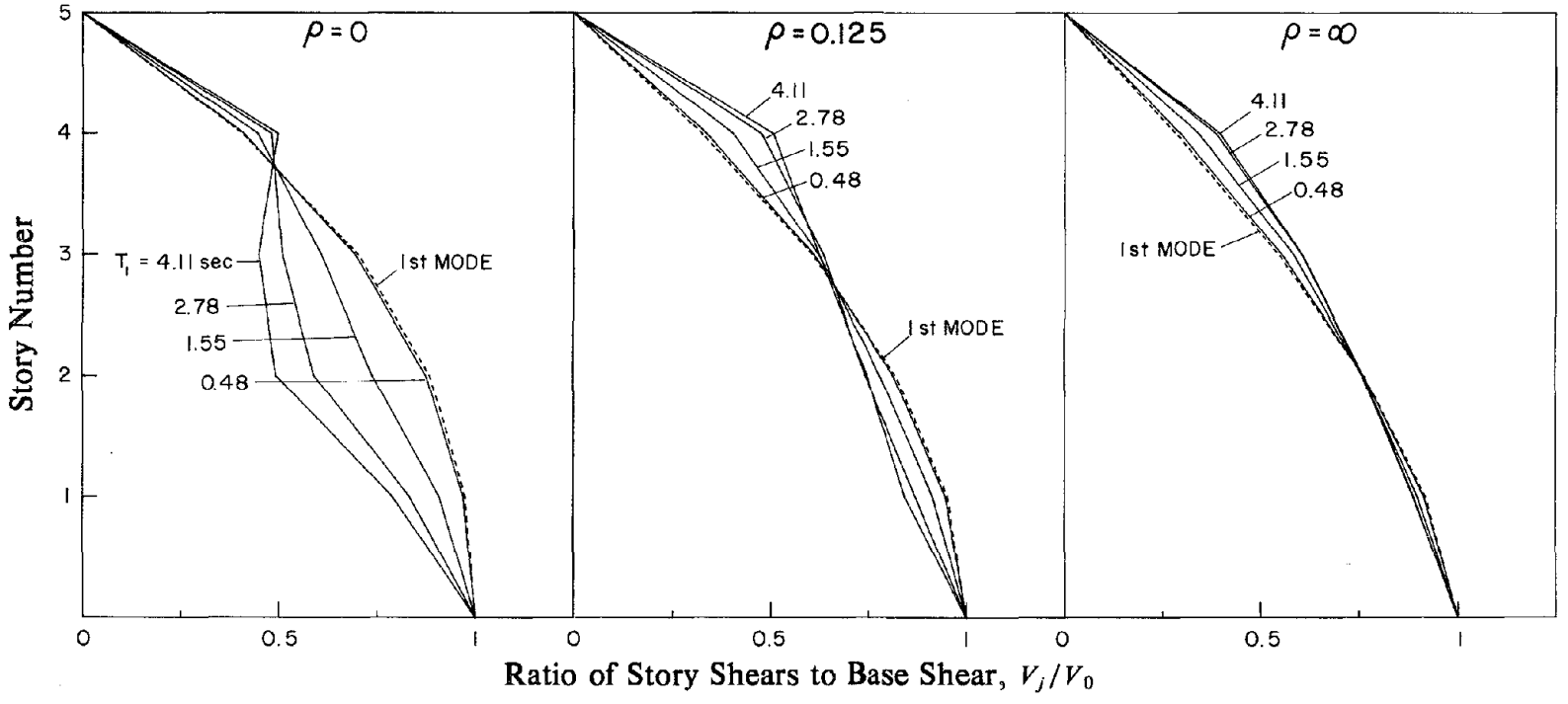

FIGURE 9 Distributions of story shears in uniform five-story frame computed by RSA including 1 or 5 modes for four values of T_1 and three values of ρ.

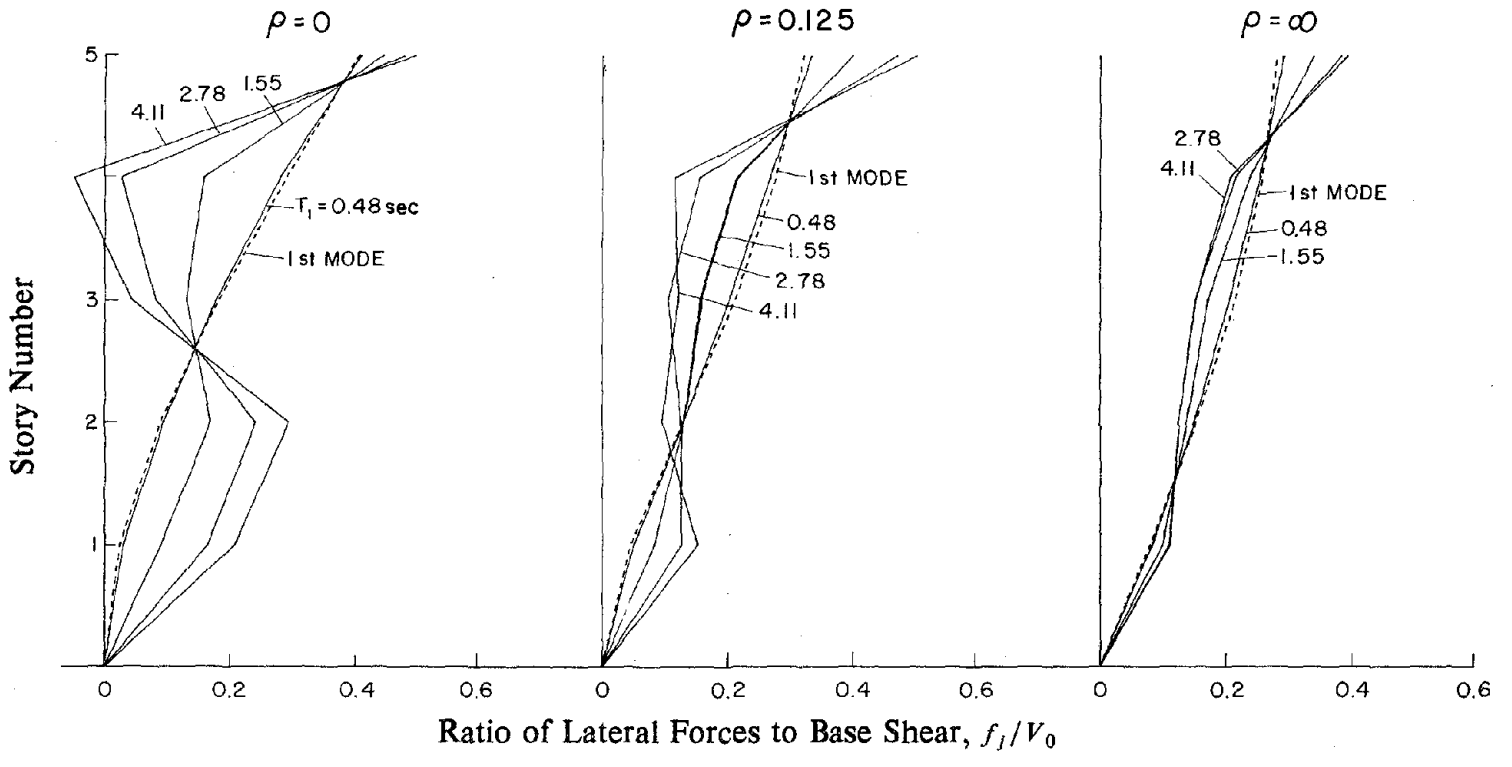

FIGURE 10 Distributions of equivalent lateral forces for uniform five-story frame determined from RSA story shears for four values of T_1 and three values of ρ.

than the four presented in Figures 9 and 10 indicated that the above observation is valid for T_1 within the acceleration-controlled region of the spectrum. The higher mode contributions become increasingly significant as T_1 increases in the velocity- or displacement-controlled regions of the spectrum. For a particular T_1 value, they are more pronounced as ρ decreases implying increasing frame action.

Figures 11 and 12 display the data presented in Figures 9 and 10 in reorganized form along with the distribution of lateral forces prescribed by the three building codes and the resulting story shears. As indicated by this comparison and other results not included here, for buildings within the acceleration-controlled region of the spectrum, the distribution of lateral forces and story shears specified by the three building codes are essentially identical and between the extremes predicted by RSA for $\rho = 0$ and ∞. With increasing fundamental vibration period T_1, the code distributions for lateral forces and story shears increasingly differ from the RSA results, especially for the smaller values of ρ, because under these conditions the higher modes contributions become more significant.

For long-period buildings, with T_1 in the velocity- or displacement-controlled regions, the higher mode contributions are pronounced enough to cause reversal of the curvature in the distribution of lateral forces, which the code formulas do not recognize. To account for this effect it has been suggested that the lateral forces be represented by a third-degree polynomial with its coefficients determined by a least-squared error fit to the RSA results [12], but this procedure appears impractical for code applications.

The RSA results and code forces presented in Figures 9-12 were all for uniform 5-story frames (Case 1). Whereas most of the plots are indicative of what to expect even for taller buildings, the lateral forces specified by UBC are an exception. In this case, the only part of the lateral force distribution that changes with vibration period T_1 is the additional force F_t concentrated at the top of the building. Therefore, as shown in Figure 13, the distribution of story shears near the top of the building is affected by the total number of stories in the building. Thus the seemingly good quality of results from UBC in Figures 11 and 12 for 5-story

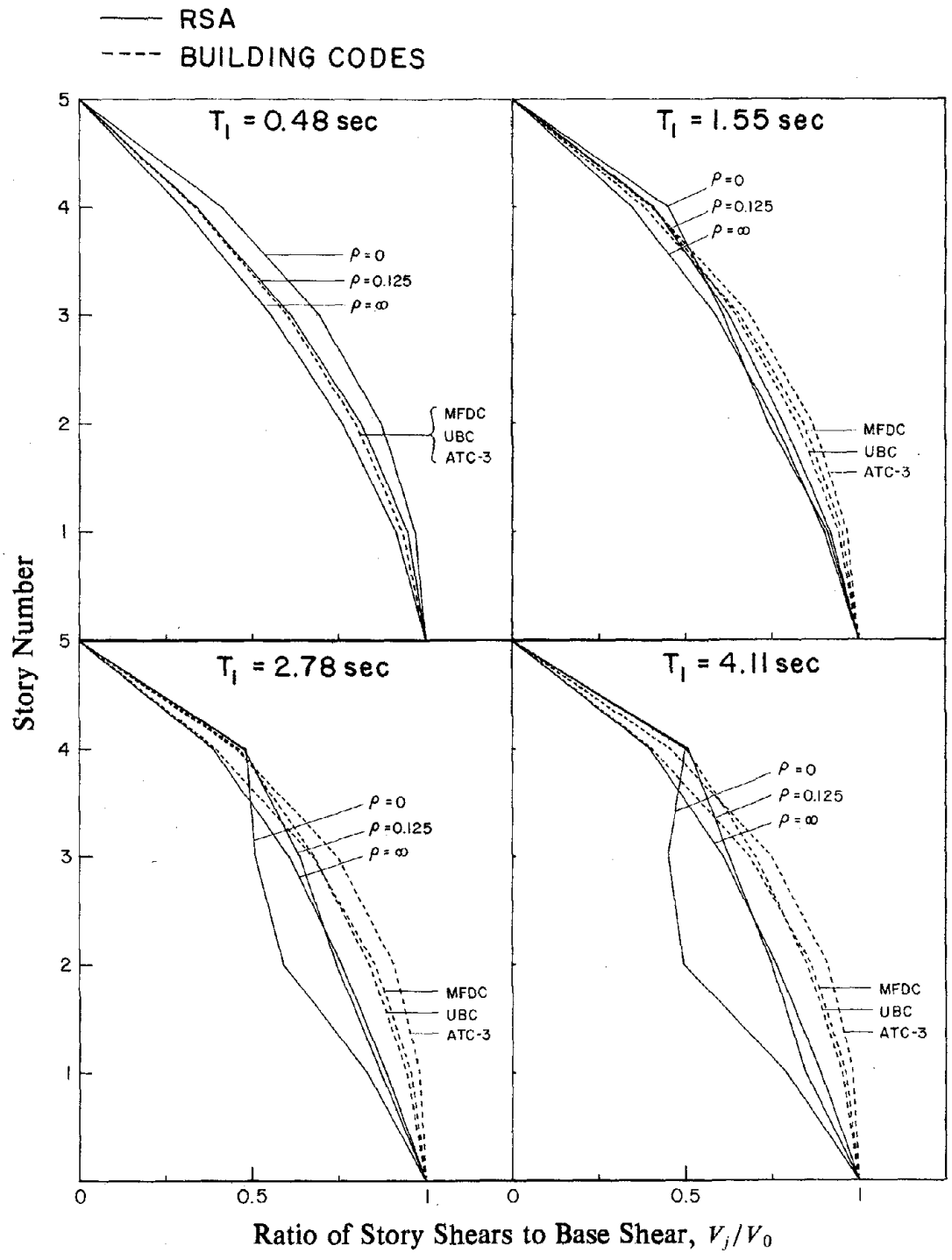

FIGURE 11 Comparison of story shear distributions for uniform five-story frame from building codes and RSA for four values of T_1 and three values of ρ.

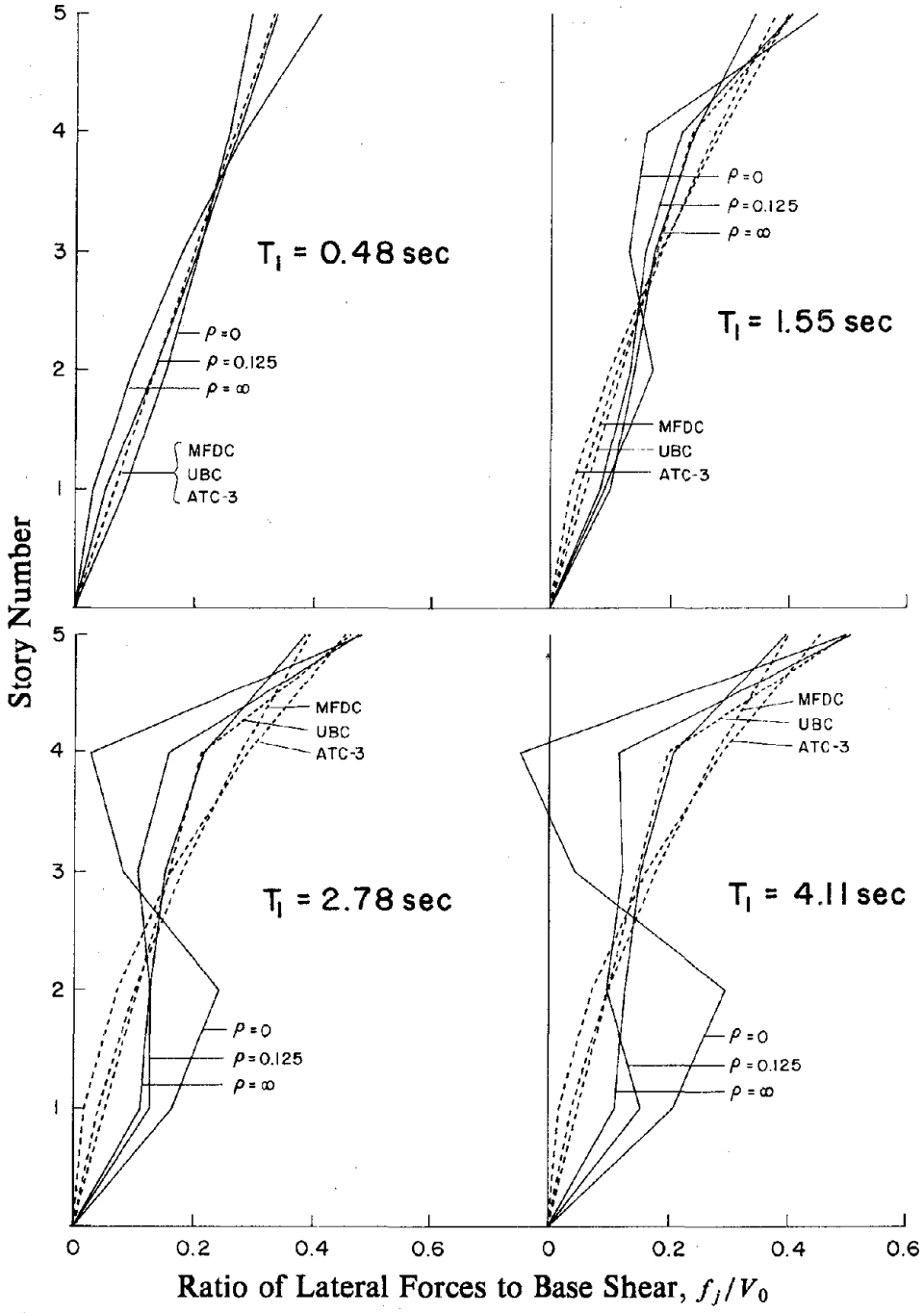

FIGURE 12 Comparison of equivalent lateral forces distributions for uniform five-story frame from building codes and RSA for four values of T_1 and three values of ρ.

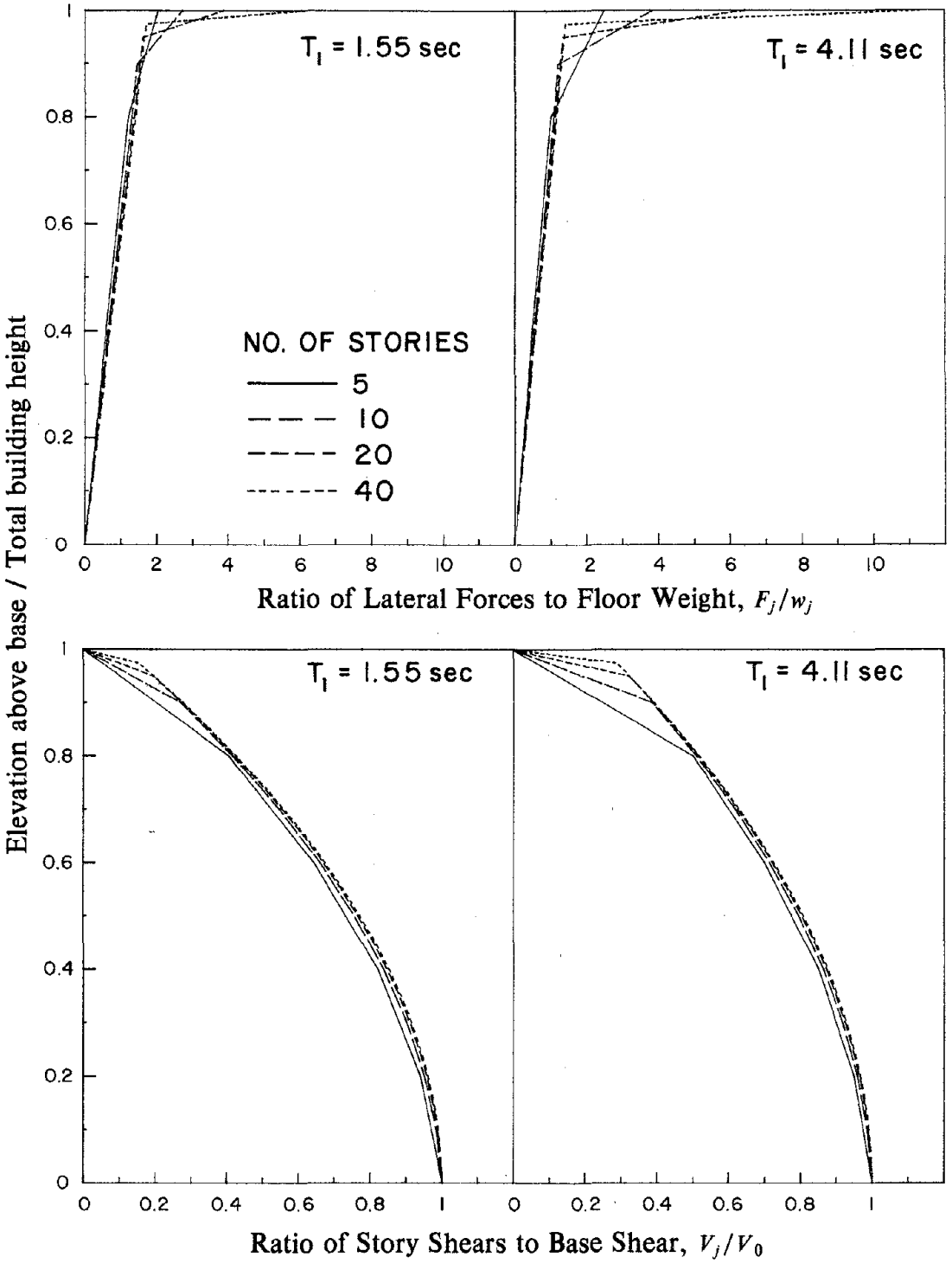

FIGURE 13 UBC distributions of equivalent lateral forces and corresponding story shears for uniform 5-, 10-, 20-, and 40-story frames.

buildings may not be valid for much taller buildings.

4.3 Overturning Moments

The maximum overturning moments due to earthquake ground motion, characterized by the design spectrum of Figure 3, were computed by including the contribution of all five modes of vibration in the response spectrum analysis (RSA) procedure. The base overturning moment is plotted in Figure 14 against the fundamental vibration period T_1 in the form of response spectra for three values of $\rho = 0$, 0.125, and ∞. The base overturning moment has been presented in dimensionless form, having been normalized with respect to $W_1^* h_1^*$, the product of the effective weight W_1^* and effective height h_1^*, both for the first vibration mode of the building. Also presented is the base overturning moment considering the contribution of only the fundamental mode of vibration, which when presented in the normalized form of Figure 14 is the same for all ρ values and is identical to the design spectrum of Figure 4. The distribution of story overturning moments over building height is presented in Figure 15 by plotting the ratio of the story moments to base moment for the same four values of T_1 selected earlier.

These figures demonstrate, similar to what was observed in the preceding sections, that the contributions of the higher modes of vibration increase with increasing T_1 and with decreasing ρ; but, as is well known, these contributions are less significant to the overturning moments compared to what they were for story shears. In particular, the higher modes contributions are negligible for buildings with T_1 within the acceleration-controlled region of the spectrum, irrespective of the ρ value; and for shear beams ($\rho = \infty$) irrespective of the T_1 value.

The RSA results of Figure 15 are displayed in Figure 16 in reorganized form along with the distributions of story overturning moments determined from the three building codes. For buildings with period T_1 within the acceleration-controlled region of the spectrum and even extending into a part of the velocity-controlled region of the spectrum, the code distributions are quite accurate. Their discrepancy relative to the RSA results increases with increasing T_1,

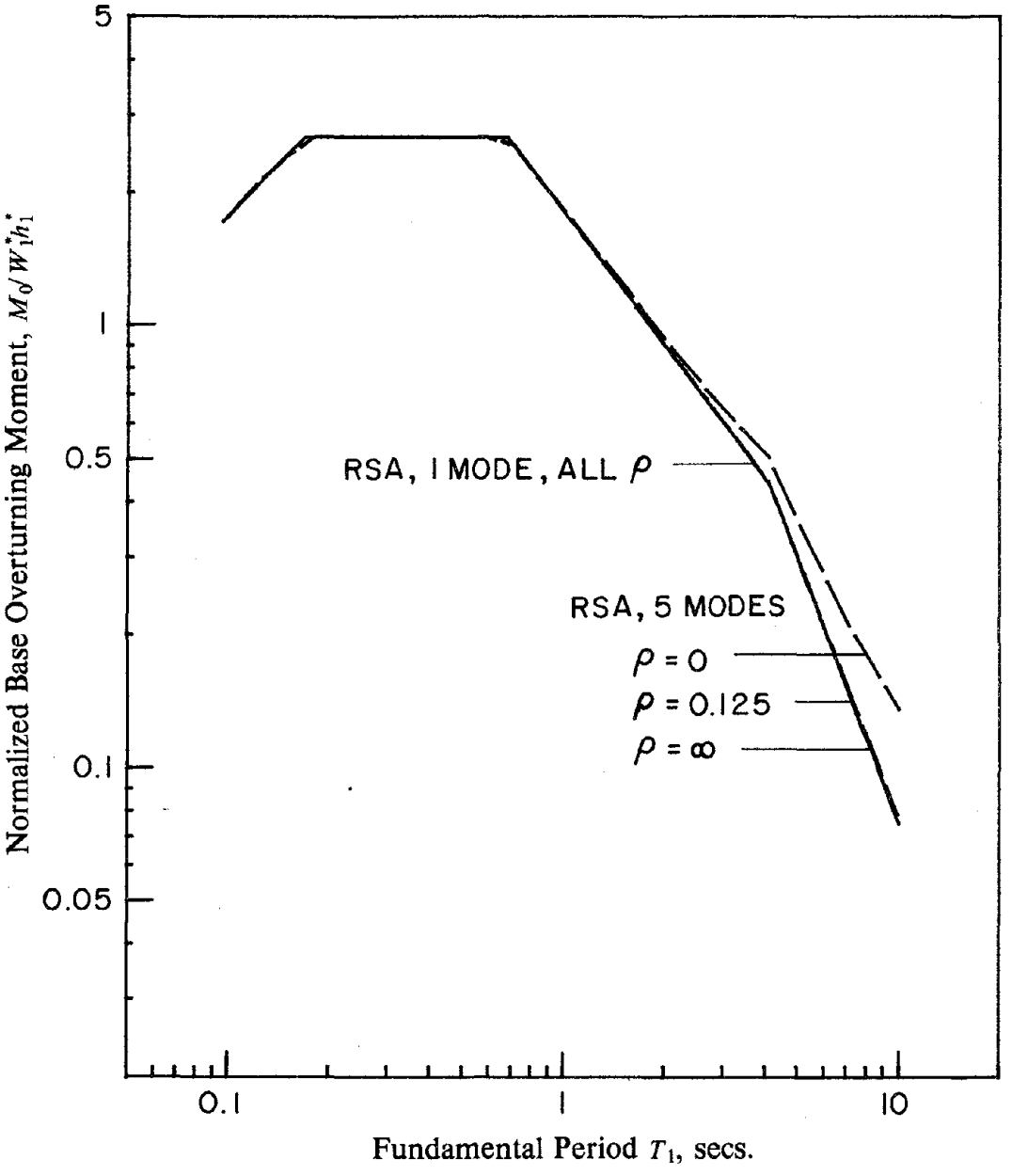

FIGURE 14 Normalized base overturning moment in uniform five-story frame computed by response spectrum analysis (RSA) for three values of ρ.

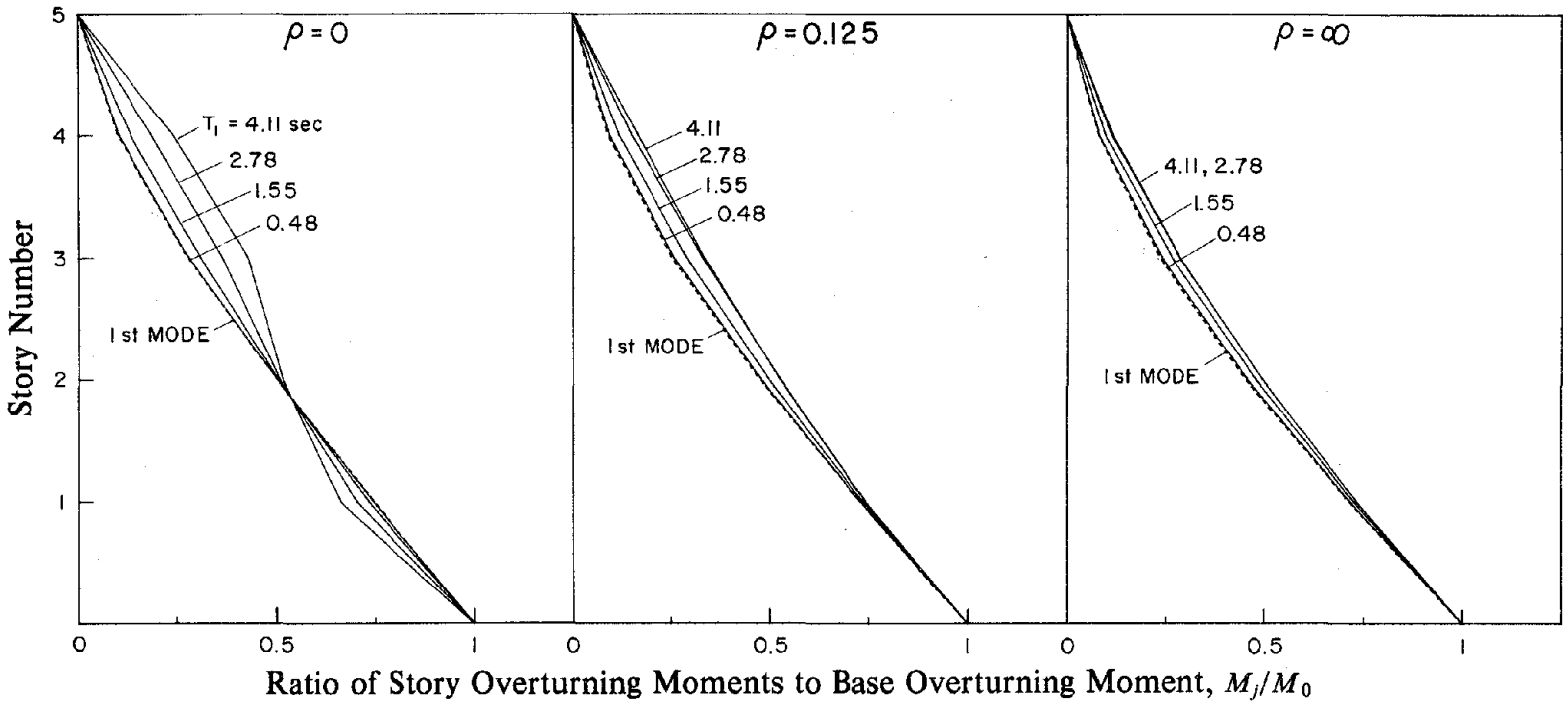

FIGURE 15 Distributions of story overturning moments in uniform five-story frame computed by RSA including 1 or 5 modes for four values of T_1 and three values of ρ.

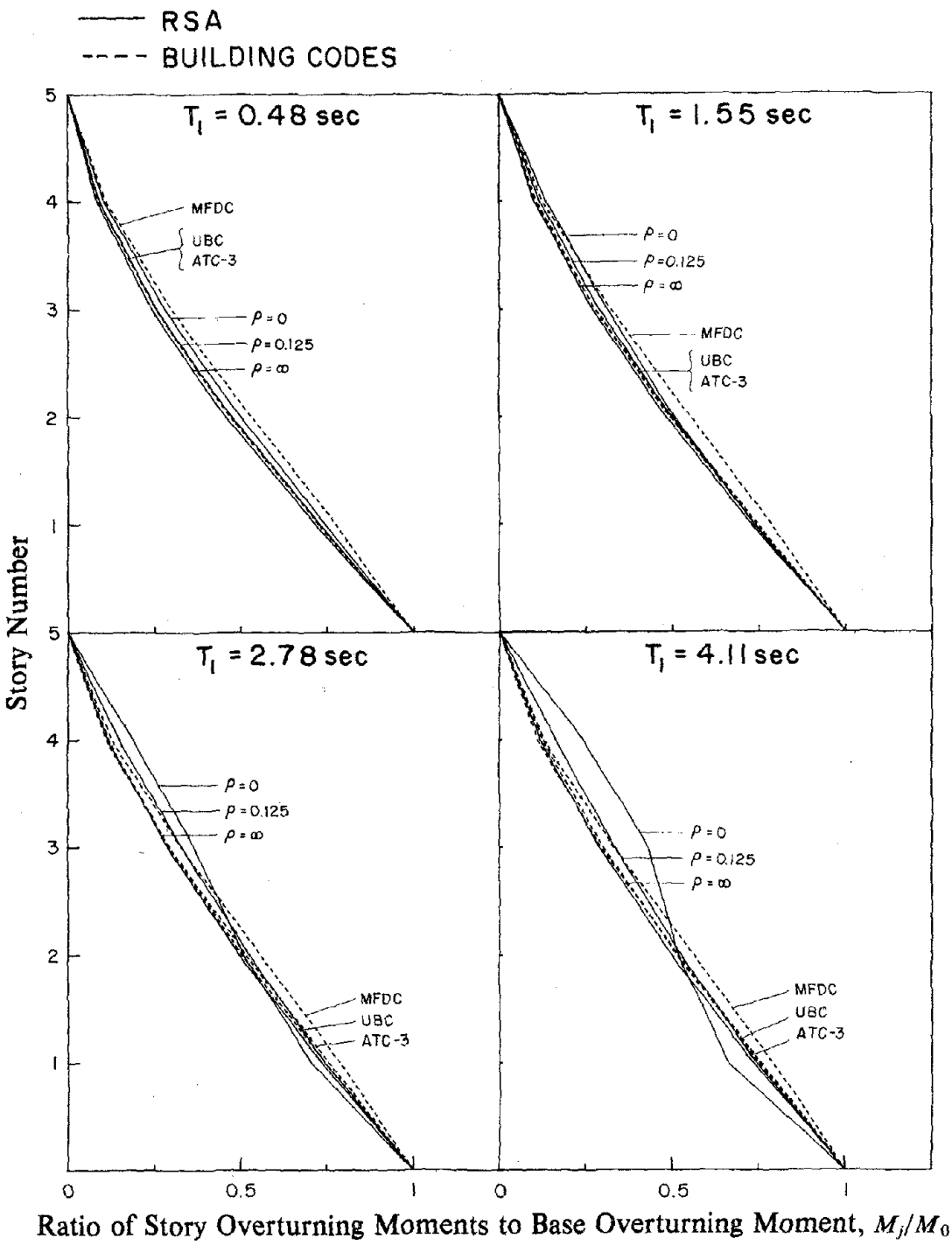

FIGURE 16 Comparison of story overturning moment distributions for uniform five-story frame from building codes and RSA for four values of T_1 and three values of ρ.

especially for buildings with smaller values of ρ, because the higher mode contributions, which become increasingly significant, are not properly recognized in the code formulas. However, the discrepancy in overturning moments computed by codes is much smaller than it was for shears, because the higher mode contributions to the moments are less significant.

A static analysis of a building with a particular T_1 and ρ subjected to the corresponding lateral forces presented in Figure 10 would provide the correct story shears, because the lateral forces were determined by statics from the story shears, but not the correct story overturning moments. This is demonstrated by presenting the ratio of overturning moments in a story computed by two procedures: (a) response spectrum analysis considering all vibration modes, presented in Figures 14 and 15; and (b) static analysis of the building subjected to the lateral forces of Figure 10. This ratio is akin to the reduction factor J specified in building codes. It is presented in Figure 17 for the base overturning moment as a function of the fundamental vibration period T_1 for three values of ρ; and in Figure 18 over the height of the building. The reduction factors never exceed unity, implying that the approximate value of overturning moment obtained from the lateral forces always exceeds the "exact" value obtained by the RSA procedure. The two values are identical for all values of T_1 if only the contribution of the fundamental vibration mode is considered. Thus, the discrepancy between the two values is directly associated with the fact that higher vibration modes contribute differently to shears and moments.

Because the lateral forces specified in building codes from which the story shears are computed by static analysis, are intended to provide estimates of story shears, the preceding observations from results of RSA procedure demonstrate that the overturning moments will be overestimated if they were also computed from the lateral forces by statics. Thus building codes usually specify reduction factors by which the statically-computed moments should be multiplied. These reduction factors defined earlier for the three codes being considered are presented in Figures 17 and 18. The reduction factors specified by UBC and MFDC are independent of the fundamental period T_1, except for the slight variation arising in the latter

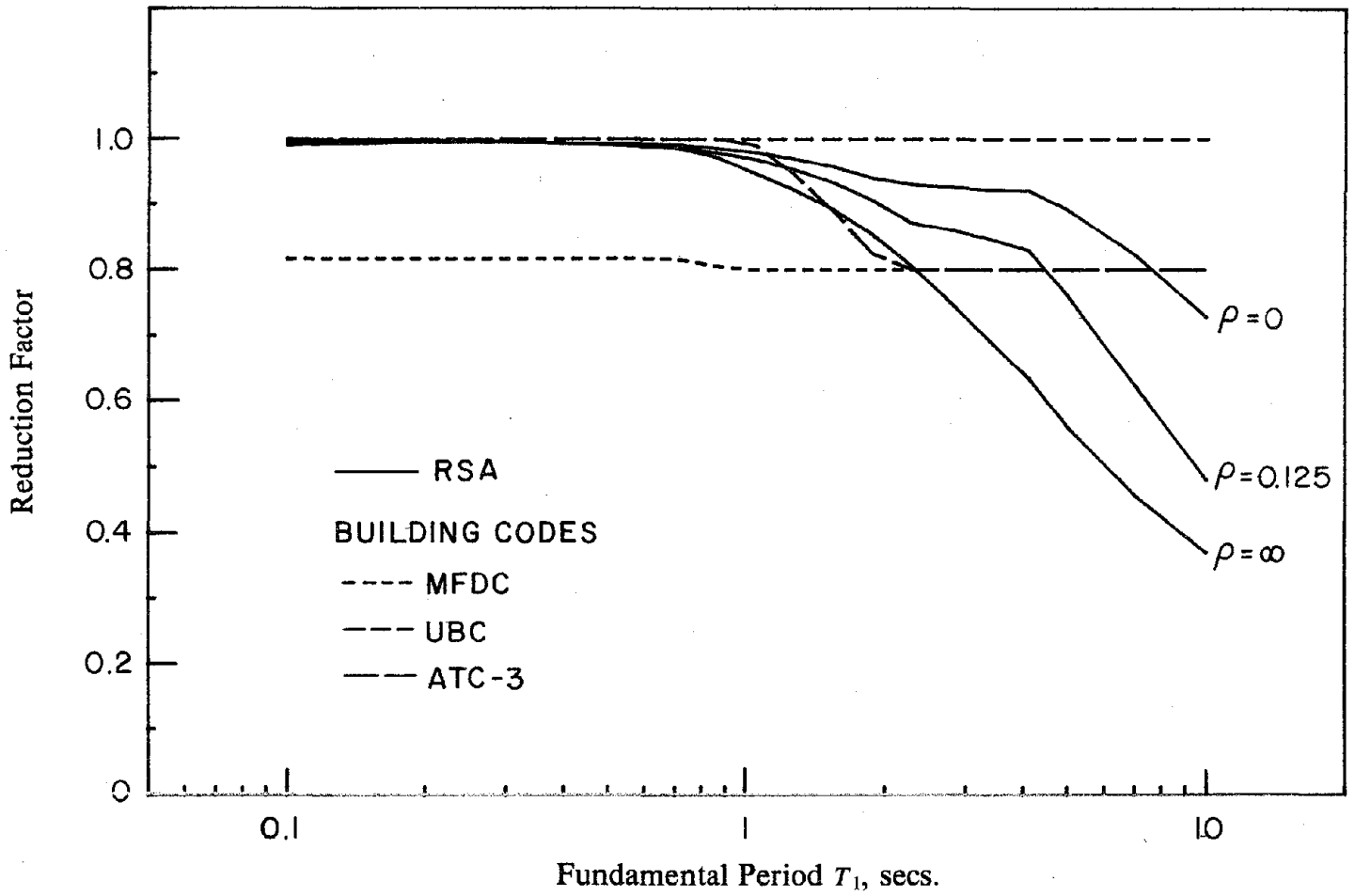

FIGURE 17 Reduction factors for base overturning moment from building codes compared with RSA results for uniform five-story frame for three values of ρ.

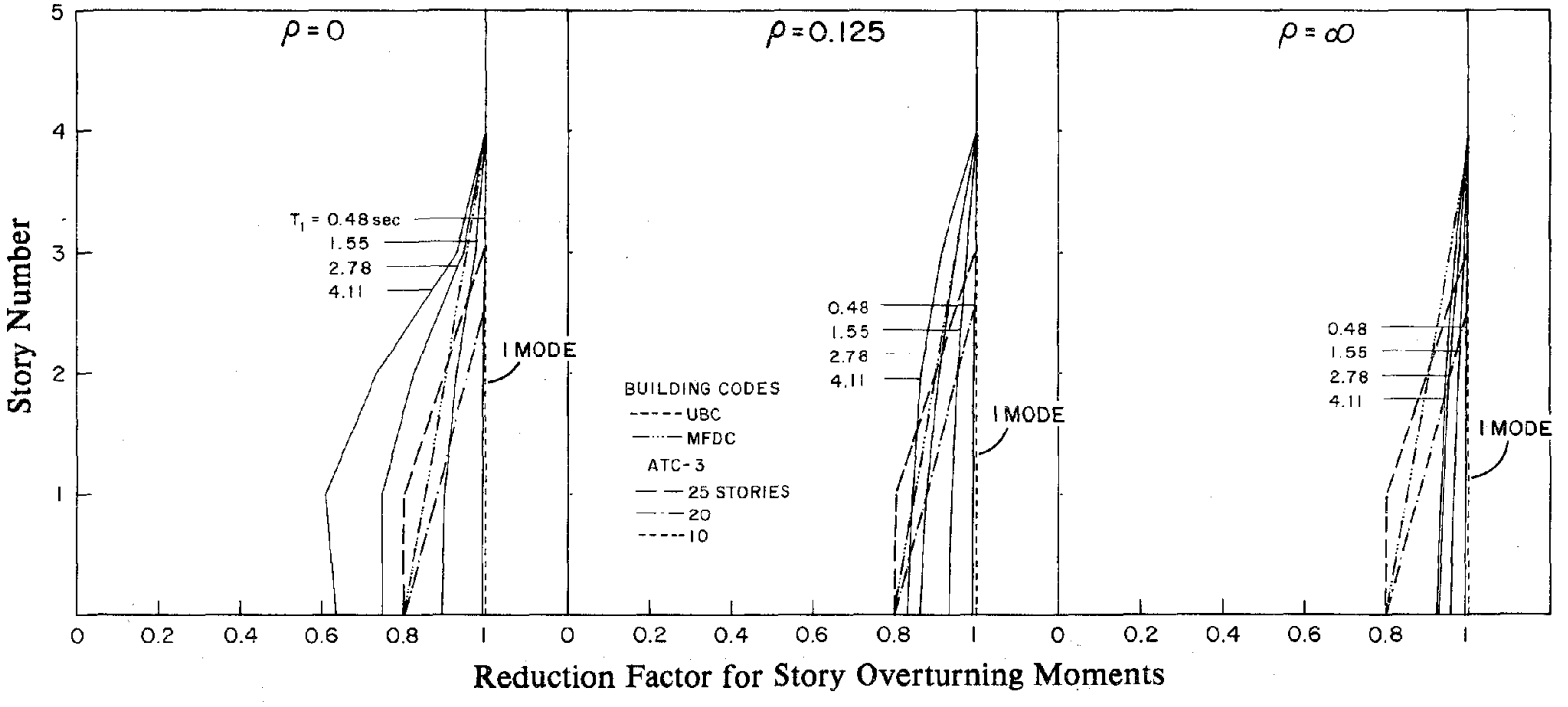

FIGURE 18 Reduction factors for story overturning moments from building codes compared with RSA results for uniform five-story frame for four values of T_1 and three values of ρ.

to satisfy an equilibrium requirement. However, the ATC-3 procedure specifies a reduction factor which depends on the total number of stories in the building. In order to include that feature the ATC-3 values are presented in Figure 17 as a function of N, the total number of stories, using the rough empirical relationship that $T_1 = 0.1\ N$; and in Figure 18 for three different values of N.

It is apparent that some reduction in the story moments relative to the statically computed values is justified in light of the results of dynamic analysis. Thus no reduction at all as in UBC is inappropriate. However, even the other two codes considered do not recognize that the reduction factor depends significantly on the building parameters T_1 and ρ.

5. IMPROVED CODE-TYPE ANALYSIS

The equivalent lateral force (ELF) analysis procedure specified in building codes is intended to provide an initial estimate of the earthquake forces without a preliminary design of the building. It was demonstrated in Sections 3 and 4 that the earthquake forces are especially affected by two overall building parameters, fundamental vibration period T_1 and beam-to-column stiffness ratio ρ; but the effects of these parameters are not properly recognized in building codes. Based on the preceding results, a procedure to estimate the earthquake forces for the initial preliminary design of buildings, which recognizes the important influence of these parameters on building response to earthquakes, is presented next.

5.1 Base Shear

Based on the results of Figure 5 and their analysis presented in Section 4.1, it is recommended that the base shear be computed from

$$\bar{V}_0 = C \quad W_1^* \tag{26}$$

where C is a seismic coefficient and W_1^* the effective weight of the building that participates in the fundamental vibration mode, both to be determined by the procedures to follow.

The seismic coefficient spectrum, showing C as a function of vibration period T_1, should be constructed by modifying the normalized pseudo-acceleration design spectrum for the site obtained by well established procedures [8]. The modifications to this spectrum are intended to directly account for the contributions of the modes of vibration higher than the fundamental mode to the base shear. These higher-mode contributions depend on building properties, the most significant of which are fundamental vibration period T_1 and stiffness ratio ρ. Based on the results of response spectrum analysis and their interpretation presented earlier the design spectrum a-b-c-d-e is modified as shown in Figure 19. The spectrum is left unchanged in the acceleration-controlled region a-b-c of the spectrum, but is modified in the velocity- and

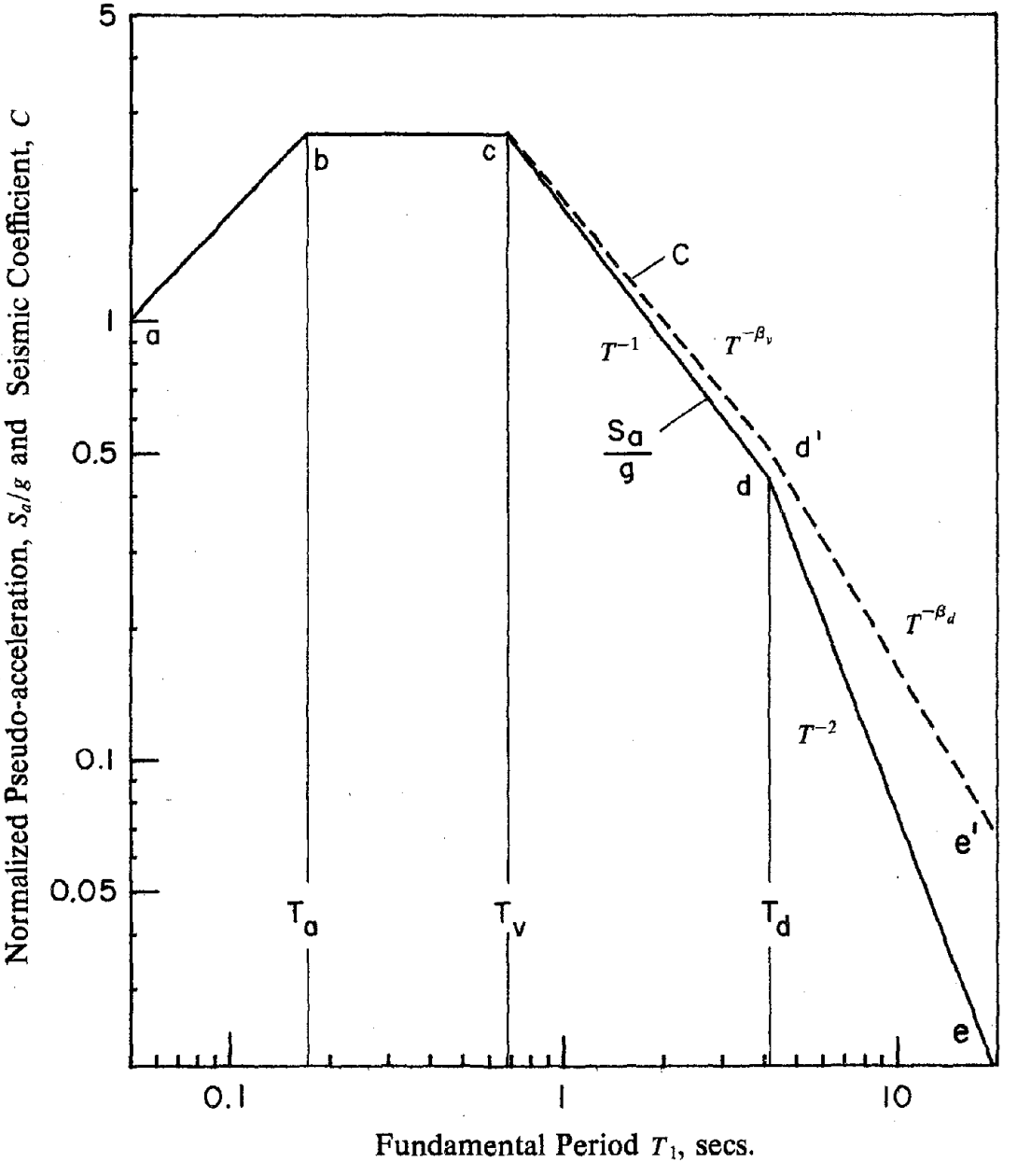

FIGURE 19 Construction of seismic coefficient spectrum from normalized pseudo-acceleration design spectrum.

displacement-controlled regions as follows: Through point c draw curve cd' proportional to $T^{-\beta_v}$ and extending to $T = T_d$; on the log-log plot of Figure 19 this will be a straight line as shown. Through point d' draw curve d'e' proportional to $T^{-\beta_d}$, which in the log-log plot of Figure 19 is another straight line. The exponents β_v and β_d depend on building properties, the most significant of which is the stiffness ratio ρ. Values for exponents β_v and β_d for the velocity- and the displacement-controlled regions of the spectrum were presented earlier in Table 3 for the five frame cases of Figure 2. These exponents were determined from a least-squared error fit, as described in Section 4.1, to the response spectrum for the normalized base shear computed by response spectrum analysis of each building frame [see Part II of this report].

The effective weight W_1^* in the fundamental vibration mode can be computed from equation (2) based on estimates of the height-wise distribution of building weight and of the fundamental mode shape. A procedure to determine an approximation to the mode shape, depending on the stiffness ratio ρ, will be described later. Alternatively, the data presented in Table 1 may be used to estimate W_1^*/W and hence W_1^*.

5.2 Modal Responses

Once the total base shear has been determined from equation (26), the next question is how should the total earthquake force given by the base shear be distributed over the height of the building. It has been demonstrated [see Parts I and II of this report] that, over a useful range of fundamental vibration periods, the earthquake response of building frames can be satisfactorily estimated by response spectrum analysis considering the contributions of only the first two modes of vibration; even the first mode alone is usually sufficient in the acceleration-controlled region of the spectrum. Thus if we could separate the total base shear into the first mode contribution and ascribe the remainder to the second mode it would be possible to distribute each modal base shear over the building height in accordance with the corresponding mode shape. This is an indirect, approximate way to determine the response in the

fundamental and second modes of vibration. The total response can then be obtained by appropriately combining the modal responses.

The base shear can be separated into two parts as follows: The base shear due to the fundamental mode of vibration is given by [4]

$$\overline{V}_{01} = \frac{S_{a1}}{g} W_1^* \tag{27}$$

An approximate value of this base shear can be obtained from equation (27) where the effective weight W_1^* for the fundamental mode is estimated as discussed above and S_{a1} is the ordinate of the pseudo-acceleration design spectrum. The remainder of the base shear, obtained under the assumption that the total base shear is best given by a SRSS combination of modal values,

$$\overline{V}_{02} = \sqrt{\overline{V}_0^2 - \overline{V}_{01}^2} \tag{28}$$

is treated as an estimate of the base shear due to the second vibration mode. Recall that if the fundamental vibration period of the building is within the acceleration-controlled region of the spectrum, the base shear is almost entirely due to the fundamental vibration mode (Figure 5) and $\overline{V}_{02}$ would be almost zero.

Having estimated the base shears due to the first two modes of vibration, the equivalent lateral forces in each mode can be determined from equation (6), provided the mode shapes can be estimated. The remainder of the analysis is the same as the standard response spectrum analysis described in Section 2.1.

5.3 Vibration Period and Mode Shapes

All that remains to be determined is the fundamental vibration period and the shapes of the first two modes of vibration; note that the second vibration period is not required in this analysis. These vibration properties can not be computed exactly without the building having been designed. In particular, the eigen-problem of equation (1) can not be formulated because

the stiffness matrix is unknown and the height-wise distribution of the building mass is known only approximately. Thus, in computing the initial estimate of earthquake forces to start the process of designing a building, the fundamental vibration period and the two mode shapes should be estimated based on overall properties of the building and its structural system.

An estimate of the fundamental vibration period is required in most of the existing building codes. For this purpose, empirical formulas have been developed [1]; these are based on only a general description of the building type --e.g. steel moment frame, concrete moment frame, shear wall system, braced frame, etc.-- and overall dimensions such as height and plan size. Such formulas may be employed in this improved code-type analysis, but it should be recognized that they often lead to significantly inaccurate values.

After considering three possible functions to describe the fundamental mode shape [Appendix A], it is recommended that the fundamental mode shape be approximated by

$$\phi_{j1} = \left(\frac{h_j}{H}\right)^{\delta}, \qquad j = 1,2,...N \tag{29}$$

where h_j = height of the jth floor above the base and H = total height of the building. The approximate mode shape of equation (29), with the exponent δ estimated from a least-squared error fit to the exact fundamental mode shape, is compared with the exact mode shape in Figure 20 for three of the building frame cases of Figure 2 and three values of stiffness ratio ρ. Although the approximate shape is not always excellent, it is obviously better than the mode shapes independent of ρ implied in building codes. As shown in Figure 21 and Table 4, the exponent δ depends on the building properties including the number of stories, height-wise variation of mass and stiffness, but perhaps most significantly on the beam-to-column stiffness ratio ρ. Because the exponent δ varies gradually with ρ, it can be estimated to a useful degree of accuracy from the data presented.

The recommended approximation to the second mode shape is

$$\phi_{j2} = \left(\frac{h_j}{h_0}\right)\left(1 - \frac{h_j}{h_0}\right) \qquad j = 1,2,...N \tag{30}$$

Table 4: Exponent δ in approximation $\phi_{j1} = (h_j/H)^{\delta}$

to the fundamental mode shape.

Frame Case	$\rho = 0$	$\rho = 0.05$	$\rho = 0.125$	$\rho = 0.5$	$\rho = 2$	$\rho = \infty$
1	1.745	1.379	1.232	1.034	0.892	0.798
2	1.814	1.188	1.092	0.982	0.911	0.864
3	1.848	1.585	1.455	1.277	1.155	1.078
4	1.815	1.507	1.360	1.162	1.028	0.942
5	1.950	1.699	1.590	1.425	1.299	1.215

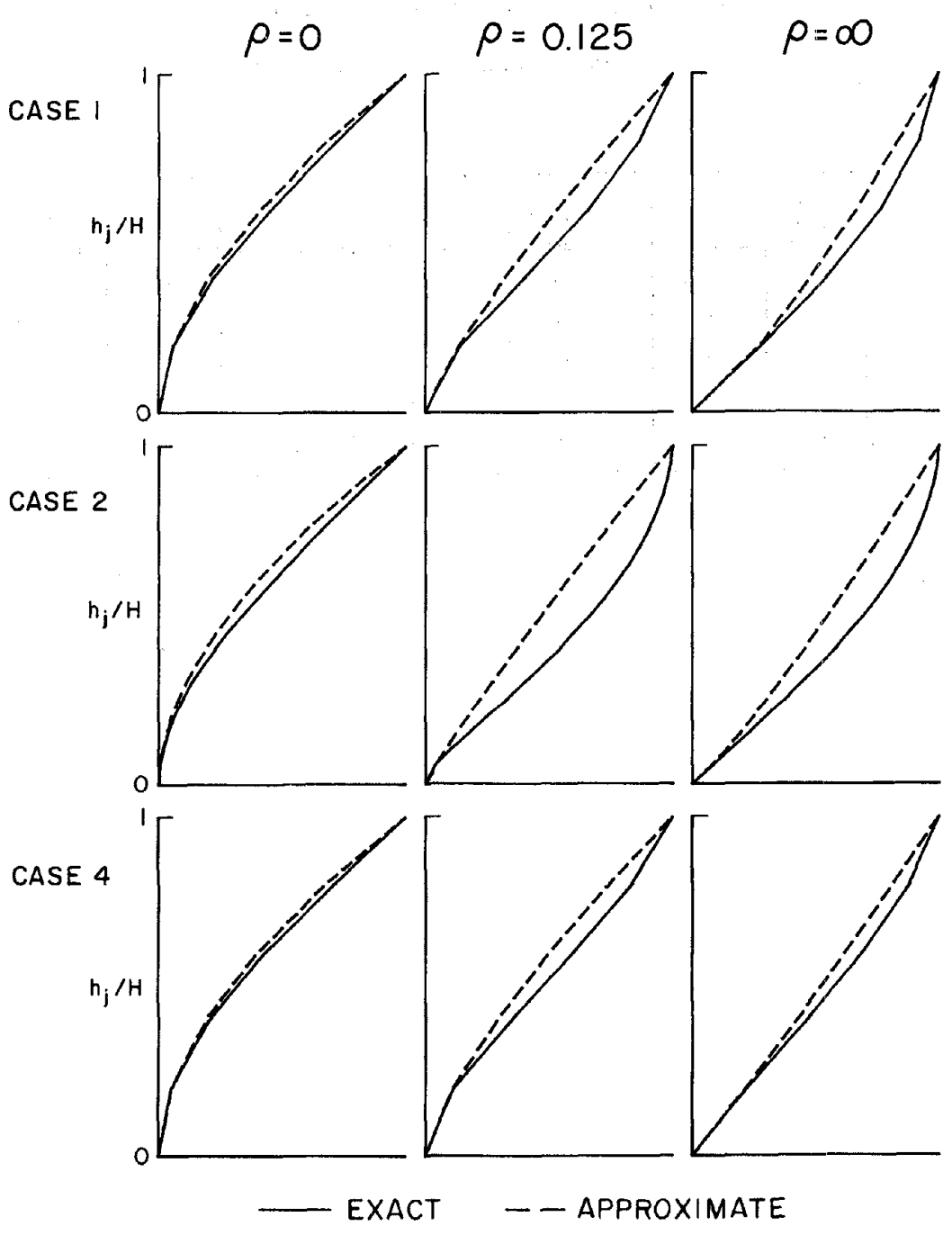

FIGURE 20 Exact fundamental mode shapes of three frame cases for three values of ρ compared with approximation $\phi_{j1} = (h_j/H)^{\delta}$.

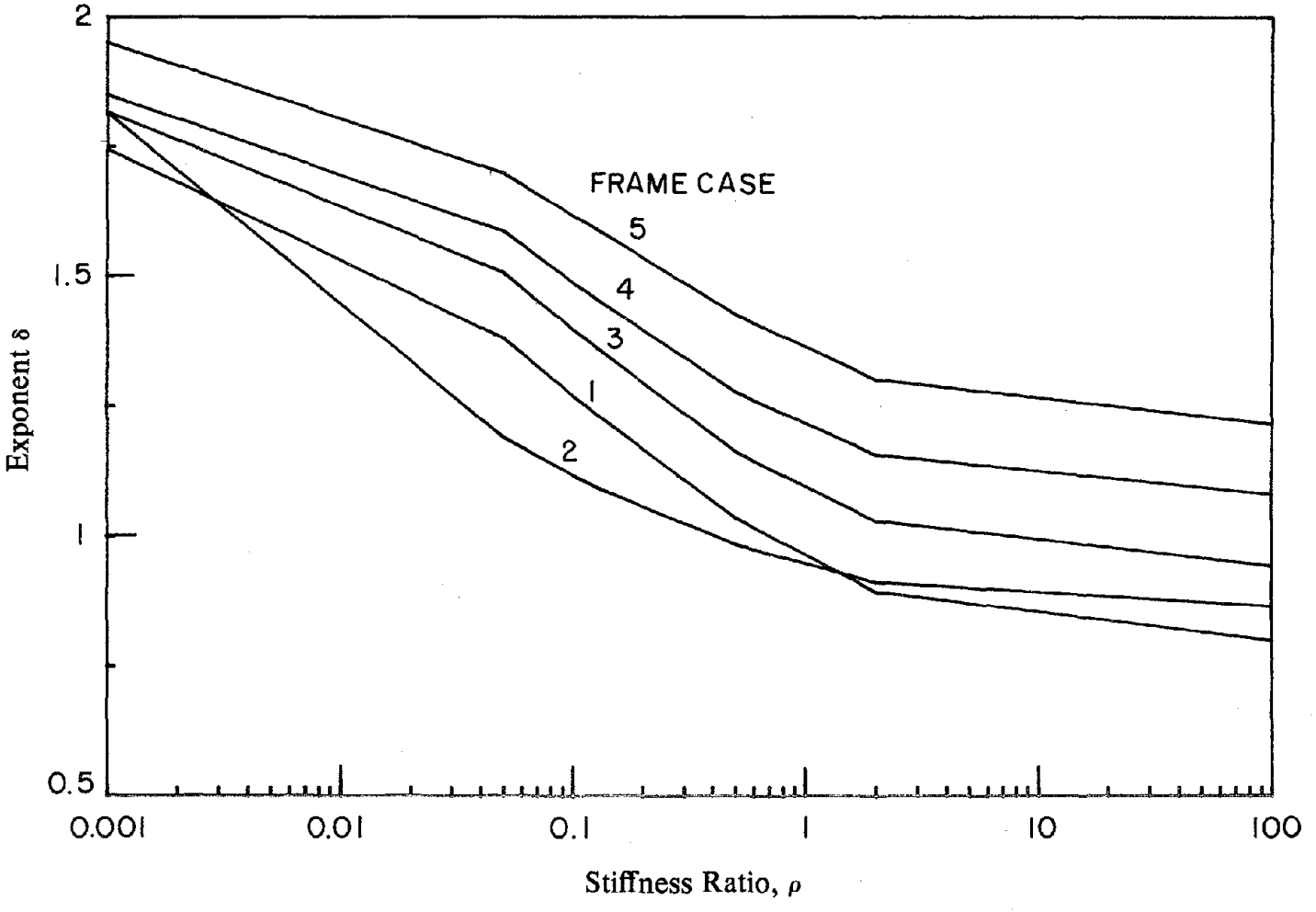

FIGURE 21 Variation of exponent δ --in approximation $\phi_{j1} = (h_j/H)^{\delta}$ to the fundamental mode shape-- with stiffness ratio ρ for five frame cases.

where h_0 is the height of the node (point of zero displacement) above the base. The approximate mode shape of equation (30), with h_0 estimated from a least-squared error fit to the exact second mode shape, is compared with the exact mode shape in Figure 22 for three of the building frame cases of Figure 2 and three values of ρ. Although the approximate shape errs significantly in some cases, for purposes of preliminary design it should be satisfactory in estimating the response due to the second mode of vibration. High degree of accuracy is not important in estimating this response because it is usually much smaller than the first mode response. As shown in Figure 23 and Table 5 the parameter h_0 is relatively insensitive to the stiffness ratio ρ, the number of stories, and other building parameters. It can therefore be estimated to a useful degree of accuracy from the data presented.

5.4 Computational Steps

The earthquake forces to be considered in the initial, preliminary design of a multistory building can be estimated from the earthquake design spectrum by the following procedure:

1. Determine the earthquake design spectrum for the building at the particular site. A spectrum for elastic design can be determined from estimates of the maximum ground acceleration, velocity and displacement and appropriate amplification factors for the various spectral regions [8]. Procedures have also been developed for constructing an inelastic design spectrum from the elastic design spectrum for the ductility factor considered allowable in the design of the building [9,14,15,16].

2. Plan the overall dimensions of the building, the number of stories and their height, heightwise distribution of building weight, and select the structural materials and structural system --moment frame, shear walls system, braced frame etc-- and estimate the stiffness ratio ρ.

3. Construct the seismic coefficient spectrum, showing C as a function of vibration period T, by modifying the earthquake design spectrum, from step 1, showing the pseudo-acceleration S_a as a function of T. The design spectrum is left unchanged in the

Table 5: Parameter h_0/H in approximation $\phi_{j2} = (h_j/h_0)(1 - h_j/h_0)$ to the second mode shape.

Frame Case	$\rho = 0$	$\rho = 0.05$	$\rho = 0.125$	$\rho = 0.5$	$\rho = 2$	$\rho = \infty$
1	0.852	0.826	0.817	0.807	0.800	0.795
2	0.801	0.755	0.751	0.749	0.747	0.746
3	0.858	0.841	0.833	0.826	0.822	0.820
4	0.792	0.768	0.758	0.746	0.739	0.734
5	0.831	0.802	0.790	0.774	0.760	0.750

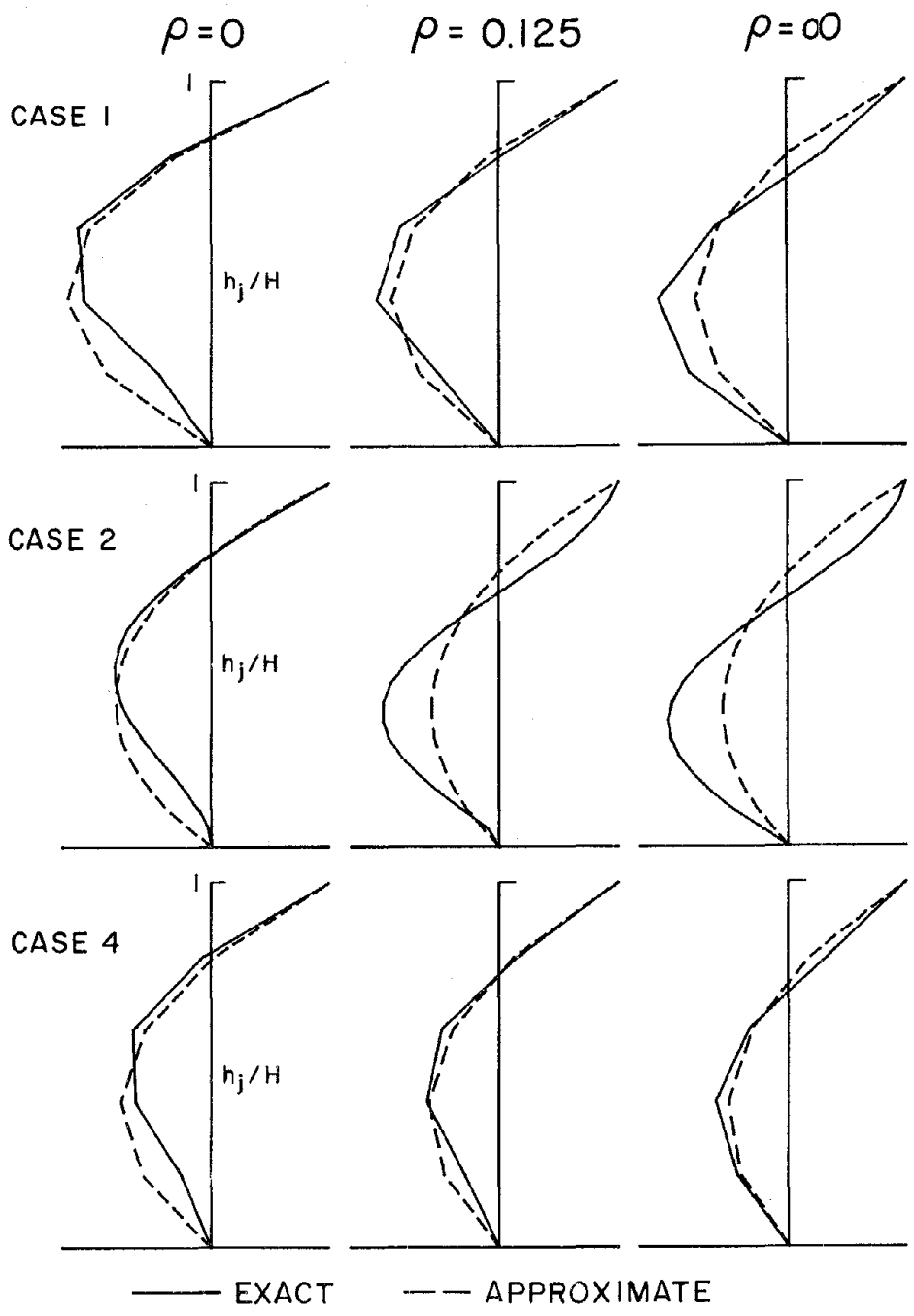

FIGURE 22 Exact second mode shapes of three frame cases for three ρ values compared with approximation $\phi_{j2} = (h_j/h_0)(1 - h_j/h_0)$.

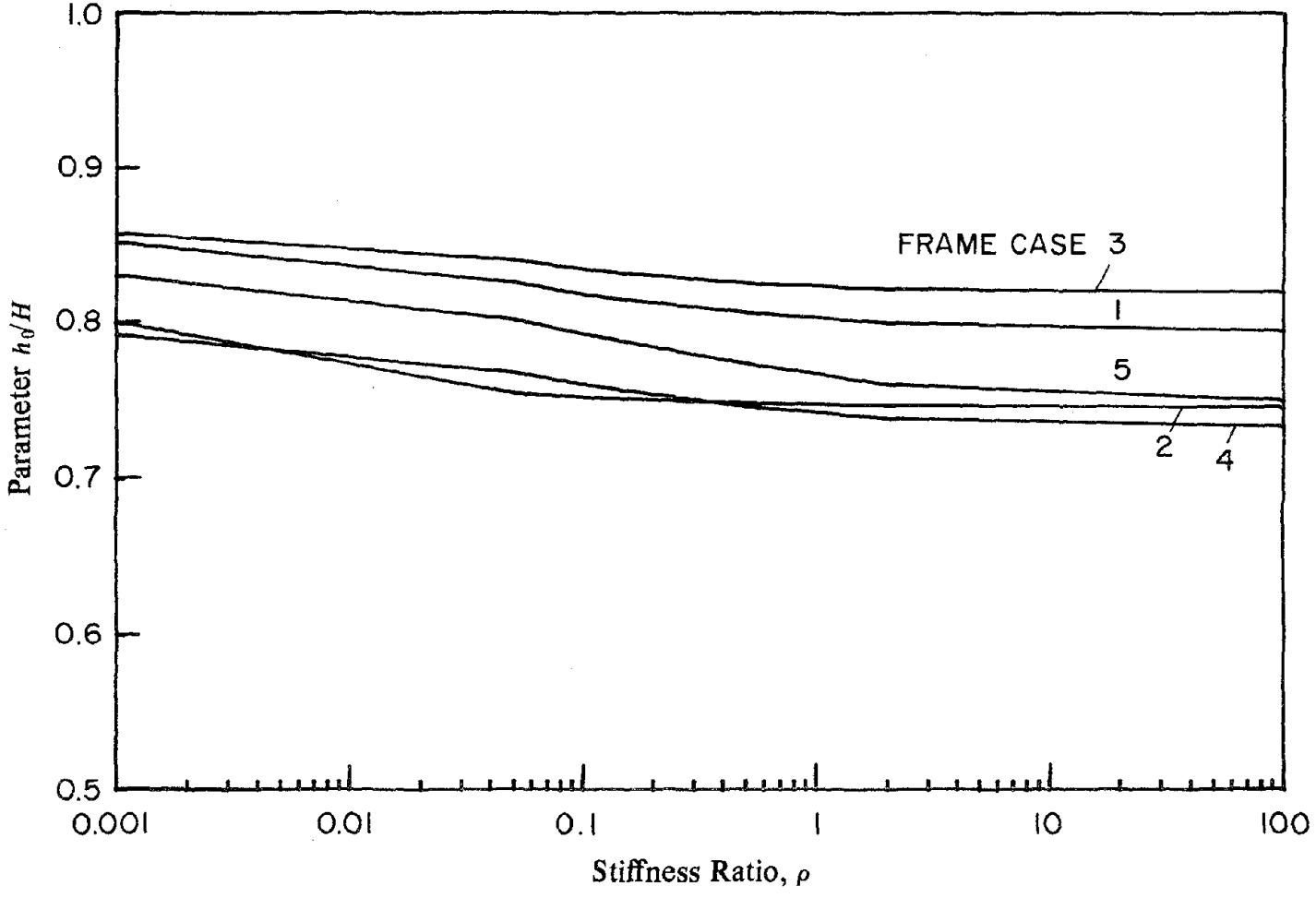

FIGURE 23 Variation of parameter h_0 --in approximation $\phi_{j2} = (h_j/h_0)(1-h_j/h_0)$ to the second mode shape-- with stiffness ratio ρ for five frame cases.

acceleration-controlled region but is raised for longer periods. The variation of S_a with T is changed from T^{-1} to $T^{-\beta_v}$ in the velocity-controlled region and from T^{-2} to $T^{-\beta_d}$ in the displacement-controlled region to obtain the seismic coefficient spectrum; see Section 5.1 for further details. The coefficients β_v and β_d are determined from data such as presented in Table 3 corresponding to ρ and other building properties from step 2.

4. Estimate the fundamental vibration period T_1. Empirical formulas included in most codes, based on a general description of the structural system and overall dimension, may be used for this estimate. However it should be recognized that these formulas often lead to significantly inaccurate values.

5. Describe the first two vibration mode shape approximately by equations (29) and (30) with the parameters δ and h_0 estimated from data of the type presented in Figures 21 and 23 and Tables 4 and 5 corresponding to ρ and other building properties from step 2.

6. Estimate the base shear $\overline{V}_0$ from equation (26) with C and W_1^* determined, corresponding to the building properties from step 2, as follows:

   (a) C is read from the seismic coefficient spectrum (from step 3) as the ordinate corresponding to T_1 and ρ (from steps 2 and 4).

   (b) W_1^* is estimated either from equation (2), based on estimates of height-wise distribution of building weight from step 2 and of the fundamental mode shape from step 5, or from data such as that presented in Table 1.

7. Separate the base shear $\overline{V}_0$ into two parts:

   (a) Fundamental vibration mode contribution $\overline{V}_{01}$ determined from equation (27), with S_{a1} read as the ordinate of the pseudo-acceleration design spectrum from step 1 corresponding to the T_1 from step 4.

   (b) Second mode contribution $\overline{V}_{02}$ determined from equation (28), with $\overline{V}_0$ and $\overline{V}_{01}$ known from steps 6 and 7(a), respectively.

8. Estimate the maximum response in individual modes of vibration by repeating the following steps for the first two modes:

   (a) Compute equivalent lateral forces $\overline{f}_{jn}$ at all floors from equation (6) with the base shear $\overline{V}_{on}$ and mode shape value ϕ_{jn} available from steps 7 and 5, respectively.

   (b) Compute story shear and moments by static analysis of the structure subjected to the equivalent lateral forces. Forces in individual structural members can not be determined until their preliminary sizes are estimated.

   (c) Compute floor displacements from equation (7).

   (d) Compute story deformations from the floor displacements using equation (8).

9. Determine an estimate of the maximum $\overline{r}$ of any response (displacement of a floor, deformation in a story, shear or moment in a story, etc.) by combining the first two modal maxima $\overline{r}_1$ and $\overline{r}_2$ for the response quantity in accordance with equation (9).

5.5 Data Base Required

Several parameters must be estimated to implement the improved code-type analysis procedure just summarized: beam to column stiffness ratio ρ in step 2; mode shape parameters δ and h_0 in step 5, and effective weight W_1^* in step 6 all of which depend on ρ and other structural properties; and exponents β_v and β_d in establishing the seismic coefficient spectrum in step 3, which depend on the shape of the design spectrum, ρ and structural properties. Obviously data must be developed to provide a basis to estimate these parameters in practical design application. The data presented in Tables 1, 3, 4, and 5 is a sub-set of the required data base. The computations necessary to develop a sufficient data base are outlined in this section.

All the aforementioned parameters depend, in part, on the stiffness ratio ρ which can not be computed formally from equation (24) without a preliminary design of the building. In the initial phase of design, therefore, ρ should be estimated from limited information: type of

structural system --moment frame, shear walls, or hybrid systems, etc.-- bay widths and story heights. The stiffness ratio can be readily estimated for limiting cases; e.g. ρ should be close to zero if a single cantilever shear wall provides the lateral resistance of the building; and it should be very large if the joint rotations are effectively restrained by stiff beams framing into flexible columns. In order to estimate ρ for a typical building somewhere between these two limiting cases, it is necessary to develop an appropiate data base.

To this end, the stiffness ratio ρ should be computed from equation (24) for actual buildings representative of each of the major types of structural systems used for buildings. Once such a data base is developed, it should be possible to estimate ρ corresponding to the structural system proposed for a building to be designed. Such a rough estimate should be satisfactory to obtain an initial estimate of the earthquake forces by the improved code-type analysis procedure presented in the preceding section. Once a preliminary design of the building is developed the ρ value can be determined from equation (24) and the computation of earthquake forces refined if necessary.

The effective weight W_1^* and mode shape parameters δ and h_0 depend only on the structural properties and these parameters have been computed (Tables 1, 4, and 5) for the five frame cases described in Figure 2 for several values of ρ. Using procedures outlined earlier, similar data should be generated for additional building cases covering the practical range of height-wise distribution of mass and stiffness, number of stories, and other important properties.

The exponents β_v and β_d for the velocity- and displacement-controlled regions of the seismic coefficient spectrum depend on the shape of the earthquake design spectrum, ρ and other structural properties. These exponents have been presented (Table 3) for the design spectrum of Figure 3, five frame cases described in Figure 2 and three ρ values. Additional data should be generated for these five frame cases to at least include all the ρ values selected in Tables 1, 4, and 5). Using procedures outlined earlier, similar data should be generated for additional building cases covering the practical range. Finally, such complete data base should

be developed for shapes of the various design spectra depending on epicentral distance, local soil conditions, etc. specified in a particular building code.

Once such a data base is developed, the improved code-type analysis procedure presented here can be conveniently implemented and included in building codes.

6. SUMMARY AND CONCLUSIONS

The Equivalent Lateral Force procedure in most building codes does not satisfactorily recognize the fact that vibration modes higher than the fundamental mode may contribute significantly to the earthquake-induced forces and deformations in a building. These higher mode response contributions increase with increasing fundamental vibration period T_1 of the building and decreasing beam-to-column stiffness ratio ρ. As a result, the code formulas for base shear, height-wise distribution of lateral forces, and reduction factor for overturning moment lead to design forces that do not satisfactorily recognize the effects of these important building parameters.

Based on the limitations of present building codes formulas identified, an improved procedure to estimate the earthquake forces for the initial, preliminary design of buildings has been presented. Starting with the earthquake design spectrum for elastic or inelastic design and the overall, general description of the proposed building, this procedure provides an indirect approach to estimate the response in the first two vibrations modes of the building. The procedure recognizes the important influence of those building properties and parameters that significantly influence its earthquake response without requiring the computations inherent in standard dynamic analysis by the response spectrum method. The procedure represents a major conceptual improvement over present building codes with very little increase in computational effort.

Several parameters must be estimated to implement this improved code-type analysis procedure. The data necessary to provide a basis for estimating these parameters in practical design application have been identified and a sub-set of the required data base has been presented.

REFERENCES

1. Applied Technology Council, "Tentative Provisions for the Development of Seismic Regulations for Buildings," *Report ATC 3-06*, NBS Special Publication 510, NSF Publication 78-08, June 1978.

2. Blume, J.A., "Dynamic Characteristics of Multi-story Buildings," *Journal of the Structural Division, ASCE*, Vol. 94, No ST2, Feb. 1968, pp 337-402.

3. Chopra, A.K., and Newmark, N.M. "Analysis," Chapter 2 in *Design of Earthquake Resistant Structures*," ed. E. Rosenblueth, Pentech Press Ltd., London, 1980.

4. Chopra, A.K., "*Dynamics of Structures, A Primer*," Earthquake Engineering Research Institute, Berkeley, California, 1982.

5. Der Kiureghian, A., "A Response Spectrum Method for Random Vibrations," *Report No UCB/EERC-80/15*, Earthquake Engineering Research Center, University of California, Berkeley, California, June, 1980.

6. International Association of Earthquake Engineering, "Mexican Code," in *Earthquake Resistant Regulations, A World List, 1980*, Tokyo, Japan, Aug., 1980, pp 503-519.

7. International Conference of Building Officials, *Uniform Buiding Code*, 1982.

8. Newmark, N.M. and W.J. Hall, "Vibration of Structures Induced by Ground Motion," Chapter 29, Part I, in *Shock and Vibration Handbook*, 2nd Ed., McGraw-Hill, 1976, pp 29-1 to 29-19.

9. Newmark, N.M. and W.J. Hall, "*Earthquake Spectra and Design*," Earthquake Engineering Research Institute, Berkeley, California, 1982.

10. Roehl, J.L., "Response of Ground Excited Building Frames," *Ph.D. Thesis* submitted to Rice University, Houston Texas, 1961.

11. Rosenblueth, E., "Seismic Design Requirements in a Mexican 1976 Code," *Earthquake Engineering and Structural Dynamics*, Vol. 7, 1979, pp 49-61.

12. Smilowitz, R. and N.M. Newmark, "Design Seismic Accelerations in Buildings," *Journal of the Structural Division, ASCE,* Vol. 105, No ST12, Dec. 1979, pp 2487-2496.

13. Structural Engineers Association of California, "*Recommended Lateral Force Requirements and Commentary,*" 1959-60.

14. Veletsos, A.S. and N.M. Newmark, "Effect of Inelastic Behavior on the Response of Simple Systems to Earthquake Motions," *Proceedings of the Second World Conference on Earthquake Engineering,* Tokyo, Japan, 1960, Vol. II, pp 895-912, 1960.

15. Veletsos, A.S., N.M. Newmark, and C.V. Chelapati, "Deformation Spectra for Elastic and Elasto-Plastic Systems subjected to Ground Shock and Earthquake Motions," *Proceedings of the Third World Conference on Earthquake Engineering,* Wellington, New Zealand, 1965, Vol. II, pp 663-682.

16. Veletsos, A.S., "Maximum Deformation of Certain Nonlinear Systems," *Proceedings of the Fourth World Conference on Earthquake Engineering,* Santiago, Chile, 1969, Vol. I, A-4, pp 156-170.

APPENDIX A:

EVALUATION OF APPROXIMATE FIRST MODE SHAPE ALTERNATIVES

A.1 Definition of Approximate First Mode Shapes

Three alternative shapes --$\mathbf{x}_1$, $\mathbf{x}_2$, and $\mathbf{x}_3$-- are considered as possible approximations to the fundamental mode shape. Their components at the jth floor level are given by:

i) $x_{1j} = (h_j/H)^{\delta}$

ii) $x_{2j} = (h_j/h_0)\ (1 - h_j/h_0)$

iii) $x_{3j} = (h_j/H)^{1/2} + \gamma\ (h_j/H)^2$

Each of the three approximate shapes is expressed in terms of one parameter which will be determined --as function of ρ and the frame characteristics-- by a least-squared error fit to the exact fundamental mode shapes for the five frame cases considered in this part of the study (Section 2).

The variation with ρ of the parameters δ, h_0, and γ for the five frame cases is presented in Figures A-1, A-2, and A-3 respectively. From a comparison of the curves in these figures it is apparent that the less sensitive of the three approximations to the fundamental mode shape to changes in the value of ρ is $\mathbf{x}_1$. This is a very important quality because ρ can not be estimated with a high degree of accuracy at the initial stages of the design process, precisely at the time when the approximation to the fundamental mode shape is going to be used. Furthermore, since the distributions of mass and stiffness over the height are only known in a very approximate manner it is also desirable that the parameter defining the approximate fundamental mode shape should not be very sensitive to them. Under these criteria, the most reliable approximation to the fundamental mode shape will be obtained from $\mathbf{x}_1$. For $\mathbf{x}_2$, precisely in the range of ρ typical of moment resisting frames (see Part I) the value of the parameter h_0 is very sensitive to changes in ρ showing a discontinuity, whose location depends on the frame characteristics (number of stories and stiffness and mass distribution over height). For $\mathbf{x}_3$ although there is no discontinuity, the dependence on the frame characteristics is somewhat

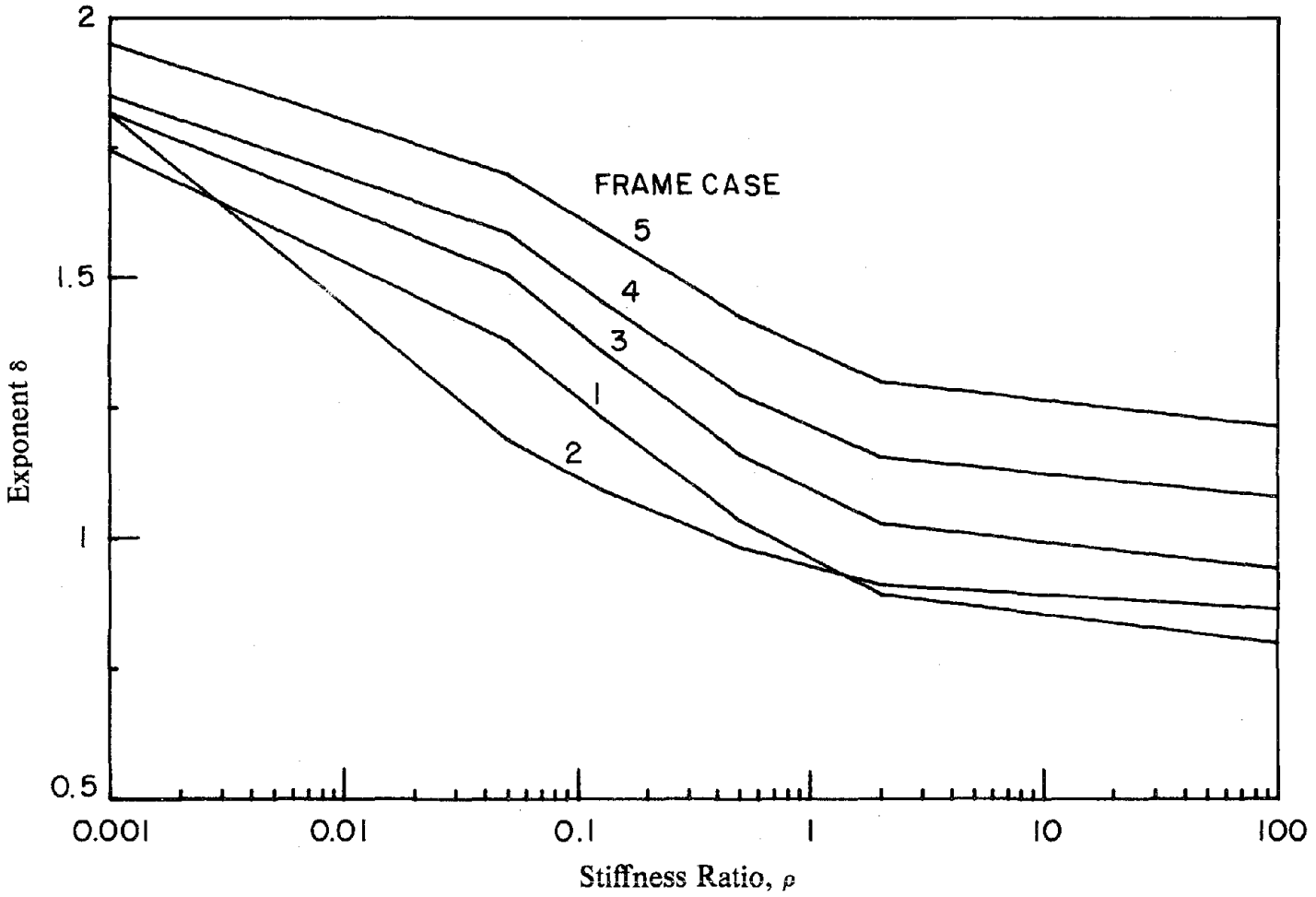

FIGURE A-1 Variation of exponent δ --in approximation $x_{j1} = (h_j/H)^{\delta}$ to the fundamental mode shape-- with stiffness ratio ρ for five frame cases.

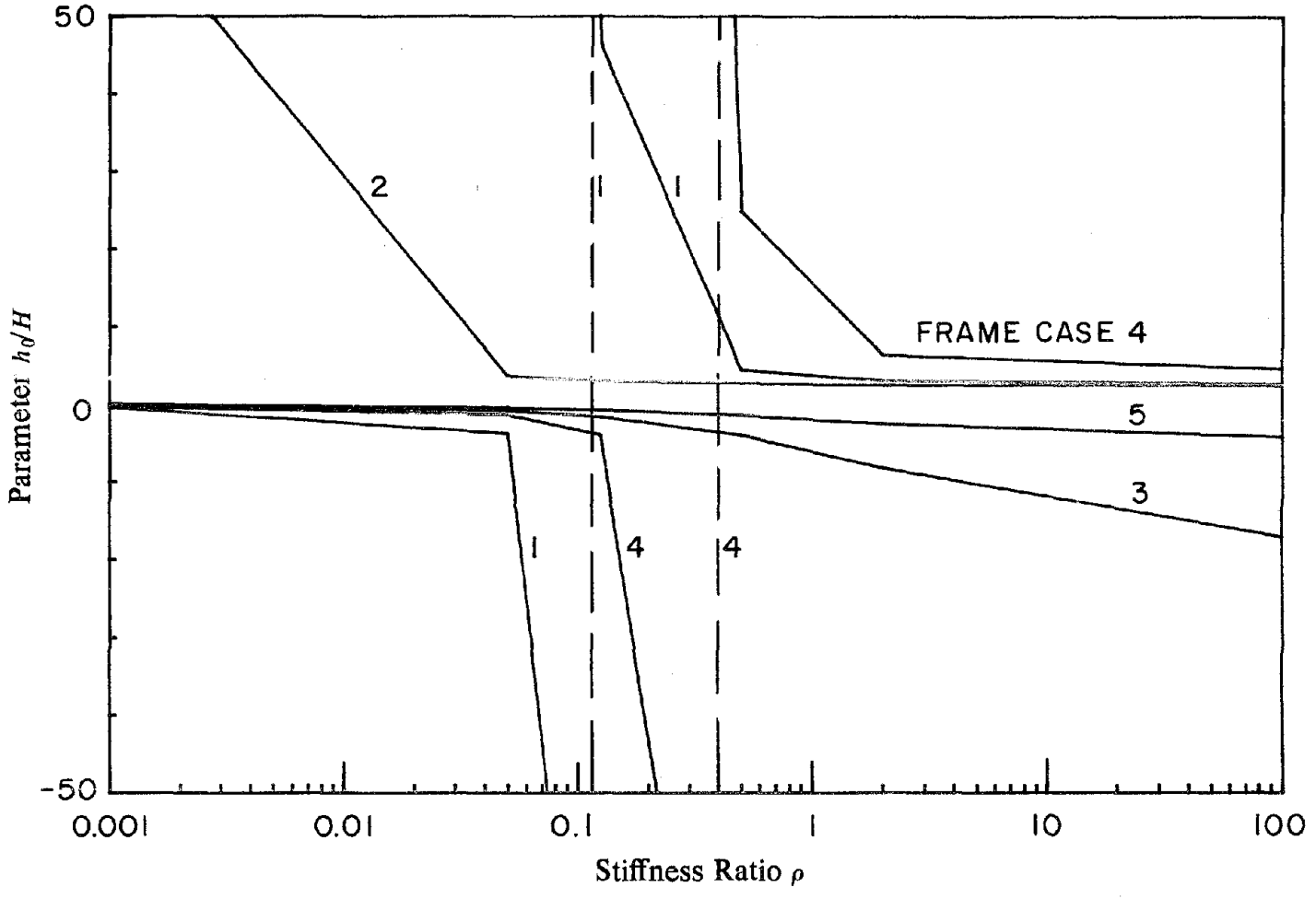

FIGURE A-2 Variation of parameter h_0 --in approximation $x_{j2} = (h_j/h_0)(1 - h_j/h_0)$ to the fundamental mode shape-- with stiffness ratio ρ for five frame cases.

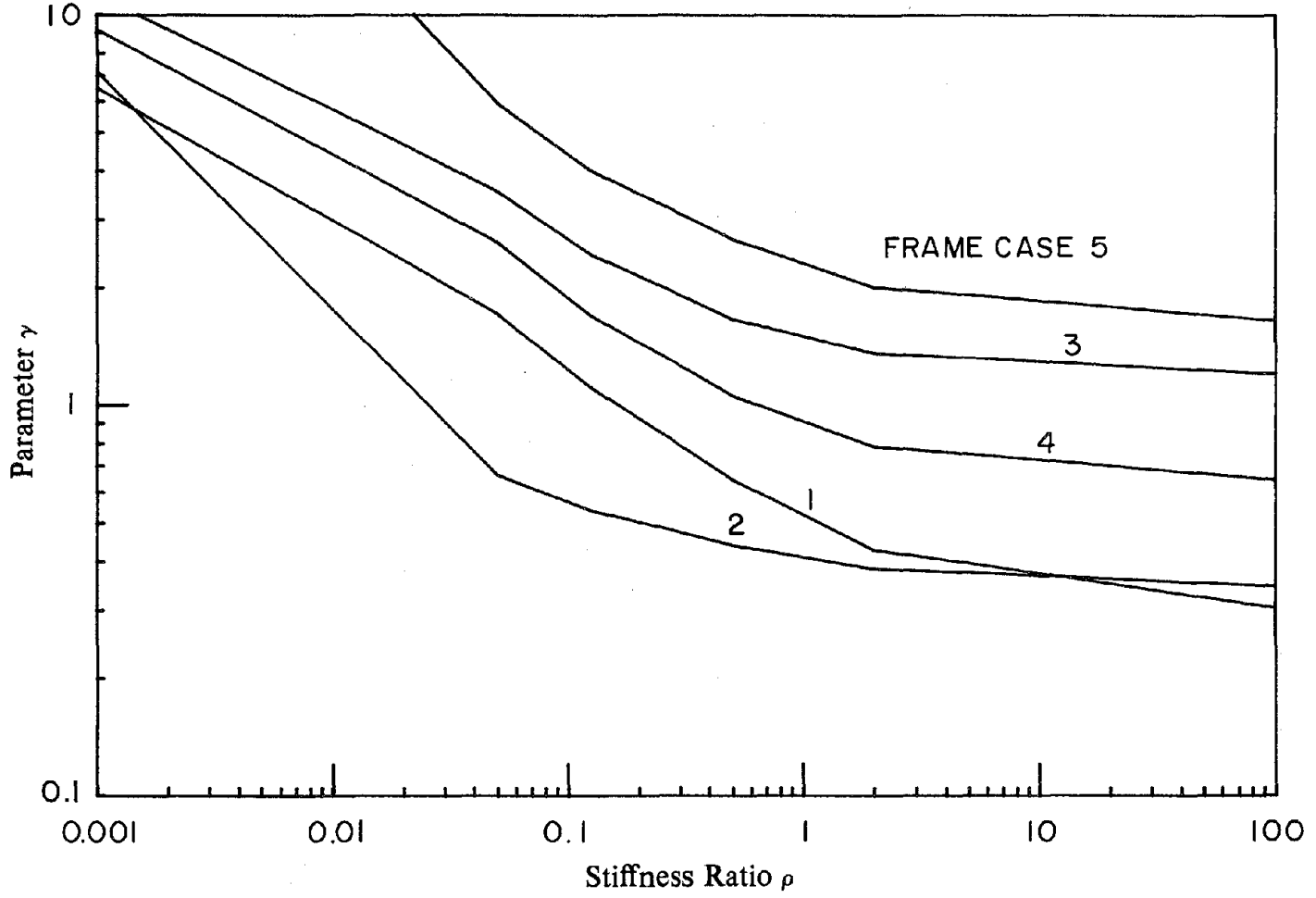

FIGURE A-3 Variation of parameter γ --in approximation $x_{j3} = (h_j/H)^{1/2} + \gamma\,(h_j/H)^2$ to the fundamental mode shape-- with stiffness ratio ρ for five frame cases.

larger and the changes in the value of γ for small changes in ρ are quite large, especially for rather small ρ values.

A.2 Errors in Approximations

An estimate of the magnitude of the errors for each of the three approximate fundamental mode shapes can be obtained from:

$$E_k = \frac{\left(\sum_{i=1}^{N} (\phi_{i1} - x_{ki})^2 \right)^{1/2}}{\left(\sum_{i=1}^{N} \phi_{i1}^2 \right)^{1/2}} \qquad k = 1, 2, 3$$

This expression corresponds to the ratio of the Euclidean norms of the error vector $(\phi_1 - \mathbf{x}_k)$ and the exact fundamental mode vector ϕ_1. The variation with ρ of this error quantity for each of the three approximate fundamental mode shapes considered is shown in Figures A-4 to A-6. They display the same general trends, the errors are largest for values of ρ about 0.1 and decrease towards both extremes. The magnitude of the error quantity E_k, for a given ρ value, is in general smallest for $\mathbf{x}_2$, but for $\mathbf{x}_1$ its largest value does not exceed 0.16. Therefore, it can be expected that the error in the individual components, at each floor level, of the approximations to the fundamental mode shape will be even smaller. In Figure A-7 the three approximate fundamental mode shapes are compared to the exact fundamental vibration mode shapes for three of the frames cases considered in this study and three values of ρ. Although there are some differences between the three approximations their overall quality is about the same. Perhaps being $\mathbf{x}_2$ the best of the three.

Although the errors for $\mathbf{x}_1$ are somewhat larger than for the other two approximations, it is still considered the most viable of the three approximate fundamental mode shapes because the differences in the errors are not large enough to offset the advantage of having a much smoother variation of the parameter that defines the shape with frame characteristics, especially ρ. Even though the errors can be rather large in some cases they can be considered acceptable given the overall level of uncertainty inherent in the preliminary design procedure.

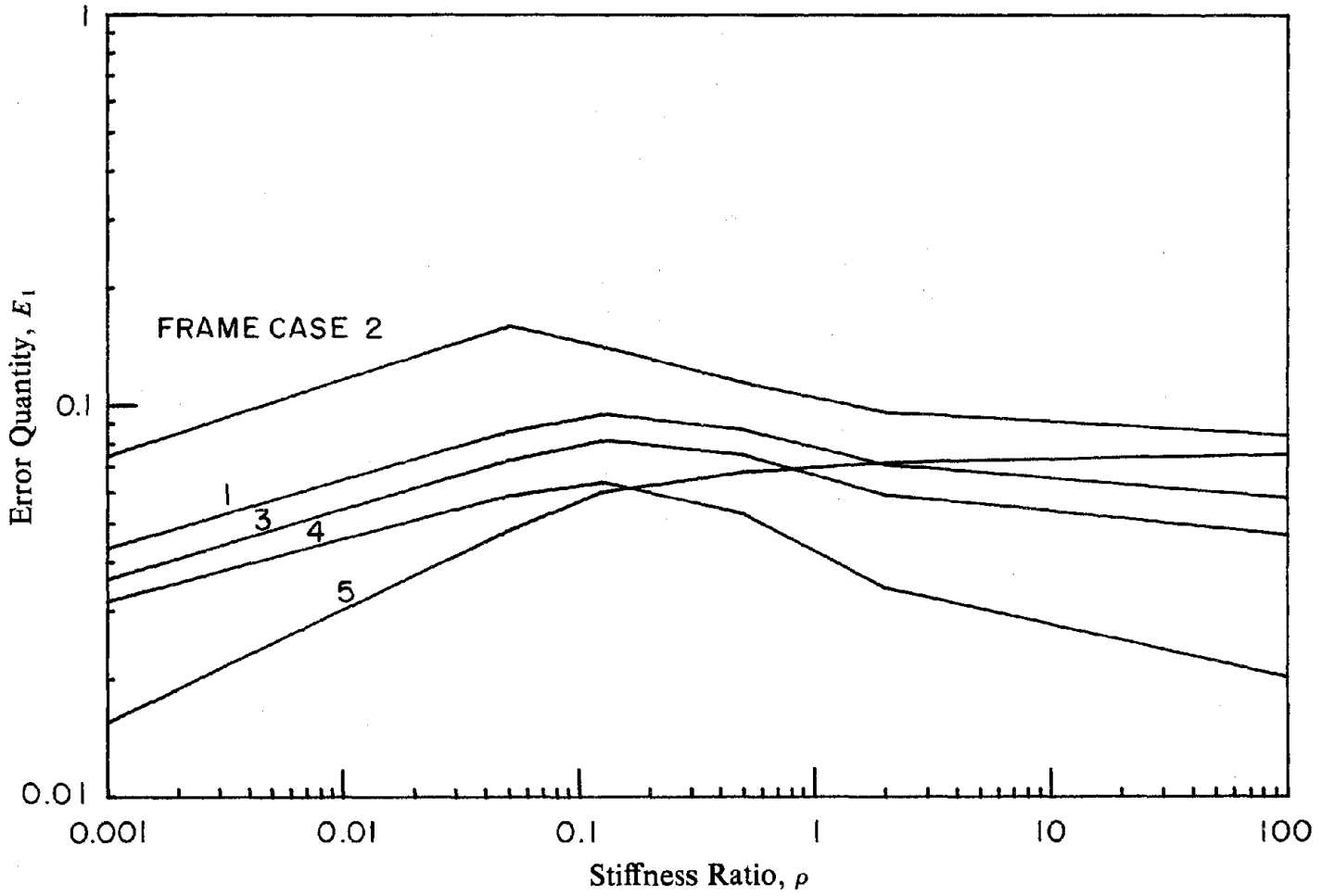

FIGURE A-4 Variation of error quantity E_1 --in approximation $x_{j1} = (h_j/H)^\delta$ to the fundamental mode shape-- with stiffness ratio ρ for five frame cases.

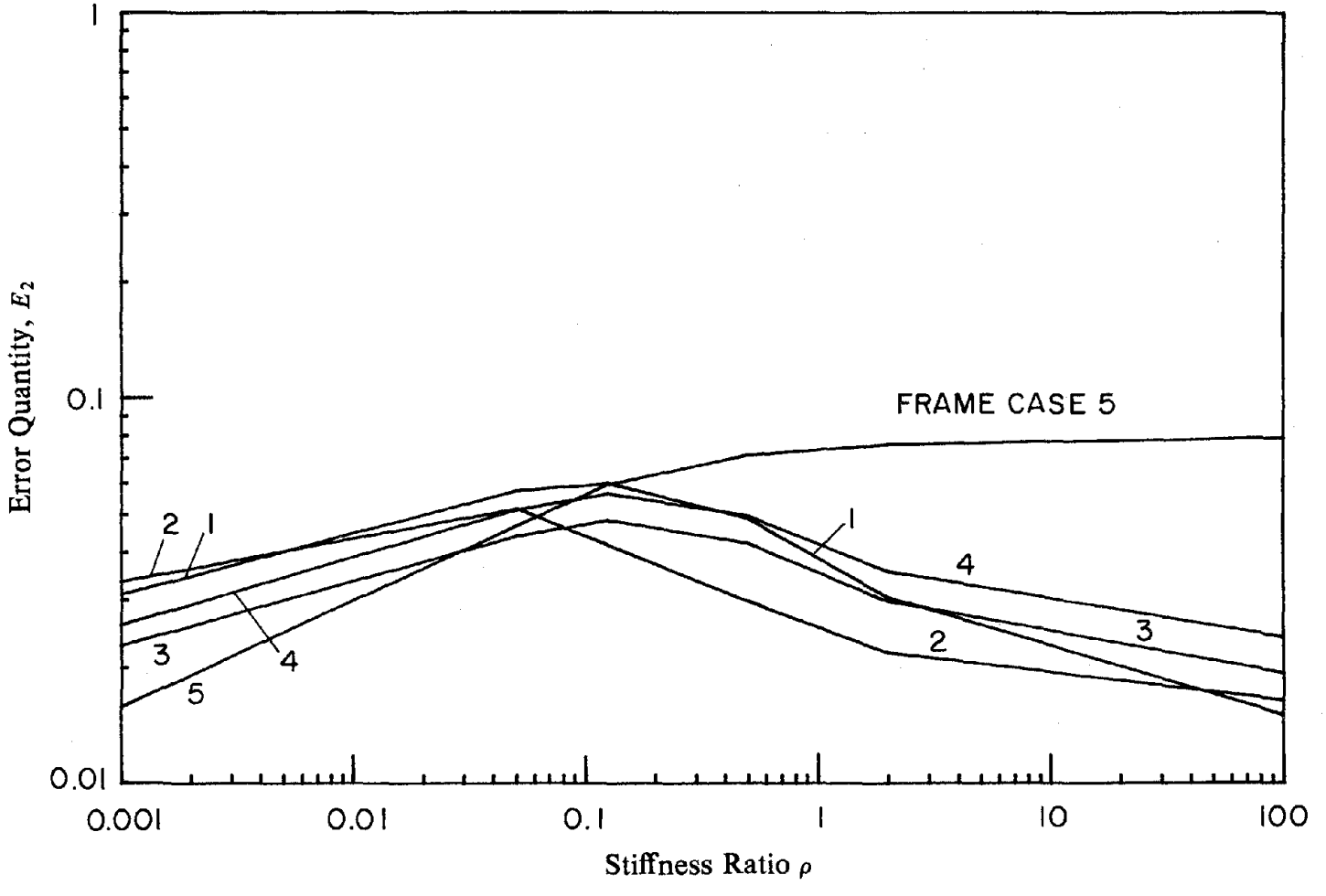

FIGURE A-5 Variation of error quantity E_2 --in approximation $x_{j2} = (h_j/h_0)(1 - h_j/h_0)$ to the fundamental mode shape-- with stiffness ratio ρ for five frame cases.

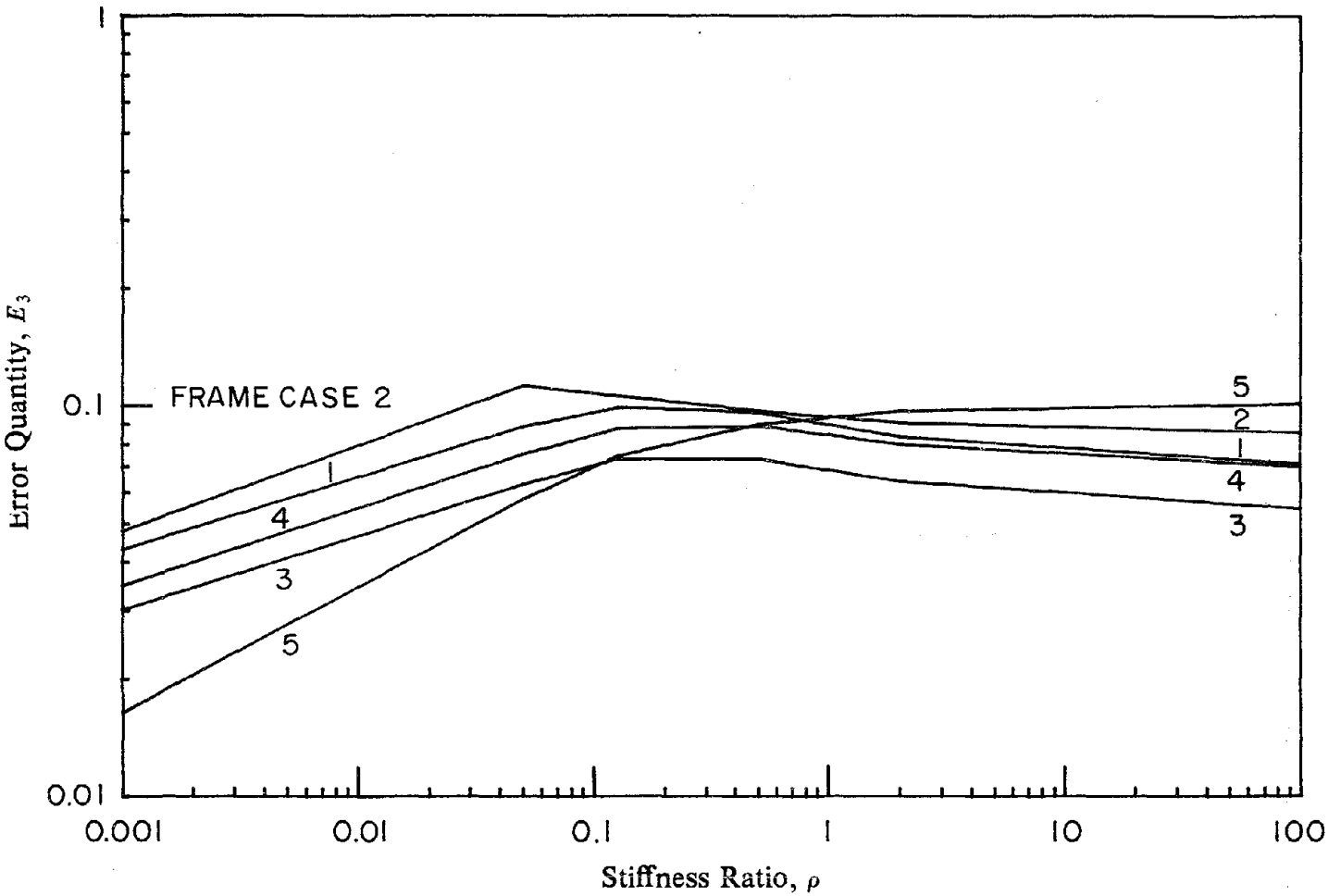

FIGURE A-6 Variation of error quantity E_3 --in approximation $x_{j3} = (h_j/H)^{1/2} + \gamma\,(h_j/H)^2$ to the fundamental mode shape-- with stiffness ratio ρ for five frame cases.

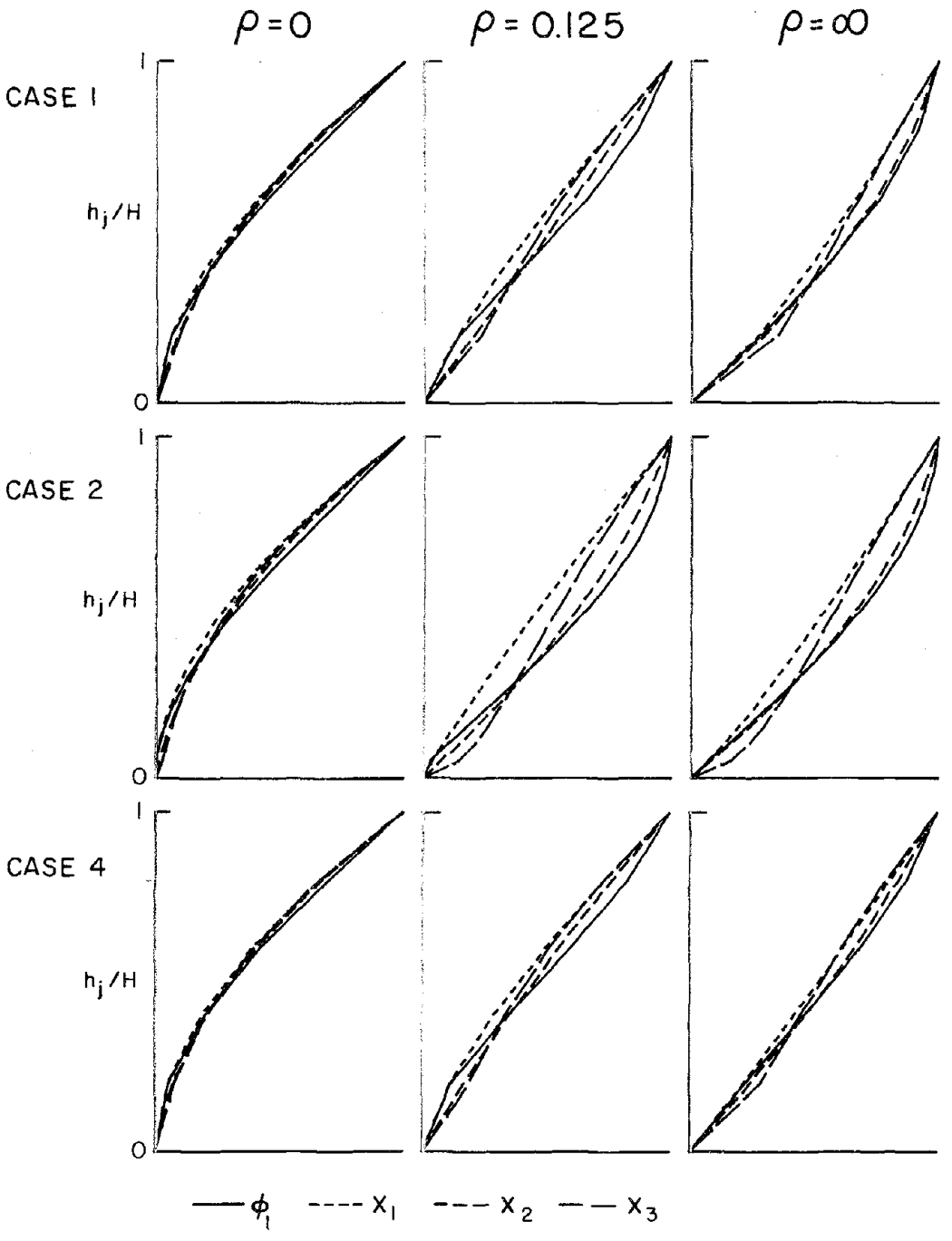

FIGURE A-7 Comparison of exact and approximate fundamental mode shapes for three values of ρ and three frame cases.

APPENDIX B: NOTATION

a_0 ordinate at zero period of the pseudo-acceleration design spectrum, Mexico's Federal District Code (MFDC)

$\overline{a}_g$ maximum ground acceleration due to earthquake ground motion

A maximum value of the pseudo-acceleration design spectrum ordinate, MFDC

A_a seismic coefficient representing effective peak acceleration, ATC-3 recommendations

A_v seismic coefficient representing effective peak velocity-related acceleration, ATC-3

C seismic coefficient in building codes

E modulus of elasticity

$\overline{f}_{jn}$ maximum equivalent lateral force at jth floor level in nth natural vibration mode

F_j lateral force at jth floor level specified by building codes

F_t addeitional force at top floor level specified by UBC

g acceleration of gravity

h story height

h_0 parameter in second mode approximation, height from base to node, equation (30)

h_j height from base to floor level j

h_n^* effective height in the nth natural vibration mode

H total height of building

I_b moment of inertia of beams

I_c moment of inertia of columns

k exponent used to define lateral force variation with height, ATC-3

$\mathbf{k}$	stiffness matrix
K	structural-type coefficient, UBC
L_b	length of beam
L_c	length of column
m_j	mass lumped at jth floor level
$M_{0n}(t)$	time-history of base overturning moment in nth mode
$\overline{M}_{0n}$	maximum value of base overturning moment in nth mode $M_{0n}(t)$
$\overline{M}_0$	maximum base overturning moment
$\overline{M}_j$	maximum overturning moment at story j
N	total number of floor levels in the structure
r	exponent of $1/T$ in decaying branch of pseudo-acceleration design spectrum, MFDC
$\overline{r}$	maximum of response quantity r
$\overline{r}_n$	maximum of nth vibration mode component of response quantity r
R	reduction factor to account for effects of inelastic behavior, ATC-3
S_a	pseudo-acceleration design spectrum
S_{an}	spectral pseudo-acceleration ordinate for nth natural vibration mode
S_d	displacement design spectrum
S_v	pseudo-velocity design spectrum
t	time variable
T	natural vibration period
T_1	fundamental vibration period of a multi-degree of freedom system
T_a	lower limit of natural period for constant pseudo-acceleration part of the design spectrum

T_d lower limit of natural period for constant displacement part of the design spectrum

T_n natural vibration period in the nth mode

T_v lower limit of natural period for the constant pseudo-velocity part of the design spectrum

$\overline{u}_g$ maximum ground displacement due to earthquake ground motion

$\overline{u}_{jn}$ maximum floor displacement at jth floor level on the nth vibration mode

$\overline{v}_g$ maximum of ground velocity due to earthquake ground motion

V_0 base shear in building code formulas

$V_0^{(1)}$ part of base shear distributed over the height proportional to h, MFDC

$V_0^{(2)}$ part of base shear distributed over the height proportional to h^2, MFDC

$\overline{V}_0$ maximum value of base shear

$\overline{V}_j$ maximum of story shear at story j

$V_{0n}(t)$ time-history of base shear in nth mode

$\overline{V}_{0n}$ maximum value of base shear in nth mode

w_j weight lumped at the jth floor level

W total weight of the structure

W_n^* effective weight that participates in the nth natural vibration mode

Z seismic zone coefficient, UBC

α scale factor in $\alpha T^{-\beta}$ least-squared error fit to normalized base shear spectrum

β exponent in $\alpha T^{-\beta}$ least-squared error fit to normalized base shear spectrum

β_d value of exponent β in the displacement-controlled region of the spectrum

β_v value of exponent β in the velocity-controlled region of the spectrum

δ	parameter in the fundamental mode approximation, exponent, equation (29)
$\overline{\Delta}_{jn}$	maximum inter-story drift at jth story in the nth natural vibration mode
ξ_n	damping ratio in the nth natural vibration mode
μ	allowable ductility factor, MFDC
μ'	reduction factor, related to μ, to account for effects of inelastic behavior, MFDC
ρ	beam-to-column stiffness ratio
ϕ_{jn}	displacement at the jth floor in the nth natural vibration mode
ϕ	eigen vector or natural vibration mode shape
ϕ_n	nth natural vibration mode shape
ω	natural vibration frequency
ω_n	nth natural vibration frequency

EARTHQUAKE ENGINEERING RESEARCH CENTER REPORTS

NOTE: Numbers in parentheses are Accession Numbers assigned by the National Technical Information Service; these are followed by a price code. Copies of the reports may be ordered from the National Technical Information Service, 5285 Port Royal Road, Springfield, Virginia, 22161. Accession Numbers should be quoted on orders for reports (PB --- ---) and remittance must accompany each order. Reports without this information were not available at time of printing. The complete list of EERC reports (from EERC 67-1) is available upon request from the Earthquake Engineering Research Center, University of California, Berkeley, 47th Street and Hoffman Boulevard, Richmond, California 94804.

UCB/EERC-79/01 "Hysteretic Behavior of Lightweight Reinforced Concrete Beam-Column Subassemblages," by B. Forzani, E.P. Popov and V.V. Bertero - April 1979(PB 298 267)A06

UCB/EERC-79/02 "The Development of a Mathematical Model to Predict the Flexural Response of Reinforced Concrete Beams to Cyclic Loads, Using System Identification," by J. Stanton & H. McNiven - Jan. 1979(PB 295 875)A10

UCB/EERC-79/03 "Linear and Nonlinear Earthquake Response of Simple Torsionally Coupled Systems," by C.L. Kan and A.K. Chopra - Feb. 1979(PB 298 262)A06

UCB/EERC-79/04 "A Mathematical Model of Masonry for Predicting its Linear Seismic Response Characteristics," by Y. Mengi and H.D. McNiven - Feb. 1979(PB 298 266)A06

UCB/EERC-79/05 "Mechanical Behavior of Lightweight Concrete Confined by Different Types of Lateral Reinforcement," by M.A. Manrique, V.V. Bertero and E.P. Popov - May 1979(PB 301 114)A06

UCB/EERC-79/06 "Static Tilt Tests of a Tall Cylindrical Liquid Storage Tank," by R.W. Clough and A. Niwa - Feb. 1979 (PB 301 167)A06

UCB/EERC-79/07 "The Design of Steel Energy Absorbing Restrainers and Their Incorporation into Nuclear Power Plants for Enhanced Safety: Volume 1 - Summary Report," by P.N. Spencer, V.F. Zackay, and E.R. Parker - Feb. 1979(UCB/EERC-79/07)A09

UCB/EERC-79/08 "The Design of Steel Energy Absorbing Restrainers and Their Incorporation into Nuclear Power Plants for Enhanced Safety: Volume 2 - The Development of Analyses for Reactor System Piping,""Simple Systems" by M.C. Lee, J. Penzien, A.K. Chopra and K, Suzuki "Complex Systems" by G.H. Powell, E.L. Wilson, R.W. Clough and D.G. Row - Feb. 1979(UCB/EERC-79/08)A10

UCB/EERC-79/09 "The Design of Steel Energy Absorbing Restrainers and Their Incorporation into Nuclear Power Plants for Enhanced Safety: Volume 3 - Evaluation of Commercial Steels," by W.S. Owen, R.M.N. Pelloux, R.O. Ritchie, M. Faral, T. Ohhashi, J. Toplosky, S.J. Hartman, V.F. Zackay and E.R. Parker - Feb. 1979(UCB/EERC-79/09)A04

UCB/EERC-79/10 "The Design of Steel Energy Absorbing Restrainers and Their Incorporation into Nuclear Power Plants for Enhanced Safety: Volume 4 - A Review of Energy-Absorbing Devices," by J.M. Kelly and M.S. Skinner - Feb. 1979(UCB/EERC-79/10)A04

UCB/EERC-79/11 "Conservatism In Summation Rules for Closely Spaced Modes," by J.M. Kelly and J.L. Sackman - May 1979(PB 301 328)A03

UCB/EERC-79/12 "Cyclic Loading Tests of Masonry Single Piers; Volume 3 - Height to Width Ratio of 0.5," by P.A. Hidalgo, R.L. Mayes, H.D. McNiven and R.W. Clough - May 1979(PB 301 321)A08

UCB/EERC-79/13 "Cyclic Behavior of Dense Course-Grained Materials in Relation to the Seismic Stability of Dams," by N.G. Banerjee, H.B. Seed and C.K. Chan - June 1979(PB 301 373)A13

UCB/EERC-79/14 "Seismic Behavior of Reinforced Concrete Interior Beam-Column Subassemblages," by S. Viwathanatepa, E.P. Popov and V.V. Bertero - June 1979(PB 301 326)A10

UCB/EERC-79/15 "Optimal Design of Localized Nonlinear Systems with Dual Performance Criteria Under Earthquake Excitations," by M.A. Bhatti - July 1979(PB 80 167 109)A06

UCB/EERC-79/16 "OPTDYN - A General Purpose Optimization Program for Problems with or without Dynamic Constraints," by M.A. Bhatti, E. Polak and K.S. Pister - July 1979(PB 80 167 091)A05

UCB/EERC-79/17 "ANSR-II, Analysis of Nonlinear Structural Response, Users Manual," by D.P. Mondkar and G.H. Powell July 1979(PB 80 113 301)A05

UCB/EERC-79/18 "Soil Structure Interaction in Different Seismic Environments," A. Gomez-Masso, J. Lysmer, J.-C. Chen and H.B. Seed - August 1979(PB 80 101 520)A04

UCB/EERC-79/19 "ARMA Models for Earthquake Ground Motions," by M.K. Chang, J.W. Kwiatkowski, R.F. Nau, R.M. Oliver and K.S. Pister - July 1979(PB 301 166)A05

UCB/EERC-79/20 "Hysteretic Behavior of Reinforced Concrete Structural Walls," by J.M. Vallenas, V.V. Bertero and E.P. Popov - August 1979(PB 80 165 905)A12

UCB/EERC-79/21 "Studies on High-Frequency Vibrations of Buildings - 1: The Column Effect," by J. Lubliner - August 1979 (PB 80 158 553)A03

UCB/EERC-79/22 "Effects of Generalized Loadings on Bond Reinforcing Bars Embedded in Confined Concrete Blocks," by S. Viwathanatepa, E.P. Popov and V.V. Bertero - August 1979(PB 81 124 018)A14

UCB/EERC-79/23 "Shaking Table Study of Single-Story Masonry Houses, Volume 1: Test Structures 1 and 2," by P. Gülkan, R.L. Mayes and R.W. Clough - Sept. 1979 (HUD-000 1763)A12

UCB/EERC-79/24 "Shaking Table Study of Single-Story Masonry Houses, Volume 2: Test Structures 3 and 4," by P. Gülkan, R.L. Mayes and R.W. Clough - Sept. 1979 (HUD-000 1836)A12

UCB/EERC-79/25 "Shaking Table Study of Single-Story Masonry Houses, Volume 3: Summary, Conclusions and Recommendations," by R.W. Clough, R.L. Mayes and P. Gülkan - Sept. 1979 (HUD-000 1837)A06

UCB/EERC-79/26 "Recommendations for a U.S.-Japan Cooperative Research Program Utilizing Large-Scale Testing Facilities," by U.S.-Japan Planning Group - Sept. 1979(PB 301 407)A06

UCB/EERC-79/27 "Earthquake-Induced Liquefaction Near Lake Amatitlan, Guatemala," by H.B. Seed, I. Arango, C.K. Chan, A. Gomez-Masso and R. Grant de Ascoli - Sept. 1979(NUREG-CR1341)A03

UCB/EERC-79/28 "Infill Panels: Their Influence on Seismic Response of Buildings," by J.W. Axley and V.V. Bertero Sept. 1979(PB 80 163 371)A10

UCB/EERC-79/29 "3D Truss Bar Element (Type 1) for the ANSR-II Program," by D.P. Mondkar and G.H. Powell - Nov. 1979 (PB 80 169 709)A02

UCB/EERC-79/30 "2D Beam-Column Element (Type 5 - Parallel Element Theory) for the ANSR-II Program," by D.G. Row, G.H. Powell and D.P. Mondkar - Dec. 1979(PB 80 167 224)A03

UCB/EERC-79/31 "3D Beam-Column Element (Type 2 - Parallel Element Theory) for the ANSR-II Program," by A. Riahi, G.H. Powell and D.P. Mondkar - Dec. 1979(PB 80 167 216)A03

UCB/EERC-79/32 "On Response of Structures to Stationary Excitation," by A. Der Kiureghian - Dec. 1979(PB 80166 929)A03

UCB/EERC-79/33 "Undisturbed Sampling and Cyclic Load Testing of Sands," by S. Singh, H.B. Seed and C.K. Chan Dec. 1979(ADA 087 298)A07

UCB/EERC-79/34 "Interaction Effects of Simultaneous Torsional and Compressional Cyclic Loading of Sand," by P.M. Griffin and W.N. Houston - Dec. 1979(ADA 092 352)A15

UCB/EERC-80/01 "Earthquake Response of Concrete Gravity Dams Including Hydrodynamic and Foundation Interaction Effects," by A.K. Chopra, P. Chakrabarti and S. Gupta - Jan. 1980(AD-A087297)A10

UCB/EERC-80/02 "Rocking Response of Rigid Blocks to Earthquakes," by C.S. Yim, A.K. Chopra and J. Penzien - Jan. 1980 (PB80 166 002)A04

UCB/EERC-80/03 "Optimum Inelastic Design of Seismic-Resistant Reinforced Concrete Frame Structures," by S.W. Zagajeski and V.V. Bertero - Jan. 1980(PB80 164 635)A06

UCB/EERC-80/04 "Effects of Amount and Arrangement of Wall-Panel Reinforcement on Hysteretic Behavior of Reinforced Concrete Walls," by R. Iliya and V.V. Bertero - Feb. 1980(PB81 122 525)A09

UCB/EERC-80/05 "Shaking Table Research on Concrete Dam Models," by A. Niwa and R.W. Clough - Sept. 1980(PB81 122 368)A06

UCB/EERC-80/06 "The Design of Steel Energy-Absorbing Restrainers and their Incorporation into Nuclear Power Plants for Enhanced Safety (Vol 1A): Piping with Energy Absorbing Restrainers: Parameter Study on Small Systems," by G.H. Powell, C. Oughourlian and J. Simons - June 1980

UCB/EERC-80/07 "Inelastic Torsional Response of Structures Subjected to Earthquake Ground Motions," by Y. Yamazaki April 1980(PB81 122 327)A08

UCB/EERC-80/08 "Study of X-Braced Steel Frame Structures Under Earthquake Simulation," by Y. Ghanaat - April 1980 (PB81 122 335)A11

UCB/EERC-80/09 "Hybrid Modelling of Soil-Structure Interaction," by S. Gupta, T.W. Lin, J. Penzien and C.S. Yeh May 1980(PB81 122 319)A07

UCB/EERC-80/10 "General Applicability of a Nonlinear Model of a One Story Steel Frame," by B.I. Sveinsson and H.D. McNiven - May 1980(PB81 124 877)A06

UCB/EERC-80/11 "A Green-Function Method for Wave Interaction with a Submerged Body," by W. Kioka - April 1980 (PB81 122 269)A07

UCB/EERC-80/12 "Hydrodynamic Pressure and Added Mass for Axisymmetric Bodies," by F. Nilrat - May 1980(PB81 122 343)A08

UCB/EERC-80/13 "Treatment of Non-Linear Drag Forces Acting on Offshore Platforms," by B.V. Dao and J. Penzien May 1980(PB81 153 413)A07

UCB/EERC-80/14 "2D Plane/Axisymmetric Solid Element (Type 3 - Elastic or Elastic-Perfectly Plastic) for the ANSR-II Program," by D.P. Mondkar and G.H. Powell - July 1980(PB81 122 350)A03

UCB/EERC-80/15 "A Response Spectrum Method for Random Vibrations," by A. Der Kiureghian - June 1980(PB81 122 301)A03

UCB/EERC-80/16 "Cyclic Inelastic Buckling of Tubular Steel Braces," by V.A. Zayas, E.P. Popov and S.A. Mahin June 1980(PB81 124 885)A10

UCB/EERC-80/17 "Dynamic Response of Simple Arch Dams Including Hydrodynamic Interaction," by C.S. Porter and A.K. Chopra - July 1980(PB81 124 000)A13

UCB/EERC-80/18 "Experimental Testing of a Friction Damped Aseismic Base Isolation System with Fail-Safe Characteristics," by J.M. Kelly, K.E. Beucke and M.S. Skinner - July 1980(PB81 148 595)A04

UCB/EERC-80/19 "The Design of Steel Energy-Absorbing Restrainers and their Incorporation into Nuclear Power Plants for Enhanced Safety (Vol 1B): Stochastic Seismic Analyses of Nuclear Power Plant Structures and Piping Systems Subjected to Multiple Support Excitations," by M.C. Lee and J. Penzien - June 1980

UCB/EERC-80/20 "The Design of Steel Energy-Absorbing Restrainers and their Incorporation into Nuclear Power Plants for Enhanced Safety (Vol 1C): Numerical Method for Dynamic Substructure Analysis," by J.M. Dickens and E.L. Wilson - June 1980

UCB/EERC-80/21 "The Design of Steel Energy-Absorbing Restrainers and their Incorporation into Nuclear Power Plants for Enhanced Safety (Vol 2): Development and Testing of Restraints for Nuclear Piping Systems," by J.M. Kelly and M.S. Skinner - June 1980

UCB/EERC-80/22 "3D Solid Element (Type 4-Elastic or Elastic-Perfectly-Plastic) for the ANSR-II Program," by D.P. Mondkar and G.H. Powell - July 1980(PB81 123 242)A03

UCB/EERC-80/23 "Gap-Friction Element (Type 5) for the ANSR-II Program," by D.P. Mondkar and G.H. Powell - July 1980 (PB81 122 285)A03

UCB/EERC-80/24 "U-Bar Restraint Element (Type 11) for the ANSR-II Program," by C. Oughourlian and G.H. Powell July 1980(PB81 122 293)A03

UCB/EERC-80/25 "Testing of a Natural Rubber Base Isolation System by an Explosively Simulated Earthquake," by J.M. Kelly - August 1980(PB81 201 360)A04

UCB/EERC-80/26 "Input Identification from Structural Vibrational Response," by Y. Hu - August 1980(PB81 152 308)A05

UCB/EERC-80/27 "Cyclic Inelastic Behavior of Steel Offshore Structures," by V.A. Zayas, S.A. Mahin and E.P. Popov August 1980(PB81 196 180)A15

UCB/EERC-80/28 "Shaking Table Testing of a Reinforced Concrete Frame with Biaxial Response," by M.G. Oliva October 1980(PB81 154 304)A10

UCB/EERC-80/29 "Dynamic Properties of a Twelve-Story Prefabricated Panel Building," by J.G. Bouwkamp, J.P. Kollegger and R.M. Stephen - October 1980(PB82 117 128)A06

UCB/EERC-80/30 "Dynamic Properties of an Eight-Story Prefabricated Panel Building," by J.G. Bouwkamp, J.P. Kollegger and R.M. Stephen - October 1980(PB81 200 313)A05

UCB/EERC-80/31 "Predictive Dynamic Response of Panel Type Structures Under Earthquakes," by J.P. Kollegger and J.G. Bouwkamp - October 1980(PB81 152 316)A04

UCB/EERC-80/32 "The Design of Steel Energy-Absorbing Restrainers and their Incorporation into Nuclear Power Plants for Enhanced Safety (Vol 3): Testing of Commercial Steels in Low-Cycle Torsional Fatigue," by P. Spencer, E.R. Parker, E. Jongewaard and M. Drory

UCB/EERC-80/33 "The Design of Steel Energy-Absorbing Restrainers and their Incorporation into Nuclear Power Plants for Enhanced Safety (Vol 4): Shaking Table Tests of Piping Systems with Energy-Absorbing Restrainers," by S.F. Stiemer and W.G. Godden - Sept. 1980

UCB/EERC-80/34 "The Design of Steel Energy-Absorbing Restrainers and their Incorporation into Nuclear Power Plants for Enhanced Safety (Vol 5): Summary Report," by P. Spencer

UCB/EERC-80/35 "Experimental Testing of an Energy-Absorbing Base Isolation System," by J.M. Kelly, M.S. Skinner and K.E. Beucke - October 1980(PB81 154 072)A04

UCB/EERC-80/36 "Simulating and Analyzing Artificial Non-Stationary Earthquake Ground Motions," by R.F. Nau, R.M. Oliver and K.S. Pister - October 1980(PB81 153 397)A04

UCB/EERC-80/37 "Earthquake Engineering at Berkeley - 1980," - Sept. 1980(PB81 205 874)A09

UCB/EERC-80/38 "Inelastic Seismic Analysis of Large Panel Buildings," by V. Schricker and G.H. Powell - Sept. 1980 (PB81 154 338)A13

UCB/EERC-80/39 "Dynamic Response of Embankment, Concrete-Gravity and Arch Dams Including Hydrodynamic Interaction," by J.F. Hall and A.K. Chopra - October 1980(PB81 152 324)A11

UCB/EERC-80/40 "Inelastic Buckling of Steel Struts Under Cyclic Load Reversal," by R.G. Black, W.A. Wenger and E.P. Popov - October 1980(PB81 154 312)A08

UCB/EERC-80/41 "Influence of Site Characteristics on Building Damage During the October 3, 1974 Lima Earthquake," by P. Repetto, I. Arango and H.B. Seed - Sept. 1980(PB81 161 739)A05

UCB/EERC-80/42 "Evaluation of a Shaking Table Test Program on Response Behavior of a Two Story Reinforced Concrete Frame," by J.M. Blondet, R.W. Clough and S.A. Mahin

UCB/EERC-80/43 "Modelling of Soil-Structure Interaction by Finite and Infinite Elements," by F. Medina - December 1980(PB81 229 270)A04

UCB/EERC-81/01 "Control of Seismic Response of Piping Systems and Other Structures by Base Isolation," edited by J.M. Kelly - January 1981 (PB81 200 735)A05

UCB/EERC-81/02 "OPTNSR - An Interactive Software System for Optimal Design of Statically and Dynamically Loaded Structures with Nonlinear Response," by M.A. Bhatti, V. Ciampi and K.S. Pister - January 1981 (PB81 218 851)A09

UCB/EERC-81/03 "Analysis of Local Variations in Free Field Seismic Ground Motions," by J.-C. Chen, J. Lysmer and H.B. Seed - January 1981 (AD-A099508)A13

UCB/EERC-81/04 "Inelastic Structural Modeling of Braced Offshore Platforms for Seismic Loading," by V.A. Zayas, P.-S.B. Shing, S.A. Mahin and E.P. Popov - January 1981(PB82 138 777)A07

UCB/EERC-81/05 "Dynamic Response of Light Equipment in Structures," by A. Der Kiureghian, J.L. Sackman and B. Nour-Omid - April 1981 (PB81 218 497)A04

UCB/EERC-81/06 "Preliminary Experimental Investigation of a Broad Base Liquid Storage Tank," by J.G. Bouwkamp, J.P. Kollegger and R.M. Stephen - May 1981(PB82 140 385)A03

UCB/EERC-81/07 "The Seismic Resistant Design of Reinforced Concrete Coupled Structural Walls," by A.E. Aktan and V.V. Bertero - June 1981(PB82 113 358)A11

UCB/EERC-81/08 "The Undrained Shearing Resistance of Cohesive Soils at Large Deformations," by M.R. Pyles and H.B. Seed - August 1981

UCB/EERC-81/09 "Experimental Behavior of a Spatial Piping System with Steel Energy Absorbers Subjected to a Simulated Differential Seismic Input," by S.F. Stiemer, W.G. Godden and J.M. Kelly - July 1981

UCB/EERC-81/10 "Evaluation of Seismic Design Provisions for Masonry in the United States," by B.I. Sveinsson, R.L. Mayes and H.D. McNiven - August 1981 (PB82 166 075)A08

UCB/EERC-81/11 "Two-Dimensional Hybrid Modelling of Soil-Structure Interaction," by T.-J. Tzong, S. Gupta and J. Penzien - August 1981(PB82 142 118)A04

UCB/EERC-81/12 "Studies on Effects of Infills in Seismic Resistant R/C Construction," by S. Brokken and V.V. Bertero - September 1981 (PB82 166 190)A09

UCB/EERC-81/13 "Linear Models to Predict the Nonlinear Seismic Behavior of a One-Story Steel Frame," by H. Valdimarsson, A.H. Shah and H.D. McNiven - September 1981(PB82 138 793)A07

UCB/EERC-81/14 "TLUSH: A Computer Program for the Three-Dimensional Dynamic Analysis of Earth Dams," by T. Kagawa, L.H. Mejia, H.B. Seed and J. Lysmer - September 1981(PB82 139 940)A06

UCB/EERC-81/15 "Three Dimensional Dynamic Response Analysis of Earth Dams," by L.H. Mejia and H.B. Seed - September 1981 (PB82 137 274)A12

UCB/EERC-81/16 "Experimental Study of Lead and Elastomeric Dampers for Base Isolation Systems," by J.M. Kelly and S.B. Hodder - October 1981 (PB82 166 182)A05

UCB/EERC-81/17 "The Influence of Base Isolation on the Seismic Response of Light Secondary Equipment," by J.M. Kelly - April 1981 (PB82 255 266)A04

UCB/EERC-81/18 "Studies on Evaluation of Shaking Table Response Analysis Procedures," by J. Marcial Blondet - November 1981 (PB82 197 278)A10

UCB/EERC-81/19 "*DELIGHT.STRUCT: A Computer-Aided Design Environment for Structural Engineering*," by R.J. Balling, K.S. Pister and E. Polak - December 1981 (PB82 218 496)A07

UCB/EERC-81/20 "Optimal Design of Seismic-Resistant Planar Steel Frames," by R.J. Balling, V. Ciampi, K.S. Pister and E. Polak - December 1981 (PB82 220 179)A07

UCB/EERC-82/01 "Dynamic Behavior of Ground for Seismic Analysis of Lifeline Systems," by T. Sato and A. Der Kiureghian - January 1982 (PB82 218 926)A05

UCB/EERC-82/02 "Shaking Table Tests of a Tubular Steel Frame Model," by Y. Ghanaat and R. W. Clough - January 1982 (PB82 220 161)A07

UCB/EERC-82/03 "Behavior of a Piping System under Seismic Excitation: Experimental Investigations of a Spatial Piping System supported by Mechanical Shock Arrestors and Steel Energy Absorbing Devices under Seismic Excitation," by S. Schneider, H.-M. Lee and W. G. Godden - May 1982 (PB83 172 544)A09

UCB/EERC-82/04 "New Approaches for the Dynamic Analysis of Large Structural Systems," by E. L. Wilson - June 1982 (PB83 148 080)A05

UCB/EERC-82/05 "Model Study of Effects of Damage on the Vibration Properties of Steel Offshore Platforms," by F. Shahrivar and J. G. Bouwkamp - June 1982 (PB83 148 742)A10

UCB/EERC-82/06 "States of the Art and Practice in the Optimum Seismic Design and Analytical Response Prediction of R/C Frame-Wall Structures," by A. E. Aktan and V. V. Bertero - July 1982 (PB83 147 736)A05

UCB/EERC-82/07 "Further Study of the Earthquake Response of a Broad Cylindrical Liquid-Storage Tank Model," by G. C. Manos and R. W. Clough - July 1982 (PB83 147 744)A11

UCB/EERC-82/08 "An Evaluation of the Design and Analytical Seismic Response of a Seven Story Reinforced Concrete Frame - Wall Structure," by F. A. Charney and V. V. Bertero - July 1982(PB83 157 628)A09

UCB/EERC-82/09 "Fluid-Structure Interactions: Added Mass Computations for Incompressible Fluid," by J. S.-H. Kuo - August 1982 (PB83 156 281)A07

UCB/EERC-82/10 "Joint-Opening Nonlinear Mechanism: Interface Smeared Crack Model," by J. S.-H. Kuo - August 1982 (PB83 149 195)A05

UCB/EERC-82/11 "Dynamic Response Analysis of Techi Dam," by R. W. Clough, R. M. Stephen and J. S.-H. Kuo - August 1982 (PB83 147 496)A06

UCB/EERC-82/12 "Prediction of the Seismic Responses of R/C Frame-Coupled Wall Structures," by A. E. Aktan, V. V. Bertero and M. Piazza - August 1982 (PB83 149 203)A09

UCB/EERC-82/13 "Preliminary Report on the SMART 1 Strong Motion Array in Taiwan," by B. A. Bolt, C. H. Loh, J. Penzien, Y. B. Tsai and Y. T. Yeh - August 1982 (PB83 159 400)A10

UCB/EERC-82/14 "Shaking-Table Studies of an Eccentrically X-Braced Steel Structure," by M. S. Yang - September 1982 (PB83 260 778)A12

UCB/EERC-82/15 "The Performance of Stairways in Earthquakes," by C. Roha, J. W. Axley and V. V. Bertero - September 1982 (PB83 157 693)A07

UCB/EERC-82/16 "The Behavior of Submerged Multiple Bodies in Earthquakes," by W.-G. Liao - Sept. 1982 (PB83 158 709)A07

UCB/EERC-82/17 "Effects of Concrete Types and Loading Conditions on Local Bond-Slip Relationships," by A. D. Cowell, E. P. Popov and V. V. Bertero - September 1982 (PB83 153 577)A04

UCB/EERC-82/18 "Mechanical Behavior of Shear Wall Vertical Boundary Members: An Experimental Investigation," by M. T. Wagner and V. V. Bertero - October 1982 (PB83 159 764)A05

UCB/EERC-82/19 "Experimental Studies of Multi-support Seismic Loading on Piping Systems," by J. M. Kelly and A. D. Cowell - November 1982

UCB/EERC-82/20 "Generalized Plastic Hinge Concepts for 3D Beam-Column Elements," by P. F.-S. Chen and G. H. Powell - November 1982 (PB83 247 981)A13

UCB/EERC-82/21 "ANSR-III: General Purpose Computer Program for Nonlinear Structural Analysis," by C. V. Oughourlian and G. H. Powell - November 1982 (PB83 251 330)A12

UCB/EERC-82/22 "Solution Strategies for Statically Loaded Nonlinear Structures," by J. W. Simons and G. H. Powell - November 1982 (PB83 197 970)A06

UCB/EERC-82/23 "Analytical Model of Deformed Bar Anchorages under Generalized Excitations," by V. Ciampi, R. Eligehausen, V. V. Bertero and E. P. Popov - November 1982 (PB83 169 532)A06

UCB/EERC-82/24 "A Mathematical Model for the Response of Masonry Walls to Dynamic Excitations," by H. Sucuoğlu, Y. Mengi and H. D. McNiven - November 1982 (PB83 169 011)A07

UCB/EERC-82/25 "Earthquake Response Considerations of Broad Liquid Storage Tanks," by F. J. Cambra - November 1982 (PB83 251 215)A09

UCB/EERC-82/26 "Computational Models for Cyclic Plasticity, Rate Dependence and Creep," by B. Mosaddad and G. H. Powell - November 1982 (PB83 245 829)A08

UCB/EERC-82/27 "Inelastic Analysis of Piping and Tubular Structures," by M. Mahasuverachai and G. H. Powell - November 1982 (PB83 249 987)A07

UCB/EERC-83/01 "The Economic Feasibility of Seismic Rehabilitation of Buildings by Base Isolation," by J. M. Kelly - January 1983 (PB83 197 988)A05

UCB/EERC-83/02 "Seismic Moment Connections for Moment-Resisting Steel Frames," by E. P. Popov - January 1983 (PB83 195 412)A04

UCB/EERC-83/03 "Design of Links and Beam-to-Column Connections for Eccentrically Braced Steel Frames," by E. P. Popov and J. O. Malley - January 1983 (PB83 194 811)A04

UCB/EERC-83/04 "Numerical Techniques for the Evaluation of Soil-Structure Interaction Effects in the Time Domain," by E. Bayo and E. L. Wilson - February 1983 (PB83 245 605)A09

UCB/EERC-83/05 "A Transducer for Measuring the Internal Forces in the Columns of a Frame-Wall Reinforced Concrete Structure," by R. Sause and V. V. Bertero - May 1983 (PB84 119 494)A06

UCB/EERC-83/06 "Dynamic Interactions between Floating Ice and Offshore Structures," by P. Croteau - May 1983 (PB84 119 486)A16

UCB/EERC-83/07 "Dynamic Analysis of Multiply Tuned and Arbitrarily Supported Secondary Systems," by T. Igusa and A. Der Kiureghian - June 1983 (PB84 118 272)A11

UCB/EERC-83/08 "A Laboratory Study of Submerged Multi-body Systems in Earthquakes," by G. R. Ansari - June 1983 (PB83 261 842)A17

UCB/EERC-83/09 "Effects of Transient Foundation Uplift on Earthquake Response of Structures," by C.-S. Yim and A. K. Chopra - June 1983 (PB83 261 396)A07

UCB/EERC-83/10 "Optimal Design of Friction-Braced Frames under Seismic Loading," by M. A. Austin and K. S. Pister - June 1983 (PB84 119 288)A06

UCB/EERC-83/11 "Shaking Table Study of Single-Story Masonry Houses: Dynamic Performance under Three Component Seismic Input and Recommendations," by G. C. Manos, R. W. Clough and R. L. Mayes - June 1983

UCB/EERC-83/12 "Experimental Error Propagation in Pseudodynamic Testing," by P. B. Shing and S. A. Mahin - June 1983 (PB84 119 270)A09

UCB/EERC-83/13 "Experimental and Analytical Predictions of the Mechanical Characteristics of a 1/5-scale Model of a 7-story R/C Frame-Wall Building Structure," by A. E. Aktan, V. V. Bertero, A. A. Chowdhury and T. Nagashima - August 1983 (PB84 119 213)A07

UCB/EERC-83/14 "Shaking Table Tests of Large-Panel Precast Concrete Building System Assemblages," by M. G. Oliva and R. W. Clough - August 1983

UCB/EERC-83/15 "Seismic Behavior of Active Beam Links in Eccentrically Braced Frames," by K. D. Hjelmstad and E. P. Popov - July 1983 (PB84 119 676)A09

UCB/EERC-83/16 "System Identification of Structures with Joint Rotation," by J. S. Dimsdale and H. D. McNiven - July 1983

UCB/EERC-83/17 "Construction of Inelastic Response Spectra for Single-Degree-of-Freedom Systems," by S. Mahin and J. Lin - July 1983

UCB/EERC-83/18 "Interactive Computer Analysis Methods for Predicting the Inelastic Cyclic Behaviour of Structural Sections," by S. Kaba and S. Mahin - July 1983 (PB84 192 012) A06

UCB/EERC-83/19 "Effects of Bond Deterioration on Hysteretic Behavior of Reinforced Concrete Joints," by F.C. Filippou, E.P. Popov and V.V. Bertero - August 1983 (PB84 192 020) A10

UCB/EERC-83/20 "Analytical and Experimental Correlation of Large-Panel Precast Building System Performance," by M.G. Oliva, R.W. Clough, M. Velkov, P. Gavrilovic and J. Petrovski - November 1983

UCB/EERC-83/21 "Mechanical Characteristics of Materials Used in a 1/5 Scale Model of a 7-Story Reinforced Concrete Test Structure," by V.V. Bertero, A.E. Aktan, H.G. Harris and A.A. Chowdhury - September 1983 (PB84 193 697) A05

UCB/EERC-83/22 "Hybrid Modelling of Soil-Structure Interaction in Layered Media," by T.-J. Tzong and J. Penzien - October 1983 (PB84 192 178) A08

UCB/EERC-83/23 "Local Bond Stress-Slip Relationships of Deformed Bars under Generalized Excitations," by R. Eligehausen, E.P. Popov and V.V. Bertero - October 1983 (PB84 192 848) A09

UCB/EERC-83/24 "Design Considerations for Shear Links in Eccentrically Braced Frames," by J.O. Malley and E.P. Popov - November 1983 (PB84 192 186) A07

UCB/EERC-84/01 "Pseudodynamic Test Method for Seismic Performance Evaluation: Theory and Implementation," by P.-S. B. Shing and S. A. Mahin - January 1984 (PB84 190 644) A08

UCB/EERC-84/02 "Dynamic Response Behavior of Xiang Hong Dian Dam," by R.W. Clough, K.-T. Chang, H.-Q. Chen, R.M. Stephen, G.-L. Wang, and Y. Ghanaat - April 1984

UCB/EERC-84/03 "Refined Modelling of Reinforced Concrete Columns for Seismic Analysis," by S.A. Kaba and S.A. Mahin - April, 1984

UCB/EERC-84/04 "A New Floor Response Spectrum Method for Seismic Analysis of Multiply Supported Secondary Systems," by A. Asfura and A. Der Kiureghian - June 1984

UCB/EERC-84/05 "Earthquake Simulation Tests and Associated Studies of a 1/5th-scale Model of a 7-Story R/C Frame-Wall Test Structure," by V.V. Bertero, A.E. Aktan, F.A. Charney and R. Sause - June 1984

UCB/EERC-84/06 "R/C Structural Walls: Seismic Design for Shear," by A.E. Aktan and V.V. Bertero

UCB/EERC-84/07 "Behavior of Interior and Exterior Flat-Plate Connections subjected to Inelastic Load Reversals," by H.L. Zee and J.P. Moehle

UCB/EERC-84/08 "Experimental Study of the Seismic Behavior of a two-story Flat-Plate Structure," by J.W. Diebold and J.P. Moehle

UCB/EERC-84/09 "Phenomenological Modeling of Steel Braces under Cyclic Loading," by K. Ikeda, S.A. Mahin and S.N. Dermitzakis - May 1984

UCB/EERC-84/10 "Earthquake Analysis and Response of Concrete Gravity Dams," by G. Fenves and A.K. Chopra - August 1984

UCB/EERC-84/11 "EAGD-84: A Computer Program for Earthquake Analysis of Concrete Gravity Dams," by G. Fenves and A.K. Chopra - August 1984

UCB/EERC-84/12 "A Refined Physical Theory Model for Predicting the Seismic Behavior of Braced Steel Frames," by K. Ikeda and S.A. Mahin - July 1984

UCB/EERC-84/13 "Earthquake Engineering Research at Berkeley - 1984" - August 1984

UCB/EERC-84/14 "Moduli and Damping Factors for Dynamic Analyses of Cohesionless Soils," by H.B. Seed, R.T. Wong, I.M. Idriss and K. Tokimatsu - September 1984

UCB/EERC-84/15 "The Influence of SPT Procedures in Soil Liquefaction Resistance Evaluations," by H. B. Seed, K. Tokimatsu, L. F. Harder and R. M. Chung - October 1984

UCB/EERC-84/16 "Simplified Procedures for the Evaluation of Settlements in Sands Due to Earthquake Shaking," by K. Tokimatsu and H. B. Seed - October 1984

UCB/EERC-84/17 "Evaluation and Improvement of Energy Absorption Characteristics of Bridges under Seismic Conditions," by R. A. Imbsen and J. Penzien - November 1984

UCB/EERC-84/18 "Structure-Foundation Interactions under Dynamic Loads," by W. D. Liu and J. Penzien - November 1984

UCB/EERC-84/19 "Seismic Modelling of Deep Foundations," by C.-H. Chen and J. Penzien - November 1984

UCB/EERC-84/20 "Dynamic Response Behavior of Quan Shui Dam," by R. W. Clough, K.-T. Chang, H.-Q. Chen, R. M. Stephen, Y. Ghanaat and J.-H. Qi - November 1984

UCB/EERC-85/01 "Simplified Methods of Analysis for Earthquake Resistant Design of Buildings," by E. F. Cruz and A. K. Chopra - February 1985